Metabolic reprograming and cancer resistance: An investigation into the metabolic control of cancer-associated fibroblasts on breast cancer cell survival and metastasis

by

Megan Irvette Mitchell

Dissertation presented for the degree of

Doctor of Philosophy in the

Faculty of Science at

Stellenbosch University

Supervisor: Prof. Anna-Mart Engelbrecht

March 2018

Declaration

By submitting this thesis electronically, I declare that the entirety of the work contained therein is my own, original work, that I am the authorship owner thereof (unless to the extent explicitly otherwise stated) and that I have not previously in its entirety or in part submitted it for obtaining any qualification.

This dissertation includes one original paper published in a peer-reviewed journal, the development and writing of the paper was the principal responsibility of myself.

Date: .....

Abstract

Introduction: Cancer-associated fibroblasts (CAFs) constitute the most abundant mesenchymal cell type present within the tumour microenvironment. Recent evidence suggests that nutrient deprived cancer cells survive as a result of their ability to undergo extensive metabolic reprogramming exploiting the metabolic capacities of surrounding CAFs. Additionally, it has been proposed that CAFs also play a role in enhancing tumourigenicity and the metastatic capability of cancer cells. However, the mechanisms underlying the interactions between epithelial cancer cells and surrounding stromal fibroblasts remain to be elucidated. We therefore hypothesize, that nutrient deprived breast cancer epithelial cells could influence cancer-associated fibroblasts (CAF's), to produce metabolites which may be utilized by cancer cells for survival, chemo-resistance and enhanced migration.

Methods: E0771 cancer cells were subjected to glucose starvation after which cell viability, oxidative stress analysis and cell death was assessed. E0771 conditioned media was then generated and proteomic analysis on conditioned media was performed. This media was also used to treat mouse embryonic fibroblast (MEF) cells. The activation of a CAF phenotype was assessed by means of Western blotting and confocal microscopy. Furthermore, cell viability assays, oxidative stress, glucose uptake and GLUT4 translocation were assessed. MEF conditioned media was then generated and again proteomic analyses were performed. MEF conditioned media was then used to treat glucose deprived E0771 cells. Where after cell viability, cell death and migration were assessed. The effects of CAFs on chemotherapy resistance and metastasis was assessed by treating E0771 cells with doxorubicin and MEF conditioned media, following which, cell viability, apoptosis and migration assays were performed. An *in vivo* tumour bearing mouse model was established using female C57/BL6 mice treated with

doxorubicin. Primary epithelial organoids were isolated from tumours and a 3D branching morphogenesis assay was performed.

Results: 12 hours of glucose deprivation resulted in no significant changes in mitochondrial reductive capacity or markers of apoptosis, however, a significant increase in mitochondrial oxidative stress was observed. Proteomic analysis of glucose deprived E0771 conditioned media revealed an increase in proteins associated with exosome-like vesicles and an increased clustering of proteins involved in epithelial-to-mesenchymal transition and glucose metabolism. 2-NBDG glucose uptake was significantly increased in conjunction with an increase in the fluorescent intensity of the HA-GLUT4-GFP construct following exposure to E0771 conditioned media, indicating the increase in glucose uptake is in part mediated by GLUT4 translocation. Furthermore the treatment of E0771s with MEF conditioned media lead to a significant increase the speed of migration and EMT. Furthermore, increased invasiveness of epithelial organoids was observed following exposure to MEF-CM in Dox treated animals, with an increase in a more epithelial-like phenotype.

Conclusion: Our data suggest that glucose deprivation induces a state of oxidative stress in the E0771 cells which is transferred to MEFs leading to the “activation” of a CAF-like phenotype, and that this “activated” phenotype contributes significantly to the pro-survival and pro-metastatic abilities of breast cancer cells. Furthermore, our results contribute significantly to the understanding of the molecular mechanisms underlying the interaction between epithelial cancer cells and fibroblasts within the tumour microenvironment.

Opsomming

Inleiding: Kanker-geassosieërde fibroblaste (KGFe) maak die grootste deel uit van die mesenkiemale selle wat in die tumor mikro-omgewing voorkom. Onlangse bewyse stel voor dat nutriënt-ontneemde kankerselle oorleef as gevolg van hul vermoë om omvattende metaboliese herprogrammering te ondergaan en die metabolise kapasiteit van omliggende KGFe te benut. Daar word ook verder voorgestel dat KGFe ‘n rol speel om die tumorigenisiteit en die metastatiese kapasitiet van kankerselle te verhoog. Die meganismes onderliggend aan hierdie interaksie tussen die epiteliale kankerselle en die omliggende fibroblaste moet egter nog ontrafel word. Ons hipotese is dus dat nutriënt-ontneemde borskanker epiteelselle KGFe beïnvloed om metaboliete te produseer wat deur die kankerselle vir oorlewing, chemo-weerstand en verhoogde migrasie benut kan word.

Metodes: E0771 borskankerselle is blootgestel aan media wat van glukose ontneem is, waarna sellewensvatbaarheid, oksidatiewe stres en merkers van seldood is geanaliseer. Gekondisioneeerde media uit E0771 selle gegenereer waarna proteomiese analises daarop uitgevoer is. Hierdie media is ook gebruik om muis embrioniese fibroblaste (MEFe) te behandel. Die aktivering van die KGF fenotipe is bepaal deur middel van westelike kladtegniek en konfokale mikroskopie. Verder is sel-lewensvatbaarheid, oksidatiewe stres, glukose opname en GLUT4 translokering, geasseseer. MEF-gekondisioneerde media is daarna gegenereer waarop daar ook proteomiese analises uitgevoer is. MEF-gekondisioneerde media is ook gebruik om glukose-ontneemde E0771 kankerselle te behandel waarna sellewensvatbaarheid, L-laktaat konsentrasies, ATP produksie en seldood gemeet is. Die effek van KGFe op chemoterapie weerstand en metastase is geasseseer deur E0771 kankerselle met doxorubicin in kombinasie met MEF gekondisioneerde media te behandel, waarna sellewensvatbaarheidsanalise, apoptose

asook ‘n migrasie bepalings uitgevoer is. Verder is daar ook ‘n *in vivo* tumor-draende muismodel gebruik waar C57/BL6 muise met doxorubicin behandel is. Primêre epiteel organoïede is vanuit tumore geïsoleer waarop daar ‘n 3D vertakkingsmorfogenese gedoen is.

Resultate: 12 ure van glukose-ontneming het geen veranderinge in mitokondriale reduktiewe kapasitiet of in merkers van apoptose teweeggebring nie, alhoewel ‘n insiggewende verhoging in mitokondriale oksidatiewe stress op daardie tydspunt waargeneem is. Proteomiese analise van glukose-ontneemde E0771-gekondisioneerde media toon ‘n toename in proteïene aan wat geassosieer word met eksosoom vesikels; proteïene wat betrokke is by epiteel-tot-mesenkiemale oorgang asook proteïene betrokke by glukose metabolisme. 2-NBDG glukose opname is ook insiggewend verhoog tesame met ‘n toename in fluoriserende intensiteit van die HA-GLUT4-GFP fragment na blootstelling aan E0771-gekondisioneerde media, wat aandui dat glukose opname gedeeltelik bemiddel is deur GLUT4 translokering. Die behandeling van E0771 selle met MEF-gekondisioneerde media het tot ‘n insiggewende verhoging in die spoed van migrasie gelei, asook ‘n toename in EMO. Daar is ook ‘n toename in ‘n epiteelfenotipe en indringing in die epiteel-organoiede waargeneem na blootstelling aan MEF-gekondisioneerde media in Dox-behandelde muise.

Gevolgtrekking: Ons data bewys dat glukose-ontneming oksidatiewe stress in E0771 kankerselle teweegbring wat dan veroorsaak dat die omliggende MEFe geaktiveer word om na ‘n KGF fenotipe te verander. Hierdie geaktiveerde fenotipe dra dan op hulle beurt insiggewend by tot die oorlewing en pro-metastatiese vermoë van nutriënt-ontneemde borskankerselle. Ons resultate maak ‘n insiggewende bydrae tot die verstaan van die molekulêre meganismes betrokke by die interaksie tussen kankerselle en fibroblaste in die tumor mikro-omgewing.

Acknowledgements

I would like to express my sincere gratitude to the following:

To my mom, I can honestly not express how thankful I am for all of your support. Thank you for your endless guidance and love and for always pushing me to do my best. None of this would have been possible for me to achieve without you encouraging me to pursue my dreams. I am truly blessed to call you my mother.

My supervisor, Prof Anna-Mart Engelbrecht, thank you so much for always believing in me even at times when I doubted myself. I will be forever grateful to you for all of the opportunities you have provided me with and for guiding me to become a better researcher. I cannot imagine having gone through my postgraduate degrees without you as my supervisor, mentor and “work-mom”. It has been an immense honour to be one of your students.

J.D. Martindale, thank you will never be enough to truly express my sincere gratitude and appreciation for all that you have done. Our long phone calls and all your encouraging words of support are ultimately what got me through the toughest of days. Thank you from the bottom of my heart for your endless support, love and motivation.

Natasha Driescher, Danzil Joseph and Dr Lydia Lacerda, thank you so much for maintaining my “sanity” over the course of this and previous degrees. Words cannot fully express my gratitude and sincere appreciation for all the coffee breaks, laughs and encouragement provided.

To Dr Bali Sishi and Dr Ben Loos thank you for always being willing to share your expertise and answer the many questions I had. Ultimately, your guidance helped contribute to making this a better project.

To Gustav thank you for your help and insight with the proteomics analyses, and for always being willing to respond to my questions and moments of sheer panic.

To Ashwin, Lize, Rozanne and Tanja, thank you all for your help and guidance throughout this project, especially during times when I needed to “McGyver” equipment in order to get things to work out.

To CRG and DSG groups, thank you all for the support, guidance and the friendly lab environment you provided - it definitely made all the long lab hours more bearable.

To Reggie Williams and CPGR, for help with the histology preparations and running of proteomic samples respectively.

A special thank you to the Postgraduate International Office (PGIO) of Stellenbosch University, Cayman Chemical and the Physiological Society of Southern Africa (PSSA) for travel bursaries which allowed me to present this work both locally and internationally.

Lastly, to the National Research Foundation (NRF) for financial support.

Dedication

I would like to dedicate this thesis in its entirety my late father, Thomas Irwin Mitchell. This one is for you daddy, even from a young age you always believed in me and were so proud of my dreams – we finally made it!

Eris Semper in Corde Meo

List of Conference Proceedings

International:

- Mitchell, M.I. and Engelbrecht, A-M. Metabolic reprograming and cancer resistance: Do cancer-associated fibroblasts contribute? Poster presented at the Keystone Symposia: Cell Plasticity in the Tumor Microenvironment. 08th-12th January 2017. Big Sky, Montana, USA.

National:

- Mitchell, M.I. and Engelbrecht, A-M. Metabolic reprograming and cancer resistance: an investigation into the metabolic control of cancer-associated fibroblasts on breast cancer cell survival. Oral presentation at the 44th meeting of the Physiology Society of Southern Africa (PSSA). 28th-31th August 2016. University of Cape Town, South Africa.
- Mitchell, M.I. and Engelbrecht, A-M. Metabolic reprograming and cancer metastasis: Do cancer-associated fibroblasts contribute? Oral presentation at the 45th meeting of the Physiology Society of Southern Africa (PSSA). 27th-31th August 2017. University of Pretoria, South Africa.

Table of Contents

List of Figures

Chapter 1

Chapter 2

Chapter 3

Chapter 5

Chapter 7

List of Tables

Chapter 2

Chapter 3

Chapter 7

List of Abbreviations

2D	Two dimensional
2-NBDG	2-(N-(7-Nitrobenz-2-oxa-1,3-diazol-4-yl)Amino)-2-Deoxyglucose
3D	Three dimensional
4E-BP1	eIF4E-binding protein
α-SMA	α-smooth muscle actin

A

Akt	Protein kinase B
ALL	Acute lymphoblastic leukaemia
AMP	Adenosine monohosphate
ANOVA	One-way analysis of variance
ATG	Autophagy-specific genes
ATP	Adenosine triphosphate

B

Bad	Bcl-2-associated death promoter
BCA	Bicinchoninic acid
BECN1	Beclin-1

BH3	Bcl-2 homology domain 3
BSA	Bovine serum albumin

C

CAF	Cancer associated fibroblast
cCaf	Circulating cancer associated fibroblast
CD81	Cluster of differentiation 81
CD-CHO	Chemically defined Chinese hamster ovary
CDK	Cyclin-dependent kinases
CHMP4B	Charged multivesicular body protein 4B
CHO	Chinese hamster ovary
CM	Conditioned media
c-Met	Tyrosine-protein kinase Met or hepatocyte growth factor receptor
CO_2	Carbon dioxide
COL4A1	Collagen type IV alpha 1 chain
COX-2	Cyclooxygenase 2
CPGR	Centre for Proteomic & Genomic Research
CTC	Circulating tumour cells
CXCL12	Stromal-derived factor 1

CXCR4	C-X-C chemokine receptor type 4

D

DAPI	4',6-diamidino-2-phenylindole
DAVID	Database for Annotation, Visualization and Integrated Discovery
DCF	2'.7'-Dichlorofluorescein
DMEM	Dulbecco's Modified Eagles Medium
DMSO	Dimethyl sulfoxide
DNA	Deoxyribonucleic acid
DNase	Deoxyribonuclease
Dox	Doxorubicin

E

E0771_C	Control E0771 conditioned media
E0771_GD	Glucose deprived E0771 conditioned media
E0771-CM	12 hr glucose deprived E0771 conditioned media
E0771-UTCM	Untreated E0771 conditioned media
ECM	Extracellular matrix

EDTA	Ethylenediaminetetraacetic acid
EGF	Epidermal Growth Factor
eGFP	Enhanced green fluorescent protein
ELISA	Enzyme linked immunosorbent assay
EMT	Epithelial-to-mesenchymal transition
EndMT	Endothelial-to-mesenchymal transition
ENO	Enolase
ERK	Extracellular signal-regulated kinase
esiRNA	Endoribonuclease-prepared small interfering ribonucleic acid
EtOH	Ethanol
Ets	E-twenty-six

F

FAC	Functional annotation clustering
FAK	Focal adhesion kinase
FAP	Fibroblast activated protein
FBS	Fetal bovine serum
FGF	Fibroblast growth factor
FITC	Fluorescein isothiocyanate

FOXC2	Forkhead box protein C2
FoxO	Forkhead box O

G

G6PD	Glucose-6-phosphate dehydrogenase
GFP	Green fluorescent protein
GLUT	Glucose transporters
GO	Gene Ontology
GSK3β	Glycogen synthase kinase 3β

H

H&E	Haemotoxylin and eosin
H_2O_2	Hydrogen peroxide
HBSS	Hanks balanced salt solution
HER	Human epidermal growth factor receptor
HGF	Hepatocyte growth factor
HIF-1α	Hypoxia inducible factor 1α
HILIC	Hydrophilic interaction chromatography
HNRNPK	Heterogeneous nuclear ribonucleoprotein K

HRP	Horseradish peroxidase
HSP	Heat shock protein

I

IGF	Insulin-like growth factor
IL-6	Interleukin 6
ITS	Insulin-transferrin-selenium X

J

JNK	c-jun N-terminal kinase

K

KEGG	Kyoto Encyclopaedia of Genes and Genomes
KGF	Keratinocyte growth factor
Kiff11	Kinesin family member 11
KOH	Potassium hydroxide

L

LC3	Microtubule-associated protein light chain-3
LC-MS	Liquid Chromatography Mass Spectrometry

LDH	Lactate dehydrogenase
LEF	Lymphoid enhancer-binding factor 1

M

MAPK	Mitogen-activated protein kinase
MBC	Metastatic breast cancer
MCP-1	Monocyte chemoattractant protein 1
MCT	Monocarboxylate transporter
MEF	Mouse embryonic fibroblast
MEF_C	Control MEF conditioned media
MEF_ECM	MEF cells treated with glucose deprived E0771 conditioned media
MEF_EUM	MEF cells treated with untreated E0771 conditioned media
MEK1	Mitogen-activated protein kinase kinase 1
MET	Mesenchymal-to-epithelial transition
miRNA	microRNA
MitoSOX™	Mitochondrial Superoxide Indicator
MMP	Matrix metalloproteases
MMT	Mesenchymal-to-mesenchymal transition
mRNA	Messenger ribonucleic acid

MSC	Mesenchymal stem cells
mTOR	mammalian Target of Rapamycin
MTT	3-(4,5-dimethylthiazol-2-yl)-2,5-diphenyltetrazolium bromide
MVB	Multi-vesicular bodies

N

NAD^+	Nicotinamide adenine dinucleotide
NADH	Nicotinamide adenine dinucleotide
NFκβ	Nuclear factor κβ
NMuMG	Normal murine mammary gland

O

O_2	Oxygen
$O_2^{\bullet-}$	Superoxide

P

p53	Tumour protein 53
p62/SQSTM1	Poly-ubiquitin protein 62/Sequestome 1
PAR1	Protease-activated receptor-1

PARP	Poly (ADP-ribose) polymerase
PBS	Phosphate buffered saline
PCA	Perchloric acid
PDC	Pyruvate dehydrogenase complex
PDGF	Platelet derived growth factor
PDGFR	Platelet derived growth factor receptor
PDH	Pyruvate dehydrogenase
PDK	Pyruvate dehydrogenase kinase
PenStrep	Penicillin/Streptomycin
PI	Propidium iodide
PI3K	Phosphatidylinositol 3-kinase
PKM	Pyruvate kinase, muscle
PMSF	Phenylmethylsulfonyl fluoride
PT-100	Small-molecule dipeptidyl peptidase inhibitor
PTEN	Phosphatase and tensin homolog
PVDF	Polyvinylidine fluoride

R

RB	Retinoblastoma

REC	Research ethics committee
REC	Research ethics committee
REVIGO	Reduce and visualize gene ontology
RhoA	Ras homolog gene family, member A
RIPA	Radio immunoprecipitation assay
RNA	Ribonucleic acid
ROS	Reactive oxygen species

S

S100A11	S100 calcium binding protein A11
S100A4	S100 calcium-binding protein A4
SDS-PAGE	Sodium dodecyl sulphate polyacrylamide gel electrophoresis
SEM	Standard error of the mean
SEM	Standard error of the mean
SIP1	Survival of motor neuron protein interacting protein 1
SMAD	Mothers against decapentaplegic homolog
SPARC	Secreted protein acidic and rich in cysteine
STAT1	Signal transducer and activator of transcription 1

T

TAM	Tumour-associated macrophage
TBS-T	Tris Buffered Saline-Tween20
TCA	Tricarboxylic acid cycle
Tcf/LEF	T-cell factor / lymphoid enhancer-binding factor 1
TGF-β	Transforming growth factor-beta
TMEM	Tumour microenvironment of metastasis
TNFα	Tumour necrosis factor α
TP53	p53 gene
TRAIL	TNF- related apoptosis inducing ligand

U

Ulk1	Unc-51-like kinase
uPAR	Urokinase plasminogen activator
UPS	Ubiquitin proteasome system

V

VEGF-A	Vascular endothelial growth factor A
vs	Versus

W

Wnt Integration site 1 (Int1) and Wingless in Drosophila

Z

ZEB1 Zinc finger E-box binding homobox 1

Units of Measurement

%	percentage
µg/ml	microgram per millilitre
µl	microlitre
µm	micrometre
µM	micromolar
g	gravitational acceleration
Hz	hertz
kD	kilodalton
l/L	litre
M	molar
mA	milli-ampere
mg	milligram
mg/ml	milligram per millilitre
min	minutes
ml	millilitres
mM	millimolar
ng/ml	nanogram per millilitre
nm	nanometre
nM	nanomolar
ºC	degrees Celsius
RPM	revolutions per minute
V	volts
w/v	weight per volume

Chapter 1: Literature Review

1.1. Introduction

The majority of human tumours are comprised of cancerous epithelial cells that coexist with a multitude of different cell types (particularly, fibroblasts, adipocytes, immune and endothelial cells) and extracellular matrix components (McAllister *et al*., 2010) together creating what is termed the cancer microenvironment (stroma). Recent evidence suggests that the different cell types comprising the tumour stroma form a complex signalling network which plays an essential role in the survival, growth and metastatic capabilities of the cancerous epithelial cells within solid tumours (Quail *et al*., 2013).

During the initial process of tumour invasion, remodelling of the tumour stroma, both molecularly and architecturally, results in the invasion of these cells into the neighbouring tissue. Invasion has been shown to rely heavily on immune cells, endothelial cells and most notably, proliferating “activated” fibroblasts (Tuxhorn *et al*., 2002). These “activated” fibroblasts within the tumour stroma have been identified as mesenchymal cells with characteristic signs of smooth muscle differentiation, and have thus been termed “myofibroblasts” (De Wever *et al*., 2002). Myofibroblasts and their interactions with the surrounding environment have been extensively studied for the critical role they play in both wound healing and chronic inflammation (Li *et al*., 2015). Due to their ability to promote angiogenesis, stimulate epithelial cell growth, migration and contraction during wound healing (Orimo *et al*., 2006), it has been postulated that these cells may play a similar role within the tumour microenvironment, thereby facilitating the growth and progression of invasive cancers.

Olumi and colleagues (Olumi *et al*., 1999) demonstrated that stromal fibroblasts isolated from human prostate carcinomas, display potent tumour-promoting properties when

injected in combination with non-tumourigenic prostate epithelial cells into immune-deficient mice, whereas normal prostate fibroblasts failed to initiate the same response. In cancer, myofibroblasts termed cancer associated fibroblasts (CAFs), are characterized by their concurrent production of α-smooth muscle actin (α-SMA) and vimentin (Sugimoto *et al*., 2006), and are found to be one of the most abundant mesenchymal cell types present within most human carcinomas. Morphologically CAFs are characterized by large spindle-shaped cells with stress fibres and highly developed fibronexi (transmembrane complex with extracellular fibronectin, integrins and intracellular actin) (Xing *et al*., 2010).

Resident fibroblasts in the surrounding stroma are an immediate source for the recruitment of CAFs. However, CAFs have been shown also to originate from three other compartments (Figure 1.1). Firstly, the recruitment of CAFs from distant sites into the tumour can occur. Evidence suggests that bone marrow derived mesenchymal stem cells and precursor cells are a source of CAFs (Karnoub *et al.,* 2007). Additionally, within the tumour stroma various other cell types including endothelial, immune and epithelial cells can undergo lineage reprogramming (known as trans-differentiation) to transform into mesenchymal cells. Furthermore, other mesenchymal cells within the stroma, such as adipocytes and vascular smooth muscle cells could also potentially trans-differentiate and give rise to CAFs. Evidence suggests that the ability of CAFs to be recruited from a range of sources leads to a heterogeneous population of CAFs displaying common tumour growth promoting functions within the tumour microenvironment (Busch *et al*., 2017).

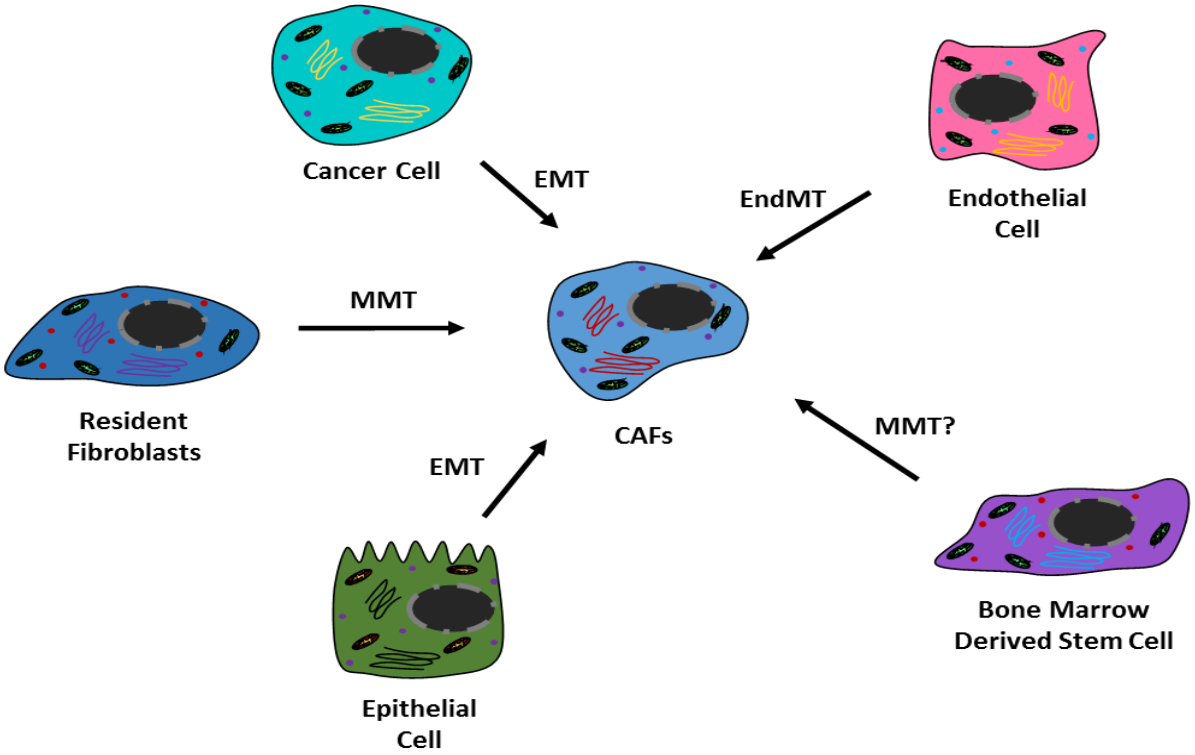

Figure 1.1: Origins of cancer-associated fibroblasts (CAFs) within the tumour stroma. CAFs are considered to be recruited from various cell types. The most immediate source of CAF recruitment comes from the "activation" of resident fibroblasts (through the process of mesenchymal-to-mesenchymal transition; MMT), from epithelial and adipocyte cells (via the process of epithelial-to-mesenchymal transition: EMT), or endothelial cells (endothelial-to-mesenchymal transition; EndMT). Finally, bone marrow derived mesenchymal stem cells can be recruited into the tumour stroma where they are thought to also undergo MMT, giving rise to CAFs. Adapted from Shiga *et al*., 2015.

1.2. Cancer-associated fibroblasts and cancer progression

The role of these "activated" fibroblasts in tumour progression appears to be multifaceted. The initial stages of tumour progression have been shown to be repressed by the action of fibroblasts, predominantly due to the formation of gap junctions between adjacent "activated" fibroblasts thereby exerting contact inhibitory effects on epithelial cancer cells (Hinz *et al*., 2007). Subsequent to the degradation of the basement membrane and the infiltration of fibroblasts into direct contact with epithelial cancer cells, the resulting activation of CAFs leads to the remodelling of the extracellular matrix (ECM) (Ao *et al*., 2015 and Neri *et al*., 2016). CAFs are predominantly responsible for the production of

essential ECM proteins (such as fibronectin and collagens) and proteases, including fibroblast activated protein (FAP) and matrix metalloproteases (MMPs) (Catteau *et al*., 2016).

In solid tumours, progressive stiffening of the ECM with a concurrent increase in matrix deposition is frequently observed, as such CAFs play a pivotal role in the remodelling of the ECM during tumour progression. Additionally, numerous cancer types show an increase in desmoplasia (increased fibrosis), characterized by an increase in collagen type I and III with a decrease in collagen type IV, which is often associated with a poor cancer prognosis (Kauppila *et al*., 1998). Interestingly, peritumoural CAFs have been implicated in the initiation of desmoplasia, through their ability to secrete a fibrillar network identical to that seen during wound healing.

A consequence of this increased desmoplasia is that the tumour stromal environment becomes more rigid, which stimulates the expression of integrins, which mediate cell-cell and cell-ECM interactions and signalling across the plasma membrane, making integrins important cell adhesion molecules (Campbell *et al*., 2011 and Löhr *et al*., 2001). In addition to ECM modulatory capabilities, integrins have also been shown to be key regulators in tumour angiogenesis. Integrins in conjunction with various pro-angiogenic factors directly influence the migratory, adhesion and proliferative abilities of endothelial cells during the formation of mature blood vessels (Cai *et al*., 2009). In terms of tumour angiogenesis the $\alpha_v\beta_3$ and $\alpha_v\beta_5$ integrins are of specific importance, as both are highly expressed in a variety of tumour cells as well as in neovascular endothelial cells (Camenisch *et al*., 2002). However, on mature endothelial cells in normal tissue, these integrins are not expressed to the same degree, making them a promising target for anti-angiogenic therapies.

It is widely accepted that cell shape and adhesion are governed by integrin signalling, and as anchorage dependence is an essential requirement for cell viability, integrins are

essential regulators in cellular responses to survival. The response of integrins to intracellular stress can occur through a range of mechanisms, as they are known to regulate both the expression and activity of several Bcl-2 protein members. Increased resistance to serum starvation in both HT29 colon carcinoma cells (O'Brien *et al*., 1996) and Chinese hamster ovary (CHO) cells (Zhang *et al*., 1995) for example is mediated by the ligation of the integrin $\alpha_5\beta_1$ which has a protective effect against apoptosis. Additionally, the binding of the integrin $\alpha_6\beta_1$ to its ligand, laminin, has been shown to be protective against apoptosis in mammary epithelial cells (Farrelly *et al*., 1999).

Furthermore, the invasiveness of gastric cancer cells has been shown to be promoted by the secretion of the chemokine CXCL12 (stromal-derived factor 1) through its ability to increase integrin β1 clustering (Izumi *et al*., 2016). In patients with chronic lymphocytic leukaemia, the tissue localization and trafficking of B cells was initially identified to be regulated by CXCL12 and its associated receptor CXCR4 (Möhle *et al*., 1999). Subsequently, it was proposed that the invasion of breast cancer cells to distant metastatic sites is also under the regulation of CXCR4. CXCR4 has been shown to be highly expressed in over 23 different tumour types, including those of the brain (Burger *et al*., 2000), prostate (Akashi *et al*., 2008), and breast (Salmaggi *et al*., 2009), whereas in normal tissue its expression level is absent or very low. Additionally, CXCL12 is also highly expressed in lymph nodes, lungs and bone marrow - organ sites where breast cancer cells most frequently metastasize (Müller *et al*., 2001). As such, the CXCL12/CXCR4 chemotactic pathway has been implicated as a critical determinant in the destination of tumour metastasis.

Increased expression of hypoxia inducible factor 1α (HIF1α) in response to a lack of oxygen availability, results in the HIF1α-dependent gene expression of both CXCL12 and CXCR4 (Hill *et al*., 2009). Recently, CXCR4 has been identified as a CAF-associated gene, signifying the existence of an autocrine feedback loop. The secretion of CXCL12 by

CAFs has been shown to increase CXCL12/CXCR4 signalling, thereby promoting angiogenesis and tumour growth in both non-small lung cancer (Wald *et al*., 2011) and breast cancer (Orimo et al., 2006). Furthermore, enhanced CXCL12/CXCR4 signalling in CAFs, has also been implicated in chemotherapeutic resistance in a variety of cancer types. In pancreatic cancer, CXCR4 is often overexpressed and activation of these cells by CXCL12 induces a cascade of downstream effects resulting in an increased resistance of pancreatic cancer cells to the chemotherapeutic drug, gemcitabine (Singh *et al*., 2010). Additionally, high basal CXCR4 expression and CXCL12 mRNA expression in patients with colorectal cancer is associated with poor prognosis and distant cancer recurrence (Saigusa *et al*., 2010).

Additionally, CAFs have been shown to play a critical role in mediating tumour-promoting inflammation through enhanced secretion of inflammatory factors including tumour necrosis factor α (TNFα), cyclooxygenase 2 (COX-2) and interleukin 6 (IL-6) leading to tumour cell invasion (Erez *et al*., 2013, Erez *et al*., 2010 and Toullec *et al*., 2010). In particular, the secretion of IL-6 and monocyte chemoattractant protein 1 (MCP-1) leads to the trans-differentiation of macrophages to a tumour-associated macrophage (TAM) phenotype. Recently, enhanced reactivity between CAFs and TAMs has been identified, the interplay of which promotes cancer cell motility and invasion (Hashimoto *et al*., 2016). In contrast, oestrogen receptor α positive CAFs have also been implicated in the suppression of prostate cancer cell invasion through a decrease in IL-6 expression and TAM infiltration into the tumour microenvironment (Yeh *et al*., 2016). Furthermore, the promotion of tumour progression and metastasis through the recruitment of TAMs is enhanced with the loss of transforming growth factor-beta (TGF-β) receptor type 2 in CAFs (Hembruff *et al*., 2010). Increased TGF-β as well as TNF-α secretion by mammary CAFs has been shown to increase matrix metalloproteinase 9 (MMP-9) expression via the

mothers against decapentaplegic homolog (SMAD), *ras* and PI3K signalling (Stuelten *et al*., 2005).

1.3. Contribution of CAFs to the "Hallmarks of Cancer"

In 2000, Douglas Hanahan and Robert Weinberg described six principle cellular physiological aspects, referred to as the 'hallmarks of cancer', which are obligate for cancer formation and progression (Hanahan *et al*., 2000). More recently, increasing evidence suggests that the evasion of cancer cells from immune destruction, and the ability to reprogram cellular metabolism are two additional hallmarks of cancer cells (Hanahan *et al*., 2011) (Figure 1.2). Although there is plenty of evidence to support their involvement in neoplastic progression of some cancer cell types, neither capability has been fully validated and as such they are referred to as emerging hallmarks. Furthermore, genomic instability and the ensuing mutations as well as tumour-promoting inflammation, are involved in the acquisition of both the emerging and principle hallmarks and as such have been characterized as consequential or enabling characteristics (Figure 1.2).

During cancer development it is thought that normal cells progressively evolve, through the acquisition of these hallmarks, to their ultimate neoplastic state. More recently, the understanding of the biology of tumours has been extended to include the effects of the tumour microenvironment in the tumourigenic process. As such the contribution of stromal cells to the "hallmarks of cancer" such as, sustaining proliferative signalling, deregulating cellular energetics, resisting cell death, inducing angiogenesis and activating invasion and metastasis, has become an intriguing area of research, which will be highlighted in the next section.

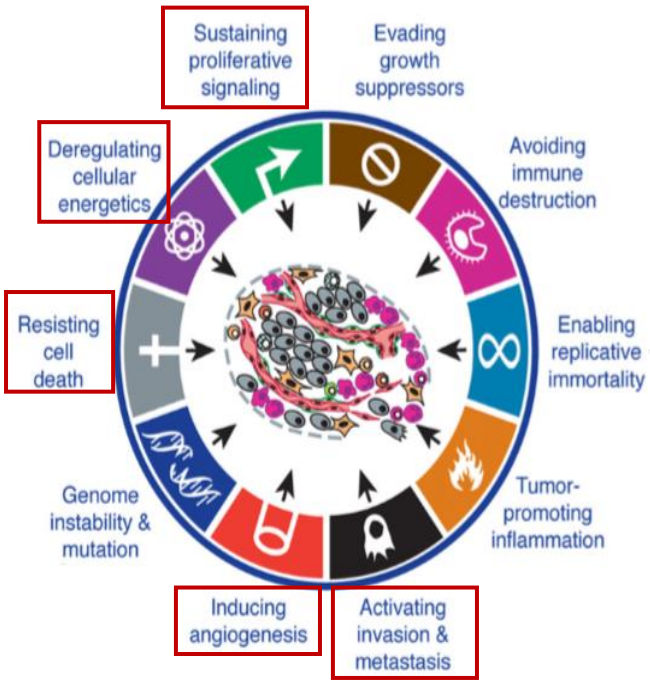

Figure 1.2: The Hallmarks of Cancer. Eight functional (six principle and two emerging) hallmarks in addition to two enabling characteristics originally described by Hanahan and Weinberg are obligate for cancer formation and progression. Hanahan and Weinberg, 2011.

1.3.1. Sustaining Proliferative Signalling (PI3K/Akt Signalling and Cancer)

The phosphatidylinositol-3-kinase (PI3K) signalling pathway plays a critical role in various aspects of cell survival and growth. The activation of PI3K/Akt signalling through both the inflammatory and chemotactic signalling cascades plays a central role in both cancer progression and metastasis (Figure 1.3). Additionally, the proliferation of fibroblasts has been shown to be promoted by the interaction between integrins and the ECM via the activation of the PI3K/Akt signalling pathway (Lu *et al*., 2010). In the context of cancer PI3K/Akt signalling is of particular importance as numerous hallmarks of cancer are regulated by Akt signalling, which highlights the importance of this signalling cascade as a potential therapeutic target for the treatment of cancer.

Activation of the PI3K pathway in response to a range of regulators, including integrin and chemokine signalling results in disturbances in both cell growth and survival. In fact, mutations arising within the PI3K/Akt signalling pathway (e.g. Ras, PTEN, or PI3K) are commonly encountered in various cancer types, including many breast cancers (Stemke--Hale *et al*., 2008). These mutations contribute to both the metastatic ability of cancer cells as well as to therapeutic resistance. Akt exerts direct effects on cell survival through the phosphorylation and inhibition of Bad (Ser^{136}), a pro-apoptotic BH3 protein, which results in the inhibition of apoptosis (Datta *et al*., 1997).

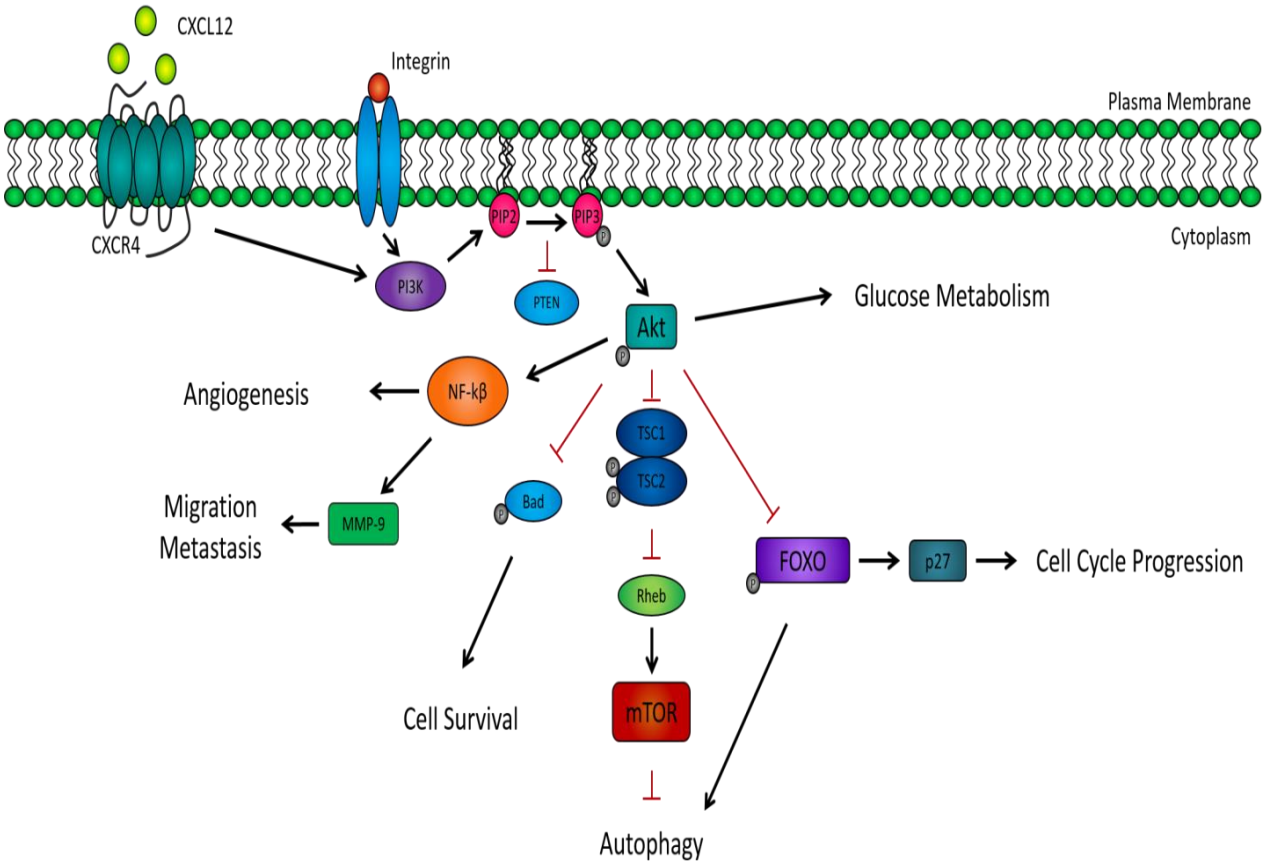

Figure 1.3: Activation of the PI3K/Akt signalling pathway through both integrin and chemotactic CXCL12/CXCR4 signalling is critical to various aspects of cancer progression. The activation of Akt downstream of PI3K results in alterations in glucose metabolism through the recruitment of GLUT transporters to the cell surface as well as increasing hexokinase (HK) and phosphofructokinase (PFK) activity. The inhibition of FOXO by Akt leads to alterations in cell cycle progression and the induction of autophagy. Furthermore, the phosphorylation and inhibition of Bad through Akt promotes cancer cell survival. Akt also promotes angiogenesis and metastasis though direct effects on the transcription factor NF-κβ.

In addition to Bad (Ser^{136}) phosphorylation, Akt also inhibits the pro-apoptotic effects of the forkhead box O (FoxO) transcription factors through their phosphorylation, thereby promoting cell survival. FoxOs have also been shown to regulate DNA repair and cell cycle progression in addition to apoptosis (Nakamura *et al*., 2000). Thus, the phosphorylation and inactivation of FoxOs by Akt, results in its cytoplasmic accumulation and altered expression of cell cycle regulators such as CDKI $p27^{Kip1}$ (Medema *et al*., 2000), retinoblastoma-related protein p130 (Kops *et al*., 2002) and cyclin D (Schmidt *et al*., 2002). Furthermore, cell survival is additionally enhanced through the inhibition of FoxOs by Akt, as FoxOs are also direct regulators of the pro-apoptotic protein TNF-related apoptosis inducing ligand (TRAIL) (Modur *et al*., 2002).

Overexpression of FoxOs has been implicated in the reduction of tumour size *in vivo* and the inhibition of tumour growth in an *in vitro* setting. Additionally, the cytoplasmic localization of FoxO correlates with a poorer prognosis in breast cancer patients, whereas FoxOs nuclear localization results in the suspension of cell cycle progression (Nakamura *et al*., 2000), and angiogenesis (Poente *et al*., 2005) as well as the induction of apoptosis (Urbich *et al*., 2005). Cumulatively, this evidence suggests that the signalling mechanisms of both the PI3K/Akt/FoxO signalling pathways and the CXCL12/CXCR4 chemotactic pathway warrant further investigation in the context of CAF-induced tumour metastasis and doxorubicin resistance in breast cancer.

In addition to its role in cell survival, stimulation of Akt through the insulin receptor is also involved in the regulation of glucose metabolism. The increased ability of tumour cells to utilize external nutrients occurs as a result of Akt-induced localization of glucose transporters, specifically GLUT-1 and GLUT-3, to the cell surface (Wieman *et al*., 2007, Rathmell *et al*., 2003 and Sommermann *et al*., 2011). As many cancer cell types are highly dependent on glucose metabolism for cell survival, this increased dependence on glycolysis has been shown to fuel apoptosis resistance in cancer cells.

1.3.2. Resisting Cell Death

The progression of tumour development and growth involves the evasion of cell death in cancer cells in addition to their sustained proliferative signalling. Therefore, in order to safeguard their proliferative capacity and survive, these cells must develop survival strategies to resist both intrinsic and extrinsic death signals. In part, pro-survival signals supplied from the tumour stroma allow for the effective evasion of cancer cells to apoptotic cell death. Insulin-like growth factor (IGF) -1 and -2 secreted by surrounding stromal CAFs, imparts critical survival signals promoting tumour growth (Strnad *et al*., 2009, LeBedis *et al*., 2002). Additionally, the ECM stiffening induced by CAFs plays a critical role in the process of malignant transformation and invasion (Leventhal *et al*., 2009).

The release of IGF1/2 as well as other growth factors, including hepatocyte growth factor (HGF), fibroblast growth factor (FGF) and platelet derived growth factor (PDGF), from CAFs (Nakagawa *et al*., 2004, Peddareddigari *et al*., 2010 and De Boeck *et al*., 2013), act via the mitogen-activated protein kinase (MAPK) and PI3K/Akt signalling pathways to induce cell proliferation, anti-apoptotic signalling and invasion (Valenciano *et al*., 2012). The activation of the PI3K/Akt and MAPK signalling pathways through the phosphorylation of human epidermal growth factor receptor 2/3 (HER2/3) and the receptor tyrosine kinase, c-Met, in colorectal cancer cells occurs as a result of HGF and neuregulin-1 found in the supernatant of CAFs (De Wever *et al*., 2004, De Boeck *et al*., 2012).

On the other hand, a less supportive microenvironment towards cancer cells is induced through tumour suppression proteins, such as p53 and retinoblastoma (RB). In response to oncogenic stress signals, the p53 gene (TP53) acts as a tumour suppressor. Upon its activation, p53-induced apoptosis or replicative senescence ensues in order to prevent enhanced proliferation of malignant cells (Childs *et al*., 2014). Therefore, protein secretion from CAFs is altered following the induction of p53, resulting in a microenvironment which is less supportive. The tumour suppressive role of p53 in CAFs is further supported by the

fact that the suppression of the chemokine CXCL12 can be repressed by the activation of p53. Furthermore, independent of direct cell-to-cell contact, p53 induction in CAFs is suppressed in lung cancer cells (Bar *et al*., 2009).

The retinoblastoma (RB) protein, another tumour suppressor, is often hyper-phosphorylated in differentiated or quiescent cells and functions to repress the transcription of essential cell cycle genes. Phosphorylation of RB, as seen in isolated human breast CAFs, leads to its inactivation and the subsequent progression of cells through the cell cycle (Mercier *et al*., 2008). Moreover, the depletion of RB in CAFs leads to the enhanced invasiveness of cancer cells. This occurs through the increased production of keratinocyte growth factor (KGF or FGF7) from CAFs, regulating invasion via an Akt-E-twenty-six (Ets)-MMP1 dependent pathway (Pickard et al., 2012). However, further research is needed in order to fully elucidate the role of both RB and p53 inhibition in CAFs and their involvement in cancer progression.

1.3.3. Induction of Angiogenesis

In addition to the secretion of pro-survival signals, CAFs also provide pro-angiogenic factors. The release of pro-angiogenic factors, including VEGF-A, from CAFs into the tumour stroma has been shown to be released in much higher quantities than that released by overt tumour cells (Thijssen *et al*., 2004). Fukumura and colleagues demonstrated that the induction of VEGF promotor activity in stromal cells is dramatically increased in mouse models of spontaneous mammary or orthotopic tumours expressing GFP-VEGF promotors (Fukumura *et al*., 1998). VEGF secreted by CAFs has been shown to be induced by bradykinin B2 receptor signalling and prostaglandin E2 produced by cyclooxygenase-2 (COX-2) (Amano *et al*., 2003, Williams *et al*., 2000 and Ikeda *et al*., 2000). Furthermore, the expression of fibroblast growth factor (FGF) 2 in CAFs is induced

by both the autocrine signalling of the cytokine, CXCL14 and paracrine activation by PDGF receptor signalling (Anderberg *et al*., 2009, Pietras *et al*., 2008 and Augsten *et al*., 2009). Finally, the recruitment of endothelial progenitor cells into the tumour neo-vasculature is enhanced by the secretion of stromal-derived factor (SDF) 1α from CAFs, resulting in the promotion of angiogenesis in the tumours of MCF-7-*ras* human breast carcinoma xenografts (Orimo *et al*., 2005).

Pericytes are essential regulators of endothelial cell function and are required for the stability of blood vessels. Signalling via PDGF receptor β is essential for the recruitment of pericytes into the blood vessels of tumours (Furuhashi *et al*., 2004). As such, perturbations in PDGFβ expression have been utilized to elucidate the role of pericytes in tumour growth and angiogenesis. A classic example of this can be seen in mouse B16 melanoma cells, where the ectopic expression of PDGFβ leads to enhanced pericyte recruitment and stabilization of the neo-vasculature (Robinson *et al*., 2008). However, in pancreatic and colon carcinoma cell lines the transfection of PDGFβ resulted in pericyte-mediated angiostatic effects and growth inhibition (McCarty *et al*., 2007). Additionally, the complex diversity of pericyte recruitment into the newly formed blood vessels of tumours is dependent on the cellular source of PDGFβ. Furthermore, a disordered and haemorrhagic vasculature, with pericytes detached from the endothelium, is seen in mouse tumours engineered to express a deletion variant of PDGFβ which is not retained near the producing cell (Abramsson *et al*., 2003). It is therefore plausible that in order to attain a balance between ideal blood vessel formation and function during angiogenesis, different subsets of pericytes need to be maintained.

1.3.4. Activating Invasion and Metastasis

During the acquisition of malignancy cancer cells attain the ability to invade into the surrounding tissue and metastasize through either the lymphatic or blood vessels. Essential to this process is the acquisition of a migratory phenotype of tumour cells and the extensive remodelling of the ECM. Sung and colleagues suggested that the exposure of epithelial cells to stromal cells results in these epithelial cells undergoing permanent pro-invasive changes (Sung *et al*., 2008).

Several pro-invasive factors such as HGF, TGFβ, secreted protein acidic and rich in cysteine (SPARC), cathepsins and matrix metalloproteases (MMPs) are secreted by CAFs. The secretion of HGF and TGFβ by CAFs contributes to enhanced invasion and metastatic capabilities of tumour cells (Bhowmick *et al*., 2004). Additionally, the prognosis of patients with resectable pancreatic cancer can be predicted by the expression of SPARC by CAFs (Infante *et al*., 2007). Furthermore, CAFs are also a key source of protease activity, including cathepsins, plasminogen activators and MMPs (Joyce *et al*., 2009). The release of these proteases into the tumour microenvironment plays a crucial role during ECM remodelling, as they lead to a loss of adhesion between adjacent tumour cells, resulting in enhanced tumour invasion and migration.

MMP-induced ECM remodelling is considered as one of the most crucial steps for tumour progression and the formation of the tumour microenvironment. Under normal physiological conditions the balance between MMPs and their inhibitors is essential in maintaining the organized structure of the ECM. However, during tumour progression the increased secretion of various MMPs in addition to their activators (such as urokinase plasminogen activator, uPAR) by CAFs play a major role in tumour cell invasion (Camps *et al*., 1990). The cleavage and subsequent upregulation of MMP activity by uPAR results in the significant degradation of the ECM and contributes to enhanced angiogenesis and metastasis (Egeblad *et al*., 2002). A wide variety of MMPs are known to contribute to

metastasis. Abnormal mammary gland branching and epithelial cell hyperplasia is stimulated by MMP3 overexpression in CAFs (Thomasset *et al*., 1998). In gliomas, pathological angiogenesis and tumour growth requires high levels of MMP2 production in stromal cells (Takahashi *et al*., 2002), and increased levels of the interstitial collagenase MMP1 has been seen in peritumoural fibroblasts isolated from melanomas (Wandel *et al*., 2000). The upregulation of MMP1 leads to the cleavage of protease-activated receptor-1 (PAR1) on the surface of cancer cells, stimulating both invasion and growth signalling. As such, MMP1 is now recognized as a putative breast cancer predictive marker (Poola *et al*., 2005). Increased MMP and uPAR activity is observed in a range of different cancer cells, indicating that fibroblasts are not the only source of MMPs. Due to the mutual interaction between tumour and stromal cells, soluble factors secreted by cancer cells also affect the expression of MMPs. For example, the direct contact of CAFs with malignant epithelial cells is essential for the expression of MMP9. Furthermore, paracrine stimulatory signals enhance the expression of MMP2 in the tumour stroma (Singer *et al*., 2002).

Collectively, several *in vivo* experiments demonstrate the significance of CAFs in cancer cell invasion, through the secretion of pro-invasive factors and the loss of cell-to-cell adhesion (Chen *et al*., 2009, Calvo *et al*., 2011). As CAFs are a major source of MMP production, which plays a critical role in metastasis, the development of novel anti-cancer treatment strategies, targeting MMP secretion from CAFs is a promising area of research.

1.3.5. Deregulating Cellular Energetics

In the presence of abundant oxygen (O_2), most non-proliferating cells in differentiated tissue rely primarily on the oxidation of glucose to carbon dioxide (CO_2) through the oxidation of glycolytic pyruvate in the tricarboxylic acid (TCA) cycle within the mitochondria (Van der Heiden *et al*., 2009). During the metabolism of glucose to CO_2 reduced nicotinamide adenine dinucleotide (NADH) is produced. NADH then behaves as a

reducing equivalent in the electron transport chain, thereby maximizing the production of adenosine triphosphate (ATP) whilst minimizing lactate production. Louis Pasteur first demonstrated that in the presence of O_2, glucose flux is reduced (termed the 'Pasteur effect'), this allows for the preservation of ATP production over a wide range of O_2 concentrations.

However, the conversion of glucose into lactate despite an abundance of O_2 (aerobic glycolysis) is seen in cancer cells. This observation, termed the 'Warburg effect', was first described by Otto Warburg in the 1920's. Warburg proposed that this altered metabolism in cancer cells, occurs as a result of defective mitochondria, thereby inhibiting their ability to effectively oxidize glucose to CO_2 (Warburg *et al*., 1926). However, evidence now suggests that mitochondria of cancer cells are not defective in their ability to carry out oxidative phosphorylation, instead they reprogram mitochondrial metabolism to cope with macromolecular synthesis (Ward *et al*., 2012).

It has been proposed that depending on the surrounding stromal conditions, epithelial cancer cells may have the propensity to preferentially produce energy via oxidative phosphorylation as opposed to increased glycolysis (Lee and Yoon, 2015). In this theory (termed the 'reverse Warburg effect'), nutrient/oxygen deprived epithelial cancer cells are thought to "educate" surrounding stromal cells to increase aerobic glycolysis, resulting in an increased production of metabolites such as lactate, which can then be converted to pyruvate and utilized by oxidative phosphorylation in epithelial cancer cells (Figure 1.4). This suggests that nutrient/oxygen deprived epithelial cancer cells present within solid tumours are able to survive these conditions, as a result of their ability to undergo extensive metabolic reprogramming (Carrer *et al*., 2015) to exploit the metabolic capacities of stromal cells within the surrounding microenvironment.

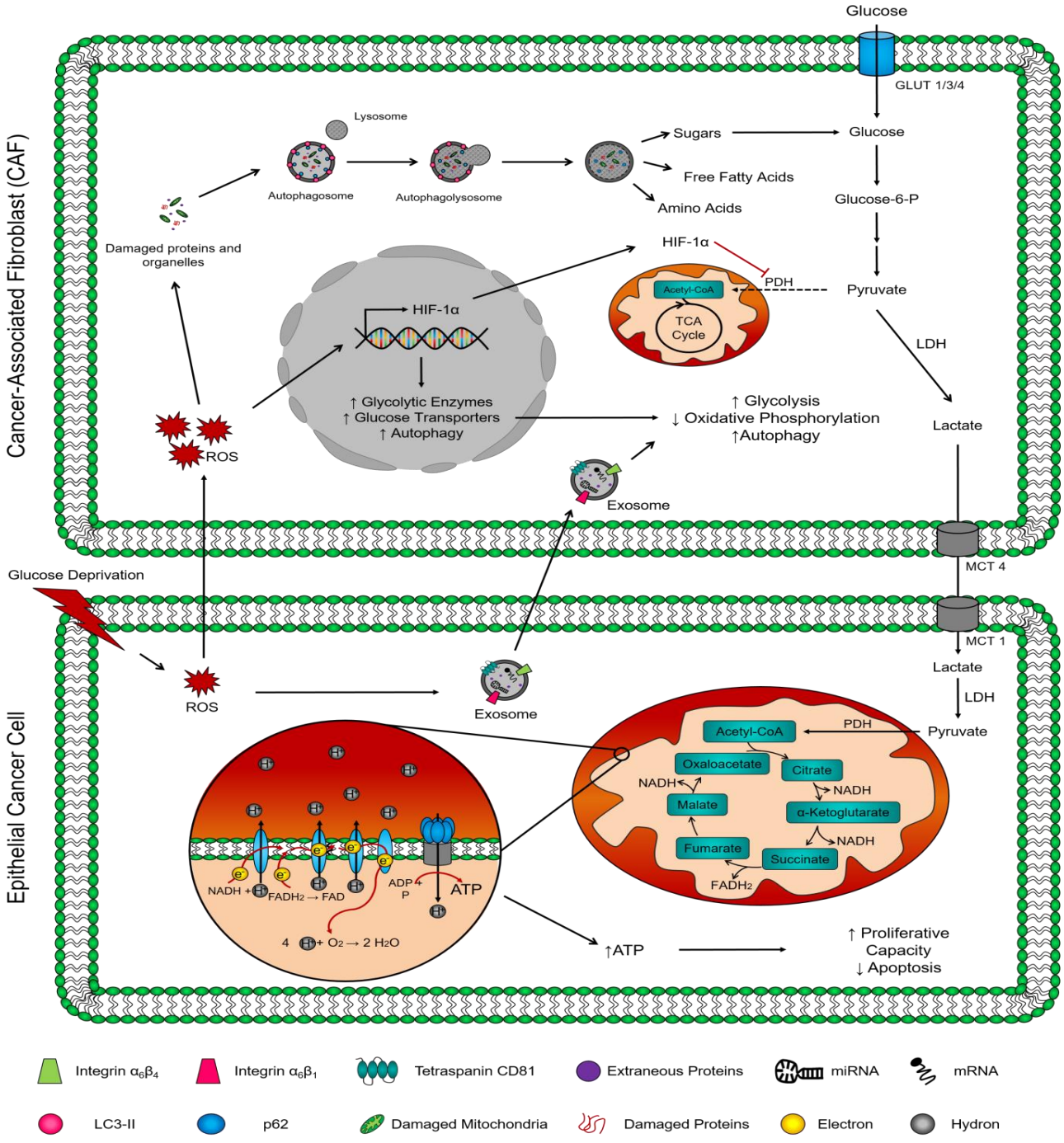

Figure 1.4: Proposed mechanism of action underlying metabolic reprogramming of cancer-associated fibroblasts promoting epithelial cancer cell survival. The induction of reactive oxygen species (ROS) in epithelial cancer cells in response to glucose deprivation results in the transcription and packaging of essential genes (mRNA and miRNA) involved in glycolysis and autophagy induction into exosomes. Additionally, ROS are directly transferred to cancer-associated fibroblasts (CAFs), the resulting increase in oxidative stress leads to the transcription and translation of hypoxia inducible factor 1α (HIF-1α). HIF-1α expression in CAFs results in an increased transcription of glucose transporters, glycolysis and autophagy and the direct inhibition of pyruvate dehydrogenase (PDH) (normally responsible for the conversion of pyruvate to acetyl-CoA) leading to the conversion of pyruvate to lactate. Intracellular build-up of lactate results in its export out of CAFs, where epithelial cancer cells are able to import and utilize lactate as a fuel source to promote cell survival. (Mitchell and Engelbrecht, 2017)

1.4. Metabolic Reprogramming and the "Reverse Warburg Effect"

The question of how epithelial cancer cells "educate" surrounding CAFs under nutrient deprived / hypoxic conditions remains to be fully elucidated. However, it has been proposed that in addition to directly increasing aerobic glycolysis, an increased production of reactive oxygen species (ROS) within epithelial cancer cells, leads to an activation of key transcription factors (HIF-1α and NFκβ) (Giannoni *et al*., 2011), and the subsequent induction of oxidative stress and autophagy in neighbouring CAFs (Pavlides *et al*., 2012). An explanation for this transfer of oxidative stress, is that the secretion of hydrogen peroxide (H_2O_2) by epithelial cancer cells into the tumour stroma acts as the driving force, leading to the induction of oxidative stress and the subsequent activation of autophagy within surrounding CAFs (Capparelli *et al*., 2011) (Figure 1.4).

Increased production of reactive oxygen species (ROS), including free radicals such as superoxide ($O_2^{\bullet-}$) and H_2O_2 induce cellular damage and ultimately cell death (Chen *et al*., 2008). Increased generation of mitochondrial ROS has been implicated in the progression of cancer as well as alterations in chemotherapy sensitivity. In addition to the release of H_2O_2 by epithelial cancer cells in response to nutrient deprivation, the removal of damaged proteins and organelles, under certain cellular conditions, can occur via the release of exosomes into the surrounding extracellular microenvironment (Okon *et al*., 2016).

Exosomes are small vesicles, typically between 30 and 100 nm in diameter that carry biological molecules, such as activated growth factor receptors, microRNA (miRNA) and mRNAs, which can be transferred to recipient cells (Figure 1.4) Exosomes have been shown to be secreted into the extracellular matrix by almost every human cell type and their cargo exhibits functionality within recipient cells (Valadi *et al*., 2007 and Kosaka *et al*., 2010), thereby highlighting their importance as intercellular signalling shuttles within

the extracellular matrix. The formation of exosomes occurs through the inward budding of the membrane of late endosomes or multi-vesicular bodies (MVBs), and their secretion into the extracellular matrix occurs predominantly through highly constitutive signalling processes (Février *et al*., 2004). However, their secretion can additionally be modulated by increased cellular stress, resulting in changes to their protein and RNA content (De Jong *et al*., 2012). The ability of cells to alter the protein and RNA content of exosomes in response to intracellular stressors, suggests that exosomes may play a significant role in cell survival as their cargo can be tailored to the specific metabolic needs of the cell.

1.5. Exosomes in cancer progression, metastasis and chemotherapy resistance

In the context of the tumour microenvironment, epithelial cancer cells have been shown to secrete exosomes which are transferred to surrounding CAFs, leading to the activation of key signalling pathways involved in both autophagy and glycolysis. Furthermore, CAFs have recently themselves also been shown to secrete exosomes in response to nutrient deprivation and increased oxidative stress (Luga *et al*., 2013). In cancer, exosomes secreted from both tumour cells and CAFs function in both a paracrine and an autocrine fashion resulting in the promotion of angiogenesis (Orimo *et al*., 2005), inflammation (Erez *et al*., 2013) and pre-metastatic niche formation (Hoffman *et al*., 2013), further highlighting them as essential intercellular signalling vesicles within the tumour stroma.

The tetraspanin molecule, CD81, has been shown to be an abundantly expressed plasma membrane protein on the surface of exosomes. The expression of CD81 on CAF-secreted exosomes has been shown to enhance the metastatic potential of breast cancer cells, specifically to the lungs (Luga *et al*., 2012). More recently, Hoshino and colleagues demonstrated that the specific integrin expression profile of circulating tumour-derived

exosomes determines the organ site of future metastasis and that these exosomes also prime the tissue site for the arrival of circulating epithelial cancer cells, thereby rendering the organ permissive to the growth of these metastatic cells. For example they have demonstrated that exosomes derived from the MDA-MB-231 sub-line which colonizes to the lung (4175-LuT), expresses the integrins $\alpha_6\beta_4$ and $\alpha_6\beta_1$ and co-localizes with S100A4+ cells within the laminin-rich microenvironment of the lung (Hoshino *et al*., 2015).

In addition to enhancing cancer metastasis, exosomes have also been implicated in the development of chemotherapy resistance (Hu *et al*., 2015). Tumours are comprised of a heterogeneous population of epithelial cancer cells with varying degrees of susceptibility to chemotherapeutic drugs. Following chemotherapeutic treatment the majority of malignant epithelial cells undergo cell death. However, a small population of these cancerous epithelial cells remain unaffected by the cytotoxic effects of the chemotherapeutic drug. These drug-resistant cells, have the ability of transferring these resistance traits through exosomes to neighbouring cells (Chen *et al*., 2014 and Xiao *et al*., 2014). Additionally, exosomes have been shown to interfere with the binding of chemotherapeutic drugs to tumour cells, for example the binding of trastuzumab to Her2 receptors, is inhibited by exosomes secreted from Her2-overexpressing breast cancer cells (Ciravolo *et al*., 2011). Furthermore, the sequestration and export of chemotherapeutic drugs as well as their metabolites by exosomes suggests that they also mediate drug efflux.

Clinically the discovery that these highly stable, cell-free exosomes are found to be circulating in the bodily fluids of cancer patients, means that they may be utilized as biomarkers in novel diagnostic and prognostic tools. Furthermore, the premise that tumour-derived exosomes act as intercellular shuttles utilized by cancerous epithelial cells to “educate” surrounding CAFs under conditions of nutrient deprivation, unlocks an

exciting new avenue of research in order to elucidate the molecular mechanisms underlying this complex interaction.

Recently, Ao and colleagues demonstrated that CAFs can be found circulating in the blood of patients with metastatic breast cancer. They showed that these circulating CAFs (cCAFs) could be detected in 88.2% of stage IV breast cancer patients with overt metastasis compared to a 23.1% in stage I breast cancer patients treated with curative therapy (Ao *et al*., 2015), suggesting that cCAFs play a direct role in facilitating breast cancer metastasis. Additionally, the discovery that cCAFs accompanied by circulating tumour cells (CTC) allows for the evasion of these cells to cell death and promotes pre-metastatic niche formation (Duda *et al*., 2010), further supports the notion that CAFs are critical role players in cancer metastasis. Based on the 'seed and soil hypothesis' described by Stephen Paget in 1889, tumour cells detached from primary tumours ('seeds') preferentially metastasize to select organs with suitable microenvironments ('soil') (Paget *et al*., 1889), therefore it is conceivable that the metabolic status of cCAFs could potentially serve as a novel tool for the assessment of primary tumour status and metastatic risk.

1.6. Autophagy and Tumour Progression

Exosome induced signalling (Baixauli *et al*., 2014) and increased reactive oxygen species (ROS) production can induce autophagy in CAFs (Karna et al., 2010), which is thought to be critical for the metabolic reprogramming of CAFs. Autophagy is a highly dynamic, evolutionary conserved self-degradative process (Kondo *et al*., 2005), which plays a critical role in maintaining cellular homeostasis and promoting cell survival (Hippert et al., 2006). Currently there are three well defined types of autophagy, namely; chaperone-mediated, micro- and macro-autophagy (Morselli *et al*., 2009). Macro-autophagy

(hereafter referred to as autophagy) constitutes the most abundant form of autophagy and involves the delivery of cytosolic cargo to lysosomes by means of a double membrane bound vesicle, called an autophagosome (Rabinowitz *et al*., 2010).

Under normal physiological conditions, low level basal autophagy serves as a housekeeping function, whereby old and redundant cellular constituents are degraded and utilized as additional energy sources for various metabolic processes (Levine, 2007). Basal autophagy serves a particularly indispensable role in quiescent and terminally differentiated cells where the aggregation of defective components may become cytotoxic, as they are not diluted through the process of cell division (Rabinowitz *et al*., 2010). Under conditions where autophagy is activated in response to cellular stressors, such as nutrient deprivation and hypoxia, the process of autophagy becomes somewhat “double-edged” (Shintani *et al*., 2004) as increased levels of autophagy, serve as a protective mechanism, whereby non-essential cellular constituents may be broken down to refuel essential cellular processes (Hippert *et al*., 2006). However, unregulated autophagy in these conditions may result in the excessive “self-cannibalization” of intracellular organelles thereby resulting in cell death (Mizushima *et al*., 2008).

Autophagosome formation is mediated by a group of autophagy-specific genes (ATG) whose products are categorized into four classes, namely; (i) an upstream autophagy regulatory complex, which responds to nutrient availability, (ii) a vesicle nucleation lipid kinase group, (iii) two ubiquitin-like protein systems, responsible for the production of modified autophagy regulatory complexes (Atg8-PE and Atg5-Atg12-Atg16) essential for autophagosome assembly and size determination (Hanada *et al*., 2007), and (iv) a group of complexes responsible for the degradation of ATG complexes (Hippert *et al*., 2006) (Figure 1.5).

The autophagy receptor p62/SQSTM1 recognises and binds to proteins tagged by ubiquitin targeting them for degradation (Komatsu *et al*., 2007). During the process of autophagosome formation, LC3 I is converted to LC3 II via a lipidation step. LC3 II is then sequestered to the inner surface of the phagophore, where it associates with p62 (Mizushima *et al*., 2008). Autophagosomal cargo is subsequently delivered to lysosomes (Rabinowitz *et al*., 2010) where the release of lysosomal digestive enzymes into the lumen of the autophagolysosome results in the degradation of p62 as well as sequestered cellular constituents, ultimately resulting in the release of free fatty acids, amino acids, nucleotides and sugars (Levine, 2007).

mTOR the predominant regulator of the autophagic process, is a sensor of intracellular nutrient status and master regulator of cell growth. mTOR serves as a negative regulator of autophagy through its ability to phosphorylate and thus inactivate Unc-51-like kinase (ULK1) and Atg13, two of the main ULK1 components, thus inhibiting the initiation of phagophore synthesis (Mathew *et al*., 2011). mTOR exists in two biologically functional signalling complexes namely, mTORC1 and mTORC2. Pharmacological administration of Rapamycin results in the detachment of RAPTOR from mTOR. RAPTOR acts as a scaffold for the recruitment and activation of mTOR substrates and thus the inhibition of mTORC1. Additionally, the mTORC1 substrates S6-kinase and eIF4E-binding protein (4E-BP1) interact with various mRNAs regulating the initiation of translation and thus controlling protein synthesis rates (Belda-Iniesta *et al*., 2011). Furthermore, mTORC1 governs the translation of regulators of cell growth, such as cyclin-D1, HIF1α and c-myc, thus promoting cellular processes such as cell cycle progression, cell growth and angiogenesis, all of which become deregulated during tumorigenesis.

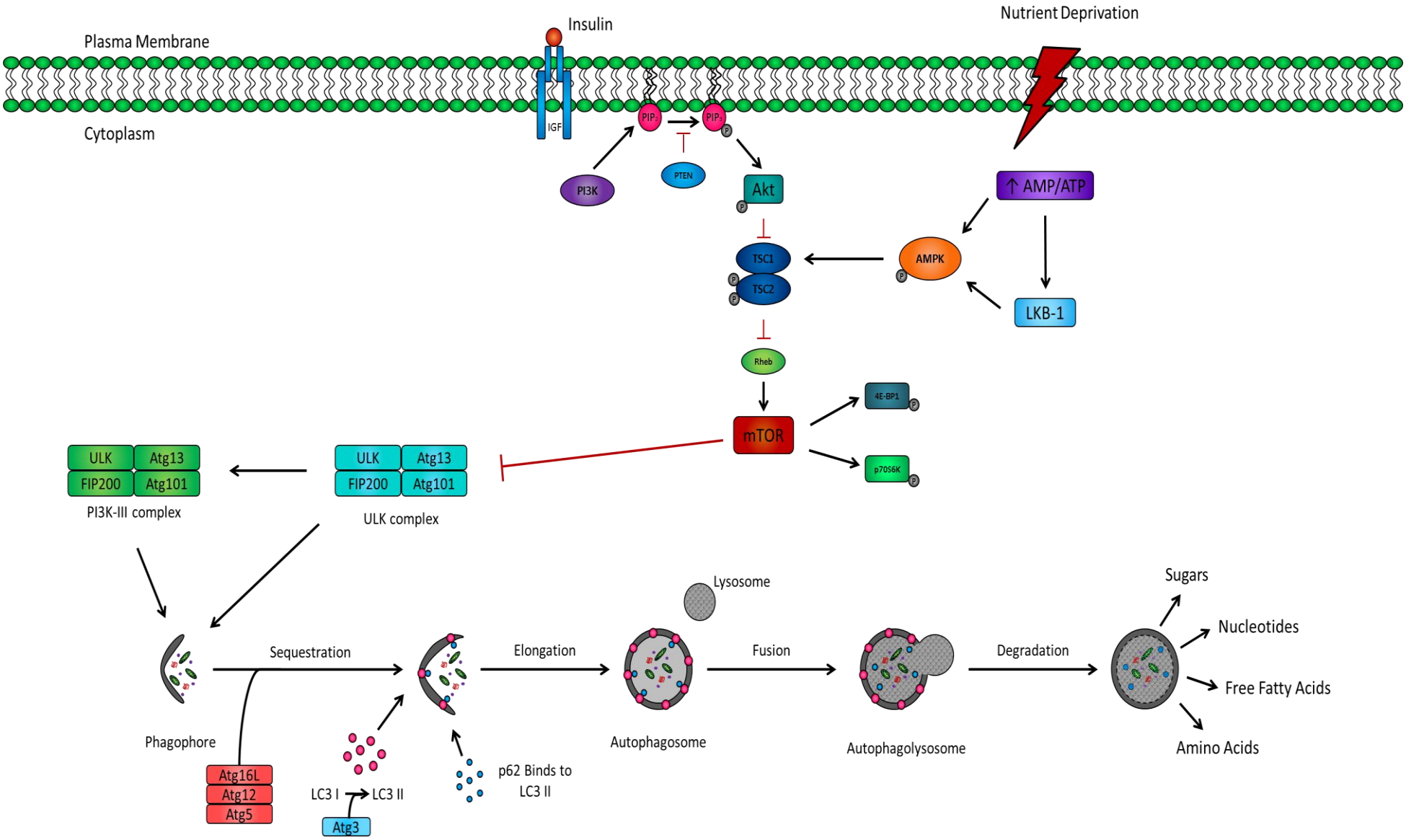

Figure 1.5: Schematic representation of the molecular pathways involved in the regulation of autophagy in mammalian cells. Adapted from: Mathew *et al*., 2011.

Enhanced tumour cell invasion and metastasis in hypoxic tumour regions is widely accepted to occur in response to the induction of the transcription factor HIF1α (Gilkes *et al*., 2013, Eisinger-Mathason *et al*., 2013). As described previously, autophagic induction in response to hypoxia favours tumour cell growth and survival, through the production of essential cellular metabolites. However, in recent years the relationship between autophagy and glycolysis has gained increasing attention following reports that increased sensitivity to reduced glucose availability is seen in cells with competent autophagy (Lock *et al*., 2010). Therefore, the induction of autophagy in CAFs during the process of metabolic reprogramming is proposed to play a critical role in enhancing glycolysis (Wang *et al*., 2017), leading to the increased production of glycolytic intermediates, such as lactate.

1.7. Lactate in the tumour microenvironment

The monocarboxylate, lactate (2-hydroxypropanoic acid), exists predominantly as the physiological enantiomer L-lactate, however, it may also exist as the stereoisomer D-lactate. Most tissues in the body produce lactate with high levels of production being found in muscle. Under normal physiological conditions, lactate is cleared predominantly by the liver and to a lesser extent by the kidneys. Systemically, lactic acid ($CH_3CH(OH)CO_2H$) is transported to the liver where it is reconverted to glucose via the Cori cycle, and thus serves as an additional energy source (Waterhouse *et al*., 1969).

The metabolism of glucose by glycolysis results in the production of pyruvate as a final product. Under normoxic conditions, the enzyme pyruvate dehydrogenase (PDH) converts pyruvate to acetyl-CoA which enters the TCA cycle. As the conversion of pyruvate to acetyl-CoA requires the presence of O_2, under conditions of limited oxygen availability,

pyruvate is converted to lactic acid by the enzymatic action of lactate dehydrogenase (Phypers *et al*., 2006).

A variety of tumour suppressor genes and oncogenes, including *myc*, Akt/protein kinase B, PI3K, mTOR and HIF-1α (Levine *et al*., 2010, DeBerardinis, 2008) are frequently mutated in many human cancers. Many of which have been shown to lead to the stimulation of genes encoding for glycolysis and glutaminolysis mediated proteins. The transcription factor HIF-1α, usually controlled by cellular O_2 conditions, can be stabilized (even under normoxic conditions) by both lactate and pyruvate, leading to its intracellular accumulation (Lu *et al*., 2002). Expression of genes regulated by HIF-1 has been shown to lead to enhanced glycolytic flux in tumour cells which is independent of oxygen concentrations, suggesting that lactate accumulation in tumours is not a direct result of hypoxia (Yaromina *et al*., 2009). In order to ensure the adequate delivery of glucose into the cell in addition to secretion of accumulated lactate out of the cell, HIF-1 targets include both glucose (GLUT-1) and lactate (MCT-4) membrane transporters. In addition to enhanced GLUT-1 translocation, glycolysis and ATP production are permitted as a result of the production of the reducing equivalent NAD^+, a direct consequence of enhanced lactate dehydrogenase A (LDH-A) expression. Moreover, the inactivation of the PDH complex, a result of HIF-1 dependent inhibition of pyruvate dehydrogenase kinase (PDK) I, contributes to the decreased flux through oxidative phosphorylation (Zimmer *et al*., 2016).

Recent evidence suggests that this metabolic switch to dysregulated glycolysis is fundamental to the tumourigenic process and may be an early event. Schafer *et al* (2009) demonstrated that enhanced glycolysis in Her2/neu^+ ductal breast carcinoma cells maintain PI3K activation, thus providing a survival advantage to these cells.

As described above, even under normoxic conditions, tumour cells preferentially convert pyruvate into lactate instead of utilizing the TCA cycle for energy production. A consequence of this Warburg effect is that increased glycolysis in cancer cells results in the secretion of large quantities of lactate into the extracellular matrix, leading to an acidification of the tumour microenvironment (pH 6.0 – 6.5) (Xie *et al*., 2014). This acidification serves as a potent signal for enhanced angiogenesis (Végran *et al.,* 2011, Sonveaux *et al*., 2012) and induced immunosuppression (Husain *et al*., 2013, Fischer *et al.,* 2007, Mendler *et al*., 2012).

Additionally, exogenous lactate, at relevant *in vivo* solid tumour concentrations (0 – 40 mmol/L) led to concentration-dependent increases in random migration in a variety of cancer cell lines, as demonstrated in classic Boyden chamber experiments. This increased lactate-dependent motility of tumour cells has also been observed by means of time-lapse microscopy for enforced bulk migration (Goetze *et al*., 2011). Several lactate-dependent changes in protein activation and signalling events (including that of β1-integrins) have been demonstrated, however, the molecular mechanisms underlying the involvement of lactate in cell motility remain to be fully elucidated. Recently, signalling of the TGF-β2 pathway has been shown to play a role in mediating lactate-associated cancer cell migration (Baumann *et al*., 2009).

The proton-linked transport of lactate (as well as other monocarboxylates, such as ketones and pyruvate) across the plasma membrane is catalysed by the transmembrane monocarboxylate transporters (MCTs) (Palmieri *et al*., 1996, Price *et al*., 1998 and Cheeti *et al*., 2006). A wide variety of cell types including tumour cells (Carpenter *et al*., 1994) have MCT transporters located on their plasma membranes. Cell types which rely on lactate as an oxidative metabolite (such as the heart and skeletal muscle) or as a substrate for gluconeogenesis (liver), are dependent on the presence of MCTs. To date four MCT isoforms (MCT 1-4) have been identified, each of which have distinctive substrate

affinities. Low level expression of MCT1 is seen in most tissues, whereas MCT2 and MCT3 expression is limited to specific tissue types namely; the liver, neurons and kidneys which primarily express MCT2 where MCT3 expression occurs in the choroid plexus and in the basolateral retinal pigment epithelium. MCT4 is highly expressed in the fibres of white skeletal muscle and low level expression is seen in other tissues, such as the placenta, testis and lung (Petrides *et al*., 2016). Furthermore, MCT4 is also expressed in specific cell types such as astrocytes (Pierre *et al*., 2007), chondrocytes (Meredith *et al*., 2002) and leukocytes (Merezhinskaya *et al*., 2006).

The different lactate affinities observed by MCTs allows for the directed influx and efflux of lactate across the plasma membrane (Brooks, 2009, Gladden, 2008). The co-transport of both lactate and protons out of the cell prevents the deleterious effects that would be observed following the accumulation of lactate and the subsequent acidification of the intercellular environment. More specifically, the intra- versus extracellular concentrations of lactate and other substrates transported by MCTs as well as the pH govern the directionality of lactate transport across the plasma membrane (Dimmer *et al*., 2000, Doherty *et al*., 2013).

The export of lactate out of glycolytic cells, such as astrocytes, can be utilized by other cell types, like neurons, as a metabolic substrate for oxidative phosphorylation (Hall *et al.,* 2012). This directed transport of lactate by cell-specific MCTs (also known as the “lactate shuttle”), has been proposed to occur as a similar phenomenon in certain cancer types, and is often referred to as metabolic symbiosis (Sonveaux *et al*., 2008).

Generally, it has been suggested that lactate is exported out of cancer cells (via MCT-4) leading to tumour microenvironment acidification thereby affecting surrounding stromal cells. However, lactate has been shown to play a fundamental role in the symbiotic relationship between hypoxic and surrounding oxygenated tumour cells (Sonveaux *et al*.,

2008). Under hypoxic conditions tumour cells have been shown to increase GLUT-1 expression and enhanced glucose uptake leading to increased glycolytic flux and lactate accumulation. Lactate export via MCT-4 from these hypoxic tumour cells can then be utilized as a metabolic substrate by aerobic tumour cells, where lactate is then converted by lactate dehydrogenase to pyruvate. Pyruvate then enters the TCA cycle resulting in enhanced energy production (Guillaumond *et al*., 2013).

The notion that tumour cells utilize metabolic symbiosis implies that the net flux of lactate occurs from hypoxic cells to oxygenated cells, and is directly related to the distance that these cells are from blood vessels within the tumour stroma (Sotgia *et al*., 2012). However, the current understanding of metabolic symbiosis in tumours fails to accurately take into account the dynamic nature of tumour progression, for instance, as a result of neovascularization, regions of perfusion are under constant modification. Furthermore, substrate and oxygen availability are not static and are also subjected to dynamic changes. As a result, tumour cells may at times be forced to alternate between available energy sources in order to survive. Taking this into account, the combined effects of metabolic symbiosis and the “reverse Warburg effect” (as described previously) may orchestrate the metabolic survival strategies utilized by tumour cells, which warrants further research attention in order to fully elucidate the molecular mechanisms governing these interactions.

Additionally, it has long been established that enhanced lactate production in tumours and subsequently increased plasma lactate levels are strongly associated with poor clinical outcomes of patients’ with metastatic cancer. In recent years, it has been demonstrated that lactate plays a causative role in the progression of breast cancer metastasis (Bonuccelli *et al*., 2010). However, the molecular mechanisms underlying the induction of metastasis by lactate still remains to be fully elucidated.

1.8. Cancer Metastasis

Tumour metastasis can be depicted as a multistep invasion-metastasis cascade in which the end-product involves the effective dissemination of cancer cells to distant organ sites and their subsequent adaptation to the foreign tissue microenvironment (Sossey-Alaoui *et al*., 2011). For successful dissemination, cancer cells from the primary tumour need to first invade through the local tissue parenchyma into nearby microvessels (known as intravasation), where they are able to undergo haematogenous dissemination and subsequent niche colonisation (McAllister *et al*., 2014, Nguyen *et al*., 2009, Redig *et al.,* 2013, Valastyan *et al*., 2011).

The simplistic classification of metastasis as an orderly sequence of basic cellular events namely; local invasion, intravasation, haematogenous dissemination, extravasation and colonization (Figure 1.6), has helped to better understand and rationalize the complexity of the signalling processes that need to be acquired in order for the successful progression towards overt metastasis. Over recent years, the biological events contributing to the metastatic process have been extensively studied and many of the genetic and epigenetic events have been identified (Kanda *et al*., 2015). Initially, oncogenic transformation is an essential event which allows for cells to sustain proliferation despite having an unstable genome. However, oncogenic transformation alone is not sufficient to maintain metastatic competence as, despite tumour cell dissemination, some patients never develop clinical metastatic disease (Klein, 2003).

Additionally, the establishment of distant metastasis does not automatically develop as seen in several oncogene-driven murine models of cancer (Moasser *et al*., 2007). As such, transformed cells require the acquisition of additional capabilities in order to overcome physiological barriers preventing metastatic dissemination (Thiery *et al*., 2006). Regardless of the method, it is clear that in order to surmount the biological challenges

which prevent cancer cell dissemination, the acquisition of a metastatic phenotype involves several complex signalling pathways which enable migration and invasion (Spano *et al*., 2012). One of the most widely understood and extensively studied processes involved in metastasis is that of epithelial-to-mesenchymal transition (EMT).

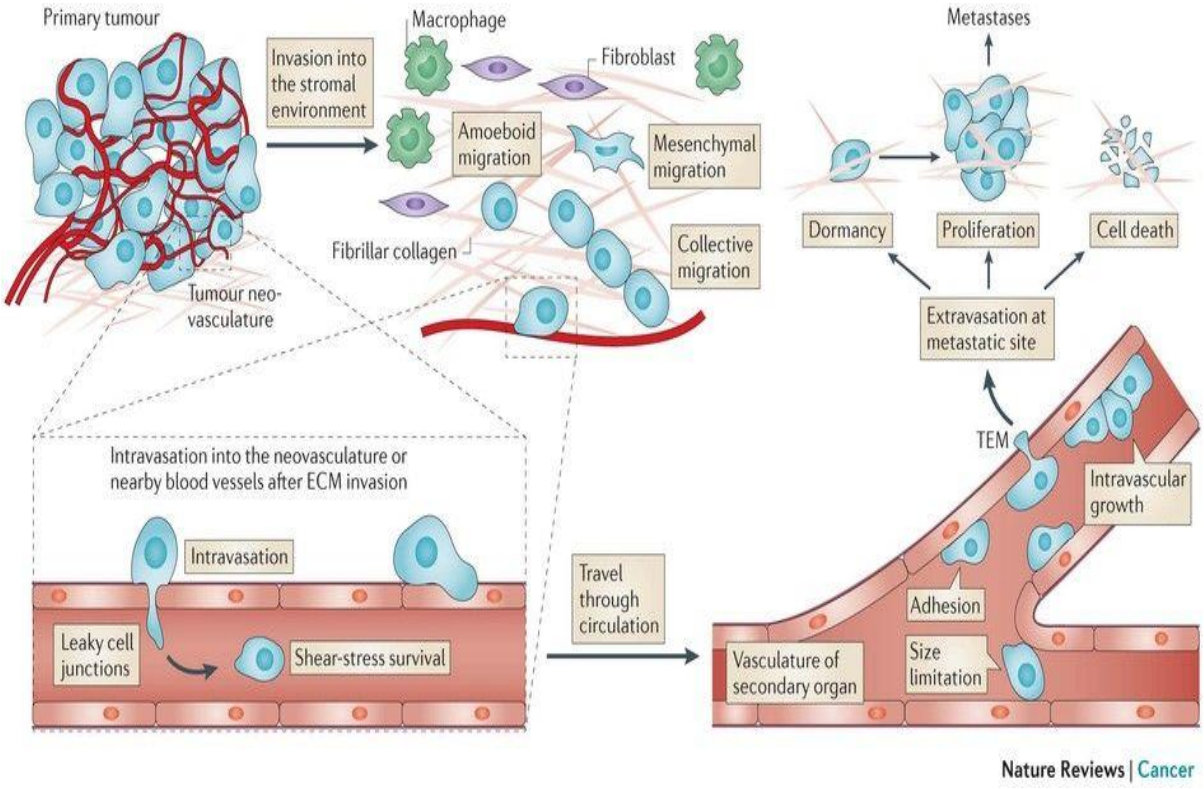

Figure 1.6: Sequential processes involved in metastatic tumour dissemination and colonization. The pre-colonization phase of metastasis comprises a series of events that occur on a timescale of minutes to hours. Local invasion of the primary tumour by cancer cells is followed by their intravasation into the tumour vasculature. The cancer cells then enter the circulatory system as single cells or clusters that are coated with platelets. On their arrest in capillaries at distant sites, the cancer cells extravasate into the parenchyma of target organs to commence colonization. Reymond *et al*., 2013.

1.9. Epithelial-to-Mesenchymal Transition (EMT)

EMT, a biological process not only unique to cancer metastasis, is essential during embryonic development, where morphogenic movements underlie the formation of organs such as the peripheral nervous system, heart, muscular system and neural crest (Huber

et al., 2005). Additionally, during tissue inflammation and wound healing enhanced EMT leads to the stimulation of new fibroblasts. However, this not only provides positive tissue healing effects, but new fibroblasts formed by EMT have the propensity to retain their mesenchymal state permanently. This is associated with increased connective tissue formation which may disrupt the underlying epithelium, ultimately invading into the surrounding stroma and leading to tissue fibrosis (Grünert *et al*., 2003, Nawshad *et al*., 2004, Balkwill, 2006, Eger *et al*., 2005).

Polarized epithelial cells usually interact with the basement membrane via their basal surface. This interaction is essential for the maintenance of their biological function, which includes endocytosis, vesicle transport and exocytosis. Regularly spaced membrane-associated junctions and keratin filaments are seen on the basolateral surface of epithelial cells; as such they closely associate with adjacent cells. This protective barrier plays a critical role to inhibit the movement of individual cells which allows for the preservation of both rigidity and structure (Denef *et al*., 2009).

Characteristic of the induction of mesenchymal cells (via the process of EMT), is the acquisition of front-rear end polarization with a loss of baso-apical polarization, thus allowing for the distinctive migratory capacity of these cells. Additionally, the acquisition of a mesenchymal phenotype is associated with elevated resistance to apoptotic cell death and increased ECM deposition (Kalluri *et al*., 2009). The initiation of EMT is characterized by the degradation of the basement membrane and the formation of a mesenchymal cell which has the ability to migrate away from its' original epithelial layer. Upon the successful establishment of secondary colonies at distant sites, EMT-derived metastatic cancer cells shed their mesenchymal phenotype through the process of mesenchymal-to-epithelial transition (MET) (Zeisberg and Kalluri, 2013).

The ability of disseminated tumour cells to undergo MET hinges on the resident microenvironment encountered after extravasation. It has been suggested that this dissemination could be as a result of the lack of heterotypic signals exposed to within the primary tumour site that lead to the initiation of EMT (Bissell *et al*., 2002, Jechlinger *et al.,* 2002, Thiery *et al*., 2009). The entire repertoire of signalling mediators involved in the metastatic dissemination (including both EMT and MET) of cancer cells remain unclear and still require experimental validation.

The initiation and completion of EMT requires the engagement of several distinctive and highly co-ordinated molecular processes. In many cancer types, the induction and activation of a series of EMT- inducing transcription factors, which include Snail, Slug, Twist, zinc finger E-box binding homobox 1 (ZEB1), FOXC2 and Goosecoid appear to be as a direct result of EMT-inducing signals such as PDGF, HGF, EGF and TGF-β, originating from the surrounding tumour stroma (Shi and Massagué, 2003, Niessen *et al*., 2008, Medici *et al*., 2008, Kokudo *et al*., 2008). Upon the activation of these transcription factors they are able to act pleiotropically and in unison to co-ordinate the execution of the EMT cascade.

The activation of EMT involves the loss of intercellular cohesion, enzymatic ECM degradation, and enhanced motility and invasion (Hartwell *et al*., 2006 and Taki *et al*., 2006). In mesenchymal cells the loss of intercellular cohesion results predominantly due to alterations in mechanical attachment sites (comprised of desmosomal, adherens and tight junctions) responsible for the regulation of the entire junctional complex (Miyoshi *et al*., 2008). Moreover, the execution of EMT depends on a sequence of intracellular signalling pathways involving MAPK, ERK, PI3K/Akt, Smads, and β-catenin, in addition to the activation of many β4 integrin cell surface proteins, including α5β1 and αvβ6 (Tse and Kalluri, 2007).

TGF-β signalling plays a critical role in the inhibition of epithelial cell proliferation and subsequently also inhibits the induction of tumourigenesis, however, there is ample evidence supporting its involvement in the advancement of tumour progression and metastasis (Bierie *et al*., 2006, Oft *et al*., 1998 and Derynck *et al*., 2001) as well as the induction of EMT (Song, 2007). Two possible signalling pathways have been implicated in the induction of EMT by TGF-β. The first involves a RhoA and p38 MAPK mediated autocrine TGF-β-induced EMT of mammary epithelial cells in NMuMG mice (Bhowmick *et al*., 2001a and Bhowmick *et al*., 2001b). The activation of the PI3K signalling pathway through Ras activation results in the inhibition of TGF-β-induced apoptosis in addition to the induction of EMT in Ras-transformed hepatocytes (Gotzmann *et al*., 2002, Oft *et al*., 1996, Janda *et al*., 2002). Additionally, the integrin αvβ6 leads to the activation of latent TGF-β, serving as an essential mediator in this signalling process (Bhowmick *et al*., 2001a and Bhowmick *et al*., 2001b). Furthermore, Ras mutant-induced EMT is mediated by both PI3K/Akt and ERK/MAPK signalling pathways, and the addition of either MAPK kinase 1 (MEK1) inhibitors or wild-type Ras results in the reversal of this EMT process (Janda *et al*., 2002).

The second signalling pathway implicated in TGF-β-induced EMT involves mothers against decapentaplegic homolog (Smad) mediated signalling (Zeisberg *et al*., 2003), wherein EMT is amplified and reinforced by the modulatory effects of inhibitory Smads and its autocrine production of TGF-β (Miyazono, 2000, Dernyck *et al*., 2001, Bhowmick *et al*., 2001a and Saika *et al*., 2004). Additionally, signalling pathways which mediate lymphoid enhancer-binding factor (LEF) and β-catenin activity cooperate with Smads inducing EMT (Eger *et al*., 2004), demonstrating the involvement of the TGF-β/Smad/LEF/PDGF signalling axis in the induction of an EMT phenotype in cancer.

The role of TGF-β-induced EMT in promoting cancer cell invasiveness has been widely explored and the absence of the TGF-β receptor expression has been shown to result in

a better cancer prognosis in mouse models of skin cancer (Cui *et al*., 1996) and in human colon cancer (Watanabe *et al*., 2001). Furthermore, TGF-β-induced EMT may be enhanced by changes in the expression of essential cell polarity proteins, for example the loss of E-cadherin in cancer cells promotes their passage through EMT (Gheldof and Berx, 2013).

1.10. E-cadherin and Epithelial-to-Mesenchymal Transition

The transmembrane glycoprotein E-cadherin (type I cadherin superfamily) is the predominant molecule in the adherent junctions of epithelial cells (Pećina-Šlaus, 2003, Li *et al*., 2012). Structurally E-cadherin is made up of an extracellular and an intracellular domain. The extracellular domain consists of 5 repeat moieties which form the E-cadherin dimers. The E-cadherin dimers of neighbouring cells interact with each other to stabilize epithelial cell adherent junctions (Stemmler, 2008). Linked to the intracellular domain is a beta- alpha- and p120-catenin containing protein complex, which interacts with actin filament networks. As such, the interactions of both E-cadherin domains creates a communication pathway, which serves as an essential integration point for both intra- and intercellular signalling pathways, including that which govern cell-to-cell contact, transcription signalling and nuclear function (Birchmeier and Behrens, 1994, Conacci-Sorrell *et al*., 2002) (Figure 1.7).

The translocation and accumulation of β-catenin in the nucleus is associated with the induction of EMT and thus the subsequent acquisition of a mesenchymal phenotype. With its nuclear translocation, β-catenin associates with the Tcf/LEF complexes (Stockinger *et al*., 2001, Gottardi *et al*., 2001). Therefore, the sequestration of β-catenin by E-cadherin maintains its cytoplasmic localization, thus maintaining an epithelial phenotype. The loss of E-cadherin in cancer cells therefore correlates with the nuclear accumulation of β-

catenin, and enhanced susceptibility of these cells to enter the EMT process to acquire a more invasive phenotype (Kim *et al*., 2002, Thiery *et al*., 2009). The importance of E-cadherin and β-catenin/LEF activity in the establishment of metastatic potential has been demonstrated in several studies (Muta *et al*., 1996, Saito *et al*., 1999).

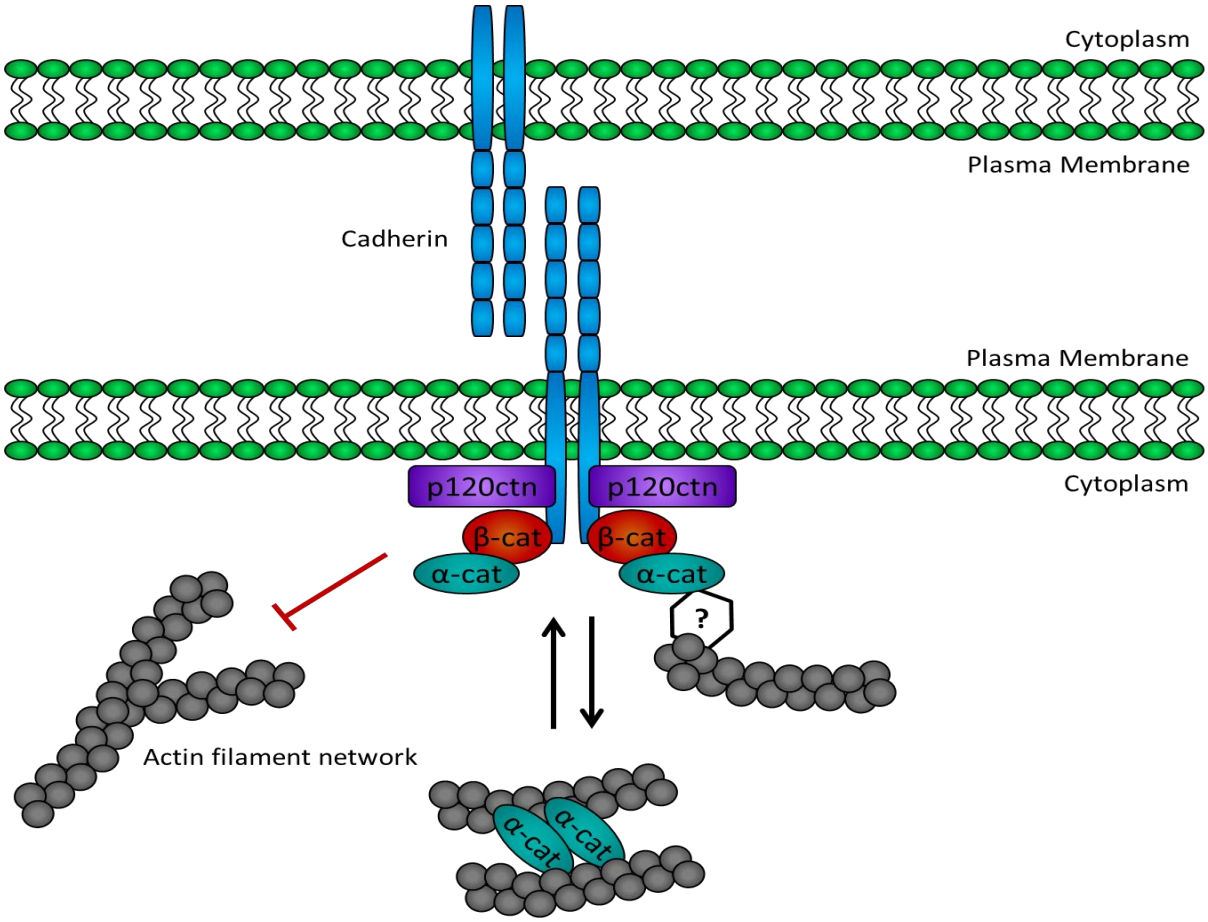

Figure 1.7: E-Cadherin/Catenin membrane complex. Structurally, E-cadherin is made up of an extracellular and an intracellular domain. The extracellular domain consists of 5 repeat moieties which form the E-cadherin dimers. Linked to the intracellular domain is a beta- alpha- and p120-catenin containing protein complex, which interacts with intracellular actin filament networks.

In studies of different human cancer types, E-cadherin expression levels vary greatly, and mutations in the *E-Cadherin* gene has been identified in cancer cell types which are more susceptible to EMT and metastatic transformation (Muta *et al*., 1996, Saito *et al*., 1999).

When transferred to immunodeficient mice, cell lines which lack E-cadherin demonstrated enhanced tumourigenicity and metastatic potential (Birchmeier *et al.*, 1994). A more in depth analysis of the mechanistic role that loss of E-cadherin plays in the metastatic progression of cancer is still required, however, it is clear that its central role in the acquisition of a mesenchymal phenotype is facilitated by the action of several other transcription factors, including that of Slug and Snail. The expression of these TGF-β-induced transcription factors result in the repression of E-cadherin expression (Medici *et al*., 2008). In mice, Snail has additionally been shown to facilitate cancer cell invasiveness (Nieto, 2002), and increased nuclear levels of Snail is associated with enhanced Wnt signalling induced by the loss of E-cadherin (Blanco *et al*., 2002). Furthermore, nuclear Snail, along with survival of motor neuron protein interacting protein 1 (SIP1), binds in an overlapping fashion to the promotor region of E-cadherin, repressing its expression (Comijn *et al*., 2001, Yokoyama *et al*., 2001).

Recently, non-coding micro-RNAs (miRNAs) have been shown to be critical components in the EMT regulatory signalling network. miR-200 and miR-205 have both been shown to inhibit ZEB1 and ZEB2, repressors of E-cadherin expression, and as such function to maintain an epithelial phenotype (Korpal *et al*., 2008, Park *et al*., 2008). Increased expression of the mesenchymal marker vimentin and decreased E-cadherin expression is correlated with the loss of miR-200 in breast carcinoma (Gregory *et al*., 2008, and Paterson *et al*., 2008), whereas, miR21 facilitates TGF-β-induced EMT and is often upregulated in many cancer types (Zavadil *et al*., 2007). Moreover, human cancer cells exhibit enhanced metastatic potential and stem cell-like properties when induced to undergo EMT (Mani *et al*., 2008).

Taken together, the generation of highly invasive cancer cells with stem cell-like properties (including that of self-renewal) and the ability to disseminate and form secondary tumours may be facilitated by EMT. However, additional direct evidence of this still remains to be

demonstrated, specifically with regards to the EMT-inducing properties of the tumour microenvironment and the role that both resident and circulating CAFs play in rendering cancerous epithelial cells permissive to EMT.

Adjuvant therapy and surgical resection remains the most effective therapeutic strategies for the treatment of well-confined primary tumours. However, this strategy remains largely ineffective in the treatment of metastatic cancer due to its enhanced chemotherapeutic resistance coupled with the systemic nature of the disease (McAllister et al., 2014). Clinically, over 90% of all cancer-associated deaths are as a direct result of the effective dissemination and metastatic spread of primary tumours to additional sites (Spano et al., 2012). As a result, extensive focus is being placed not only on elucidating the mechanisms involved in tumour dissemination, but also on understanding the role that the tumour microenvironment plays in both cancer progression and metastatic dissemination.

1.11. Clinical Implications - Overcoming cancer resistance through metabolic manipulation of CAFs

Anthracyclines, such as doxorubicin (Dox), are considered as some of the most effective chemotherapeutic agents for the treatment of various solid cancers, including those arising in the breast (Barrett-Lee *et al*., 2009). Unfortunately, anthracyclines are also cytotoxic and affect a wide variety of systems. Aside from these severe cumulative dose-dependent side effects, resistance of cancer cells to chemotherapeutic strategies has become an ongoing complex issue faced by many cancer patients and oncologists alike. Currently it is believed that chemoresistance accounts for over 90% of the failure rate seen with the treatment of metastatic breast cancer (Coley *et al*., 2008). Furthermore, the majority of patients diagnosed with breast cancer will at some point have a recurrence of the disease, resulting in poorer clinical outcomes. Due to the highly variable responses

seen with the treatment of breast cancer in particular, a critical need for new strategies aimed at overcoming these issues and improving cancer cell susceptibility has arisen. The failure of current chemotherapeutic strategies may partially be attributed to an underestimation of the stromal influence exerted on epithelial cancer cells. Furthermore, many preclinical models fail to accurately represent the influence of the tumour microenvironment (Singh *et al*., 2010). Therefore, one approach to increase tumour susceptibility and overcome chemotherapeutic resistance, involves the development of novel treatment strategies which interfere with the metabolic capacity of the surrounding tumour microenvironment.

Exposure of CAFs to chemotherapeutic drugs has been shown to result in changes in the expression of metabolic enzymes, myofibroblastic differentiation markers, and key proteins involved in autophagy (Peiris-Pagès *et al*., 2015). Additionally, increased accumulation of CAFs in colon cancer xenograft tumours occur in response to exposure to the chemotherapeutic drug oxaliplatin (Li *et al*., 2016). Increased production of cytokines (such as TGF-β, osteopontin and FGF-2) is induced by chemotherapy. This leads to HIF-1α expression which has been shown to promote cancer cell growth and metastasis (Yang *et al*., 2008, Wei *et al*., 2013 and Schioppa *et al*., 2003), and could also account for the increased recruitment of CAFs seen in tumours following chemotherapy treatment (Kojima *et al*., 2010). In pancreatic cancer models chemoresistance has been shown to be enhanced by myofibroblasts through the induction of CpG DNA-hypermethylation and DNA methyltransferase 1 expression, leading to a reduction in caspase expression (Caspase-8, -9, -7 and -3) as well as the epigenetic inhibition of STAT1 (Müerköster *et al*., 2008). Due to their abundance within the tumour stroma coupled with the profound effects they exert on tumour growth, progression, metastasis and chemoresistance, CAFs have become an attractive target for novel chemotherapeutic strategies.

Recently, pharmacological inhibition of the protein synthesis (mTOR/4E-BP1) pathway in CAFs has been shown to abolish the resistance of pancreatic cancer cells to gemcitabine (Duluc *et al*., 2015). Additionally, the *in vivo* use of targeted fibroblast activated protein (FAP) inhibition with PT-100 (a small-molecule dipeptidyl peptidase inhibitor) in combination with oxaliplatin was shown to reduce tumour angiogenesis, CAF-associated cytokine levels and significantly repressed tumour growth (Li *et al*., 2016). Furthermore, the use of a DNA-based vaccine against the tumour-stromal FAP antigen in combination with doxorubicin treatment results in enhanced chemotherapy uptake, increased survival and reduced tumour growth in an *in vivo* model of breast cancer metastasis (Loeffler *et al*., 2006).

Due to encouraging pre-clinical evidence, several clinical trials are in progress to assess the effects of various metabolic therapies for the treatment of cancer. Based on the fact that oxidative stress and autophagy play a central role in the metabolic “education” of CAFs, modulators of both may be attractive anti-CAF targets. The anti-malarial drug chloroquine, a potent inhibitor of autophagy, significantly reduces tumour growth in both human tumours and in *in vivo* xenograft models by targeting fibroblasts (Hiraki *et al*., 1963, Hiraki *et al*., 1964a and Hiraki *et al*., 1964b). As such the inhibition of autophagy by chloroquine prevents the production of high energy metabolites, thereby disrupting the ability of epithelial cancer cells to “activate” CAFs (Martinez-Outschoorn *et al*., 2010). However, in cancer the autophagic process becomes somewhat of a “double-edged sword” (Shintani *et al*., 2004), as it can serve as both a pro-death (Mizushima *et al*., 2008) and a pro-survival (Degenhardt *et al*., 2006) process depending on cellular conditions. As such the paradoxical nature of autophagy makes this treatment strategy quite challenging. It is therefore conceivable that the inhibitory effect of chloroquine on autophagy could in fact promote cancer growth and progression.

Autophagic induction within the stromal compartment has been shown to promote the resistance of carcinoma cells to cell death. In particular, the loss of caveolin-1 expression in CAFs results in the upregulation of both autophagy and p53-induced glycolysis in cancer cells (Martinez-Outschoorn et al., 2010), which is associated with poor clinical outcomes in cancer patients (Wietkiewicz *et al*., 2009, Wu *et al*., 2011 and Qian *et al*., 2011). Additionally, stromal expression of the autophagy-associated marker beclin-1 (BECN1) in tumours is associated with increased cancer cell proliferation and is associated with poor pathological and clinical outcomes in patients with invasive breast cancer (Ueno *et al*., 2016). Therefore, the assessment of stromal caveolin-1 and beclin-1 expression in CAFs could potentially serve as markers for the prediction of patient outcome. However, extensive research is still needed to fully elucidate the significance of both autophagy and CAF involvement in the clinical outcome of cancer patients.

Additionally, therapeutic strategies aimed at interfering with the ability of epithelial cancer cells to utilize the metabolites provided by surrounding CAFs could prove to be effective in overcoming CAF-induced chemoresistance. The use of L-asparaginase as an anti-cancer agent for the treatment of paediatric acute lymphoblastic leukaemia (ALL), exerts its cytotoxic effects by depriving ALL cancer cells of the amino acids asparagine and glutamine. However, due to its toxic side effects at higher doses the use of L-asparaginase in adults is limited (Oettgen *et al*., 1970), making this therapeutic strategy severely restricting. As cancer cells are highly reliant on the presence of exogenous glutamine as a fuel source to replenish intermediates of the tricarboxylic acid (TCA) cycle (anaplerosis) (Eagle *et al*., 2001) the use of sodium phenylbutyrate could prove to be a viable strategy as it decreases plasma glutamine levels, and thereby exploits the “addiction” of cancer cells to glutamine. Currently the efficacy of sodium phenylbutyrate is awaiting clinical approval for its use in the treatment of solid tumour malignancies (Gilbert *et al*., 2001 and Phuphanich *et al*., 2005). A major aspect of the ‘reverse Warburg effect’ involves the

transfer of CAF-produced lactate to the epithelial cancer cell. Therefore, the use of an inhibitor of either lactates' export from CAFs or its import into cancer cells could prove effective. Currently, a phase I clinical trial (NCT01791595) to assess the safety and potential side effects of AZD3965, a monocarboxylate 1/2 inhibitor) in patients with advanced cancer is underway.

Collectively, current pre-clinical and clinical trials show promising results in overcoming tumour progression and chemoresistance through targeted CAF-based therapies. However, several key mechanisms still remain to be elucidated in order to fully understand the role that CAFs play in cancer progression and chemoresistance. Once answered, the understanding of the complex signalling network that exists between cancer cells and CAFs will open an exciting new avenue in cancer drug discovery.

1.12. Problem Statement

The highly complex nature of the tumour microenvironment in conjunction with an underestimation of the influence that stromal cells, particularly cancer-associated fibroblasts (CAFs), exert on the metabolic and migratory ability of cancerous epithelial cells, results in an increase in the failure of current chemotherapeutic strategies. As such, there is a critical need for the development of novel pre-clinical models which effectively recapitulate the metabolic and metastatic influences of stromal cells on epithelial cancer cells within the tumour microenvironment.

1.13. Hypothesis

Based on this collective evidence, we hypothesize that nutrient deprived breast cancer epithelial cells influence cancer-associated fibroblasts (CAF's), leading to the production

of metabolites which may be utilized by these cancer cells for survival, chemo-resistance and enhanced migration. Furthermore, we hypothesize that the manipulation of autophagy in CAFs could inhibit the migratory capacity of these nutrient deprived epithelial breast cancer cells.

1.14. Aims

In vitro

- To induce oxidative stress in E0771 breast cancer cells without significant cell death (simulating the tumour microenvironment where cancer cells are deprived of nutrients and oxygen) in order to generate conditioned media to treat CAFs.
- To determine changes in the metabolic profile of CAF's treated with conditioned media (CM) derived from cancer cells.
- To determine the metabolic response of E0771 cancer cells exposed to CAF derived conditioned media (CM).
- To assess whether CAFs contribute to doxorubicin resistance and enhanced metastatic capabilities of E0771 cancer cells.
- To determine whether autophagy in CAFs plays a role in mediating epithelial-to-mesenchymal transition (EMT) and migration of E0771 cancer cells.

In vivo

- To establish a physiologically relevant tumour-bearing mouse model.
- To determine if any ultrastructural changes occur in tumours and mammary fat pads in response to systemic doxorubicin administration.

- To determine the extent of collagen deposition in tumours following doxorubicin administration.
- To determine the degree of CAF infiltration in tumours in response to doxorubicin exposure.
- To establish a primary epithelial organoid model which accurately recapitulates the 3D environment of tumour epithelial cells.
- To determine if differences exist between *in vitro* and *in vivo* models of cancer cell migration and epithelial-to-mesenchymal transition (EMT).

Chapter 2: Materials and Methods

2.1. Cell Culture

For this study the E0771 murine breast cancer (CH3 BioSystems) and the mouse embryonic fibroblast (MEF) (ATCC #SCRC-1008) cell lines were utilized. Both E0771 and MEF cells were cultured in Dulbecco's Modified Eagles Medium (DMEM) (Life Technologies) that was supplemented with 10% Foetal Bovine Serum (Scientific Group) and 1% Penicillin Streptomycin (PenStrep) (Life Technologies) collectively known as growth medium. Cells were cultured as a monolayer and maintained at an atmosphere of 37 ºC and 5% CO_2 humidity. Growth media was refreshed every 2 days and cells were regularly sub-cultured once a confluency 70 - 80% was reached. Upon reaching confluency, cells were split and seeded with fresh media for experiments. Seeding was accomplished by washing the cell monolayer with warmed Phosphate Buffered Saline (PBS) before incubation in 4 ml 0.25% Trypsin EDTA (1X) (Life Technologies) until all cells had loosened from the surface of the flask.

2.2. Treatment Strategies

2.2.1. Glucose Deprivation

Prior to treatment, media was aspirated and cell monolayers were washed twice with warm PBS to ensure all cell debris was removed. In order to determine optimal treatment times, time responses were carried out for treatment periods of 4, 8, 12, 24, 48 and 72 hours using glucose free DMEM (Life Technologies, #A1443001). Treatment time was then selected based on cell viability and oxidative stress analysis, with the treatment time

producing the least toxic effect while still increasing oxidative stress levels in the E0771 cancer cells being used.

2.2.2. Doxorubicin

Prior to treatment, media was aspirated and the cell monolayer was washed twice with warm PBS to ensure all cell debris was removed. In order to determine optimal concentrations, concentration curves were done for a treatment period of 24 hours for doxorubicin (LKT Laboratories, #D5794) with the following concentrations: 0.1, 1.0, 2.5, 5.0 and 10.0 µM. The concentration of doxorubicin was determined based on cell viability, with the lowest concentration that lead to a significant decrease in mitochondrial reductive capacity in the E0771 cancer cells being selected.

2.3. MTT Assay

A MTT cell viability assay was conducted to assess the percentage of metabolically viable cells. The principle of this assay is based on the reduction of MTT to yield purple formazan crystals by various reduction enzymes present within the mitochondria. Under conditions whereby cells have undergone or are in the process of apoptosis MTT will not be reduced. Cells from each cell line where arbitrarily divided into four treatment groups and seeded at a cell density of 5×10^5 cells per well into 24 well plates (Cellstar, Greiner bio-one). Cells were left for 24 hours to attach and proliferate in 1 ml of growth media after which media was refreshed and treatments administered as described above. Subsequent to treatments, all media was aspirated (Mini-vac power, PeqLab biotechnologie GmbH) and 500 µl of MTT working solution (0.001 g MTT/ml PBS) was added to each well. As MTT is a light sensitive compound this experiment was conducted in the dark and 24 well plates

were covered in tin foil. After the addition of MTT working solution to wells, cells were incubated for 1.5 hours at a 37ºC, 5% CO_2 humidified environment (C01901R, Snijders Scientific). Subsequent to incubation, 500 µl Isopropanol:HCl/ Triton-X-100 solution was added to each well, and the tinfoil wrapped plate was placed on a heated shaker (37ºC, 200 RPM) for a period of ± 5 min until formazan crystals generated by healthy cells had dissolved. Plates were then analysed using KCjunior software on a universal micro plate reader (EL800, Bio-Tek Instruments Inc.) where absorbance values were determined at a wavelength of 595 nm. All groups were analysed in triplicate and three independent experiments (biological replicates) were conducted. Absorbance values were all expressed as a percentage of MTT reduction versus the untreated control.

2.4. Oxidative Stress Analysis

Oxidative stress analysis was performed using flow cytometry by staining cells with DCF (2'.7'-Dichlorofluorescein) (Sigma Aldrich, #35848) or MitoSOX™ Red Mitochondrial Superoxide Indicator (Life Technologies, #M36008). Prior to treatments E0771 and MEF cells were seeded into T25 flasks at a density of 4 x 10^5 cells. Media was discarded and the cell monolayer was washed twice with warm PBS, cells were trypsinized and centrifuged at room temperature for 5 min at 300 x g. Supernatant was discarded and the pellet gently re-suspended in 1 ml of the PBS, and DCF or MitoSox was added to unfixed cells to obtain final concentrations of 50 µM and 5 µM respectively. Cells were incubated in the dark at 37 ºC for 10 min. Hydrogen peroxide (H_2O_2) was used as a positive control. Samples were analysed on the flow cytometer (BD FACSAria I) and a minimum of 10 000 live cell events were acquired for each sample using a 488 nm laser and 610 LP, 616/23 BP emission filters. Mean percentages from three separate experiments were used to perform statistical comparisons.

2.5. Western Blot Analysis

In order to carry out western blot analysis cells were seeded into T25 flasks (25 cm^2, NEST) with 4 ml of growth media per flask. Flasks were all incubated in a 37 ºC, 5% CO_2 environment for 24 hours to allow cells to attach and proliferate.

2.5.1. Protein Extraction and Quantification

After treatment, media was aspirated from T25 flasks and cells were immediately placed on ice. The cell monolayer was washed with 1 ml cold PBS, which was repeated twice more. 100 µl modified radioprecipitation (RIPA) buffer comprising of 2.5 mM Tris-HCL, 1 mM EDTA, 1 mM dithiothreitol, 0.1 mM phenylmethylsulfonyl fluoride (PMSF), 1 mM benzamidine, 50 mM NaF, 4 mg/ml SBTI, 10 mg/ml leupeptin, 0.1% SDS 0.5%, Na deoxycholate and 1% NP40, calibrated to pH 7.4, was added to each petri dish and allowed to stand for 5 min on ice in order to extract total cell protein. Cells were then detached from the flask surface with the use of a cell scraper that was cleaned using EtOH between samples. Whole cell lysates were sonicated on ice at 3 Hz for 8 seconds and centrifuged at 8000 RPM for 30 seconds. The supernatant was then decanted into Eppendorf tubes and stored at -80 ºC ready for protein quantification. A Direct Detect® infrared spectrometer (DDHW00010-WW, Merck) was used to determine the protein content of samples from each cell line.

2.5.2. Sample Preparation

Samples used for western blots were prepared following protein determination. Aliquots were prepared containing 20 µg protein content and diluted with sample buffer. Prepared samples were then stored at -80 ºC for further western blot analysis.

2.5.3. SDS-PAGE and Western Blot Analysis

Cell lysates were subsequently separated on 4-15% polyacrylamide precast gels (mini-PROTEAN® TGX™ Gels, Bio-Rad) by sodium dodecyl sulphate polyacrylamide gel electrophoresis (SDS-PAGE). 5 µl of a protein marker ladder (PeqGold) was loaded into the first well of each gel run; this is used for orientation of gels as well as for determination of molecular weights of separated proteins. Prepared cell lysates were heated to a temperature of 95 ºC for 5 minutes in order to denature proteins and pulse centrifuged, after which 50 µg of protein was added to each lane following the ladder.

Gels were run at 100 V (constant) and 400 mA for a period of more or less 90 minutes (Power Pac 300, BioRad). On completion of SDS-PAGE, proteins were transferred to prepared polyvinylidine fluoride (PVDF) membranes using a semi-dry electrotransfer system (TransBlot® Turbo™ v1.02, BioRad) for 30 minutes at 25 V and 1.0 A. Membranes were visualized using the stain free blot protocol provided on a Chemi-Doc™ MP (BioRad) system in order to visualize that proteins transferred correctly. Membranes were subsequently washed in 0.1% Tris Buffered Saline-Tween20 (TBS-T) and blocked for 2 hours in 5% (w/v) non-fat milk and TBS-T, whilst being gently agitated at room temperature, this prevents non-specific binding of the antibody. Membranes were then incubated at 4 ºC overnight in TBS-T diluted primary antibodies (1:1000). The following day membranes were removed from the primary antibody and washed with TBS-T before being incubated in anti-rabbit IgG horseradish peroxidase conjugated secondary antibody (1:10000) (from donkey) (Cell Signalling Technologies) with gently agitation at room temperature for 1 hour. Subsequent to the incubation period membranes were washed in TBS-T before antibodies were detected with the use of an ECL western blotting substrate detection kit (Pierce®, Thermo Scientific) and protein bands visualised with the use of ImageLab 4.0 software on a Chemi-Doc™ MP (BioRad) imaging system. Exposed bands were visualized and quantification was done with the use of BioRad ImageLab software

where samples were normalized to total protein present on the same membrane. Bands for each specific protein were quantified as normalized readings comparative to the control sample present on the same blot.

2.6. Generation of Conditioned media

E0771 and MEF cells were seeded into T75 flasks at a density of 1 x 10^5 cells. After the treatment period, media was collected and centrifuged at 5000 RPM for 10 min at a temperature of 4 ^{0}C. The pellet was discarded and centrifuged conditioned media was filtered using a 0.2 µm filter. Conditioned media was then snap frozen in liquid nitrogen and stored at -80 ^{0}C for no longer than 4 weeks until further use / analysis. For analysis purposes conditioned media was collected from three flasks and pooled to provide a single technical replicate. In order to account for variance conditioned media was collected from four separate cultures for analysis.

2.6.1. Conditioned Media Treatment Strategies

Prior to treatment, media was aspirated and cell monolayers were washed twice with warm PBS to ensure all cell debris was removed. Conditioned media was thawed and allowed to reach a temperature of 37 ^{0}C. Following this, cells were treated for 24 hours with conditioned media that was diluted with fresh DMEM (50:50) in order to maintain cellular viability whilst still eliciting a desired response. Treatment groups were established as described in table 2.1 below.

Table 2.1: This study was divided into two main experimental groups utilizing conditioned media which consisted of the following treatment groups:

Experimental Group 1	Control	Control Conditioned Media **(Control-CM)**	E0771 Untreated Conditioned Media **(E0771-UTCM)**	E0771 Conditioned Media **(E0771-CM)**
	Untreated	NO cells	untreated E0771	12 hr glucose deprived E0771
Experimental Group 2	Control	Control Conditioned Media **(Control-CM)**	MEF Untreated Conditioned Media **(MEF-UTCM)**	MEF Conditioned Media **(MEF-CM)**
	Untreated	NO cells	Untreated MEF	E0771-CM treated MEF

2.7. Proteomics Analysis of Conditioned Media

E0771 and MEF cells were seeded individually into T75 flasks at a density of 1.5 x 10^6 cells per flask. After 2 days, DMEM media was discarded and the cell monolayer washed twice using 1 x DPBS (Life Technologies). Following this, 15 ml of chemically defined Chinese hamster ovary (CD-CHO) serum-free media (Invitrogen) supplemented with 8 mM glutamine (Invitrogen) was added to each flask. Flasks were then allowed to incubate

at a 37ºC, 5% CO_2 humidified environment (C01901R, Snijders Scientific) for the required treatment times. Conditioned media generated was collected as previously described and media from four T75 flasks were pooled to obtain a total volume of 60 ml conditioned media per sample, and a total of four biological replicates per treatment group for each cell line were generated for proteomics analysis. Proteins present in the conditioned media were concentrated and liquid chromatography mass spectrometry (LC-MS) was performed by the Centre for Proteomic & Genomic Research (CPGR), an ISO 9001:2008 accredited facility.

2.7.1. Sample Purification and Concentration

Overnight passivation of spin filters was achieved using 5% TWEEN-20 (Sigma, #9005-64-5). Spin columns were then three times washed for 30 minutes each using water prior to use. Columns were then placed inside collection tubes and 500 µl of Millipore water was spun through. Following which, columns were conditioned using 500 µl of 50 mM ammonium bicarbonate (Sigma, #40867) spun for 15 minutes at 12 000 x g at 4˚C. Five hundred µl from each sample was then added to the spin filters and spun through at the same settings as above. This was repeated three times so that a final volume of 1.5 ml of sample was concentrated to less than 50 µl. Samples were then washed three times with 500 µl of 50 mM ammonium bicarbonate leaving a residual volume of less than 40 µl. Samples were then transferred to protein LoBind tubes and a final volume of 60 µl was achieved using 50 mM ammonium bicarbonate (final concentration), 2% SDS (Sigma, #71736). Protein quantification was achieved using the QuantiPro BCA assay kit (Sigma, #QPBCA).

2.7.2. On-bead Hydrophilic Interaction Chromatography (HILIC) Digestion

Protein reduction was achieved by incubating samples for 1 hour at 60˚C in 10 mM final concentration tris(2-carboxyethyl) phosphine per sample (Sigma, #646547). Once cooled to room temperature, samples were alkylated with 10 mM final concentration methylmethanethiosulphonate (Sigma, #208795) per sample, where samples were allowed to incubate at room temperature for 15 minutes. Prior to HILIC magnetic bead workflow, beads were aliquoted into a new tube to remove shipping solution. Subsequently, beads were washed twice with 250 µl wash buffer (15% acetonitrile, 100 mM ammonium acetate (Sigma, #14267) pH 4.5) for one minute. Beads were then re-suspended in loading buffer (30% acetonitrile, 200 mM ammonium acetate, pH 4.5). For digestion, 50 µg of protein or the entire sample was transferred to a protein LoBind plate and HILIC magnetic beads were added at an equal volume to that of the sample (at a ratio of 5:1 total protein). The plate was then transferred to a shaker at 900 RPM and incubated for 30 minutes to allow for binding of protein to beads. After binding, beads were washed twice with 500 µl of 95% acetonitrile for one minute. For digestion, 200 µl trypsin (Promega, #PRV5111), made up in 50 mM triethylammonium bicarbonate (Sigma,# T7408) was added at a ratio of 1:10 total protein and the plate was incubated at 37˚C on a shaker for 4 hours. After digestion, the supernatant containing peptides was removed and dried down, after which samples were re-suspended in LC loading buffer (0.1% formic acid, 2.5% acetonitrile).

2.7.3. Liquid Chromatography Mass Spectrometry (LC-MS)

LCMS analysis was conducted with a Q-Exactive quadrupole-Orbitrap mass spectrometer (Thermo Fisher Scientific, USA) coupled with a Dionex Ultimate 3000 nano-HPLC system. Peptides were dissolved in 0.1% formic acid (Sigma, #56302), 2% acetonitrile (Burdick & Jackson, #BJLC015CS) and loaded on a C18 trap column (300 µm × 5 mm × 5 µm). Chromatographic separation was performed using a PepAcclaim C18 column (75 µm × 25 cm × 2 µm) and LC water (Burdick and Jackson, #BJLC365); 0.1% formic acid (solvent A) and acetonitrile, 0.1% formic acid (solvent B) was employed as the solvent system. The multi-step gradient for peptide separation was generated at 300 nL / min as follows: time change 6 min, gradient change: 3.5 – 9% solvent B, time change 45.5 min, gradient change 9 – 24.6% solvent B, time change 2 min, gradient change 24.6 – 38.7% solvent B, time change 2.1 min, gradient change 38.7 – 52.8% solvent B. The mass spectrometer was operated in positive ion mode with a capillary temperature of 320°C, and an electrospray voltage of 1.95 kV was applied.

2.7.4. Data Analysis

Progenesis QI (Nonlinear, UK) was used in order to determine the relative quantification of protein abundance in each sample. Data processing included peak picking, run alignment and normalisation and relative quantification was based on four biological replicates per condition using non-conflicting peptides. Proteins, containing at least two unique peptides that were above the first false positive protein identified for each sample, were reported. A protein with a fold change greater than or equal to two with a corresponding p-value <0.05 was considered regulated. Identified peptides were then

matched to proteins using a human database source from UniProt (www.uniprot.org) dated 23/03/2017 by means of Byonic Software (Protein Metrics, USA).

2.7.5. Gene Ontology (GO) Approach

Data generated using 'omics' platforms are in themselves not very informative as the share scale of the data generated renders any direct insight into biological significance inaccessible. In this regard, a number of techniques have been developed to 'condense' a data set into a meaningful description of the information generated. Often, these approaches involve grouping genes or proteins into categories, such as their shared involvement in a metabolic or signalling pathway.

In this study, the Gene Ontology (GO) approach was implemented. A heuristic way of understanding the GO approach can be provided by analogy to the central dogma of life; similarly to the way in which DNA is transcribed to RNA and subsequently translated to protein, the protein itself can in turn be 'assigned' a particular relevance (i.e. protein be 'translated' into a function or activity). These 'assigned relevance' or GO terms describe gene products in terms of three ontologies; molecular function, biological process and cellular component. For example, 'molecular function' includes "iron-binding", whereas 'biological process' describes the process in which the molecular function is implemented (e.g. iron sequestration as a host response during an infection). Structure denotes the physical location of the gene product (e.g. nucleus or cytosolic) or the structure into which the component is incorporated (e.g. a subunit of the apoptosome).

A second feature of GO terms is that they are hierarchically arranged, that is to say that a more descriptive GO term is nested in a less descriptive GO term. As an example, the GO term "response to gamma radiation" is contained in the less descriptive (i.e. more generic)

term “response to ionizing radiation”. The interaction between GO terms are via ‘controlled vocabularies’. For example, the GO term ‘protein kinase activity’ is related to ‘protein phosphorylation’ by the fact that ‘protein kinase activity’ is part of the biological process ‘protein phosphorylation’. These main aspects give rise to a hierarchal network of descriptive terms that can be used to identify proteins with the same functionality or involvement in the same process as well as the location of these proteins **(Figure 2.1)**.

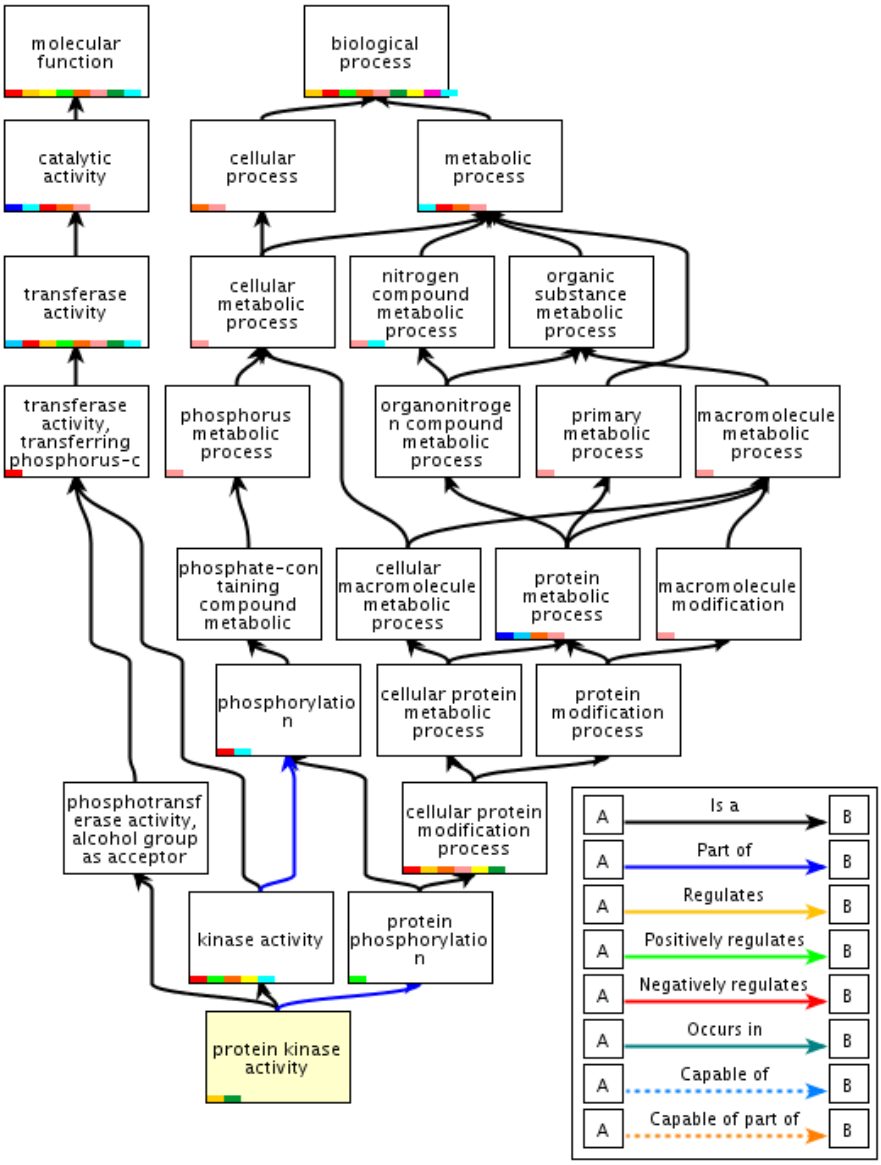

Figure 2.1: A graphical representation of the GO term “protein kinase activity” (GO:0004672) generated in *AmiGO 2*.

2.7.6. Bioinformatics Analysis

From the list of regulated proteins provided by CPGR, a list of UniProt accession numbers of all regulated proteins where extracted. Protein sets for each treatment condition were then grouped according to proteins which were upregulated and those that were downregulated. A basic descriptive overview of differentially regulated proteins between groups where visualised by generating Venn diagrams using Venny 2.1 (http://bioinfogp.cnb.csic.es/tools/venny/). Next, GO terms were assigned by submitting the list of regulated proteins into DAVID (Database for Annotation, Visualization and Integrated Discovery) version 6.8 [Systematic and integrative analysis of large gene lists using DAVID bioinformatics resources]. The list of GO terms and their associated P-values (Benjamini–Hochberg procedure to control for multiple testing) was subsequently submitted to REVIGO (which summarizes and visualizes long lists of gene ontology terms) in order to visualise GO terms and their associations. REVIGO provides a number of graph-based tools to visualise and inspect the association between GO terms, allowing for the identification of protein clusters as well as the identification of interactions occurring between clusters.

Interesting associations between GO terms were followed up with more detailed analysis using various tool suits provided in DAVID. For example, DAVID allows for the quick access to KEGG (Kyoto Encyclopaedia of Genes and Genomes), where regulated proteins in a pathway can be visualised. In this manner, the ‘condensed’ information in a GO term can be revisited to gain a more refined view of the proteins’ biological relevance within a metabolic pathway. DAVID also provides a 2D-viewer **(Figure 2.2)**, wherein a set of proteins involved in common processes or pathways (“Annotation Cluster”) can be visualized more informatively.

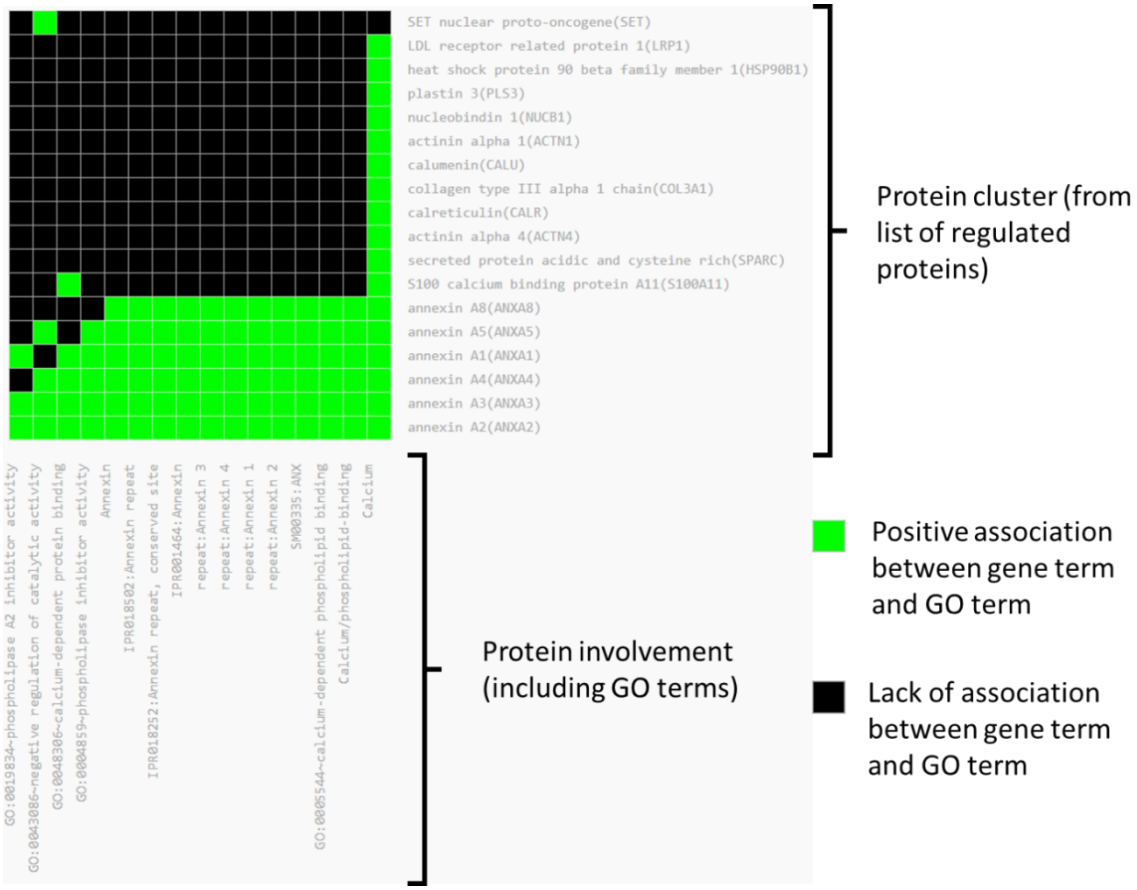

Figure 2.2: A representative 2D-graph of proteins ('y-axes') and their annotation terms ('x-axes). Green blocks indicate shared annotation clustering between proteins, whereas black indicates the lack of shared association between proteins.

To summarize, the interrogation of the list of regulated proteins between groups provided by CPGR, followed a three phase process **(Figure 2.3)**. Firstly, data sets were cleaned and prepared for subsequent analysis by extracting Uniprot accession numbers. Next, GO terms were extracted and visualised in REVIGO. After which, interesting GO terms as well as their interactions observed were followed up by more detailed investigations using DAVID tool suits, which included functional annotation clustering (2D-graph viewer) as well as pathway analysis (KEGG).

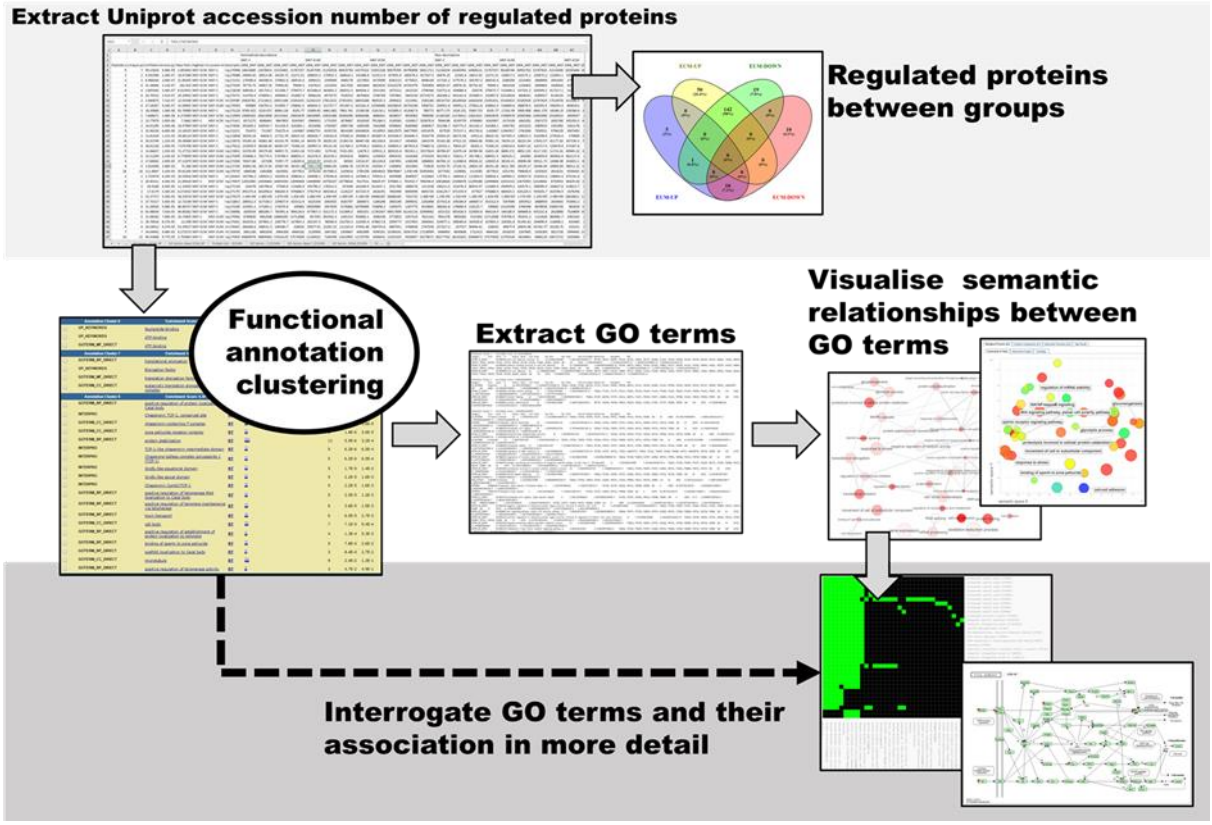

Figure 2.3: A brief outline of the procedures followed to explore proteomic data sets.

2.8. Immunocytochemistry

MEF cells were grown in 8-well chamber slides (Lab-Tek, Thermoscientific) at a density of 1.2 x 10^4 cells cells/well. After the treatment period, growth medium was removed and cells were washed with PBS. Cells were fixed with ice-cold methanol and acetone (1:1) and left to incubate on ice for 10 min. The fixative mixture was then removed and cells were allowed to air-dry for 20 min. After being rinsed twice with PBS, non-specific binding was prevented by incubating cells in a 1% BSA/PBS blocking solution for 30 min at RT. After this time period, the blocking solution was drained off and primary monoclonal antibodies against alpha smooth muscle actin (α-SMA) (Abcam, #ab7817) and vimentin (Cell Signalling Technologies, #D21H3) diluted in PBS (1:50 and 1:100 respectively) were added to cells and allowed to incubate overnight at 4°C. Cells were then rinsed three times

with PBS and allowed to incubate with the appropriate secondary antibody for 30 min at room temperature. In this case an Alexa Fluor 488 conjugated donkey anti-mouse secondary antibody (Life Technologies, #A-21206) and an Alexa Fluor 647 conjugated goat anti-rabbit secondary antibody (Life Technologies, #A-21244) was used. After incubation, Hoechst 33342 dye (1:200) was additionally added and kept in contact with cells for a further 10 min incubation period. Next, cells were rinsed and mounted with DAKO fluorescent mounting medium (DAKO Inc., CA, USA). Chambers were kept wrapped in foil at -20 °C until image acquisition was performed using the Zen imaging software on a Carl Zeiss LSM780 confocal microscope (Carl Zeiss, Germany) using a 60x oil immersion objective.

2.9. Glucose Uptake Assay

MEF cells were seeded into 6-well plates at a density of 2.5 x 10^5 cells/well. After the treatment period, media was discarded and the cell monolayer was washed twice with warm PBS, after which 2 ml 0.25% Trypsin EDTA (Life Technologies) was added to each well for 3-4 min until all cells had detached. The cell suspension was then added to 15 ml Falcon tubes (BD Biosciences) and centrifuged at 1500 RPM for 3 min. The supernatant was removed and the pellet re-suspended in 1 ml PBS. 2-NBDG (2-(N-(7-Nitrobenz-2-oxa-1,3-diazol-4-yl)Amino)-2-Deoxyglucose) (Life Technologies, #N13195) and Propidium Iodide (PI) (Sigma-Aldrich, # P4170) was added to the unfixed cells to obtain final concentrations of 100 µM and 1 mg/ml respectively, and incubated for 10 min before being analysed on the flow cytometer (BD FACSAria I). A minimum of 10 000 live cell events were collected and analysed. As PI has an emission spectrum of 550 – 720 nm a bandpass filter of 585/42 was employed to detect light emitted between 564 and 606 nm by stained cells. PI inclusion signified loss in membrane integrity and cell death as such

only live cells (signified by PI exclusion) were evaluated for glucose uptake. Values were represented as a percentage of the control and mean percentages from three separate experiments were used to perform statistical comparisons.

2.10.GLUT4 Translocation Assay

Translocation of GLUT4 to the cell membrane was determined through the expression of the HA-GLUT4-GFP fusion protein (A kind gift from Prof. M.F. Essop and Dr D. Joseph, Stellenbosch University, RSA). Transfection of HA-GLUT4-GFP was achieved by electroporation using the Neon® transfection system (Invitrogen, Carlsbad, CA, USA). Prior to seeding, MEF cells were washed with warm PBS and centrifuged at 400 x *g* for 5 min at room temperature. Supernatant was discarded and the pellet gently re-suspended in the supplied re-suspension buffer R to a final density of 1 x 10^7 cells/ml and gently pipetted to obtain a single cell suspension. A Neon® tube containing 3 ml Electrolytic buffer was placed into the Neon® pipette station. 500 ng of the HA-GLUT4-GFP construct was added to a cell suspension at a density of 5 x 10^6 cells/ml and cells were pulsed once at a voltage of 1350 and pulse width of 30 ms using a 10 µl tip. Transfected cells were then seeded onto 8-well chamber slides (Lab-Tek, Thermoscientific) at a density of 12 000 cells/well and plates were gently swirled and incubated at an atmosphere of 37 ºC and 5% CO_2 humidity for 24 hours. GLUT4 expression was confirmed following transfection in cells demonstrating positive GFP fluorescence. After the treatment period, growth medium was removed and cells were washed twice with warm PBS. Cells were fixed using a 4% paraformaldehyde solution and incubated for 15 min at RT. The fixative solution was then removed and cells were allowed to air-dry for 20 min. After being rinsed twice with PBS, non-specific binding was prevented by incubating cells in a 1% BSA/PBS blocking solution for 30 min at RT. After this time period, the blocking solution was drained off and an anti-

HA Alexa Fluor 647 conjugated antibody diluted in PBS (1:100) was added to cells and allowed to incubate overnight at 4°C. Cells were then rinsed three times with PBS and mounted with DAKO fluorescent mounting medium (DAKO Inc., CA, USA). Chambers were kept wrapped in foil at -20°C until image acquisition was performed using the Zen imaging software on a Carl Zeiss LSM780 confocal microscope (Carl Zeiss, Germany) using a 60x oil immersion objective.

2.11.Pyruvate dehydrogenase (PDH) Assay

Assessment of intracellular pyruvate dehydrogenase activity was achieved by means of a commercially available pyruvate dehydrogenase (PDH) Combo (Activity + Profiling) Microplate Assay Kit (Abcam, ab110671). This assay combines two independent kits to assess relative PDH protein concentration and activity as well as relative specific activity (activity / protein concentration).

2.11.1. Sample Preparation

MEF cells were seeded into T75 flasks at a density of 1.5 x 10^6 cells/flask. Following treatment, cell monolayers were washed with warm PBS, and 4 ml 0.25% Trypsin EDTA (Life Technologies) was added to each well for 3-4 min until all cells had detached. The cell suspension was then added to 15 ml Falcon tubes (BD Biosciences) and centrifuged at 1500 RPM for 3 min. The supernatant was removed and the pellet re-suspended in PBS. Prior to sample solubilisation the protein concentration of each sample was measured and adjusted using PBS to obtain a concentration of 15 mg/ml. Intact, functional PDH was solubilized with the addition of an appropriate volume of the supplied

detergent solution in order to produce a final protein concentration of 13.5 mg/ml. Samples were then incubated on ice for 10 min and centrifuged at 1 000 x *g* for 10 min at 4 ^{0}C.

2.11.2. PDH Enzyme Activity Assay

The colorimetric PDH enzyme activity assay relies on the immunocapture of the PDH enzyme within the wells and the subsequent reduction of NAD+ to NADH, coupled to the reduction of a reporter dye producing a change in colour (λmax = 450 nm) which can be then be detected spectrophotometrically.

2.11.2.1. Assay Procedure

A 1 x buffer solution was prepared by diluting the supplied 20 x buffer with dH_2O, and samples were diluted appropriately in order to obtain a concentration of 500 µg / 200 µl/well (which falls within the linear working range of 100 – 1000 µg / 200 µl/well). 200 µl of each sample was then added to each well of the microplate, additionally two positive control samples (100 µg / 200 µl/well and 1000 µg / 200 µl/well) in addition to the negative buffer control was included and the microplate was then allowed to incubate at room temperature for 3 hours. A working stabilizer solution was prepared by diluting the 5 x stock stabilizer solution provided in the kit with freshly prepared 1 x buffer solution. Following incubation the wells of the microplate were emptied and 300 µl of the 1 x stabilizer solution was added to each well, this was then repeated for a second time. Finally the wells were emptied and 200 µl of prepared assay solution was added to each well and absorbance was then measured at 450 nm at room temperature using a universal micro plate reader (EL800, Bio-Tek Instruments Inc.) set to kinetic program for 30 minutes

with readings being taken every 42 seconds. PDH activity was then expressed as the initial rate of reaction, determined by the slopes of the generated curves.

2.11.3. PDH Protein Profiling Microplate Assay

This “sandwich” ELISA assay relies on the purification and immobilization of the PDH enzyme by an anti-PDH capture antibody pre-coated in the wells of a microplate. The amount of PDH which is captured is determined with the addition of a second anti-PDH antibody which binds to captured PDH. Once bound the addition of a HRP conjugated anti-mouse secondary antibody results in a change in colour (colourless to blue) of the HRP development solution. This colour change (absorbance) is directly proportional to the amount of captured PDH.

2.11.3.1. Assay Procedure

200 µl of previously prepared samples was added to each well of the supplied microplate. The same two positive control samples in addition to the negative buffer control was included and the microplate was then allowed to incubate at room temperature for 3 hours. 1 x buffer solution was freshly prepared by diluting the supplied 20 x buffer with supplied incubation buffer. The wells of the microplate were then emptied by inverting the plate over a receptacle and firmly shaking out the well contents in a single rapid downward motion. Wells were washed twice by rapidly adding 300 µl of 1 x stabilizer solution to each well and then removing the solution. Following the second wash the plate was inverted onto a paper towel in order to remove excess liquid. 200 µl of 1 x detector antibody was added to each well and plates were covered and incubated at room temperature for 1

hour. Following incubation, wells were washed twice using 1 x buffer solution (without stabilizer). 200 µl of the provided 1 x HRP label was then added to each well and plates were covered and incubated for a further 1 hour at room temperature. Plates were then washed for a total of three times before 200 µl of the provided HRP development solution was added to each well. Absorbance was then measured at 600 nm at room temperature using a universal micro plate reader (EL800, Bio-Tek Instruments Inc.) set to a kinetic program for 30 minutes with readings being taken every 42 seconds. PDH activity was then expressed as the initial rate of reaction, determined by the slopes of the generated curves.

2.12.L-Lactate Assay

Assessment of intracellular L-Lactate levels was achieved by means of a commercial colorimetric L-Lactate assay kit (Abcam, ab65331). This assay relies on the oxidation of lactate by lactate dehydrogenase. The resulting product interacts with the provided probe to produce a change in colour (λmax = 450 nm) which can be then be detected.

2.12.1. Sample Preparation

MEF and E0771 cells were seeded into T25 flasks at a density of 4 x 10^5 and 8 x 10^5 cells respectively. Following treatment, cell monolayers were washed with warm PBS and 2 ml 0.25% Trypsin EDTA (Life Technologies) was added to each well for 3 - 4 min until all cells had detached. The cell suspension was then added to 15 ml Falcon tubes (BD Biosciences) and centrifuged at 1500 RPM for 3 min. The supernatant was removed and the pellet washed with cold PBS. The cells were centrifuged again at the same specifications and the supernatant was removed as before. 500 µl of lactate assay buffer

provided in the kit was added to re-suspend each pellet. Cells were then homogenized by quickly pipetting up and down a few times. Insoluble debris was then removed by means of centrifugation at top speed (5 min at 4 ^{0}C). The supernatant was then kept and a deproteinization step was performed in order to remove endogenous lactate dehydrogenase which could lead to lactate degradation. Deproteinization was achieved by adding ice cold perchloric acid (PCA) to each sample at a final concentration of 1 M. Samples were then incubated on ice for 5 min and centrifuged at 13 000 x *g* for 2 min at 4^{0}C. Supernatants were then transferred to clean tubes and excess PCA was precipitated out by adding ice cold 2 M potassium hydroxide (KOH) to equal 34% of the supernatant volume. pH was assessed (testing 1 µl on litmus paper) and each sample was adjusted to a pH of 6 – 8.5. Samples were then centrifuged at 13 000 x *g* for 2 min at 4 ^{0}C and the supernatant collected.

2.12.2. Assay Procedure

Working solutions of lactate standards were prepared using the stock solution provided in the kit. Triplicates of serially diluted lactate standards (0 – 10 nmol/well) were pipetted into wells of a 96-well microtiter plate. Duplicates of prepared protein samples (50 µl) were pipetted, followed by the addition of 50 µl reaction mix (lactate enzyme mix, substrate mix and assay buffer) to all wells. Plates were then allowed to incubate at room temperature for 30 min where after absorbance was read at 450 nm using KCjunior software on a universal micro plate reader (EL800, Bio-Tek Instruments Inc.). Lactate concentrations were then calculated by using the sample amount from the standard curve (Lα) in nmol, sample volume (Sv) and dilution factor (D) in the following equation: Lactate concentration = (Lα/Sv) x D. Values were represented as a percentage of the control.

2.13.Cell Death Analysis

E0771 cells were grown in T25 flasks at a seeding density of 8 x 10^5 cells/flask. After the treatment period, 2 ml 0.25% Trypsin EDTA (Life Technologies) was added to each flask for 3 - 4 min until all cells had detached. The cell suspension was then added to 15 ml Falcon tubes (BD Biosciences) and centrifuged at 1500 RPM for 3 min. The supernatant was removed and the pellet washed with 0.1 M PBS. The cells were centrifuged again at the same specifications and the supernatant was removed as before. Propidium Iodide (PI) (Sigma-Aldrich) and Hoechst 33342 was added to the unfixed cells to obtain final concentrations of 1 mg/ml, incubated for 10 min and analysed on the flow cytometer (BD FACSAria I). A minimum of 10 000 events were collected and analysed using a 488 nm laser and 610LP, 616/23BP emission filters. PI inclusion signified loss in membrane integrity and cell death. Values were represented as a percentage of the control and mean percentages from three separate experiments were used to perform statistical comparisons.

2.14. ATP Analysis

Intracellular ATP concentrations were assessed by means of the ENLITEN® ATP bioluminescent assay kit (Promega, Madison WI). In this assay, recombinant luciferase is utilized to catalyze the reaction:

$$\text{ATP} + \textit{D}\text{-Luciferin} + O_2 \rightarrow \text{Oxyluciferin} + \text{AMP} + \text{PPi} + \text{Light (560 nm)}$$

In this ATP dependent reaction the ATP concentration present is directly proportional to the light intensity emitted. As such, the measurement of emitted light using a luminometer allows for the direct quantification of intracellular ATP concentrations.

2.14.1. Sample Preparation

MEF and E0771 cells were seeded into T25 flasks at a density of 4 x 10^5 and 8 x 10^5 cells respectively. Subsequent to treatments, media was discarded and the cell monolayer washed with sterile PBS. Cells were detached from flasks using 2 ml 0.25% Trypsin EDTA (Life Technologies). Detached cells were collected and centrifuged at 1500 RPM for 3 min at 4 ^{0}C. The supernatant was discarded and cell pellets washed using sterile PBS. Following a second centrifugation step, pellets were re-suspended in 50 µl ice cold lysis buffer comprising of 100 mM Tris-HCl, and 4 mM EDTA calibrated to pH 7.75 (Essmann *et al*., 2003). Immediately following re-suspension 150 µl of boiling lysis buffer was added to each sample and incubated at 99 °C for 2 min. Samples were then centrifuged at 8,000 x g, for 1 min at 4 ^{0}C. The resulting supernatant was then collected for ATP analysis and protein determination.

2.14.2. Assay Procedure

A working solution of ATP standards was prepared using the stock solution provided in the kit, and triplicates of serially diluted ATP standards (0 – 100 nmol/well) was pipetted into wells of a white 96-well luminometer plate (Glomax Promega, Madison WI). 50 µl of prepared samples was then added to wells in triplicate. For this assay an ATP standard served as a positive control and ATP-free water as a negative control, which was added to triplicate wells (50 µl). The provided luciferase rL/L reagent was reconstituted as per manufacturer's instructions and 50 µl added to samples followed by immediate analysis using a Glomax-96 luminometer (Promega, Madison WI).

2.15. Migration Assay

In order to assess cell migration capabilities, cell migration (wound healing) assays were performed. This assay involves the introduction of a linear wound (with the use of a sterile 200 µl tip) to a confluent monolayer and then relies on the ability of these cells to move into and fill the gap introduced.

2.15.1. Mitomycin C Preparation

The cytostatic agent Mitomycin C was used to inhibit cellular proliferation, thus excluding any effects that may be as a result of proliferation. Mitomycin C is an antibiotic produced from *Steptomyces caespitosus* which acts as a powerful inhibitor of DNA synthesis (Ueda *et al.,* 1984). A 0.4 mg/ml stock solution of Mitomycin C (Sigma Aldrich, #) was prepared and aliquots were shielded from light and stored at 4 ^{0}C for no longer than one week as a toxic precipitate may form if stored longer than prescribed. A dose response assay was performed in order to determine the optimal concentration of Mitomycin C needed to effectively inhibit cellular proliferation. Briefly, E0771 cells were seeded onto sterile glass coverslips in 6-well plates at a density of 1 x 10^5 cells/well and plates were gently swirled and incubated at an atmosphere of 37 ºC and 5% CO_2 humidity for 24 hours. Triplicate wells were then treated with a range of Mitomycin C concentrations (1 µg/ml, 2 µg/ml, 5 µg/ml and 10 µg/ml) for 24 hours. Following treatment, coverslips were removed from wells and gently washed twice with warm PBS. Cells were then fixed with ice-cold 100% methanol and left to incubate on ice for 5 min. Methanol fixative was then removed and cells were washed three times with PBS. 200 µl of Hoechst 33342 (Sigma Aldrich, #) at a final concentration of 10 µg/ml was added to each coverslip and allowed to incubate at room temperature for 10 min. Following staining, coverslips were rinsed and mounted onto glass slides with DAKO fluorescent mounting medium (DAKO Inc., CA, USA). Slides were

then allowed to air dry for 2 hours at RT and kept wrapped in foil at -20 °C. Imaging was performed with the use of a Nikon Eclipse E400 microscope equipped with a DS-Fi2 colour digital camera (Nikon, Japan) with a DAPI barrier filter (excitation 340 - 380 nm, emission 435 - 483 nm). A total of nine random fields of view images per slide were acquired, and nuclear counts compared to control groups (0 and 24 hours) were performed as an indication of cellular proliferation.

2.15.2. Assay Procedure

E0771 cells were cultured in 6-well plates at a density of 6 x 10^5 cells/well. Cells were allowed to adhere for 24 hours, after which, three linear wounds were made in each well using a sterile 200 µl pipette tip. Cell monolayers were then washed with warm PBS to remove cell debris and fresh growth medium was added to each well. Control (0 hr) images were acquired for each well using an Olympus® Cell^R system and Olympus® IX81 inverted fluorescence microscope (Olympus®, GMBH Japan), which is equipped with a temperature-controlled incubator system that was set to 37 °C and a motorized stage control that allows exact coordinate positions to be saved and accessed at a later point in time. For each well, a total of three positions across the three wounds were saved and used in all subsequent time-points (6, 12, 18 and 24 hrs). Subsequent to the acquisition of the first images, wells were treated with appropriate conditioned media supplemented with Mitomycin C and doxorubicin. As both Mitomycin C and doxorubicin are light sensitive, treatment proceeded after the acquisition of initial images in order to avoid excessive light exposure. Image analysis was performed using ImageJ analysis software where wound area was calculated using the software by demarcating the migration front on scaled images. Percentage wound closure and rate of wound closure (% per hour) was then calculated by using the following equations:

$$\%\ wound\ closure\ at\ x\ hr = \frac{wound\ area\ at\ (0\ hr) - wound\ area\ (x\ hr)}{wound\ area\ (0\ hr)} \times 100$$

$$rate\ of\ wound\ closure\ at\ x\ hr\ (\%.hr^{-1}) = \frac{\%\ wound\ closure\ (x\ hr)}{x} \times 100$$

2.16. Atg5 Knockdown

Cells were transfected by means of electroporation using the Neon® transfection system (Invitrogen, Carlsbad, CA, USA). Prior to seeding, MEF cells were washed with warm PBS and centrifuged at 400 x *g* for 5 min at room temperature. Supernatant was discarded and the pellet gently re-suspended in supplied re-suspension buffer R to a final density of 1 x 10^7 cells/ml and gently pipetted to obtain a single cell suspension. A Neon® tube containing 3 ml Electrolytic buffer was placed into the Neon® pipette station. 500 ng of an endoribonuclease-prepared siRNA (esiRNA) targeted against Atg5 (Sigma-Aldrich, Mission® esiRNA mouse Atg5 (esiRNA1) # EMU038061) was added to a cell suspension at a density of 5 x 10^6 cells/ml and cells were pulsed once at a voltage of 1350 and pulse width of 30 ms. Transfected cells were then seeded either into 6-well plates (Whitehead Scientific, #S00023) or into T25 flasks at a seeding density of 1 x 10^5 cells/well and 4 x 10^5 cells/flask respectively. Plates or flasks were gently swirled and incubated at an atmosphere of 37 ºC and 5% CO_2 humidity for 24 hours. esiRNA against Mouse Kif11 (Sigma-Aldrich, Mission esiRNA mouse Kiff11 #EMU017691) was used as a positive control, and esiRNA against enhanced green fluorescent protein (eGFP) (Sigma-Aldrich, Mission esiRNA eGFP #EHU019931) served as a negative control.

2.17. *In vivo* Tumour-bearing Mouse Model

Ethical approval for the *in vivo* animal study was obtained from the animal research ethics committee (REC) of Stellenbosch University (no. SU-ACUD15-00027). All protocols in this study were carried out according to the guidelines for the care and use of laboratory animals implemented at Stellenbosch University. Eight week-old female C57BL/6 mice were obtained from the University of Stellenbosch Tygerberg breeding facility and housed at the Stellenbosch University animal unit under reverse dark/light cycle and temperature controlled conditions. For the duration of the study all animals were maintained on a standard chow diet and tap water *ad lib*. A total of 40 mice were utilized for this study. Prior to induction of cancer, female mice were randomized (into two groups, n=20 per group) and placed into one of two groups. One group was inoculated with tumours (using the syngeneic E0771 murine breast cancer cell line) and upon tumour appearance, each group was further divided into two sub-groups (n=10) where only one sub-group received doxorubicin treatment. Animals were routinely monitored and weighed twice a week prior to the initiation of the experiment, after which tumour volume and weight was recorded every second day for the duration of the study.

2.17.1. Tumour Inoculation

Mice were inoculated subcutaneously on the right pad of the fourth mammary gland with 200 µl of 2.5 x 10^5 E0771 cells suspended in Hanks Balanced Salt Solution (HBSS) (Sigma Chemical Co., St Louis, MO, USA), using a 23-gauge needle. The use of the murine E0771 breast cancer cell line in this tumour-bearing mouse model, previously established in our lab, is a more physiologically relevant model as it makes use of normal (non-immunocompromised) C57BL/6 mice with a syngeneic cancer cell line for tumour inoculation. Tumour dimensions were obtained every second day using digital callipers

where length (longest dimension) and width (dimension perpendicular to length) was recorded. Tumour volume was then calculated using the following equation:

$$\text{Tumour volume } (mm^3) = \frac{length \times width^2}{2}$$

2.17.2. Doxorubicin Treatment

Doxorubicin (LKT Laboratories, #D5794) stock solutions for the *in vivo* animal study were prepared in Hanks Balanced Salt Solution (HBSS) and made up to a concentration of 2 mg/ml. Once tumours became palpable doxorubicin treatment was initiated and was administered via intraperitoneal (i.p.) injection using a 25 gauge needle every third day. Animals were weighed prior to the preparation of the doxorubicin and further dilutions in HBSS were performed to obtain a final injection volume of 100 µl per mouse. Animals received three doses of 4 mg/kg doxorubicin (resulting in a cumulative dosage of 12 mg/kg), whereas, control animals received an isovolumetric i.p. injection of HBSS.

2.17.3. Animal Euthanasia and Tissue Harvesting

The study was terminated when tumours reached a volume of 400 mm^3. Additional humane endpoints were established in the event that animals lost more than 10% body weight or upon the occurrence of bleeding ulcers at the tumour site. Animals were anaesthetised using 3% isofluorane (Isofor, Safeline Pharmaceuticals) and euthanasia was achieved by means of exsanguination through cardiac puncture. Tumours were then carefully excised and processed appropriately. Tumours from some of the animals (6 animals per group) were divided into two parts. One part was snap frozen in liquid nitrogen and subsequently stored at -80 °C for further analysis by means of Western blot

experiments. The second part, was stored in formalin at room temperature for additional immunohistochemistry analysis. Tumours from the remaining animals (4 animals per group) were placed in a sterile petri dish for 3D culture of isolated epithelial organoids.

2.18. 3D Culture of Isolated Tumour Epithelial Organoids

Organoids are defined as being miniaturized and simplified organs which are produced *in vitro* through the dissociation of harvested tissue. When cultured in three dimension (3D) they depict a realistic micro-anatomy. Organoids are currently a widely accepted model in cancer research due to the fact that they better recapitulate the physiological structure and response of tumours *in vivo*.

2.18.1. Isolation of Mammary Epithelial Organoids

Under sterile conditions in a tissue culture hood, harvested tumour and mammary fat pad samples used for primary 3D cell culture models were minced using a scalpel (25 – 50 times per sample) until the tissue relaxed. Minced samples were then transferred into a sterile 50 ml tube containing 10 ml filtered collagenase solution (DMEM/F12 media containing 2 mg/ml collagenase (Sigma-Aldrich, collagenase from *Clostridium histolyticum* #C2139), 2 mg/ml trypsin (Life Technologies, #27250018), 5% FBS (Scientific Group), 5 µg/ml Insulin (Sigma-Aldrich, #I9278) and 50 µg/ml gentamicin (Life Technologies, #15750037)). The suspension was shaken at 110 – 150 RPM for 30 - 40 min in an orbital shaker set to 37ºC until the tissue was broken up into smaller pieces and relatively dispersed (care was taken to ensure that the samples were not over-digested). Samples were then centrifuged at 1500 RPM for 10 min at room temperature. The top opaque fatty layer was carefully removed using a sterile pipette coated with a BSA solution and placed

into a sterile BSA coated 15 ml tube. At this stage samples have been separated into three distinct layers; a top fatty layer, middle aqueous layer and a red epithelial pellet layer at the bottom. As the top fatty layer could still contain additional epithelial organoids which can be harvested, this layer was removed and placed into a clean BSA coated 15ml Falcon tube. The fatty layer was then dispersed by pipetting the solution up and down vigorously prior to being centrifuged again. Following the second centrifugation step, the pellets from both samples were combined and re-suspended in 10 ml of DMEM/F12. Samples were then centrifuged again at the same settings and the resultant pellet was re-suspended in 4 ml DMEM/F12 media. DNase I (2 U/µl) was then added to each sample and gently inverted by hand at room temperature for 2 – 5 min. The addition of DNase I to the solution allows for clusters of cells to be broken up, in addition it also allows for the detachment of organoids from single cells. Samples were then centrifuged again at 1500 RPM for 10 min at room temperature. Finally, differential centrifugation was performed in order to obtain a pellet containing epithelial cell organoids without single cells.

2.18.2. Organoid Density Determination

The density of the organoids obtained from each tumour was determined by re-suspending the final pellet in 10 ml of fresh DMEM/F12 media. Once a homogenous solution was obtained, 50 µl was transferred to a sterile 30 mm Petri dish and the number of organoids visible counted under a microscope. The total number of organoids collected from each tumour sample was calculated using the following equation:

$$Total\ number\ of\ organoids = \frac{number\ of\ organoids}{sample\ volume\ (50\ \mu l)} \times remaining\ volume\ (9950\ \mu l)$$

Samples were then adjusted to 1000 organoids / ml in order to simplify the allocation of organoids to ECM gels. The required number of organoids for each experiment was then calculated and the appropriate volume of each sample was aliquoted into sterile BSA-coated 1.5 ml microcentrifuge tubes. Tubes were then centrifuged at 1500 RPM for 5 min at room temperature and the appropriate volume of ECM solution was added to each tube in order to obtain a final density of 2 organoids / µl.

2.18.3. Plating of Organoids in Matrigel

Prior to plating, growth factor reduced Matrigel (BD Biosciences, #354230) was allowed to thaw at 4 ºC for 3 – 4 hours. In the meantime, a 24-well black glass bottomed plate was pre-incubated at 37 ºC for 5 min before being placed directly onto a heating block set to 37 ºC inside a tissue culture hood. The appropriate volume of liquid Matrigel needed was then placed into the sterile microcentrifuge tube containing the organoid pellet. The organoid pellet was re-suspended by gently pipetting the Matrigel solution up and down on ice. The appropriate volume of Matrigel / organoid solution was then plated into each well. The plate was then placed on the heating block set to 37 ºC for several minutes in order to allow for further gelation before being incubated at 37 ºC, 5% CO_2 for 30 – 60 minutes. Pre-warmed organoid medium (DMEM/F12 containing 1% PenStrep and 1% insulin-transferrin-selenium X (ITS) (Life Technologies, #51500) and 2.5 nM EGF (Sigma Aldrich, #F0291) was added to each well. In order to prevent dehydration of samples, sterile PBS was added to empty wells. Plates were then incubated for 24 hours before treatment commenced.

2.18.4. Branching Morphogenesis and Invasion Assays

Subsequent to plating, isolated organoids were allowed to equilibrate at 37 ºC, 5% CO_2 for 24 hours. Control (0 hr) images were acquired using an Olympus® Cell^R system and Olympus® IX81 inverted fluorescence microscope (Olympus®, GMBH Japan), which is equipped with a temperature-controlled incubator system that was set to 37 °C and a motorized stage control that allows exact coordinate positions to be saved and accessed at a later point in time. For each animal two separate wells were imaged for each treatment group and a total of 12 organoids across each group were imaged and used in all subsequent time-points (0, 12, 24, 36, and 48 hours). Subsequent to the acquisition of the first images, organoids were treated with freshly collected MEF conditioned media. Across the imaging time points, organoids were refreshed with new media every 24 hours. Image analysis was performed using ImageJ analysis software where branching morphogenesis and the rate of invasion was calculated using the software by demarcating the leader cell migration front on scaled images and then calculating the distance travelled over time as a ratio of organoid surface area.

2.19.Western Blotting Analysis of Whole Tumour Samples

In order to carry out western blot analysis snap frozen tumour and mammary fat pad samples were divided into two smaller sections. One section was then processed for Western blot analysis and the other section was frozen and stored at -80 °C and utilized.

2.19.1. Protein Extraction and Quantification

Samples were immediately placed on ice and allowed to thaw at 4 °C. 300 µl of ice cold modified radioprecipitation (RIPA) buffer comprising of 2.5 mM Tris-HCL, 1 mM EDTA, 1

mM dithiothreitol, 0.1 mM phenylmethylsulfonyl fluoride (PMSF), 1 mM benzamidine, 50 mM NaF, 4 mg/ml SBTI, 10 mg/ml leupeptin, 0.1% SDS 0.5%, Na deoxycholate and 1% NP40, calibrated to pH 7.4, was added to each sample and allowed to stand for 5 min on ice in order to extract total cell protein. Samples were then homogenized on ice, with the blades of the homogeniser being cleaned using EtOH between each sample in order to prevent cross contamination of proteins. Upon the formation of a homogenous liquid which contained no lumps of whole tissue, samples were centrifuged at 14 000 RPM for 1 hour at 4 °C. At this stage, samples had been separated into four distinct layers, two top fat layers, a middle supernatant layer and a bottom pellet. In order to prevent the oily fat layer from mixing into the supernatant and causing smudges to form during SDS-PAGE, sterile 23-guage needles were used to remove the supernatant from the sides of Eppendorf tubes. The supernatant was then placed into clean Eppendorf tubes and samples were centrifuged again at 14 000 RPM for 30 minutes at 4 °C. The process of removing the supernatant was repeated and samples were stored at -80 ºC ready for protein quantification. A Direct Detect® infrared spectrometer (DDHW00010-WW, Merck) was used to determine the protein content of each sample and aliquots were prepared containing 20 µg protein content diluted with sample buffer. SDS-PAGE was performed for each sample as previously described (Section 2.7.3).

2.20. Tissue Processing and Sectioning

Formalin fixed tissue samples were placed into individually labelled cassettes and underwent (i) dehydration, (ii) “clearing” and (iii) impregnation with paraffin wax using an automated tissue processor (Leica Biosystems, #TP1020) set to follow a 20 hour pre-programmed time-schedule. Dehydration of samples was achieved by soaking samples in an increasing concentration series of ethanol solutions, namely; 2 rounds of 70%

ethanol for 90 minutes each, 90% ethanol for 90 minutes, 2 rounds of 95% ethanol for 90 minutes each, 2 rounds of 100% ethanol for 90 minutes each and then a final 100% ethanol solution for 120 minutes. Clearing of tissues was then achieved through a 90 minute xylene incubation step followed by a second xylene incubation for 120 minutes. Finally, wax impregnation was achieved with two 120 minute paraffin wax incubation steps. Following the automated tissue processing protocol, samples were placed into clean individually labelled cassettes, where samples were orientated in such a way as to achieve a longitudinal section through the sample. Cassettes were then filled with hot paraffin wax and allowed to cool on a cold block, before being sectioned into 5 µm sections using a microtome (Leica Biosystems, #RM2235). Three sections of each sample was placed onto a slide and slides were placed to on a pre-warmed heating plate to dry. Prior to any staining procedures samples were deparaffinised and rehydrated using an automated stainer (Leica Biosystems, # ST4020), where samples were dipped in xylene twice, 100% ethanol, 90% ethanol, 70% ethanol and 50% ethanol, samples remained in each solution for a period of 2 minutes before being placed into distilled water (dH_20), ready for subsequent staining steps.

2.20.1. Histological Staining

Following sectioning, deparaffinization and rehydration, tissue samples were stained for ultrastructure changes (haemotoxylin and eosin (H&E) staining) as well as for fibrosis (picrosirius red staining). H&E staining of tissue samples was achieved using an automated tissue stainer (Leica Biosystems, # ST4020), where slides where dipped into a haemotoxylin solution, followed by dH_2O, scott's tap water, dH_2O, eosin and dH_2O. Samples remained in each solution for a period of 2 minutes before coverslips were mounted using DPX mounting media. Picrosirius red staining for fibrosis was achieved by

staining sections for 1 hour at room temperature using a 0.1% Sirius red solution dissolved in aqueous picric acid. Samples were then washed twice using 0.5% hydrogen chloride (acidified) water, dehydrated and then mounted with DPX mounting media.

2.20.2. Immunofluorescent Staining of Tumour Samples

Following sectioning onto poly-L-lysine coated glass slides, tumour samples were deparaffinised and rehydrated. Tumour sections were then fixed for 8 minutes at room temperature with a 0.25% Triton-x-100 solution made up in DPBS. The fixative mixture was then removed and sections were placed back into Coplin jars containing dH_20. During the process of formalin fixation, methylene bridges form causing the cross-linking of proteins, and thus allowing for the preservation of cellular and subcellular structure. Protein cross-linking results in the antigenicity of some cell structures to be reduced, causing the obstruction of antibody binding. In order to overcome this cross-linking, heat-induced antigen retrieval was performed by boiling a Coplin jar containing a 10 mM sodium citrate, 0.05% Tween 20 (pH 6.0) solution in a 95 °C water bath and then placing samples into the solution for 20 minutes. Coplin jars containing samples were removed from the water bath and allowed to cool to room temperature before samples were removed and blocked using 5% donkey serum for 1 hour. Samples were then incubated overnight at 4 ºC in primary antibodies against alpha smooth muscle actin (α-SMA) (Abcam, #ab7817) and vimentin (Cell Signalling Technologies, #D21H3) diluted in PBS containing 3% BSA (1:250). Samples were then rinsed three times with PBS and allowed to incubate with the appropriate secondary antibody for 1 hour at room temperature. In this case Alexa Fluor 488 conjugated donkey anti-mouse secondary antibody (Life Technologies, #A-21206) and Alexa Fluor 564 conjugated donkey anti-rabbit secondary antibody (Life Technologies, #A-21244) were used. Tumour samples were rinsed and mounted with

DAKO fluorescent mounting medium (DAKO Inc., CA, USA). All samples were kept wrapped in foil at -20 °C until analysis on a Zeiss confocal microscope. In each condition, three images across two different sections were obtained.

2.21.Statistical Analysis

All statistical analyses was carried out using GraphPad Prism 5. All data was assessed using mean ± standard error of the mean (SEM). All *In vitro* experiments made use of both technical (three separate wells or flasks) and biological (three separate experiments) replicates One-way or two-way analysis of variance (ANOVA) with Bonferroni post hoc test as well as t-tests were conducted where appropriate. A p-value ≤0.05 was considered statistically significant.

Chapter 3: Results

3.1. Induction of Oxidative Stress without Cell Death in E0771 Breast Cancer Cells

3.1.1. Time-Dependent Changes in Viability Following Glucose Deprivation

In order to establish a time course of glucose deprivation that elicits the least cytotoxic effect in E0771 cancer cells, while still producing a significant increase in oxidative stress, E0771 murine breast cancer cells were treated for various time points with glucose free DMEM. MTT cell viability assays were carried out to determine the relative percentage cell death at different treatment time points.

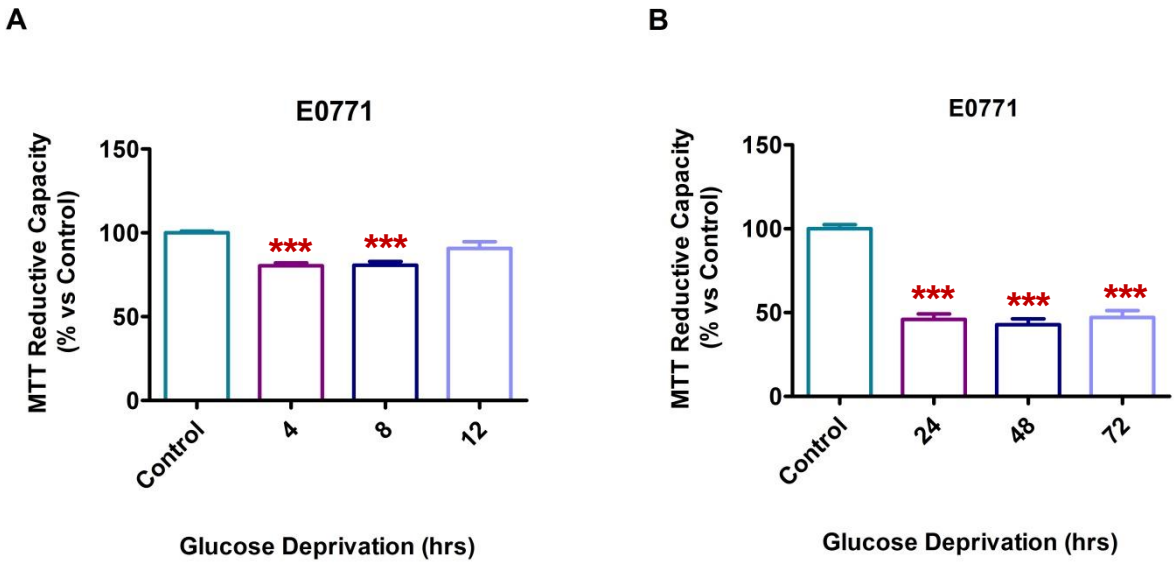

Figure 3.1: The effects of short (A) and long (B) term glucose deprivation on the viability of E0771 murine breast cancer cells. E0771 cells were incubated in 25 mM glucose containing DMEM (Control), or glucose free (0 mM) DMEM for 4, 8 and 12 hours or for 24, 48 and 72 hours. Cell viability was assessed using the MTT assay. Statistical analysis: One way ANOVA with Bonferroni post hoc correction. All results are presented as mean ± SEM (n=3). *** = $p<0.001$ vs control.

When compared to control, a significant decrease in MTT reductive capacity was observed in E0771 murine breast cancer cells following 4, 8, 24, 48 and 72 hours of glucose deprivation (4 hours: 80.42% ± 1.687% vs 100% ± 1.011%, $p<0.001$; 8 hours: 80.75% ± 2.197% vs 100% ± 1.011%, $p<0.05$; 24 hours: 45.90% ± 3.321% vs 100% ± 2.475%, $p<0.0001$; 48 hours: 42.76% ± 3.476% vs 100% ± 2.475%, $p<0.0001$ and 72 hours: 47.069% ± 4.149% vs 100% ± 2.475%, $p<0.0001$). However when subjected to 12 hours of glucose deprivation no significant change in reductive capacity was observed (90.67% ± 3.959% vs 100% ± 1.011%, $p=0.1445$) when compared to control.

In order to determine if the increased mitochondrial reductive capacity observed after 12 hours of glucose deprivation is a cell line specific compensation, we carried out time responses for glucose deprivation in four other human triple negative cancer cell lines. A significant reduction in MTT reductive capacity was observed in the MDA-MB-23 human breast cancer cell line across all time points following glucose deprivation (4 hours: 66.44% ± 2.410% vs 100% ± 3.600%, $p<0.0001$; 8 hours: 73.32% ± 1.248% vs 100% ± 3.600%, $p<0.0001$; 12 hours: 81.52% ± 3.511% vs 100% ± 3.600%, $p<0.0001$; 24 hours: 71.80% ± 2.033% vs 100% ± 3.408%, $p<0.0001$; 48 hours: 63.22% ± 1.566% vs 100% ± 3.408%, $p<0.0001$ and 72 hours: 61.30% ± 2.111% vs 100% ± 2.475%, $p<0.0001$). However, an increase in MTT reductive capacity was seen following 12 hours of glucose deprivation in MDA-MB-231 cells when compared to the 8 hour time point (81.52% ± 3.511% vs 73.90% ± 1.248%, $p<0.0001$

In comparison to control, a significant reduction in MTT reductive capacity was observed in HCC-70 human breast cancer cells following 4, 24, 48 and 72 hours of glucose deprivation (4 hours: 86.81% ± 2.269% vs 100% ± 2.269%, $p<0.0001$; 24 hours: 73.71% ± 4.052% vs 100% ± 1.465%, $p<0.0001$; 48 hours: 77.37% ± 5.202% vs 100% ± 3.408%, $p<0.0001$ and 72 hours: 80.24% ± 6.110% vs 100% ± 1.465%, $p<0.0029$).

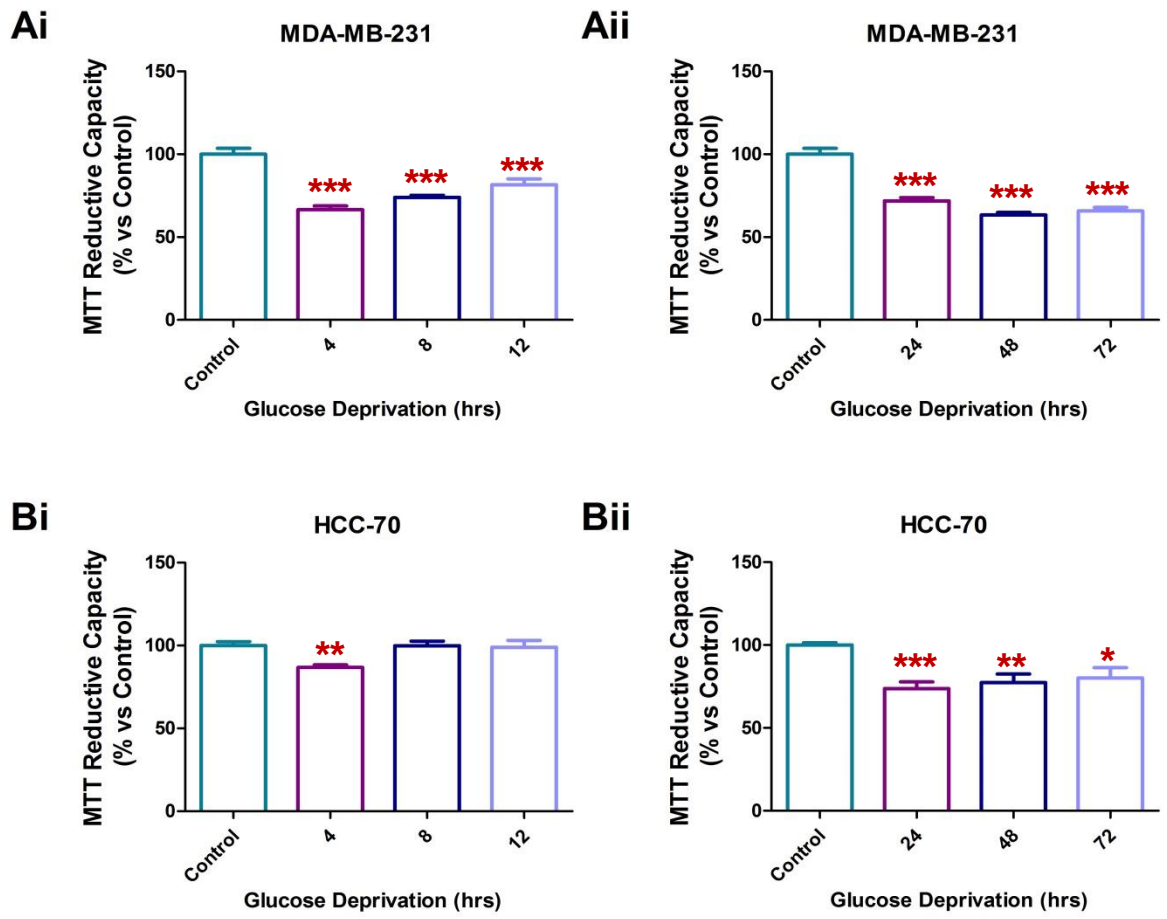

Figure 3.2: The effects of short (A) and long (B) term glucose deprivation on the viability of human MDA-MB-231 and HCC-70 breast carcinoma cells. MDA-MB-231 and HCC-70 cells were incubated in 25 mM glucose containing DMEM (Control), or glucose free (0 mM) DMEM for 4, 8 and 12 hours or for 24, 48 and 72 hours. Cell viability was assessed using the MTT assay. Statistical analysis: One way ANOVA with Bonferroni post hoc correction. All results are presented as mean ± SEM (n=3). * = $p<0.05$ vs control, ** = $p<0.001$ vs control and *** = $p<0.001$ vs control.

Assessment of mitochondrial reductive capacity in BT-549 human breast cancer cells showed a significant reduction in MTT reduction following 8, 24, 48 and 72 hours of glucose deprivation when compared to control (79.80% ± 2.104% vs 100% ± 3.612%, $p<0.0001$, 24 hours: 73.55% ± 4.756% vs 100% ± 1.401%, $p<0.0001$; 48 hours: 77.03% ± 5.438% vs 100% ± 1.401%, $p=0.0002$ and 72 hours: 77.10% ± 5.099% vs 100% ± 1.401%, $p<0.0001$). However, when BT-549 cells were subjected to both 4 and 12 hours of glucose deprivation no significant reduction in MTT reductive capacity was observed.

Finally, the subjection of the non-adherent DU4475 human breast cancer cells to glucose deprivation resulted in a significant reduction in mitochondrial reductive capacity following 8, 24, 48 and 72 hours (8 hours: 90.18% ± 1.867% vs 100% ± 1.552%, p=0.0005, 24 hours: 83.61% ± 2.038% vs 100% ± 2.734%, p<0.0001; 48 hours: 74.38% ± 2.773% vs 100% ± 2.734%, p<0.0001 and 72 hours: 75.58% ± 3.302% vs 100% ± 2.734%, p<0.0001) when compared to control. In comparison to the 8 hour glucose deprivation time point in DU4475 cells a significant increase in MTT reduction was observed following 12 hours of glucose deprivation (96.43% ± 1.920% vs 90.18% ± 1.730%, p=0.0264).

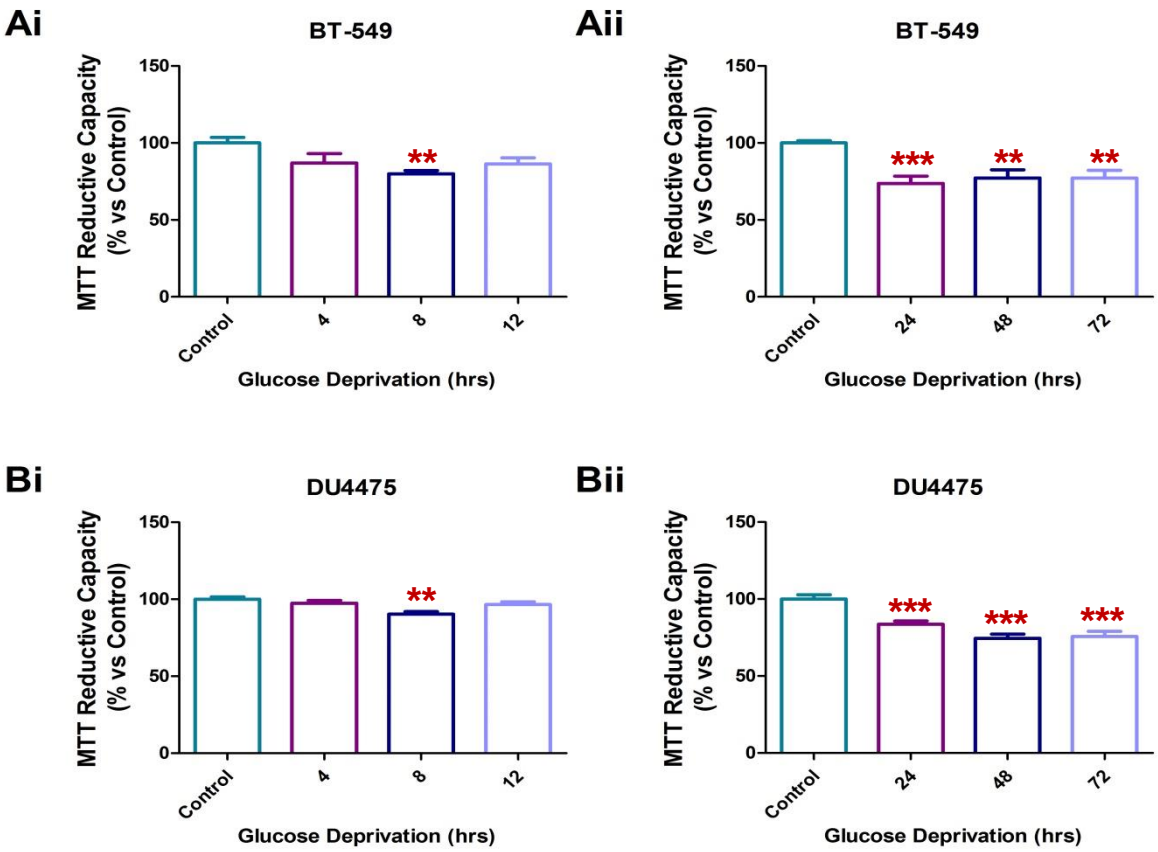

Figure 3.3: The effects of short (A) and long (B) term glucose deprivation on the viability of human BT-549 and DU4475 breast carcinoma cells. BT-549 and DU4475 cells were incubated in 25 mM glucose containing DMEM (Control), or glucose free (0 mM) DMEM for 4, 8 and 12 hours or for 24, 48 and 72 hours. Cell viability was assessed using the MTT assay. Statistical analysis: One way ANOVA with Bonferroni post hoc correction. All results are presented as mean ± SEM (n=3). ** = p<0.001 vs control and *** = p<0.001 vs control.

Based on initial time responses and cell death analyses, long term (24 – 72 hours) glucose deprivation in the E0771 murine breast cancer cells lead to a significant reduction in MTT reductive capacity with a significant increase in the protein expression of key cell death markers, therefore these time points were disregarded for all subsequent experiments.

3.1.2. Effect of Glucose Deprivation on Cell Death Induction

3.1.2.1. PARP-cleavage

Poly (ADP-ribose) Polymerase (PARP) is a 116 kDa nuclear protein that plays a critical role in DNA damage repair mechanisms (Grasso *et al*., 2012). PARP is synthesized upon the fragmentation of DNA in the presence of nuclear poly-ADP ribosylated proteins. Its activation then occurs when PARP binds to broken DNA strands. Through the poly (ADP-ribosylation of various nuclear proteins, PARP utilizes nicotinamide adenine dinucleotide (NAD^+) as a substrate. Therefore, it was originally thought that PARP contributes to apoptotic cell death via cellular depletion of NAD^+ and ATP. However, PARP has been shown to be cleaved by caspase-3 during the initial stages of apoptosis into 24- and 89 kDa fragments respectively containing the enzymatic DNA –binding domains and active sites (Boulares *et al*, 1999). Once cleaved the smaller 24 kDa fragment binds to fragmented DNA ends, inhibiting the access of DNA repair enzymes, and thus ensuring the cells' commitment to apoptosis (Grasso *et al*., 2012).

Therefore, PARP expression was assessed as a marker of nuclear damage and apoptosis induction in the E0771 cancer cells in response to glucose deprivation. Although Western blots show a trend towards an increase in PARP expression following 8 hours of glucose deprivation no statistically significance was seen across all treatment groups when compared to control.

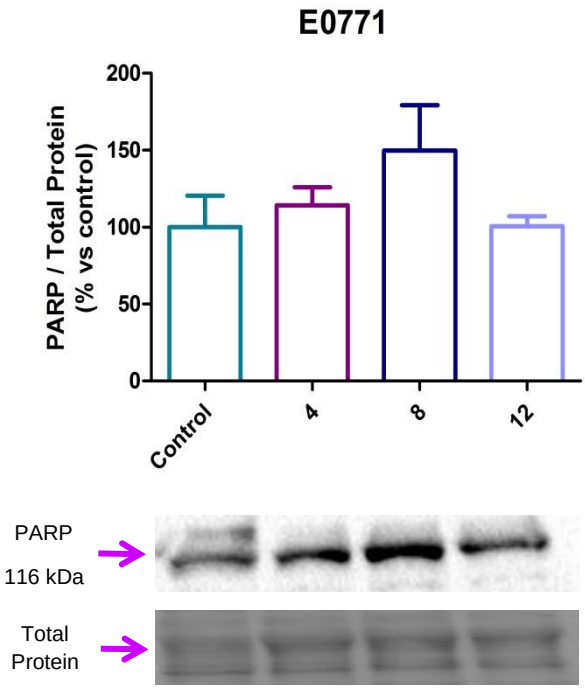

Figure 3.4: Western Blot analysis of PARP in E0771 mouse breast cancer cells following glucose deprivation. E0771 cells were subjected to (1) Control, (2) 4, (3) 8 and (4) 12 hours of glucose deprivation. Statistical analysis: One way ANOVA with Bonferroni post hoc correction. All results are presented as mean ± SEM (n=6).

3.1.2.2. Ratio of Cleaved Caspase-3 to Caspase-3

Caspase-3 is an executioner caspase which leads to the induction of apoptotic cell death upon its cleavage by upstream initiator caspases. Western blot analysis for both caspase-3 and cleaved caspase-3 was used to assess apoptotic activity in E0771 cells following glucose deprivation. A significant increase in cleaved caspase-3 was seen following 8 hours of glucose deprivation (144.5 ± 18.19% vs 100% ± 6.186%, p=0.0432) when compared to control. However, when total caspase-3 protein expression was compared to control no significant differences were observed across all three treatment groups. As the cleavage of caspase-3 is required for the initiation of apoptosis the ratio of cleaved caspase-3 to total caspase-3 protein expression, could provide a better understanding of the initiation of cell death in E0771 cells following glucose deprivation.

When compared to control, a significant increase in the ratio of cleaved caspase-3 to caspase-3 was seen in both the 4 hour and 8 hour glucose deprived treatment groups (4 hours: 161.0 ± 17.58% vs 100% ± 10.58%, p=0.0138 and 8 hours: 150.2 ± 18.11% vs 100% ± 10.58%, p=0.0404).

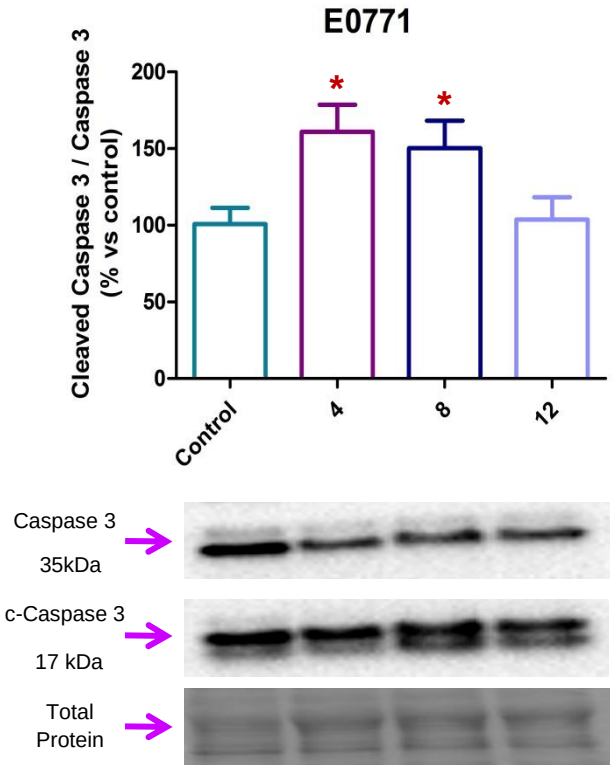

Figure 3.5: Western Blot analysis of the ratio of cleaved caspase-3 to total caspase-3 in E0771 mouse breast cancer cells following glucose deprivation. E0771 cells were subjected to (1) Control, (2) 4, (3) 8 and (4) 12 hours of glucose deprivation. Statistical analysis: One way ANOVA with Bonferroni post hoc correction. All results are presented as mean ± SEM (n=6). * = $p<0.05$ vs control.

3.1.3. Effects of Glucose Deprivation on Oxidative Stress

In order to determine the effects of glucose deprivation on oxidative stress, E0771 cells were stained with either DCF (cytosolic H_2O_2) or MitoSOX (mitochondrial $O_2^{\bullet}$-) and the mean fluorescent intensity was measured by means of flow cytometry. No significant increases in the ability of glucose deprivation to generate cytoplasmic hydrogen peroxide

were observed across all three time points. However, a significant increase in mitochondrial superoxide was observed following 12 hours of glucose deprivation alone in comparison to control (146.1 ± 8.938% vs 100 ± 1.586%, p=0.0001).

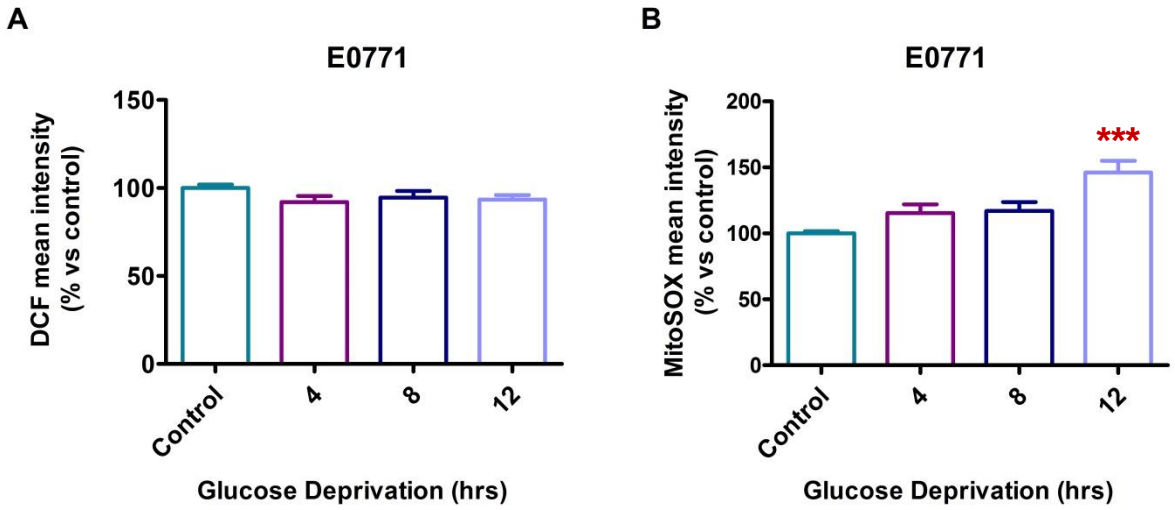

Figure 3.6: The effects of short term glucose deprivation on cytosolic H_2O_2 (A) and mitochondrial $O_2^{\bullet-}$ (B) production in E0771 murine breast cancer cells. E0771 cells were incubated in 25 mM glucose containing DMEM (Control), or glucose free (0 mM) DMEM for 4, 8 and 12 hours. Oxidative stress was assessed by means of flow cytometry. Statistical analysis: One way ANOVA with Bonferroni post hoc correction. All results are presented as mean ± SEM (n=3). *** = p<0.001 vs control.

Based on initial time responses for glucose deprivation, a treatment time of 12 hours did not lead to a significant reduction in cell viability, however, an increase in oxidative stress in the E0771 murine breast cancer cells was observed. Therefore this time point was chosen for all subsequent experiments.

3.2: Proteomics Analysis of E0771 Conditioned Media

3.2. Proteomic Analysis of E0771 Conditioned Media

In order to determine the protein composition present in conditioned media generated from E0771 murine breast cancer cells following glucose deprivation proteomic analysis was performed, wherein protein abundance of regulated proteins adhering to the predetermined selection criteria (see section 2.4.4), were normalized to control (for list of regulated proteins refer to section 7.1.1). Briefly, a total of 62 protein elements were found exclusively in the glucose deprived E0771 conditioned media, whereas a total of 41 protein elements were displayed exclusively in control conditioned media. A total of 3 protein elements were found to be present in both conditions.

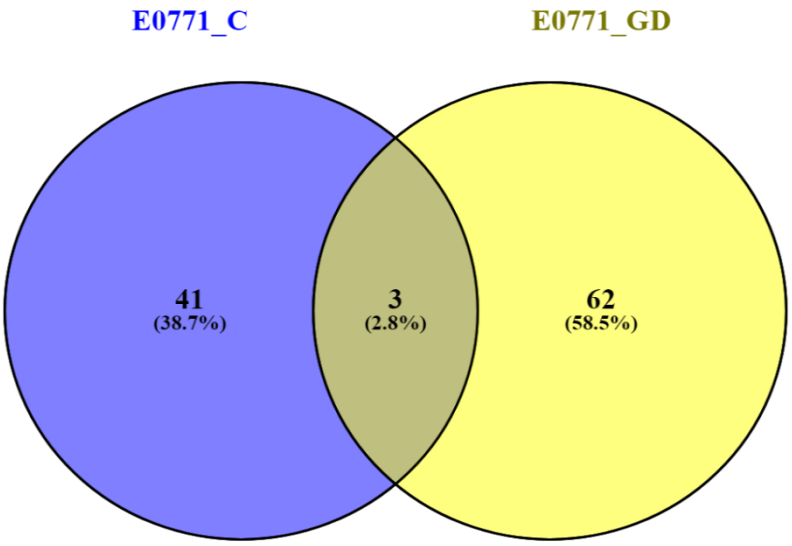

Figure 3.7: Broad overview of protein elements differentially regulated between control and glucose deprived conditioned media generated from E0771 breast cancer cells. E0771 cells were incubated in 25 mM glucose containing DMEM (E0771_C), or glucose free (0 mM) DMEM (E0771_GD) for 12 hours. Diagram generated by CPGR using Venny freeware.

3.2.1. Biological Processes Downregulated in the Glucose Deprived Group

GO terms obtained from the list of proteins found to be downregulated in conditioned media derived from E0771 breast cancer cells were submitted into REVIGO and proteins

were clustered according to biological processes. Although a number of GO terms were identified to be downregulated in response to glucose deprivation, REVIGO collapsed all of these terms into a single biological process. The size of “bubbles” (nodes) generated by REVIGO is indicative of the number of specific GO terms collapsed into it. Therefore larger nodes imply a lower specificity. Although all nodes displayed are significant ($p<0.05$ translates to a –log[p-value] >1.3) the colour of the node is representative of the significance of terms collapsed into it. Based on the fact that REVIGO clustered our list of downregulated proteins into a single biological process with a low significance, these were not interrogated further using DAVID.

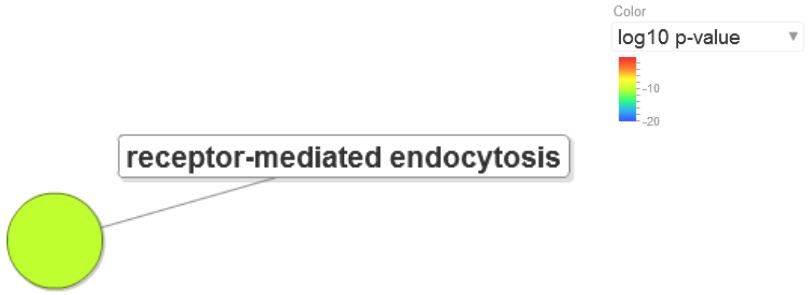

Figure 3.8: Scatterplot view of biological processes downregulated in E0771 cancer cells following 12 hours of glucose deprivation. Graph generated in REVIGO using GO terms.

3.2.2. Biological Processes Upregulated in the Glucose Deprived Group

Again as mentioned above, GO terms obtained for proteins upregulated in response to glucose deprivation were submitted into REVIGO, and a scatterplot view of protein clusters for biological processes which are upregulated was generated. A large number of biological processes were found to be upregulated in the conditioned media of glucose deprived E0771 breast cancer cells, many of which were observed to be involved in cell migration and metabolism. In terms of cell migration, a significant upregulation in the Wnt signalling pathway, ephrin receptor signalling pathway, ARP2/3 complex-mediated actin nucleation as well cell-cell adhesion was observed. An upregulation of both canonical

glycolysis and gluconeogenesis was also observed. Of additional interest, we also observed a significant upregulation in the cellular response to reactive oxygen species as well as processes involved in protein polyubiquitination.

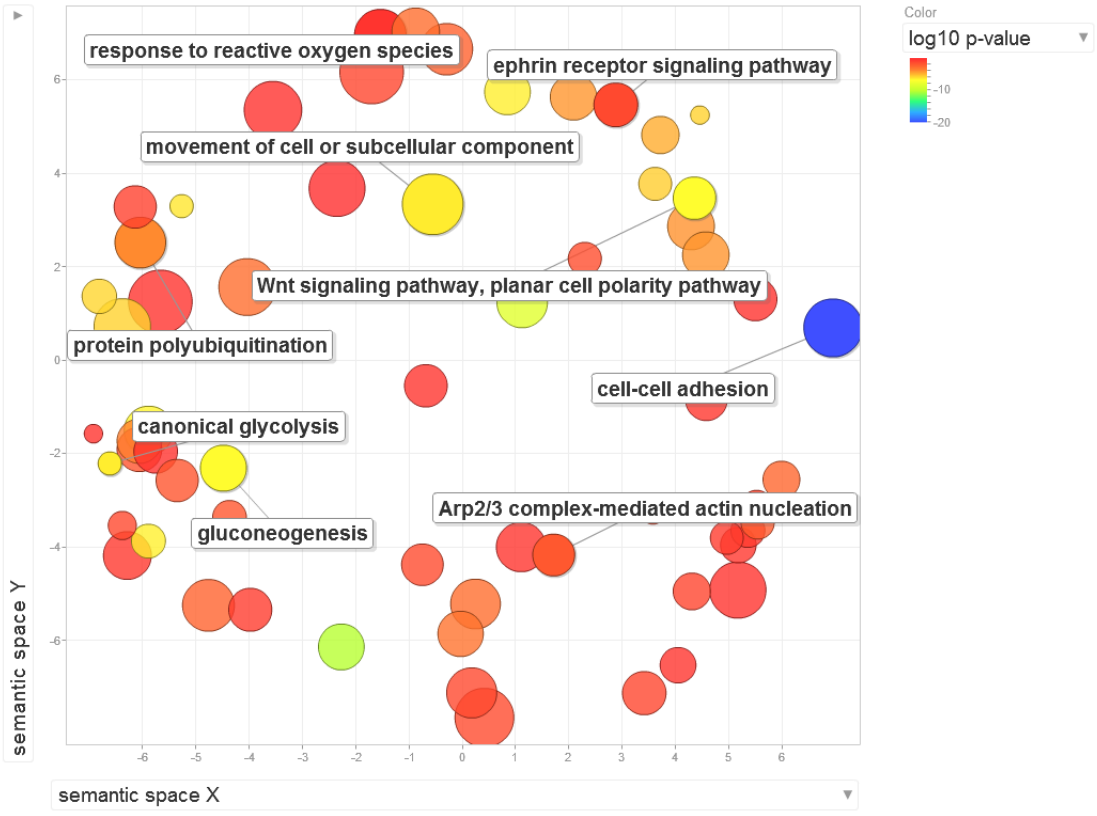

Figure 3.9: Scatterplot view of biological processes upregulated in E0771 cancer cells following 12 hours of glucose deprivation. Graph generated in REVIGO using GO terms.

Based on the interesting biological processes we observed to be upregulated in REVIGO, we further interrogated the protein list for similar clustering using Functional Annotation Clustering (FAC) in DAVID. Clustering of common processes in both REVIGO and DAVID can be interpreted as highly significant, as different clustering algorithms are used by the two software programs. Interrogation of functional clustering in DAVID also revealed a significant upregulation in cell-cell adhesion processes with a large number of proteins found to be clustered together.

Proteins involved in cell-cell adhesion of most interest, within the context of this study, were found to be the upregulation of vinculin (VCL), AHNAK nucleoprotein (AHNAK), profilin 1 (PFN1) and heat shock proteins (HSP) 70 and 90.

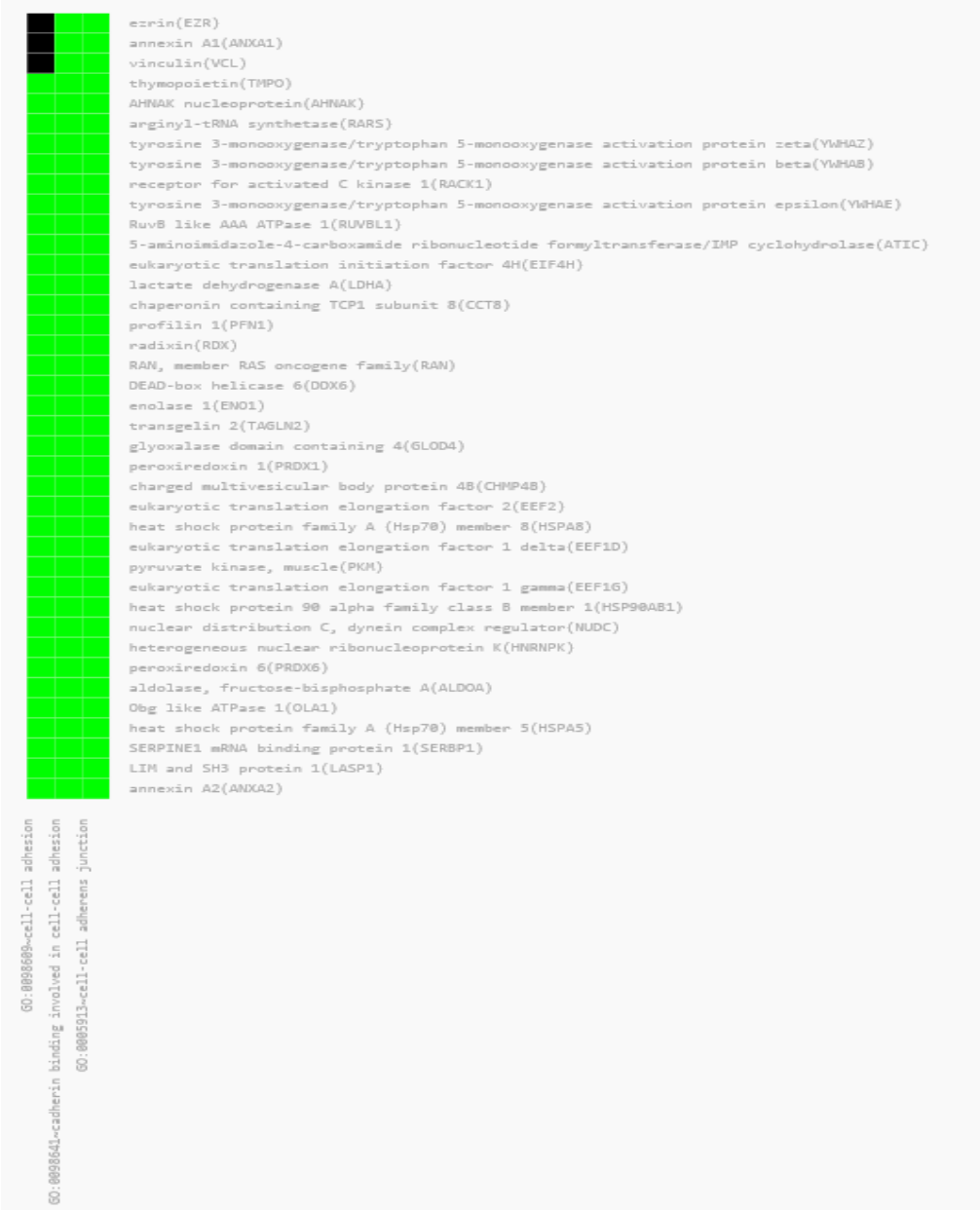

Figure 3.10: 2D viewer of functional annotation clustering of upregulated proteins involved in cell-cell adhesion in E0771 cancer cells following 12 hours of glucose deprivation. Graph generated in DAVID using UniProt accession numbers.

A significant clustering of proteins involved in glycolysis, gluconeogenesis and a variety of metabolic pathways were also observed in DAVID. Again proteins, of interest in the context of

this study, involved in cellular metabolism were identified to be glucose-6-phosphate dehydrogenase (G6PD), lactate dehydrogenase A (LDHA), pyruvate kinase, muscle (PKM), enolase -1 (ENO1) and -3 (ENO3).

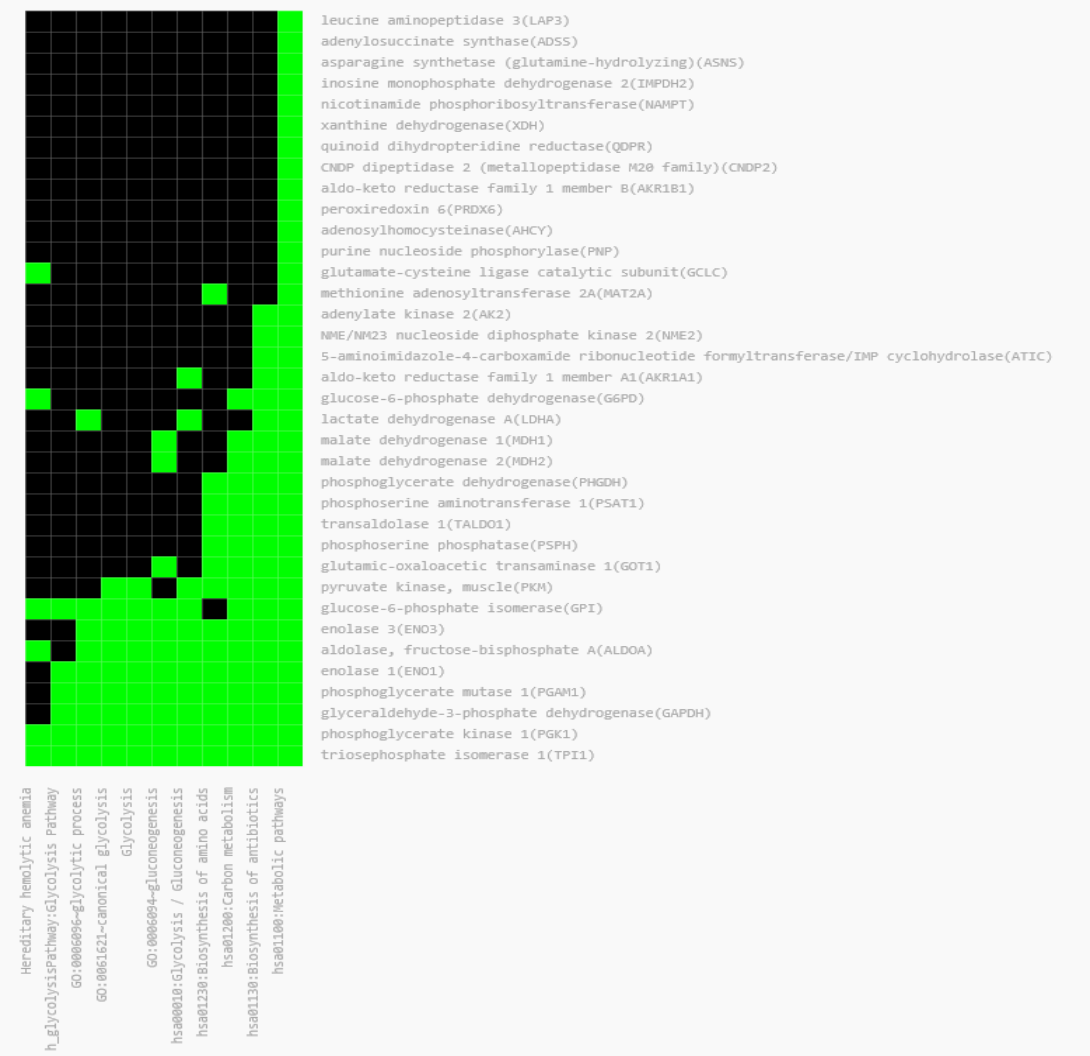

Figure 3.11: 2D viewer of functional annotation clustering of upregulated proteins involved in glycolytic, gluconeogenesis and metabolic pathways in E0771 cancer cells following 12 hours of glucose deprivation. Graph generated in DAVID using UniProt accession numbers. Proteins are displayed horizontally and their functional relationship is displayed vertically.

Additionally, significant clustering of proteins involved in PI3K/Akt signalling was observed in glucose deprived E0771 conditioned media. Of particular interest for this study is the

upregulation of the proteins, collagen type IV alpha 2 chain (COL4A2), laminin subunit gamma I (LAMC1), heat shock protein 90 (HSP90) and insulin like growth factor 1 (IGF1).

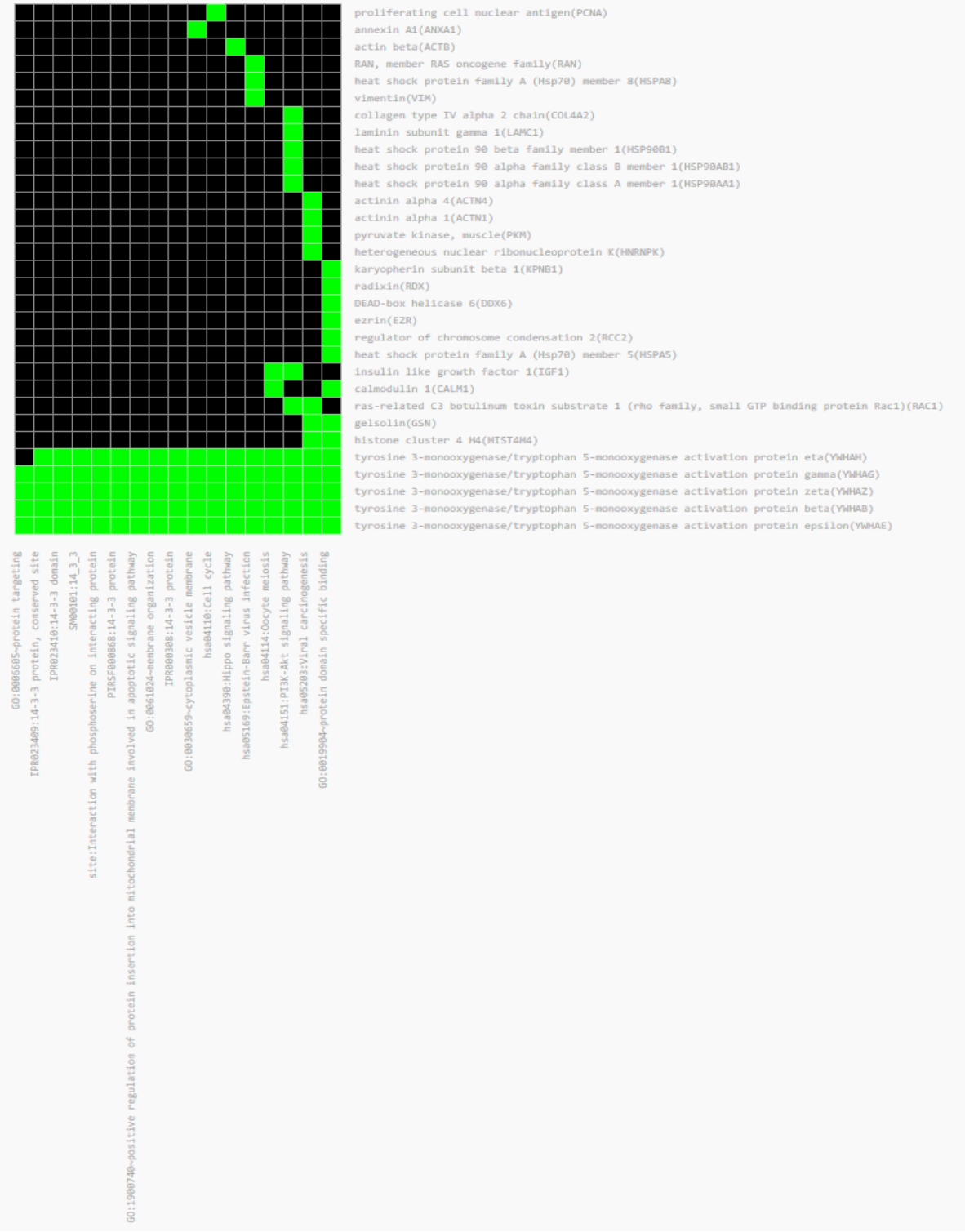

Figure 3.12: 2D viewer of functional annotation clustering of upregulated proteins involved in PI3K/Akt signalling in E0771 cancer cells following 12 hours of glucose deprivation. Graph generated in DAVID using UniProt accession numbers.

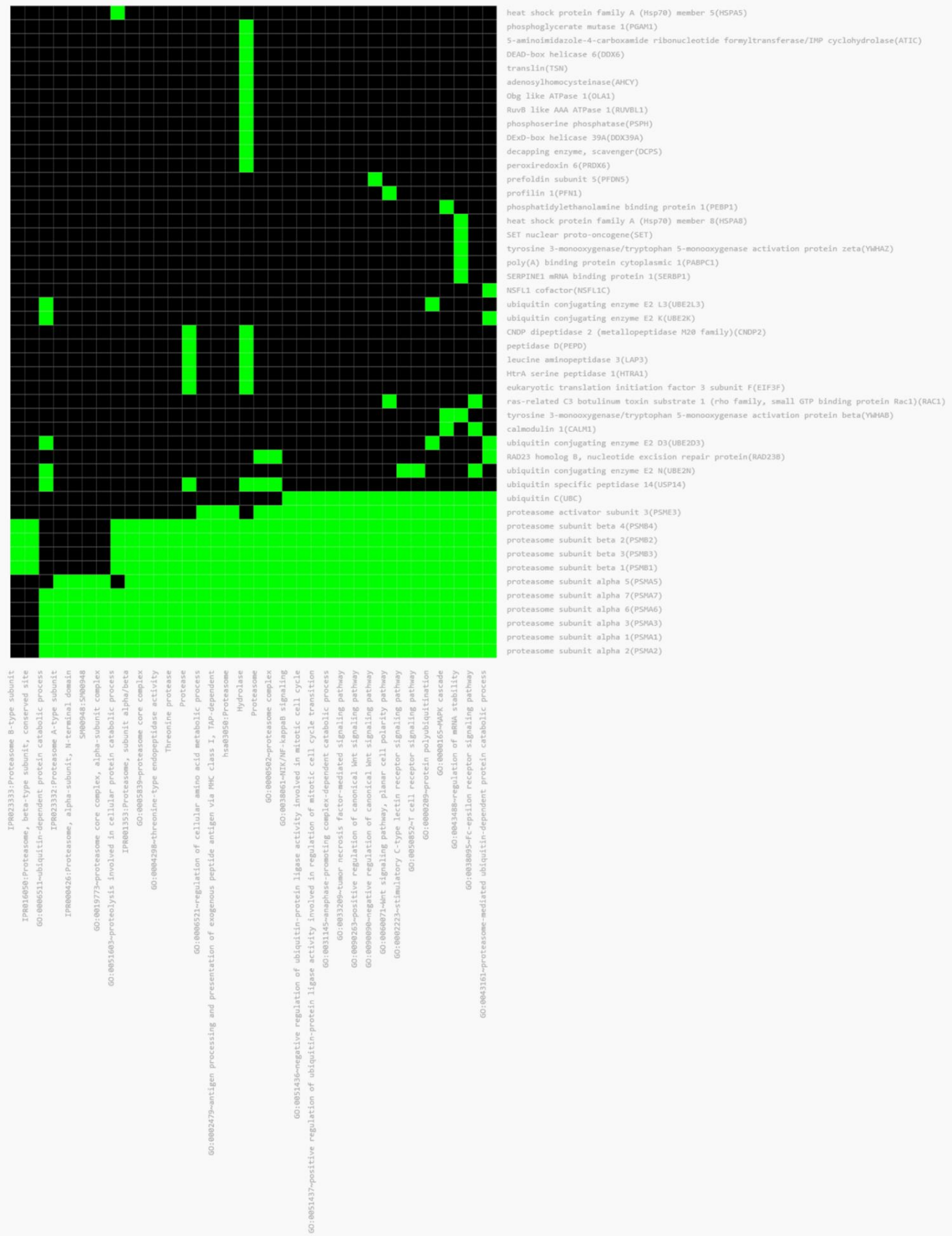

Figure 3.13: 2D viewer of functional annotation clustering of upregulated proteins involved in Wnt signalling, protein catabolism and protein polyubiquitination in E0771 cancer cells following 12 hours of glucose deprivation. Graph generated in DAVID using UniProt accession numbers. Proteins are displayed horizontally and their functional relationship is displayed vertically.

Finally, the functional clustering of proteins involved in the Wnt signalling pathway, protein polyubiquitination and protein catabolism using DAVID revealed an upregulation in the proteasome subunits alpha (PSMA) 1, 2, 3, 5, 6 and 7, involved in Wnt signalling, protein catabolism and polyubiquitination. Additionally, an upregulation was seen in the proteasome subunits beta (PSMB) 1, 2, 3 and 4 and ubiquitin C (UBC), all of which are linked to both Wnt signalling and protein polyubiquitination.

3.3: Effects of E0771 Conditioned Media on Cancer-Associated Fibroblasts Metabolism

3.3. Effects of E0771 Conditioned Media on Cancer-Associated Fibroblasts Metabolism

3.3.1. Verifying the "Activation" of Cancer-Associated Fibroblast

Currently, there is not one unique marker that identifies a cancer-associated fibroblast, currently the concurrent expression of several protein markers are rather used to define CAFs within the tumour microenvironment (Giannoni *et al*., 2010, Erez *et al*., 2010). Therefore, in order to determine whether mouse embryonic fibroblasts were able to "activate" a cancer-associated fibroblast phenotype in response to treatment with glucose deprived E0771 conditioned media, MEF cells were cultured under standard cellular conditions and following treatment, confocal microscopy and Western blot analysis was performed to assess the relative expression of the protein markers; α-smooth muscle actin (α-SMA), platelet derived growth factor receptor α (PDGFRα), vimentin and E-cadherin.

3.3.1.1. Confocal Microscopy

To assess the "activation" of MEFs to a cancer-associated phenotype in response to treatment with glucose deprived E0771 conditioned media, MEF cells were cultured under standard cellular conditions until reaching confluency; following treatment, cells were immunostained with α-SMA:AlexaFluor 488, vimentin: AlexaFluor 595 and Hoechst 33342 and visualized using confocal fluorescent microscopy. Visually a distinct increase in fluorescent intensity was observed in both the mesenchymal markers α-smooth muscle actin (α-SMA) and vimentin in MEF cells that were treated with either untreated E0771 conditioned media or glucose deprived E0771 conditioned media.

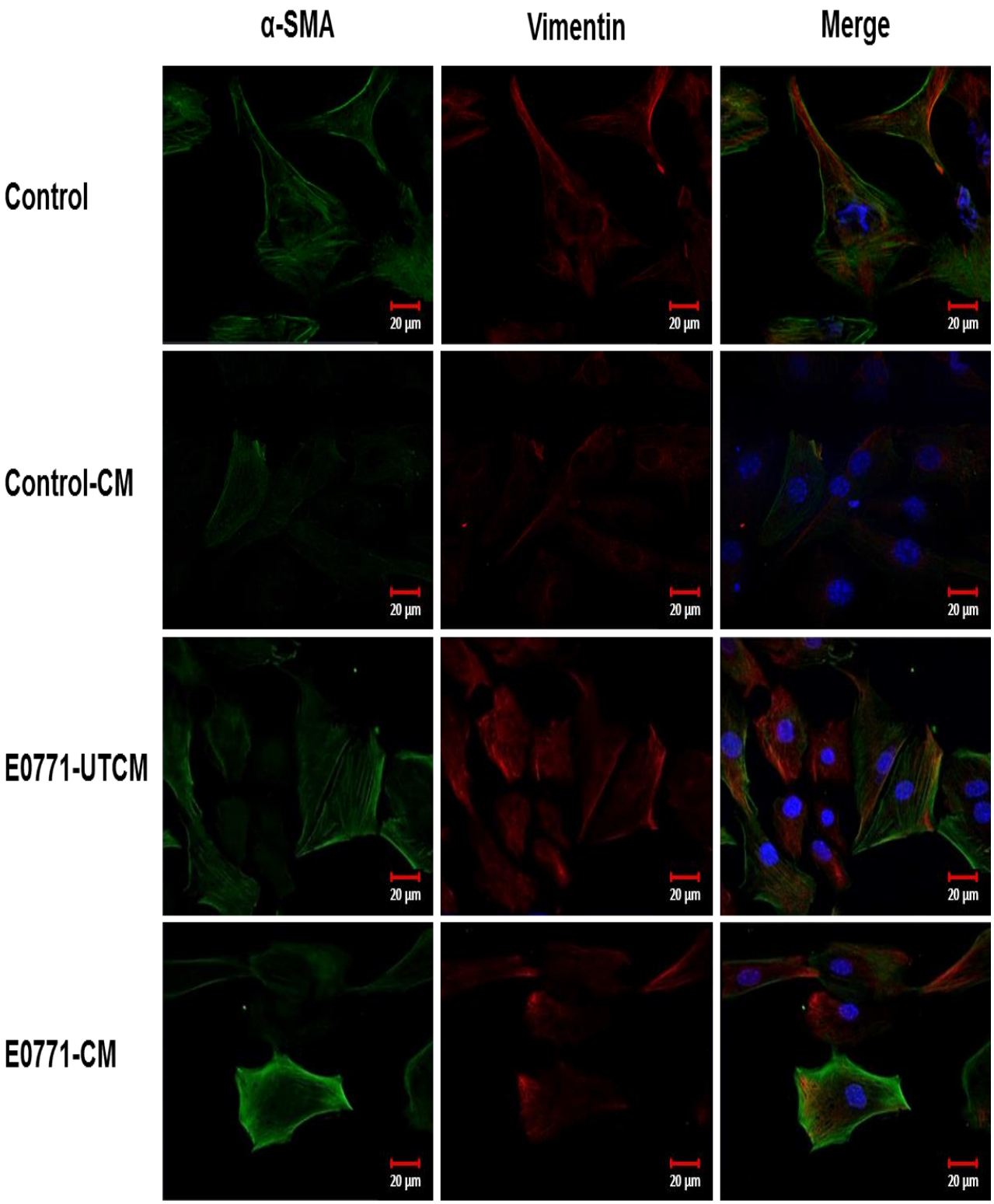

Figure 3.14: Characterization of cancer-associated fibroblast "activation" of mouse embryonic fibroblasts (MEF) cells. MEF cells were cultured under standard control cellular conditions in 8-well chamber plates. MEF cells were then subjected to (1) Control, (2) Control conditioned media, (3) E0771 untreated conditioned media and (4) glucose deprived E0771 conditioned media for 24 hours. Cells were immunostained for α-SMA (Green), vimentin (Red) and Hoechst 33342 (Blue) and visualized using fluorescent confocal microscopy. Images acquired at 60x magnification.

3.3.1.2. Western blot Analysis of CAF Markers

3.3.1.2.1. α-SMA and PDGFRα

The mouse embryonic fibroblast (MEF) cells showed a significant increase in α-smooth muscle actin (α-SMA) protein levels following treatment with E0771-CM in comparison to control (166.8% ± 21.71% vs 100% ± 11.67%, p=0.0133) and Control-CM (166.8% ± 21.71% vs 103.3% ± 13.07%, p=0.0214). Although α-SMA levels were increased following treatment with E0771-UTCM they were not significant, when compared to either control (131.0 ± 16.39% vs 100% ± 11.67%, p=0.1460) or control-CM (131.0 ± 16.39% vs 103.3% ± 13.07%, p=0.2075). Furthermore, no statistically significant differences in PDGFRα across all treatment groups were observed when compared to control.

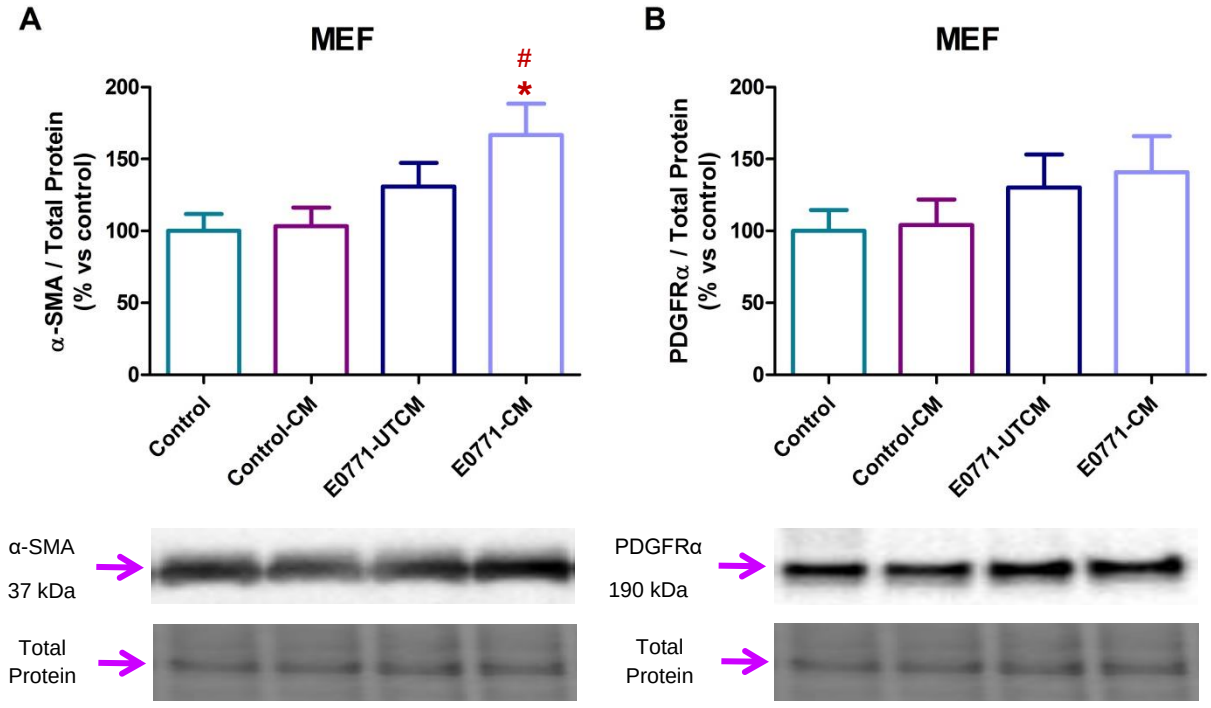

Figure 3.15: Western blot analysis of α-SMA and PDGFRα in mouse embryonic fibroblast (MEF) cells following E0771 conditioned media treatment. MEF cells were subjected to (1) Control, (2) Control conditioned media (Control-CM), (3) E0771 untreated conditioned media (E0771-UTCM) and (4) glucose deprived E0771 conditioned media (E0771-CM) for 24 hours. Statistical analysis: One way ANOVA with Bonferroni post hoc correction. All results are presented as mean ± SEM (n=6). * = $p<0.05$ vs control. # = $p<0.05$ vs control-CM.

3.3.1.2.2. Vimentin and E-cadherin

Examination of vimentin protein expression revealed a significant increase in protein levels with E0771-CM treatment when compared to control (253.5% ± 39.91% vs 100% ± 16.85%, p<0.0001) and control-CM (253.5% ± 39.91% vs 122.6% ± 16.67%, p=0.0073). Additionally, an increase vimentin expression was seen with E0771-UTCM treatment (173.4% ± 20.92% vs 100% ± 16.85%, p=0.0172) when compared to control.

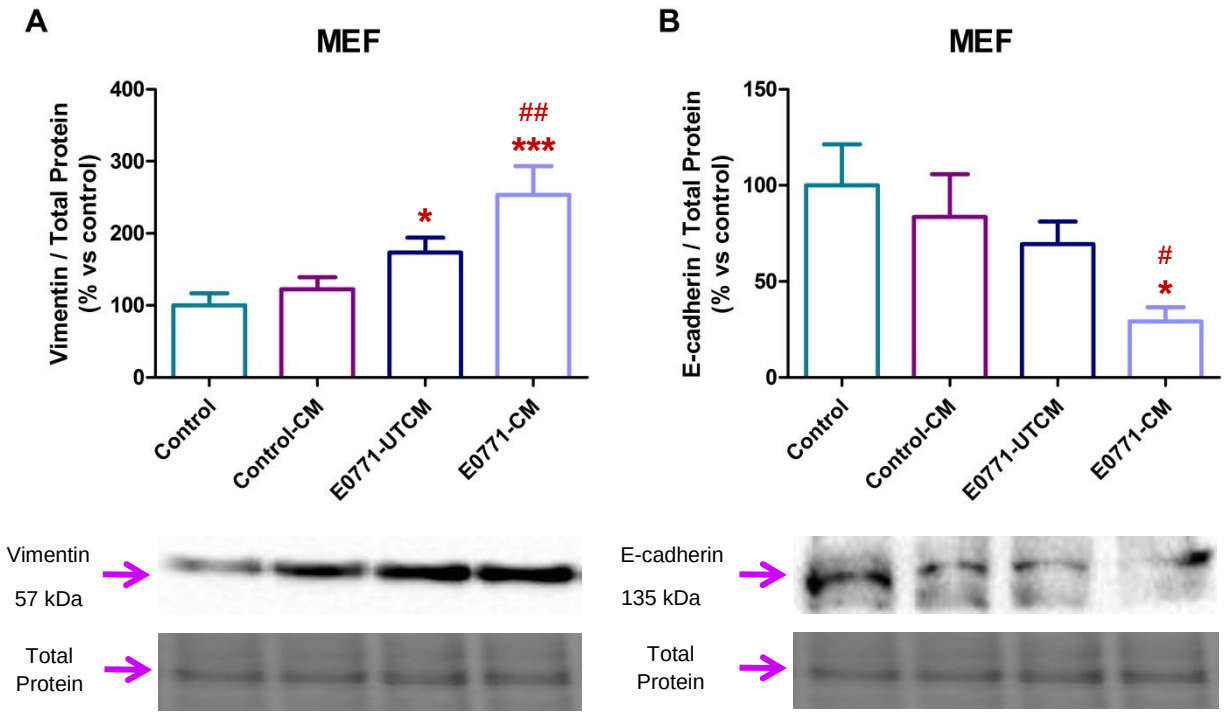

Figure 3.16: Western blot analysis of vimentin and E-cadherin in mouse embryonic fibroblast (MEF) cells following E0771 conditioned media treatment. MEF cells were subjected to (1) Control, (2) Control conditioned media (Control-CM), (3) E0771 untreated conditioned media (E0771-UTCM) and (4) glucose deprived E0771 conditioned media (E0771-CM) for 24 hours. Statistical analysis: One way ANOVA with Bonferroni post hoc correction. All results are presented as mean ± SEM (n=6). * = p<0.05 vs control, *** = p<0.0001 vs control, # = p<0.05 vs control-CM, ## = p<0.01 vs control-CM.

We also observed a significant decrease in the protein expression of the epithelial marker, E-cadherin, in MEF cells following E0771-CM treatment when compared to control (29.13% ± 7.375% vs 100% ± 21.29%, p=0.0071) and control-CM (69.38% ± 11.76% vs 83.62% ± 22.14%, p=0.0350). However, no statistical differences in E-cadherin

expression were seen following E0771-UTCM treatment when compared to either the control (69.38% ± 11.76% vs 100% ± 21.29%, p=0.2286) or control-CM (69.38% ± 11.96% vs 83.62% ± 22.14%, p=0.5792) groups.

3.3.2. Cell Viability

Subsequent to the verification of CAF "activation", MTT cell viability assays were carried out to assess the effects of E0771 conditioned media on mitochondrial reductive capacity. No significant changes in reductive capacity were observed following treatment with either control-CM or E0771-UTCM in comparison to control. However, a significant increase in MTT reductive capacity was seen following treatment with glucose deprived E0771-CM when compared to control (118.4 ± 2.899% vs 100% ± 2.976%, p<0.0001) as well as when compared to control-CM (118.4 ± 2.899% vs 97.36 ± 2.932%, p<0.0001).

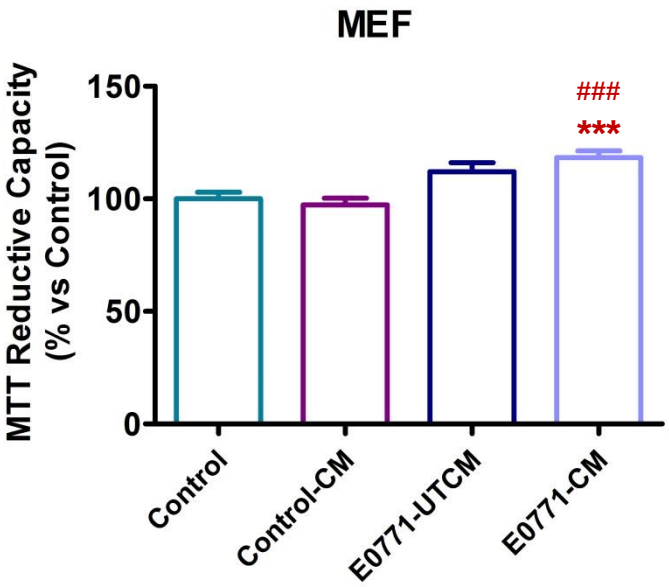

Figure 3.17: Determination of the effects of E0771 conditioned media on the viability of mouse embryonic fibroblast (MEF) cells. MEF cells were subjected to (1) Control, (2) Control conditioned media (Control-CM), (3) E0771 untreated conditioned media (E0771-UTCM) and (4) glucose deprived E0771 conditioned media (E0771-CM) for 24 hours. Statistical analysis: One way ANOVA with Bonferroni post hoc correction. All results are presented as mean ± SEM (n=3). *** = p<0.0001 vs control and ### = p<0.0001 vs control-CM.

3.3.3. Oxidative Stress Analysis

Oxidative stress was assessed based on the understanding that the secretion of hydrogen peroxide (H_2O_2) by epithelial cancer cells in response to either hypoxia and nutrient deprivation acts as the driving force for the induction of oxidative stress and the subsequent activation of autophagy within surrounding CAFs (Capparelli *et al*., 2011).

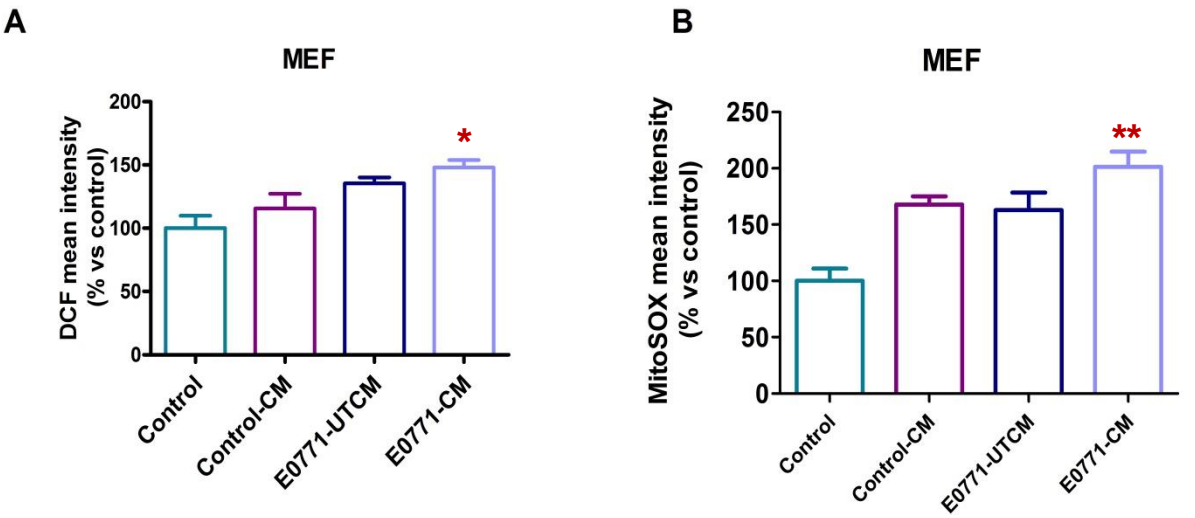

Figure 3.18: Determination of the effects of E0771 conditioned media on oxidative stress in mouse embryonic fibroblast (MEF) cells. MEF cells were subjected to (1) Control, (2) Control conditioned media (Control-CM), (3) E0771 untreated conditioned media (E0771-UTCM) and (4) glucose deprived E0771 conditioned media (E0771-CM) for 24 hours. Oxidative stress was assessed by means of flow cytometry following staining with either DCF or MitoSOX. Statistical analysis: One way ANOVA with Bonferroni post hoc correction. All results are presented as mean ± SEM (n=3). * = $p<0.05$ vs control and ** = $p<0.001$ vs control.

Oxidative stress was assessed following treatment with E0771 conditioned media by staining MEF cells with either DCF (cytosolic H_2O_2) or MitoSOX (mitochondrial $O_2^{\bullet}$-) and measuring mean fluorescent intensity using flow cytometry. Significant increases in both DCF (148.1% ± 5.719% vs 100% ± 9.960%, p=0.0138) and MitoSOX (201.4% ± 13.58% vs 100% ± 10.88%, p=0.0135) mean fluorescent intensity were observed following treatment with glucose deprived E0771-CM. However, no significant differences were observed across all treatment groups when compared to control-CM.

3.3.4. HIF-1α Protein Expression

ROS induced stabilization of HIF-1α has been shown to occur under hypoxic as well as normoxic conditions. Based on the significant induction of both cytosolic and mitochondrial ROS we observed in MEF cells subjected to 24 hour treatment with E0771 conditioned media, we aimed to assess the relative protein expression levels of HIF-1α to determine if ROS-induced HIF-1α expression plays a role in the metabolic reprogramming of CAFs. A significant increase in HIF-1α expression was seen following E0771-CM treatment when compared to both control (175.8% ± 14.31% vs 100% ± 15.28%, p=0.0223) and control-CM (175.8% ± 14.31% vs 71.02% ± 8.745%, p=0.0033).

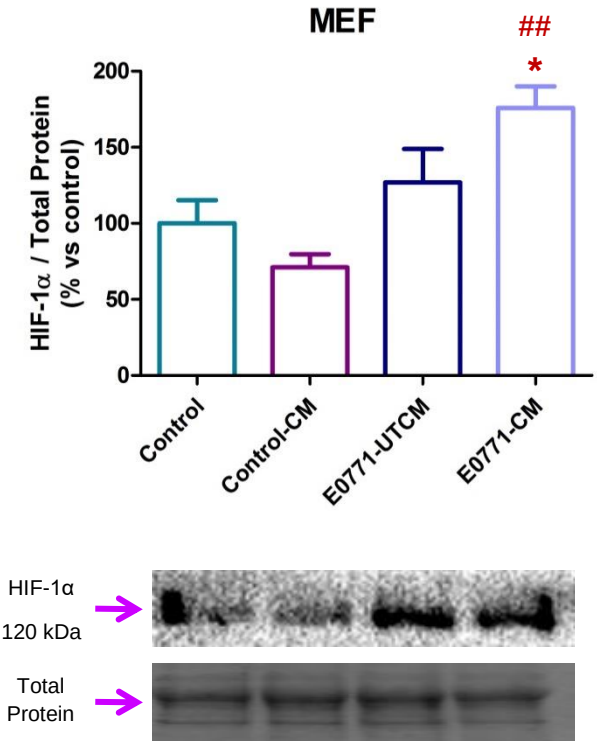

Figure 3.19: Western blot analysis of HIF-1α protein expression in MEF cells treated with E0771 conditioned media. MEF cells were subjected to (1) Control, (2) Control conditioned media (Control-CM), (3) E0771 untreated conditioned media (E0771-UTCM) and (4) glucose deprived E0771 conditioned media (E0771-CM) for 24 hours. Statistical analysis: One way ANOVA with Bonferroni post hoc correction. All results are presented as mean ± SEM (n=3). * = $p<0.05$ vs control and $^{\#\#}$ = $p<0.01$ vs control-CM

3.3.5. Autophagy Assessment

In order to determine whether treatment of MEF cells with E0771 conditioned media results in the induction of the autophagic process, Western blot analysis was carried out using recognised markers of autophagy, namely; mTOR, p62 and LC3.

3.3.5.1. p-mTOR (Ser2448) and mTOR

In comparison to the control group, a significant decrease in mTOR phosphorylation (Ser2448) was observed following E0771-UTCM (62.56% ± 7.071% vs 100% ± 7.699%, p=0.0231) and E0771-CM (45.02% ± 17.44% vs 100% ± 7.699%, p=0.0448) treatment.

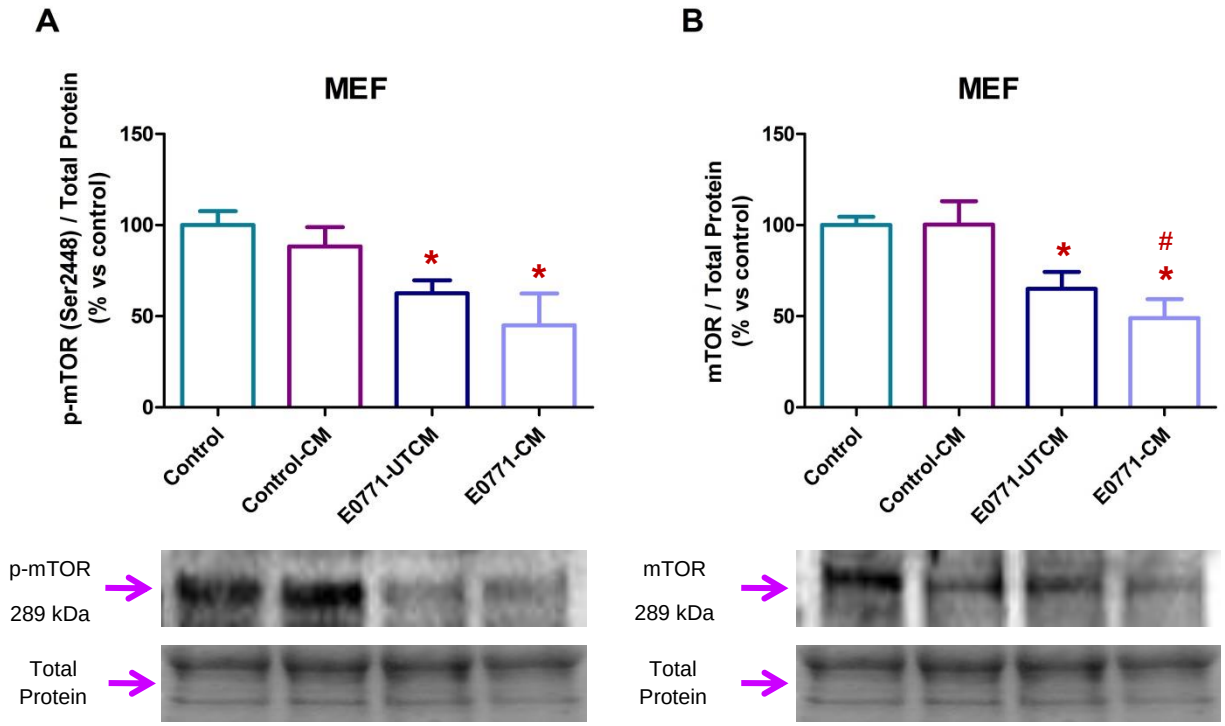

Figure 3.20: Western blot analysis of p-mTOR and total mTOR protein expression in MEF cells treated with E0771 conditioned media. MEF cells were subjected to (1) Control, (2) Control conditioned media (Control-CM), (3) E0771 untreated conditioned media (E0771-UTCM) and (4) glucose deprived E0771 conditioned media (E0771-CM) for 24 hours. Statistical analysis: One way ANOVA with Bonferroni post hoc correction. All results are presented as mean ± SEM (n=3). * = $p<0.05$ vs control, and # = $p<0.05$ vs control-CM.

Total mTOR assessment revealed a significant decrease in mTOR protein expression following E0771-UTCM (65.02% ± 9.242% vs 100% ± 4.529%, p=0.0273) and E0771-CM (48.88% ± 10.44% vs 100% ± 4.529%, p=0.0109) treatment in comparison to control. When compared to control-CM a significant decrease in total mTOR protein expression was only observed in the E0771-CM (48.88% ± 10.44% vs 100.4% ± 12.65%, p=0.0349) treated group.

3.3.5.2. LC3 II and p62

Assessment of LC3 II protein expression showed no significant differences across all treatment groups when compared to both control and control-CM.

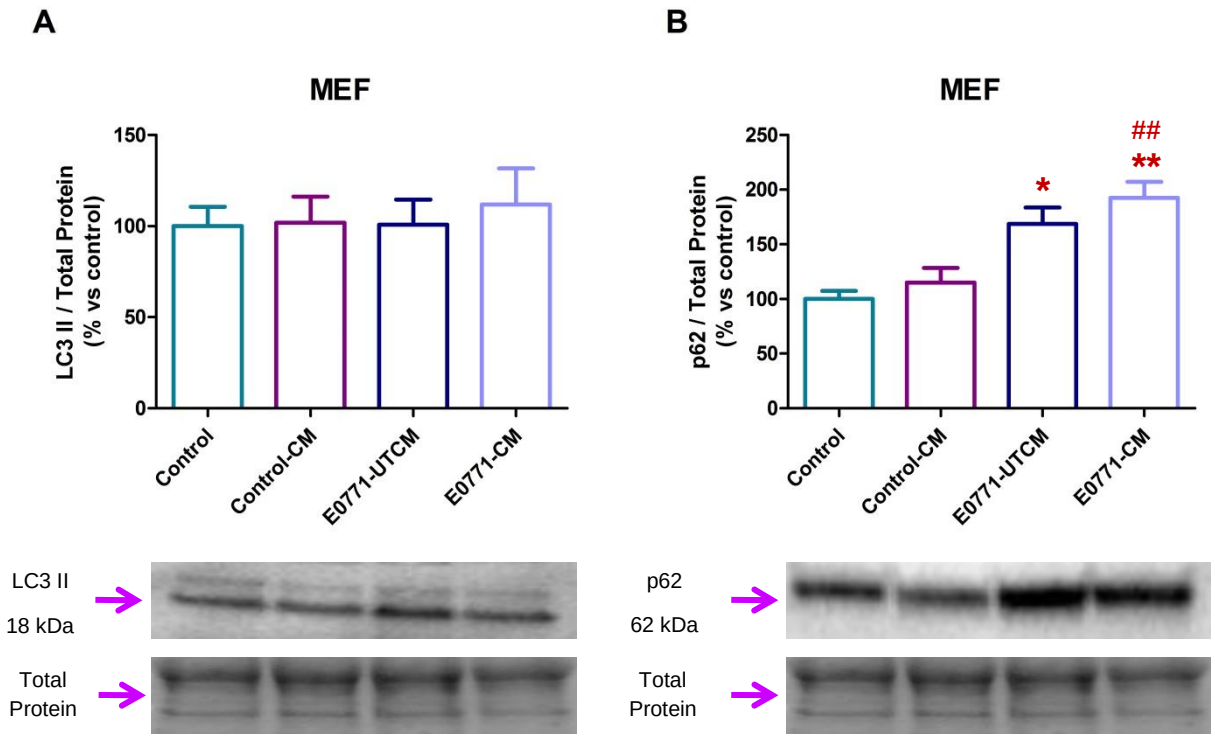

Figure 3.21: Western blot analysis of LC3 II and p62 protein expression in MEF cells treated with E0771 conditioned media. MEF cells were subjected to (1) Control, (2) Control conditioned media (Control-CM), (3) E0771 untreated conditioned media (E0771-UTCM) and (4) glucose deprived E0771 conditioned media (E0771-CM) for 24 hours. Statistical analysis: One way ANOVA with Bonferroni post hoc correction. All results are presented as mean ± SEM (n=3). * = p<0.05 vs control, ** = P<0.01 vs control and ## = p<0.01 vs control-CM.

A significant increase in p62 protein expression was seen in MEF cells following treatment with both E0771-UTCM (168.7% ± 14.90% vs 100% ± 7.353%, p=0.0061) and E0771-CM (192.6% ± 14.61% vs 100% ± 7.353%, p=0.0013) when compared to control. Furthermore, when compared to control-CM a significant increase in p62 expression was also observed in the E0771-CM (192.6% ± 14.61% vs 115.1% ± 13.38%, p=0.0079).

3.3.6. Glucose Uptake Assay

The effects of glucose deprived E0771 conditioned media on glucose uptake in MEFs was achieved by means of flow cytometry with the utilization of 2-NBDG, a fluorescently labelled deoxyglucose analog. A significant increase in 2-NBDG mean fluorescent intensity was observed in MEF cells following treatment with glucose deprived E0771-CM when compared to control (132.1% ± 10.95% vs 100% ± 3.722%, p=0.0107) and when compared to control-CM (132.1% ± 10.95% vs 105.8% ± 6.120%, p=0.0475).

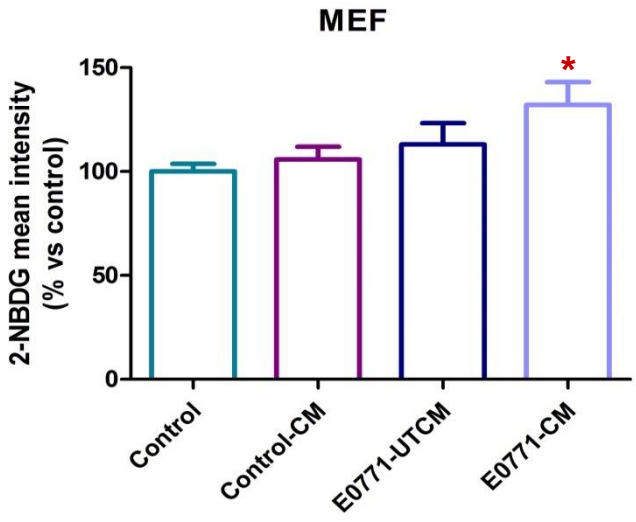

Figure 3.22: Determination of the effects of E0771 conditioned media on glucose uptake in mouse embryonic fibroblast (MEF) cells. MEF cells were subjected to (1) Control, (2) Control conditioned media (Control-CM), (3) E0771 untreated conditioned media (E0771-UTCM) and (4) glucose deprived E0771 conditioned media (E0771-CM) for 24 hours. Statistical analysis: One way ANOVA with Bonferroni post hoc correction. All results are presented as mean ± SEM (n=3). * = p<0.05 vs control.

3.3.7. GLUT4 Translocation

In order to determine whether the increase in glucose uptake observed in MEF cells following treatment with glucose deprived E0771-CM is in part mediated by the translocation of the GLUT4 transporter to the plasma membrane, MEF cells were first transfected with a HA-GLUT4-GFP expressing plasmid and then visualized using confocal microscopy.

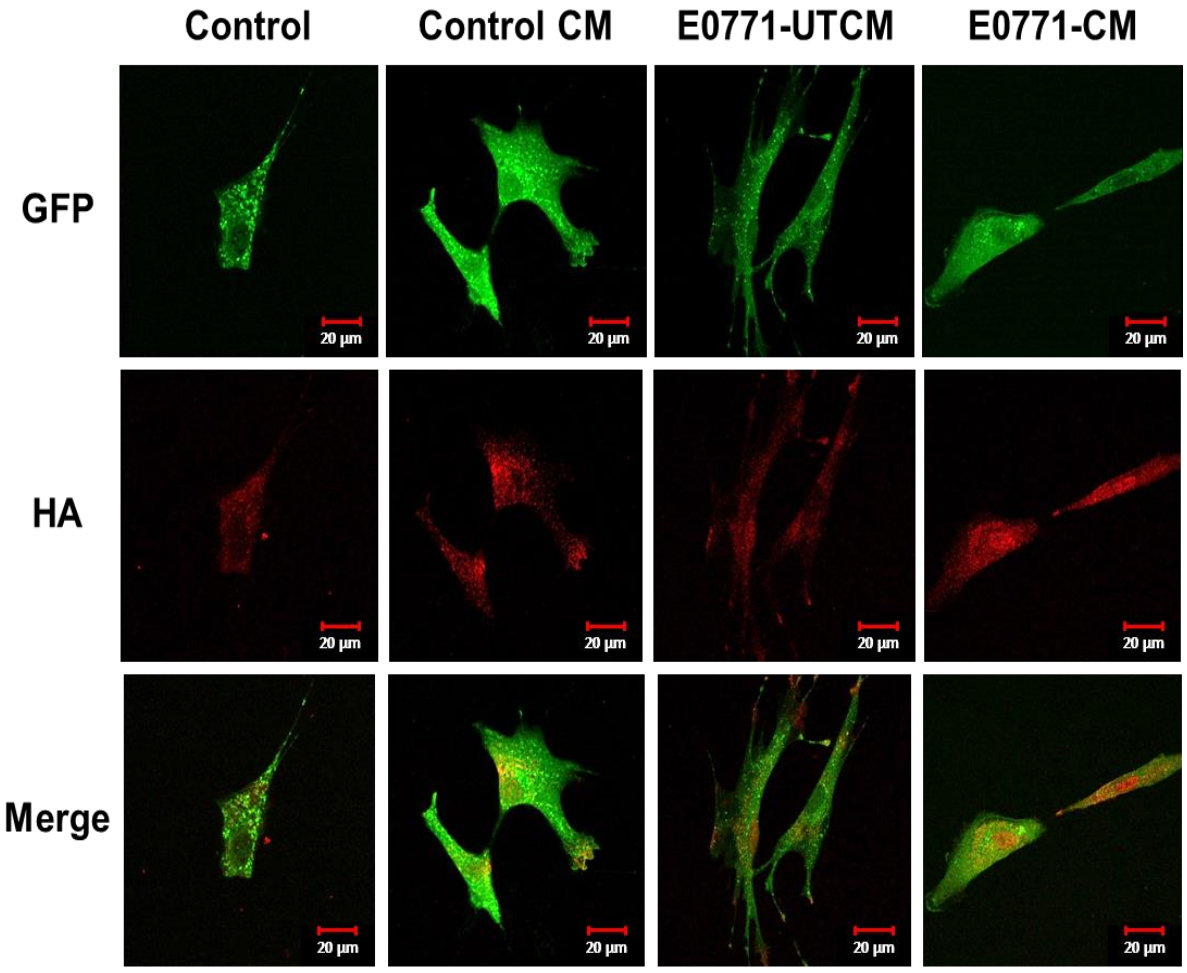

Figure 3.23: Assessment of GLUT4 translocation in MEF cells following treatment with E0771 conditioned media. MEF cells were subjected to (1) Control, (2) Control conditioned media (Control-CM), (3) E0771 untreated conditioned media (E0771-UTCM) and (4) glucose deprived E0771 conditioned media (E0771-CM) for 24 hours. Cells were then immunostained for the HA tag using an Alexa Fluor 647 secondary antibody (Red). GFP and HA expression were visualized using fluorescent confocal microscopy. Images acquired at 60x magnification

As the translocation of the GLUT4 transporter to the plasma membrane results in the extracellular expression of the bound HA tag, staining of the HA-tag using an Alexa Fluor 647 specific antibody indicates total GLUT4 translocation. Thus the ratio between cytosolic - (GFP fluorescent intensity) and translocated GLUT4 (HA:Alexa Fluor 647 fluorescent intensity) can be determined, and used as an indicator of glucose uptake via GLUT4 (Zeigerer *et al*., 2002, Martin *et al*., 2005). Visually GFP fluorescent intensity (total GLUT4) remained fairly constant across all treatment groups. However, HA:Alexa Fluor 647 fluorescent intensity (translocated GLUT4) appeared to be increased in MEF cells in response to treatment with either untreated E0771 conditioned media (EUM) or glucose deprived E0771 conditioned media (ECM) in comparison to both the control and control conditioned media treated cells (CCM).

3.3.8. Pyruvate dehydrogenase (PDH) Assay

The catabolism of glucose via glycolysis in cells, under normal oxygen tension, results in the generation of pyruvate, which is converted to acetyl-CoA and further catabolized within the mitochondria to produce energy via oxidative phosphorylation (Randle, 1986). Pyruvate dehydrogenase catalyzes the irreversible conversion of pyruvate to acetyl-CoA, and therefore serves as the rate-limiting connection between glycolysis and oxidative phosphorylation (Koukourakis *et al*., 2005). However, under conditions of hypoxia the activation of HIF-1α results in the inhibition of PDH, through the activation of the PDH antagonizer pyruvate dehydrogenase kinase (PDK), leading to decreased energy production via oxidative phosphorylation (Kim *et al*., 2006). Additionally, decreased oxidative phosphorylation resulting in enhanced lactate production is a key metabolic feature of the “reverse Warburg effect”. Therefore, in order to determine whether the E0771 conditioned media results in the induction of the “reverse Warburg effect” in MEF

cells, we assessed the protein profile of PDH in MEF cells following 24 hour treatment with E0771 conditioned media.

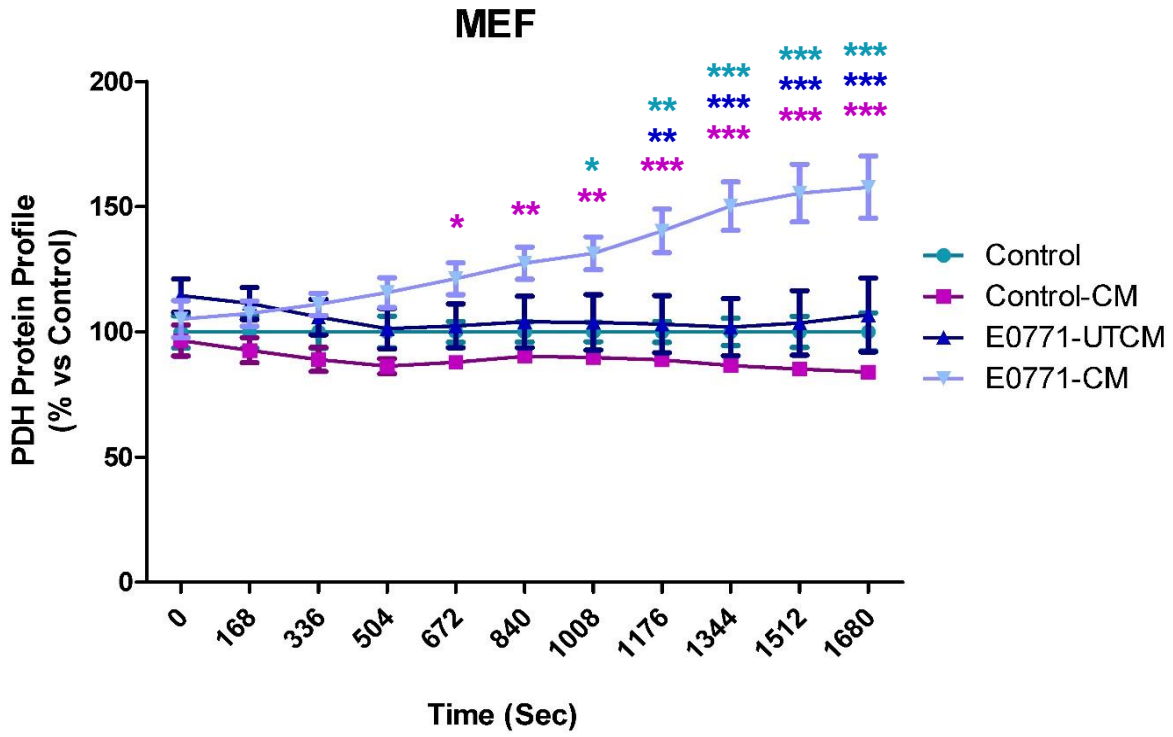

Figure 3.24: Determining the effect of E0771 conditioned media on the protein profile of PDH in mouse embryonic fibroblasts (MEF) cells. MMEF cells were subjected to (1) Control, (2) Control conditioned media (Control-CM), (3) E0771 untreated conditioned media (E0771-UTCM) and (4) glucose deprived E0771 conditioned media (E0771-CM) for 24 hours. Statistical analysis: Two-way ANOVA with Bonferroni post hoc correction. All results are presented as mean ± SEM (n=3). * = p<0.05 vs control, ** = p<0.01 vs control, *** = p<0.0001 vs control, * = p<0.05 vs control-CM, ** = p<0.01 vs control-CM, *** = p<0.0001 vs control-CM, * = p<0.05 vs E0771-UTCM, ** = p<0.01 vs E0771-UTCM, *** = p<0.0001 vs E0771-UTCM.

Our results show a significant increase in total amount of PDH present in MEF cells that had been treated with glucose deprived E0771 conditioned media (E0771-CM) at the 1008 second time point (131.4% % ± 6.554% vs 100% % ± 3.898%, p<0.05), which steadily increased over the remaining time course of the assay when compared to control. A similar statistical result was obtained when compared to the control-CM group. However, the amount of PDH increased significantly from the 672 second time point (121.2% ± 6.414%

vs 87.88% % ± 2.185%, p<0.05) onwards. Furthermore, when compared to the E0771-UTCM treatment group a statistically significant increase was only seen from the 1176 second time point (140.3% ± 8.718% vs 103.1% % ± 11.04%, p<0.01).

3.3.9. PDH Enzyme Activity Assay

As the enzymatic activity of PDH is a determinant of the metabolic conversion of pyruvate to acetyl-CoA, assessment of PDH activity provides partial insight into the flux of pyruvate into oxidative phosphorylation. No statistically significant differences in the enzymatic activity of PDH was observed across all treatment groups when compared to control.

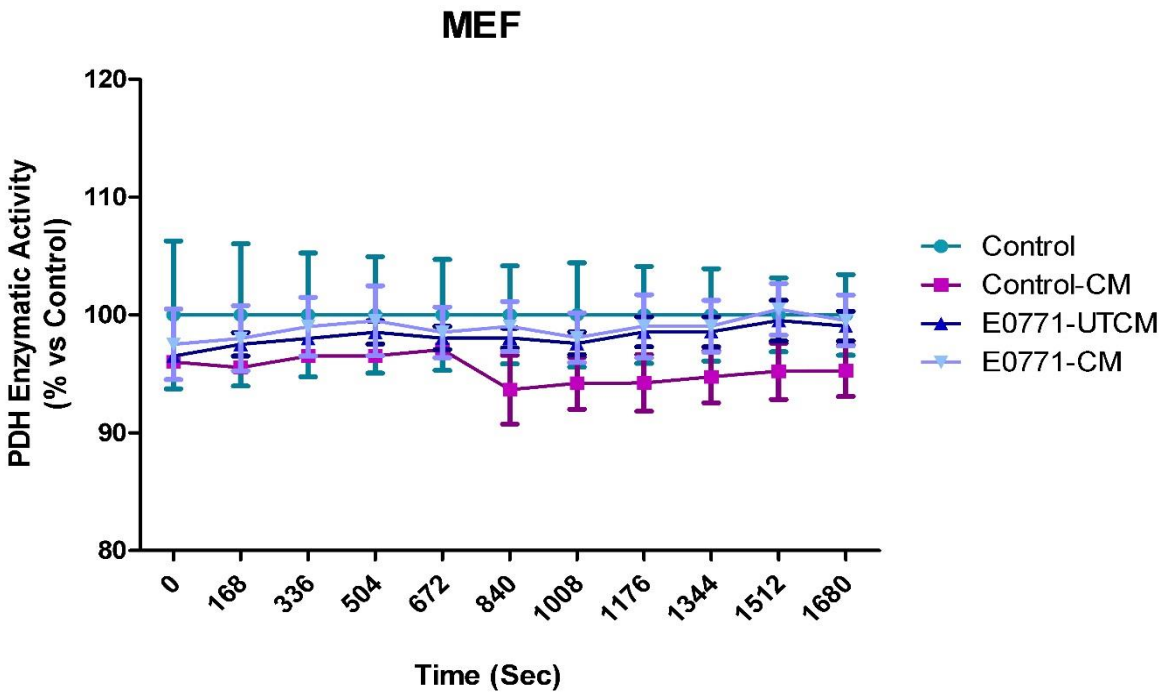

Figure 3.25: Determining the effect of E0771 conditioned media on the enzymatic activity of PDH in mouse embryonic fibroblasts (MEF) cells. MEF cells were subjected to (1) Control, (2) Control conditioned media (Control-CM), (3) E0771 untreated conditioned media (E0771-UTCM) and (4) glucose deprived E0771 conditioned media (E0771-CM) for 24 hours. Statistical analysis: One way ANOVA with Bonferroni post hoc correction. All results are presented as mean ± SEM (n=3).

3.3.10. L-Lactate Assay

As the activation of HIF-1α results in the inhibition of pyruvate dehydrogenase and a shunting of pyruvate away from oxidative phosphorylation, leading to the increased production of lactate (Kim *et al*., 2006, Papandreou *et al*., 2006), L-lactate concentrations were therefore assessed by means of a commercially available colorimetric assay. A significant increase in L-lactate production was observed following the treatment of MEF cells with glucose deprived E0771-CM in comparison to both control (340.2% ± 50.13% vs 100% ± 11.70%, p=0.0009) and control-CM (340.2% ± 50.13% vs 128.0% ± 21.35%, p=0.0030). Treatment of MEF cells with E0771-UTCM resulted in a significant increase in L-lactate concentrations in comparison to control (214.4% ± 38.34% vs 100% ± 11.70%, p=0.0172) alone.

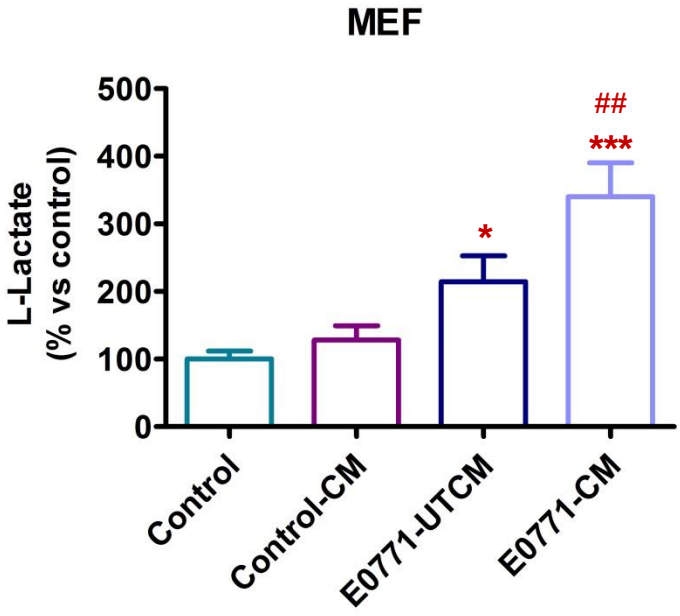

Figure 3.26: Determination of the effects of E0771 conditioned media on L-lactate concentrations in mouse embryonic fibroblast (MEF) cells. MEF cells were subjected to (1) Control, (2) Control conditioned media (Control-CM), (3) E0771 untreated conditioned media (E0771-UTCM) and (4) glucose deprived E0771 conditioned media (E0771-CM) for 24 hours. Statistical analysis: One way ANOVA with Bonferroni post hoc correction. All results are presented as mean ± SEM (n=3). * = p<0.05 vs control, *** = p<0.0001 vs control and ## = p<0.01 vs control-CM.

3.3.11. Lactate Transporter Expression

Assessment of the relative protein expression levels of the monocarboxylate transporters (MCT) 1 and 4, allows for the inference of the transport of monocarboxylates, such as L-lactate, across the plasma membrane. Our results revealed a significant decrease in MCT-1 protein expression levels in MEF cells treated with E0771-CM (49.78% ± 12.28% vs 100% ± 10.98%, p=0.0381) when compared to control. No significant differences in MCT-4 protein expression levels were observed across all treatment groups when compared to control.

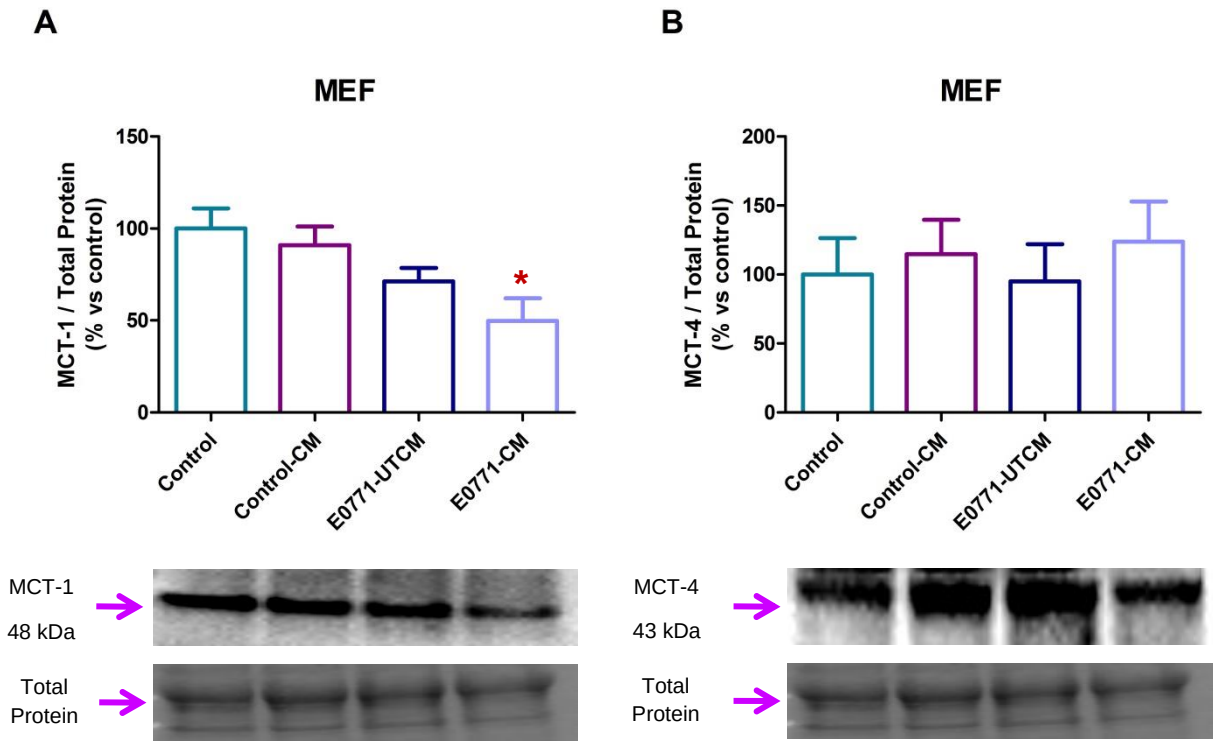

Figure 3.27: Western blot analysis of MCT-1 and MCT-4 protein expression in MEF cells treated with E0771 conditioned media. MEF cells were subjected to (1) Control, (2) Control conditioned media (Control-CM), (3) E0771 untreated conditioned media (E0771-UTCM) and (4) glucose deprived E0771 conditioned media (E0771-CM) for 24 hours. Statistical analysis: One way ANOVA with Bonferroni post hoc correction. All results are presented as mean ± SEM (n=3). * = $p<0.05$ vs control.

3.4: Proteomics Analysis of MEF Conditioned Media

3.4. Proteomics Analysis of MEF Conditioned Media

Assessment of the protein composition of conditioned media generated from MEF cells that had been treated with E0771 conditioned media for 24 hours was achieved as previously described (see section 3.2) (refer to section 7.1.2 for the list of regulated proteins). In this section, a total of 23 protein elements were found exclusively in the conditioned media generated from MEF cells treated with glucose deprived E0771 CM (MEF_ECM), and a total of 7 protein elements found exclusively in the conditioned media generated from MEF cells treated with untreated E0771 CM (MEF_EUM), whereas a total of 32 protein elements were displayed exclusively in conditioned media generated from control MEF cells. A total of 9 elements were found common to both MEF_C and MEF_ECM, 17 common elements to MEF_C and MEF_EUM, and a total of 24 protein elements were found to be present in all three conditions.

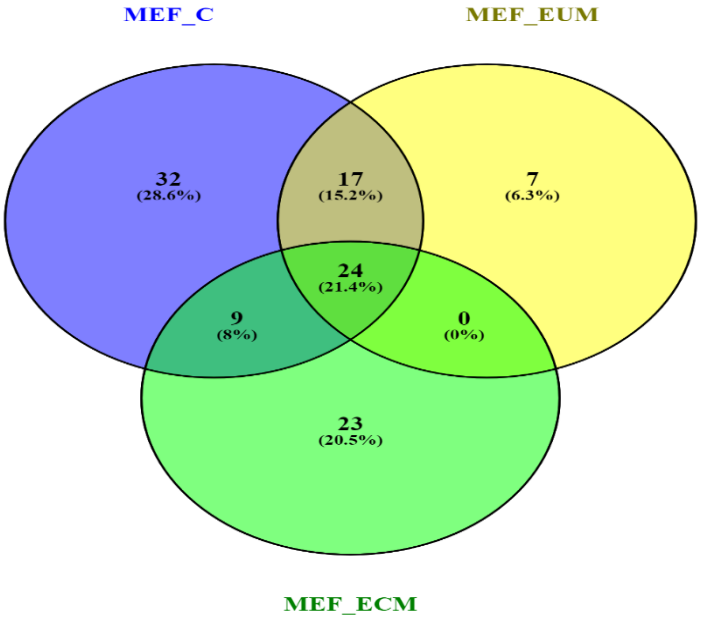

Figure 3.28: Broad overview of the total number of protein elements identified between control, MEF_EUM and MEF_ECM conditioned media groups. MEF cells were incubated in either control DMEM (MEF_C), untreated E0771 conditioned media (MEF_EUM) or glucose deprived E0771 conditioned media (MEF_ECM) for 24 hours. Diagram generated by CPGR using Venny freeware.

3.4.1. Biological Processes Downregulated in MEF_EUM Conditioned Media

As described previously, GO terms obtained from the list of proteins found to be downregulated in conditioned media generated from MEF cells treated with untreated E0771 conditioned media (MEF_EUM) were submitted into REVIGO and proteins clustered according to their involvement in various biological processes.

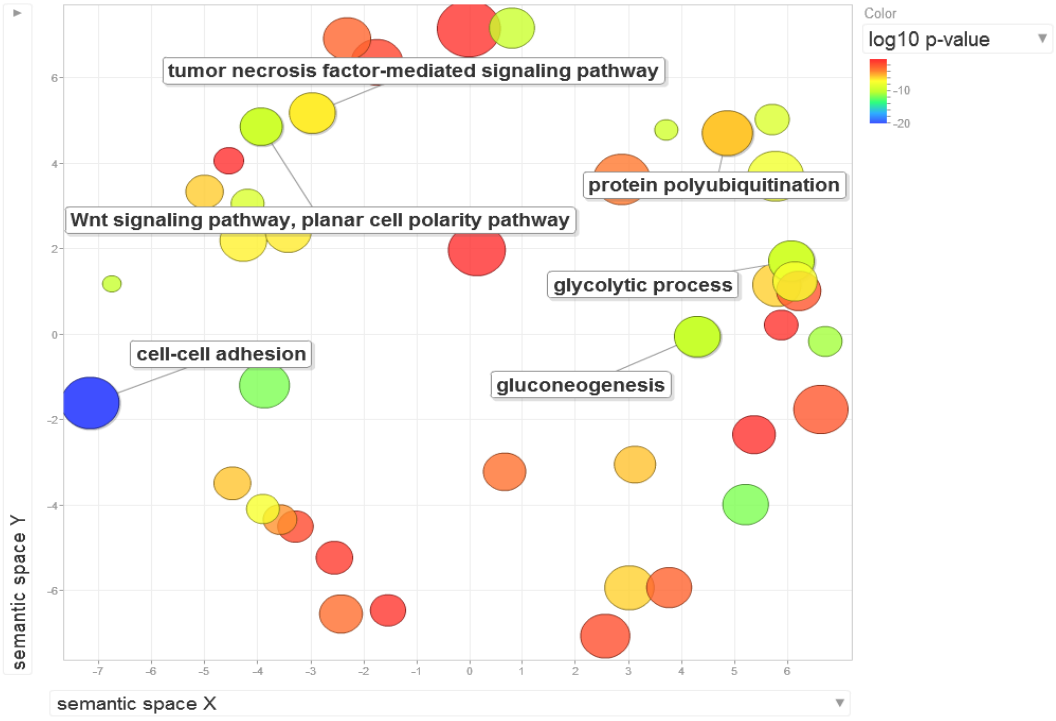

Figure 3.29: Scatterplot view of biological processes downregulated in MEF conditioned media following 24 hours of treatment with untreated E0771 conditioned media (MEF_EUM). Graph generated in REVIGO using GO terms.

A variety of biological processes involved in cell migration and metabolism were found to be significantly downregulated in MEF_EUM conditioned media. Again, within the context of this study, a downregulation in the Wnt signalling pathway, cell-cell adhesion, glycolysis, gluconeogenesis and protein polyubiquitination was observed. Of additional interest, we also observed a significant downregulation in tumour necrosis factor (TNF) mediated signalling.

To gain a better understanding of the interactions between interesting biological processes identified in REVIGO, additional interactive graphs were assessed. Interactive graphs generated in REVIGO, also display both the specificity of the terms (larger nodes indicate more GO terms which have been collapsed and as such indicates a lower specificity) as well as the significance of the term (deeper-red nodes show greater significance). Furthermore, interconnections between nodes represent the hierarchical relationship between collapsed GO terms.

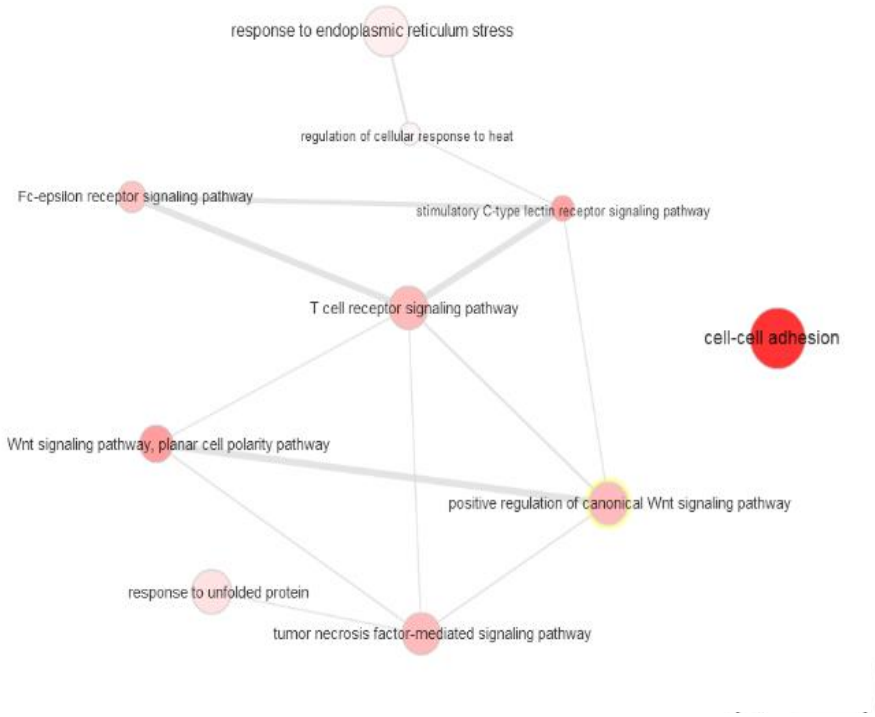

Figure 3.30: Interactive graph of downregulated biological processes involved in cell migration in MEF conditioned media following 24 hours of treatment with untreated E0771 conditioned media (MEF_EUM). Graph generated in REVIGO using GO terms.

From the interactive graphs generated in REVIGO for the downregulation of biological processes involved in cell migration, a distinct hierarchical interaction between the Wnt signalling pathway and tumour necrosis factor mediated signalling is observed, both of which being highly specific.

Assessment of the interactive graph containing a wide variety of metabolic processes, revealed a hierarchical interaction between protein catabolism and glycolysis. Additionally, interactions between protein polyubiquitination and MAPK signalling as well as NK/NF-kappaB signalling and MAPK signalling were observed. This is of particular interest as MAPK signalling is seen to have further interactions with both glycolysis and proteolysis involved in cellular protein catabolism.

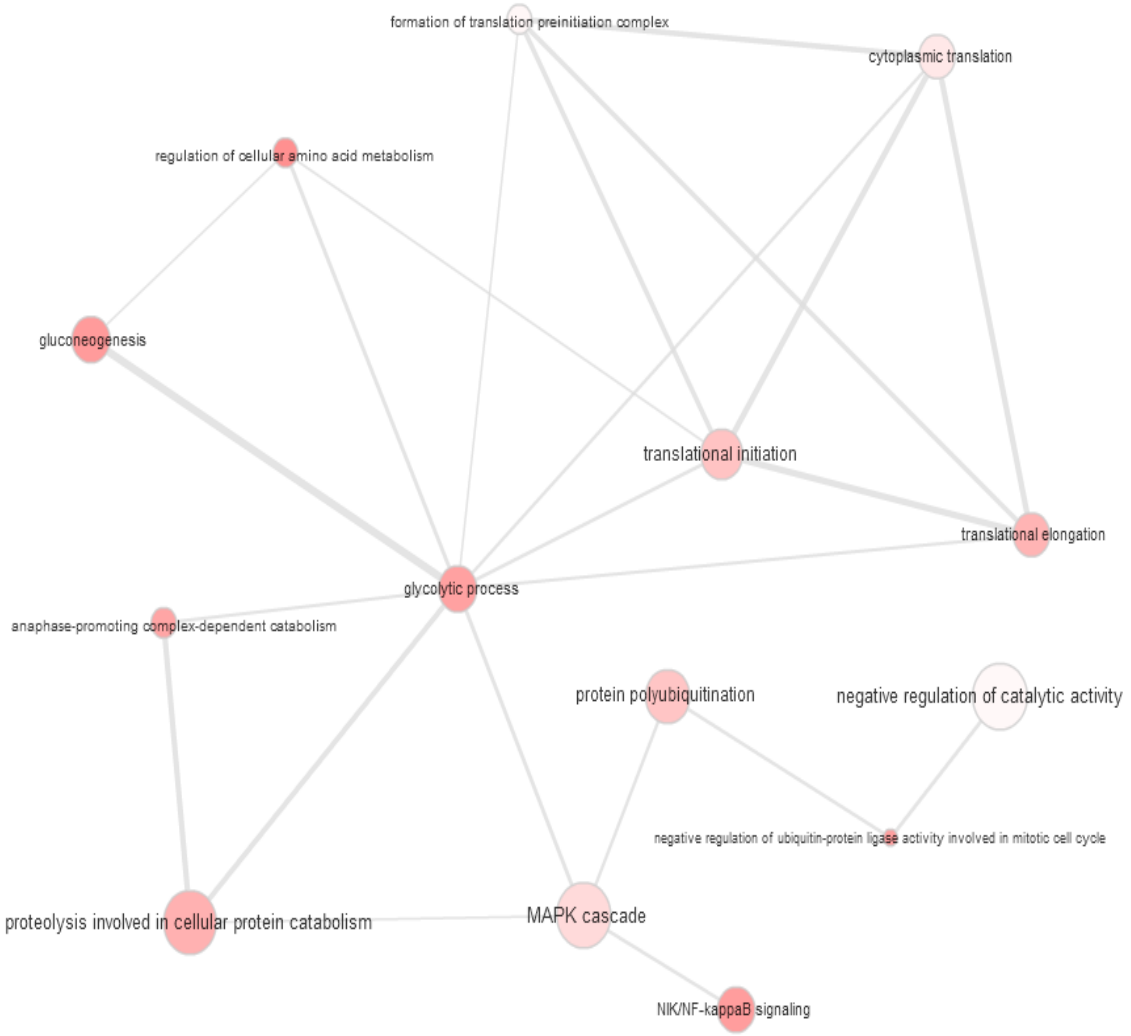

Figure 3.31: Interactive graph of downregulated biological processes involved in cellular metabolism in MEF conditioned media following 24 hours of treatment with untreated E0771 conditioned media (MEF_EUM). Graph generated in REVIGO using GO terms.

Furthermore, submission of UnitProt accession numbers generated from downregulated proteins in MEF_EUM conditioned media into DAVID also showed significant clustering of proteins involved in cell-cell adhesion and metabolism. Interrogation of proteins clustered into cell-cell adhesion pathways, showed a significant downregulation of enolase I (ENO1), annexin I (ANXA1), profilin 1 (PFN1) and charged multivesicular body protein 4B (CHMP4B).

Figure 3.32: 2D viewer of functional annotation clustering of downregulated proteins involved in cell-cell adhesion processes in MEF_EUM conditioned media. Graph generated in DAVID using UniProt accession numbers. Proteins are displayed horizontally and their functional relationship is displayed vertically.

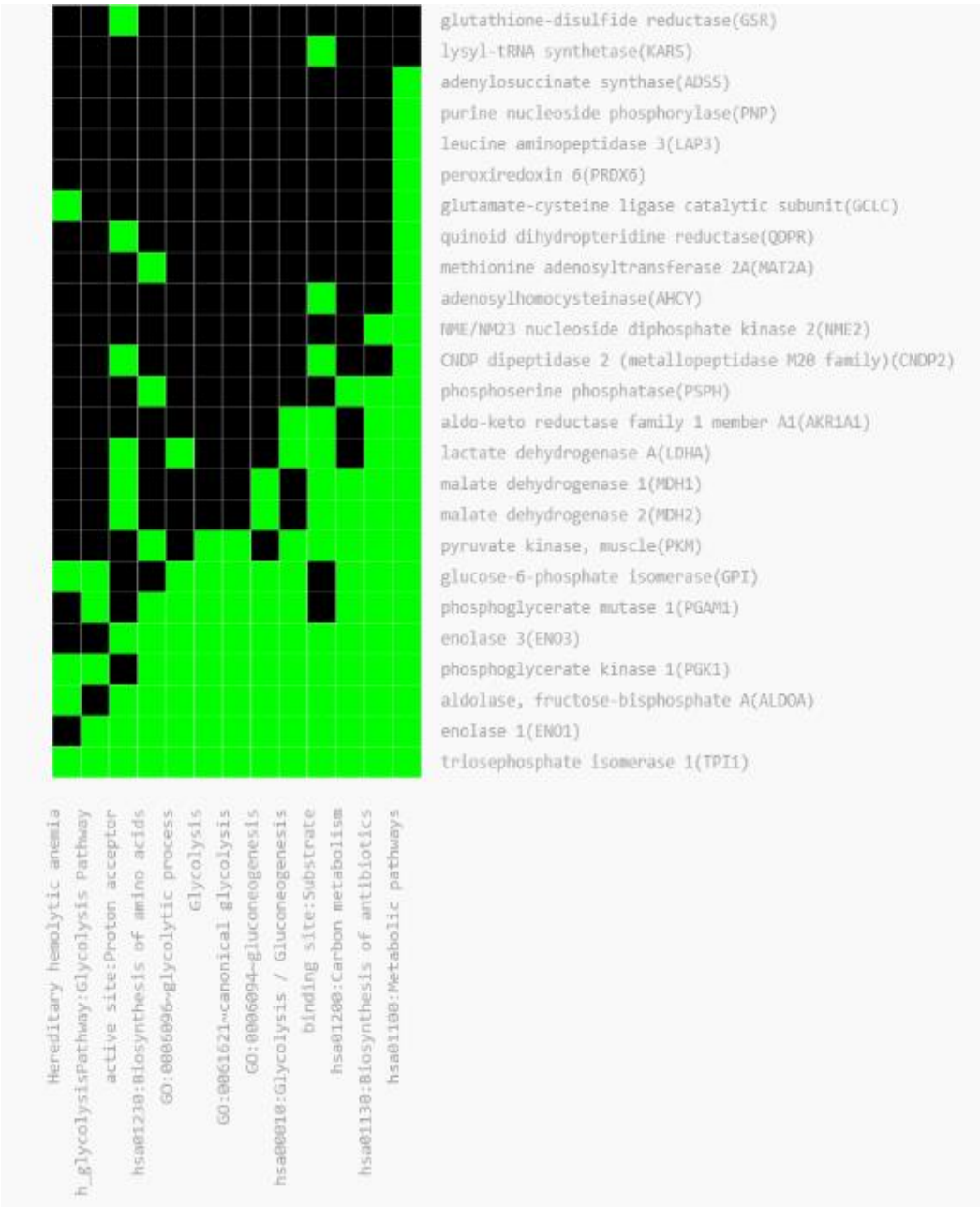

Figure 3.33: 2D viewer of functional annotation clustering of downregulated proteins involved in metabolic processes in MEF_EUM conditioned media. Graph generated in DAVID using UniProt accession numbers. Proteins are displayed horizontally and their functional relationship is displayed vertically.

In depth assessment of protein clustering involved in glycolysis, gluconeogenesis and/or carbon metabolism in MEF_EUM, showed a downregulation of lactate dehydrogenase A (LDHA), malate dehydrogenase (MDH) -1 and -2, pyruvate kinase, muscle (PKM) and enolase (ENO) -1 and -3.

3.4.2. Biological Processes Upregulated in MEF_EUM Conditioned Media

Upregulated GO terms for MEF_EUM conditioned media, when submitted into REVIGO, resulted in a collapse of these terms into only a few clusters associated with cellular components. No biological processes were shown to be upregulated in MEF_EUM conditioned media. The scatterplot view generated for clusters associated with cellular components in REVIGO proved to not to be very informative, therefore, only the interactive graph is displayed as the hierarchical interactions between the extracellular space, extracellular region and cytoplasm as well as their significance can be easily interpreted. Again based on the fact that very few clusters were generated in REVIGO, none of which were found to be involved in any biological processes, these were not submitted into DAVID for further analysis in this study.

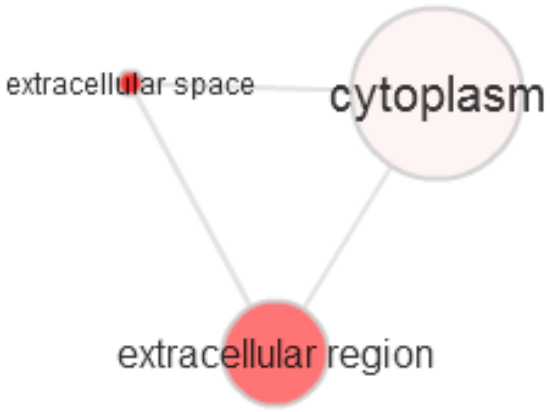

Figure 3.34: Interactive graph of upregulated cellular components in MEF conditioned media following 24 hours of treatment with untreated E0771 conditioned media (MEF_EUM). Graph generated in REVIGO using GO terms.

3.4.3. Biological Processes Downregulated in MEF_ECM Conditioned Media

Bioinformatic analysis of MEF_ECM was conducted using the same pipeline as described above. Interestingly, we noted an opposite effect in MEF_ECM as to that seen in the analysis of MEF_EUM conditioned media, where REVIGO showed that no biological

processes were downregulated in MEF_ECM, and GO terms were clustered into very few nodes involved in cellular components. Again, for the purpose of this study, these were not analysed further using DAVID and only the interactive graph of downregulated cellular components, showing the interaction between the extracellular region and extracellular space, is displayed below.

Figure 3.35: Interactive graph of downregulated cellular components in MEF conditioned media following 24 hours of treatment with glucose deprived E0771 conditioned media (MEF_ECM). Graph generated in REVIGO using GO terms.

3.4.4. Biological Processes Upregulated in MEF_ECM Conditioned Media

Protein clustering analysis for biological processes upregulated in MEF_ECM conditioned media using REVIGO, showed significant clustering of processes heavily involved in cell migration and metastasis, namely; the Wnt signalling pathway, ephrin signalling pathway, ARP2/3 complex-mediated actin nucleation, movement of cell or subcellular component and cell-cell adhesion. Additionally, significant clustering was also observed in processes involved in cell metabolism, including; glycolysis, gluconeogenesis and protein polyubiquitination.

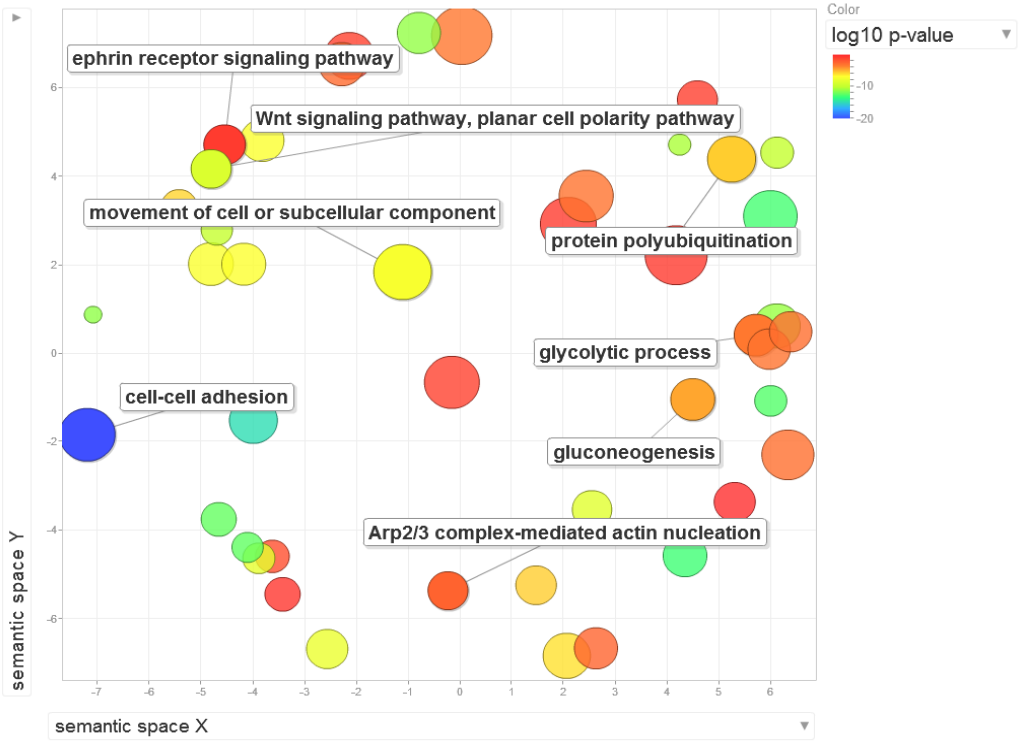

Figure 3.36: Scatterplot view of biological processes upregulated in MEF conditioned media following 24 hours of treatment with glucose deprived E0771 conditioned media (MEF_ECM). Graph generated in REVIGO using GO terms.

As described in the previous section, interactive graphs were generated in REVIGO in order to assess the hierarchical interactions between nodes of upregulated biological processes in MEF_ECM conditioned media. Assessment of the REVIGO interactive graph, which displays the interactions of several biological processes involved in cell migration, demonstrates a hierarchical association between ephrin signalling and Wnt signalling. Tumour necrosis factor-mediated signalling was observed to interact with both ephrin and Wnt signalling pathways, in addition to the response to unfolded proteins.

Significant interactions were also observed between nodes of upregulated biological processes involved in cell metabolism. In MEF_ECM conditioned media we observed hierarchical interactions between glycolysis, gluconeogenesis and protein catabolism. Interactions between protein polyubiquitination - MAPK signalling and NK/NF-kappaB signalling - MAPK signalling were also observed.

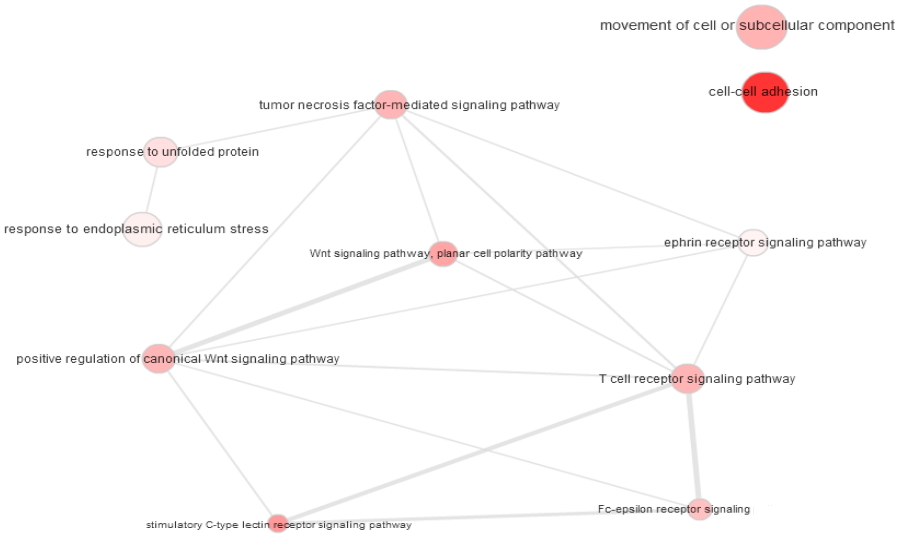

Figure 3.37: Interactive graph of upregulated biological processes involved in cell migration in MEF conditioned media following 24 hours of treatment with glucose deprived E0771 conditioned media (MEF_ECM). Graph generated in REVIGO using GO terms.

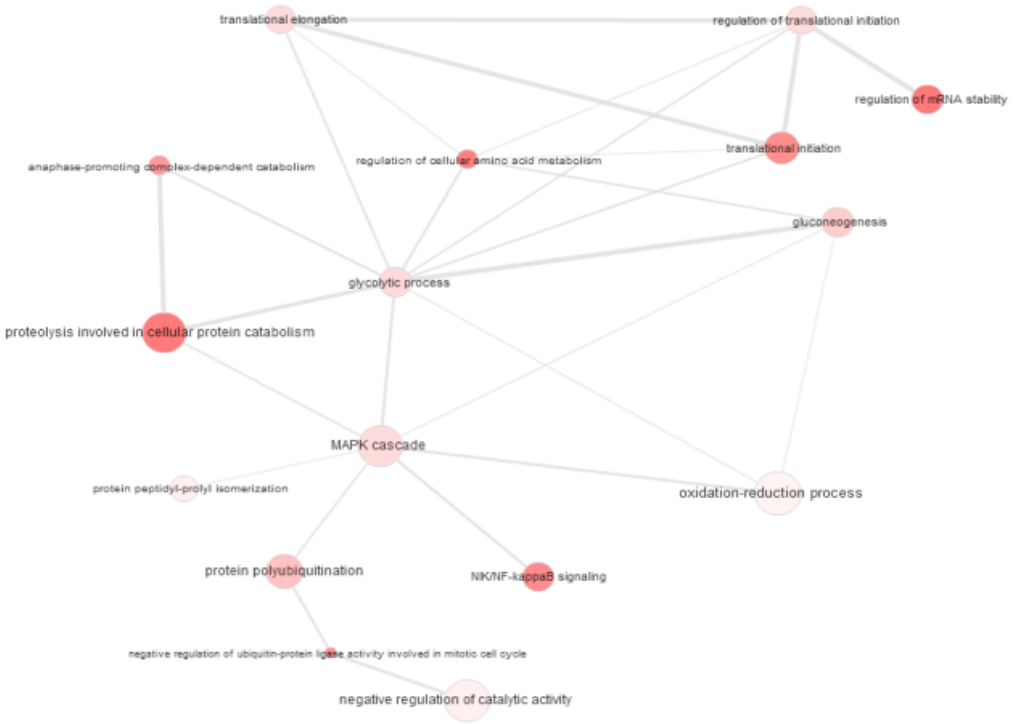

Figure 3.38: Interactive graph of upregulated biological processes involved in metabolic processes in MEF conditioned media following 24 hours of treatment with glucose deprived E0771 conditioned media (MEF_ECM). Graph generated in REVIGO using GO terms.

Significant clustering of proteins involved in cell-cell adhesion and cadherin binding involved in cell adhesion were observed. Upregulated proteins of interest involved in cell adhesion in MEF_CM, within the context of this study, were identified and include; annexin A1 (ANXA1), charged multivessicular body protein 4B (CHMP4B), heat shock protein family A (HSP70) member -5 (HSPA5) and -8 (HSPA8), heat shock protein 90 alpha family class B member 1 (HSP90AB1), lactate dehydrogenase A (LDHA), S100 calcium binding protein A11 (S100A11) and enolase 1 (ENO1).

Figure 3.39: 2D viewer of functional annotation clustering of upregulated proteins involved in cell-cell adhesion processes in MEF_ECM conditioned media. Graph generated in DAVID using UniProt accession numbers. Proteins are displayed horizontally and their functional relationship is displayed vertically.

Upregulated proteins of interest clustering in processes involved in cell metabolism in MEF_CM were also assessed. Proteins of interest found to be positively associated with glycolysis and gluconeogenesis were identified as, glucose-6-phosphate isomerase (GPI), enolase -1 (ENO1) and -3 (ENO3), lactate dehydrogenase A (LDHA) and aldo-keto reductase family 1 member A1 (AKR1A1).

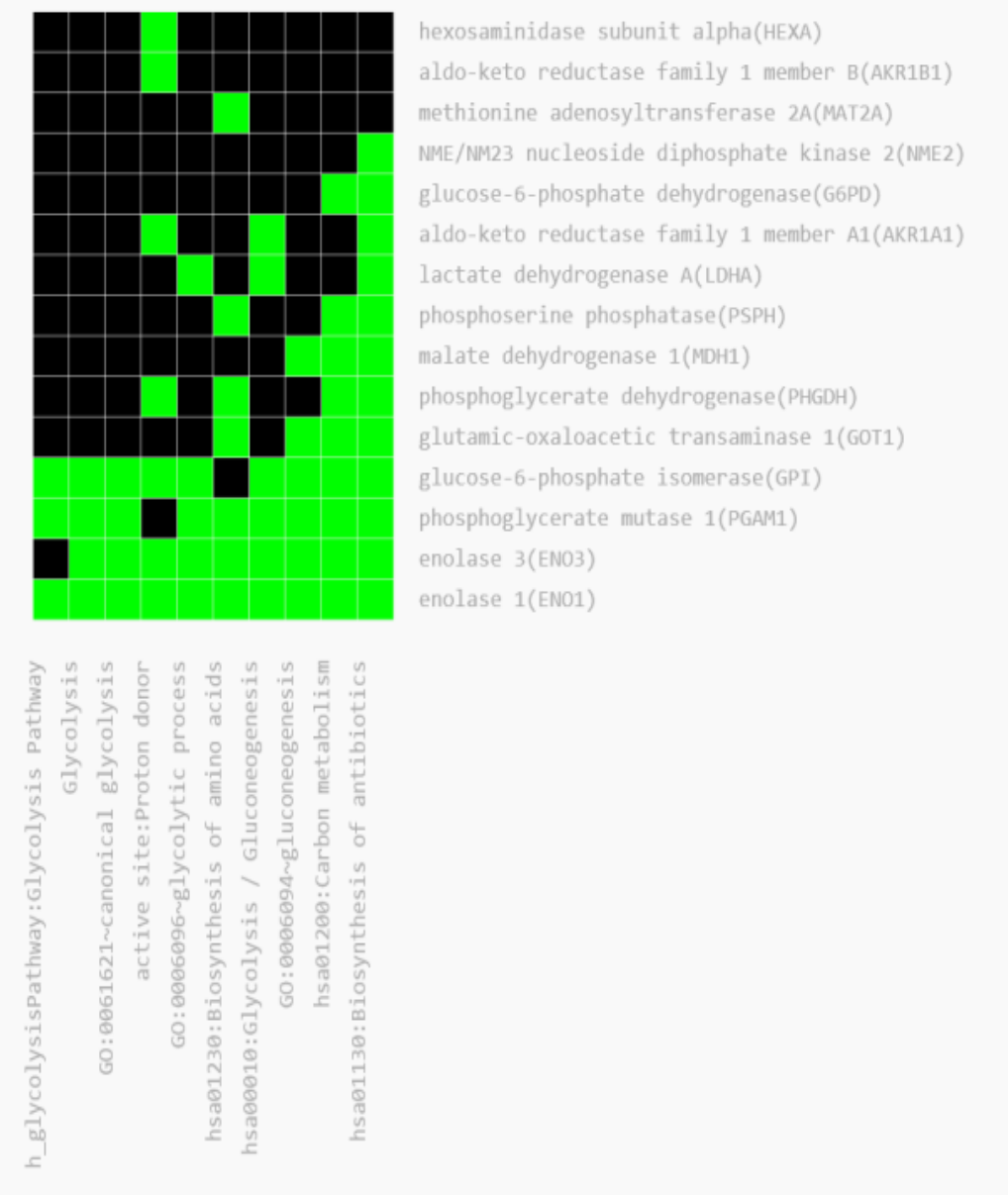

Figure 3.40: 2D viewer of functional annotation clustering of upregulated proteins involved in metabolic processes in MEF_ECM conditioned media. Graph generated in DAVID using UniProt accession numbers. Proteins are displayed horizontally and their functional relationship is displayed vertically.

We also observed a significant clustering of proteins involved in PI3K/Akt signalling in MEF_ECM conditioned media. An upregulation of the proteins, laminin subunit gamma I (LAMC1), collagen type IV alpha 2 chain (COL4A2), insulin like growth factor 1 (IGF1) and heat shock protein 90 (HSP90) were observed.

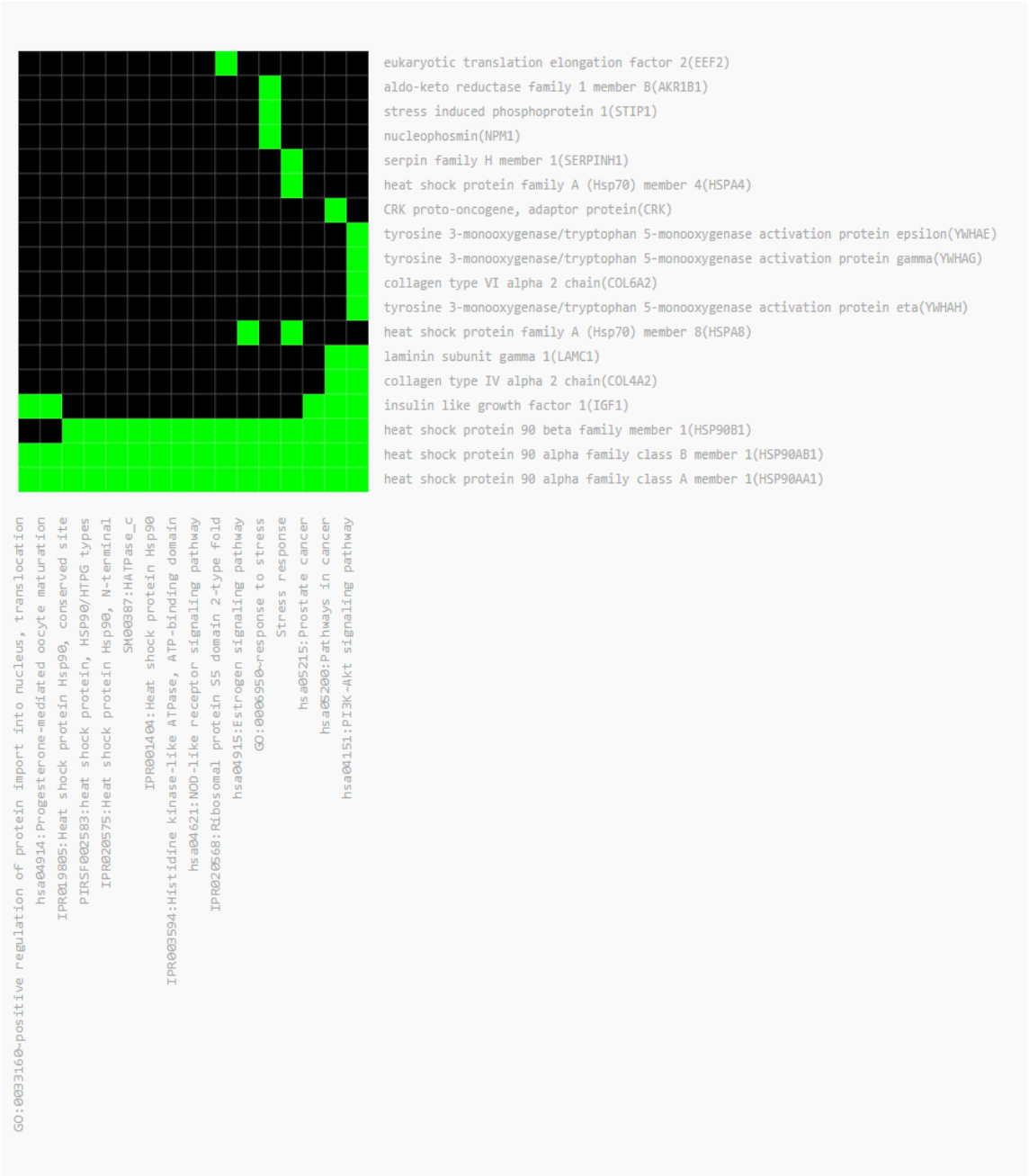

Figure 3.41: 2D viewer of functional annotation clustering of upregulated proteins involved in PI3K/Akt signalling in MEF_ECM conditioned media. Graph generated in DAVID using UniProt accession numbers. Proteins are displayed horizontally and their functional relationship is displayed vertically.

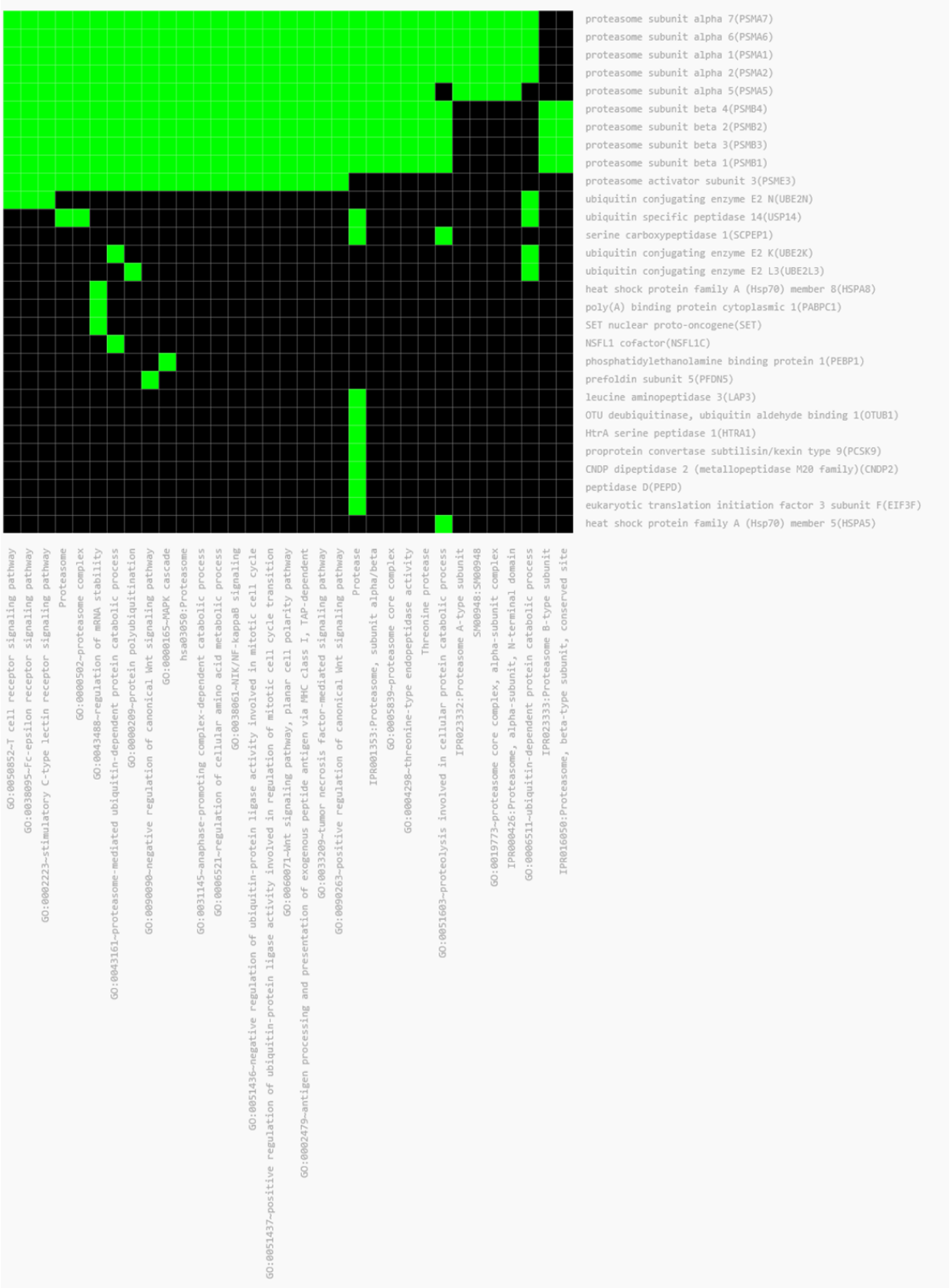

Figure 3.42: 2D viewer of functional annotation clustering of upregulated proteins involved in Wnt signalling, protein catabolism and protein polyubiquitination in MEF_ECM conditioned media. Graph generated in DAVID using UniProt accession numbers. Proteins are displayed horizontally and their functional relationship is displayed vertically.

Finally, the functional clustering of proteins involved in the Wnt signalling pathway, protein polyubiquitination and protein catabolism using DAVID were identified. As observed previously (see section 3.2) an upregulation in the proteasome subunits alpha (PSMA) 1, 2, 5, 6 and 7, known to play a role in the Wnt signalling pathway, protein catabolism and protein polyubiquitination were also seen in MEF_ECM conditioned media. Additionally, an upregulation was seen in the proteasome subunits beta (PSMB) 1, 2, 3 and 4, which are linked to both Wnt signalling and protein polyubiquitination. Of additional interest, DAVID also identified an upregulation in ubiquitin conjugating enzyme E2 K (UBE2K) which is critically involved in both the processes of proteasome-mediated ubiquitin-dependent protein catabolism and ubiquitin-dependent protein catabolism.

3.5: Effects of MEF Conditioned Media on E0771 Breast Cancer Cell Metabolism

3.5. Effects of MEF Conditioned Media on E0771 Breast Cancer Cell Metabolism

Based on the interesting results we obtained for the proteomics analysis of MEF_ECM conditioned media, we therefore set out to determine the effects of MEF derived conditioned media on both the metabolic profile and the migratory capacity of glucose deprived E0771 breast cancer cells.

3.5.1. Cell Viability

In order to determine the effects of MEF conditioned media on the metabolic capabilities of glucose deprived E0771 cancer cells, MTT cell viability assays were performed following treatments.

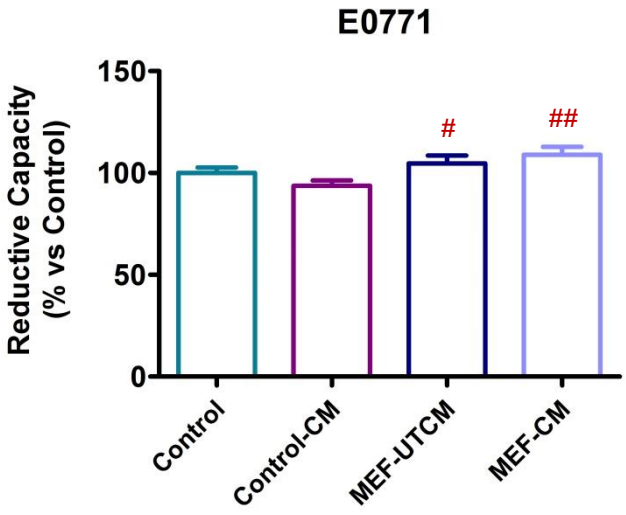

Figure 3.43: Determination of the effects of MEF conditioned media on the viability of glucose deprived E0771 murine breast cancer cells. Subsequent to 12 hours of glucose deprivation (0 mM glucose DMEM), E0771 cells were subjected to (1) Control, (2) Control conditioned media (Control-CM), (3) Untreated MEF conditioned media (MEF-UTCM) and (4) E0771 treated MEF conditioned media (MEF-CM) for 24 hours. Cell viability was assessed using the MTT assay. Statistical analysis: One way ANOVA with Bonferroni post hoc correction. All results are presented as mean ± SEM (n=3). # = $p<0.05$ vs control-CM and ## = $p<0.01$ vs control-CM.

No significant differences in mitochondrial reductive capacity was seen when E0771 breast cancer cells were treated with control conditioned media for 24 hours following 12 hours of glucose deprivation. However, when glucose deprived E0771 cells were treated with MEF-CM a significant increase in MTT reductive capacity was observed when compared to control-CM (108.9% ± 3.957% vs 93.68% ± 2.644%, p=0.0016) as well as when these cells were treated with MEF-UTCM when compared to control-CM (104.7% ± 3.786% vs 93.68% ± 2.644%, p=0.0170) alone.

3.5.2. Cell Death Assessment (Hoechst + PI)

In order to validate the data obtained from the MTT cell viability assay, cell death was assessed further by means of flow cytometry by staining E0771 cells with Hoechst 33342 and propidium iodide (PI) following all treatments. Our results showed no significant differences in either the live or dead cell populations across all treatment groups.

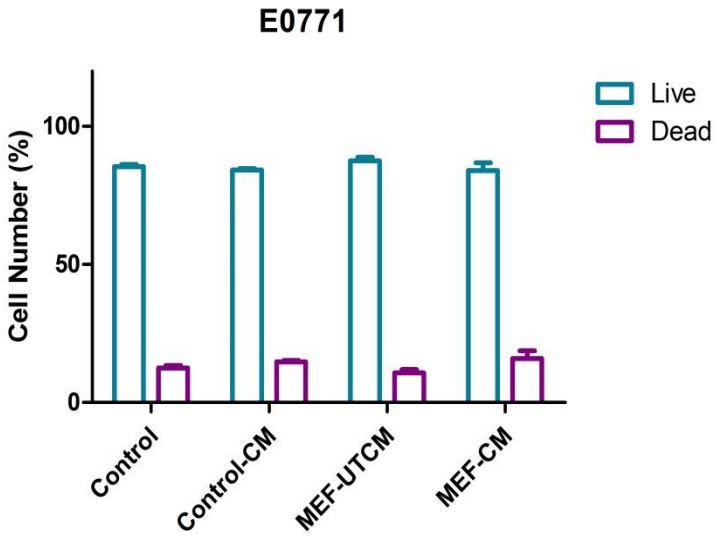

Figure 3.44: Determination of the effects of MEF conditioned media on cell death in glucose deprived E0771 murine breast cancer cells. Subsequent to 12 hours of glucose deprivation (0 mM glucose DMEM), E0771 cells were subjected to (1) Control, (2) Control conditioned media (Control-CM), (3) Untreated MEF conditioned media (MEF-UTCM) and (4) E0771 treated MEF conditioned media (MEF-CM) for 24 hours. Statistical analysis: One way ANOVA with Bonferroni post hoc correction. All results are presented as mean ± SEM (n=3).

3.5.3. MCT-1/4 Protein Expression

As previously described, changes in the relative expression levels of the monocarboxylate transporters (MCT) of E0771 breast cancer cells can provide insight into the degree to which monocarboxylates, including L-lactate, are transported across the plasma membrane. We observed a significant increase in the relative protein expression levels of the importer MCT-1 following both MEF_UTCM (232.9% ± 28.95% vs 100% ± 27.56%, p=0.0292) and MEF_CM (227.7% ± 9.004% vs 100% ± 27.56%, p=0.0116) treatment when compared to the control group.

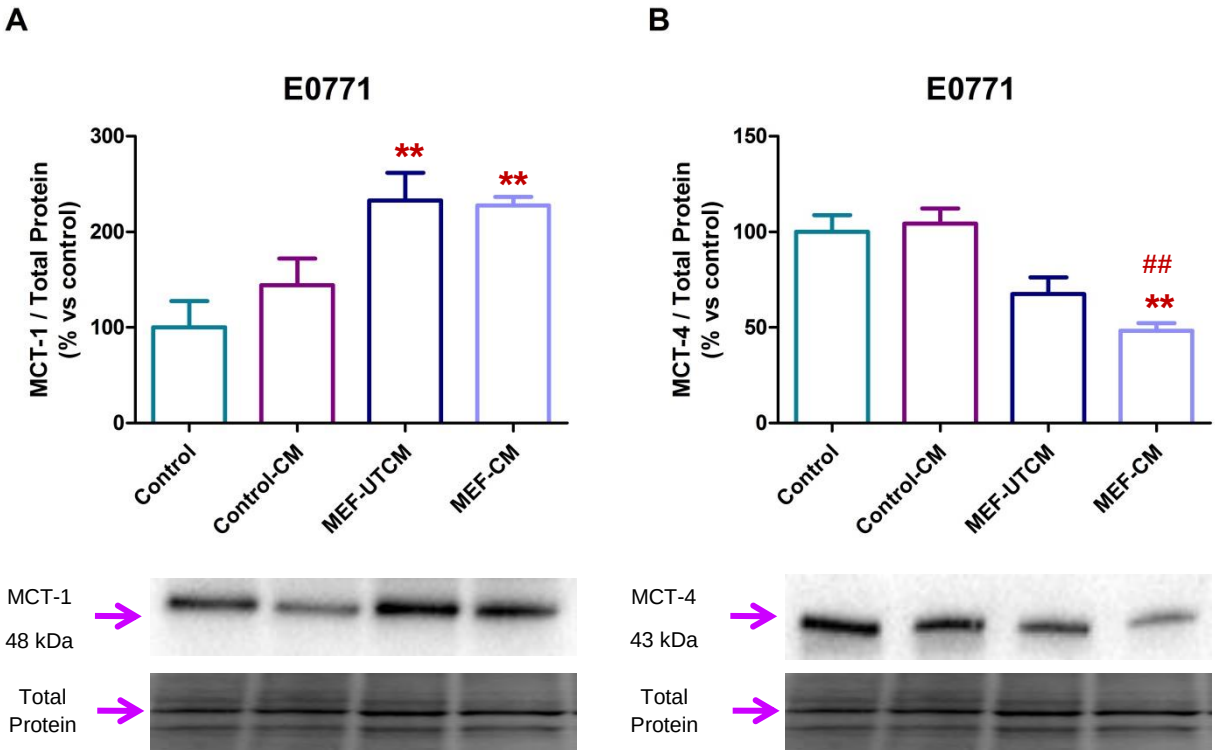

Figure 3.45: Western blot analysis of MCT-1 and MCT-4 protein expression in E0771 breast cancer cells treated with MEF conditioned media. Subsequent to 12 hours of glucose deprivation (0 mM glucose DMEM), E0771 cells were subjected to (1) Control, (2) Control conditioned media (Control-CM), (3) Untreated MEF conditioned media (MEF-UTCM) and (4) E0771 treated MEF conditioned media (MEF-CM) for 24 hours. Statistical analysis: One way ANOVA with Bonferroni post hoc correction. All results are presented as mean ± SEM (n=3). **= p<0.01 vs control and ## = p<0.01 vs control-CM

Additionally, we observed a concomitant decrease in the expression levels of the exporter MCT-4 following MEF-CM (48.34% ± 4.006% vs 100% ± 8.812%, p=0.0059) treatment alone when compared to control and control-CM (48.34% ± 4.006% vs 104.4% ± 7.962%, p=0.0033).

3.5.4. L-Lactate Assay

As described previously, in the "reverse Warburg effect" lactate generated and exported from CAFs can be utilized by either oxygen or nutrient deprived cancer cells as an energy source to promoting cancer cell survival (Lee *et al*., 2015), L-lactate concentrations were therefore assessed following treatment of glucose deprived E0771 cells with MEF conditioned media by means of a commercially available colorimetric assay.

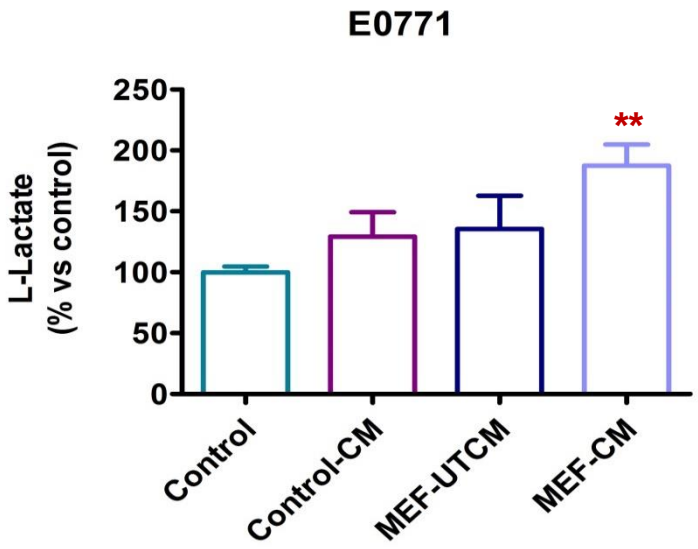

Figure 3.46: Determination of the effects of MEF conditioned media on L-lactate concentrations in E0771 murine breast cancer cells. Subsequent to 12 hours of glucose deprivation (0 mM glucose DMEM), E0771 cells were subjected to (1) Control, (2) Control conditioned media (Control-CM), (3) Untreated MEF conditioned media (MEF-UTCM) and (4) E0771 treated MEF conditioned media (MEF-CM) for 24 hours. Statistical analysis: One way ANOVA with Bonferroni post hoc correction. All results are presented as mean ± SEM (n=3). ** = p<0.01 vs control.

A significant increase in L-lactate production was observed following the treatment of glucose deprived E0771 cells with MEF-CM (211.5% ± 13.49% vs 100% ± 4.706%, p=0.0083) in comparison to control. However, no significant differences were observed when MEF-CM treated E0771 cells were compared to those treated with control-CM.

3.5.5. ATP Production Assay

Following the treatment of E0771 murine breast cancer cells with MEF conditioned media, ATP production was assessed by means of a commercially available bioluminescent assay kit. A significant increase in ATP concentrations were observed in glucose deprived E0771 cancer cells following 24 hour treatment with MEF-CM in comparison to both the control (28.37 ± 1.008 % vs 10.50 ± 0.4346 %, p<0.0001) and the control-CM (28.37 ± 1.008 % vs 17.76 ± 2.874 %, p<0.001) groups.

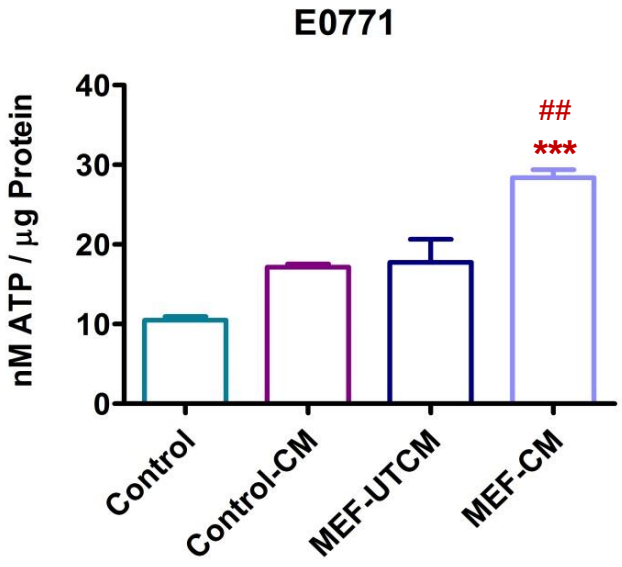

Figure 3.47: Determining the effects of MEF conditioned media on ATP production in E0771 murine breast cancer cells. Subsequent to 12 hours of glucose deprivation (0 mM glucose DMEM), E0771 cells were subjected to (1) Control, (2) Control conditioned media (Control-CM), (3) Untreated MEF conditioned media (MEF-UTCM) and (4) E0771 treated MEF conditioned media (MEF-CM) for 24 hours. Statistical analysis: One way ANOVA with Bonferroni post hoc correction. All results are presented as mean ± SEM (n=3). *** = p<0.0001 vs control and ## = p<0.01 vs control-CM.

3.5.6. Pyruvate dehydrogenase (PDH) Assay

In order to determine the relative substrate availability for oxidative phosphorylation in E0771 breast cancer cells in response to treatment with MEF-derived conditioned media, the total PDH protein profile was assessed using a commercially available “sandwich” ELISA assay. Analysis of the protein profile of PDH in glucose deprived E0771 cells subjected to treatment with conditioned media derived from “activated” MEF cells, showed no significant differences in the amount of PDH present in E0771 breast cancer cells across all treatment groups and analysis time points when compared to both the control and control-CM groups.

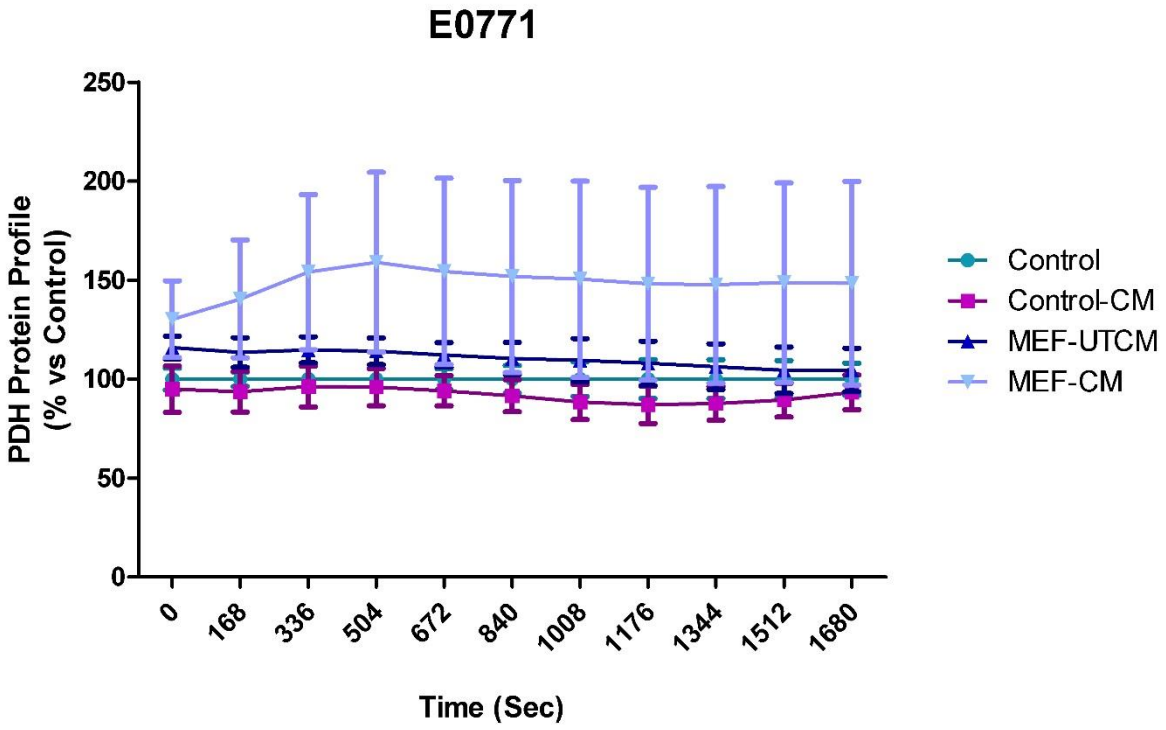

Figure 3.48: Determination of the effects of MEF conditioned media on the protein profile of PDH in E0771 murine breast cancer cells. Subsequent to 12 hours of glucose deprivation (0 mM glucose DMEM), E0771 cells were subjected to (1) Control, (2) Control conditioned media (Control-CM), (3) Untreated MEF conditioned media (MEF-UTCM) and (4) E0771 treated MEF conditioned media (MEF-CM) for 24 hours. Statistical analysis: Two-way ANOVA with Bonferroni post hoc correction. All results are presented as mean ± SEM (n=3).

3.5.7. PDH Enzyme Activity Assay

Assessment of the relative enzymatic activity of PDH in E0771 breast cancer cells following MEF conditioned media treatment was achieved using a commercially available kinetic assay. Our results showed no statistically significant differences in the enzymatic activity of PDH in E0771 cancer cells across all treatment groups for the entire duration of the assay when compared to control and control-CM.

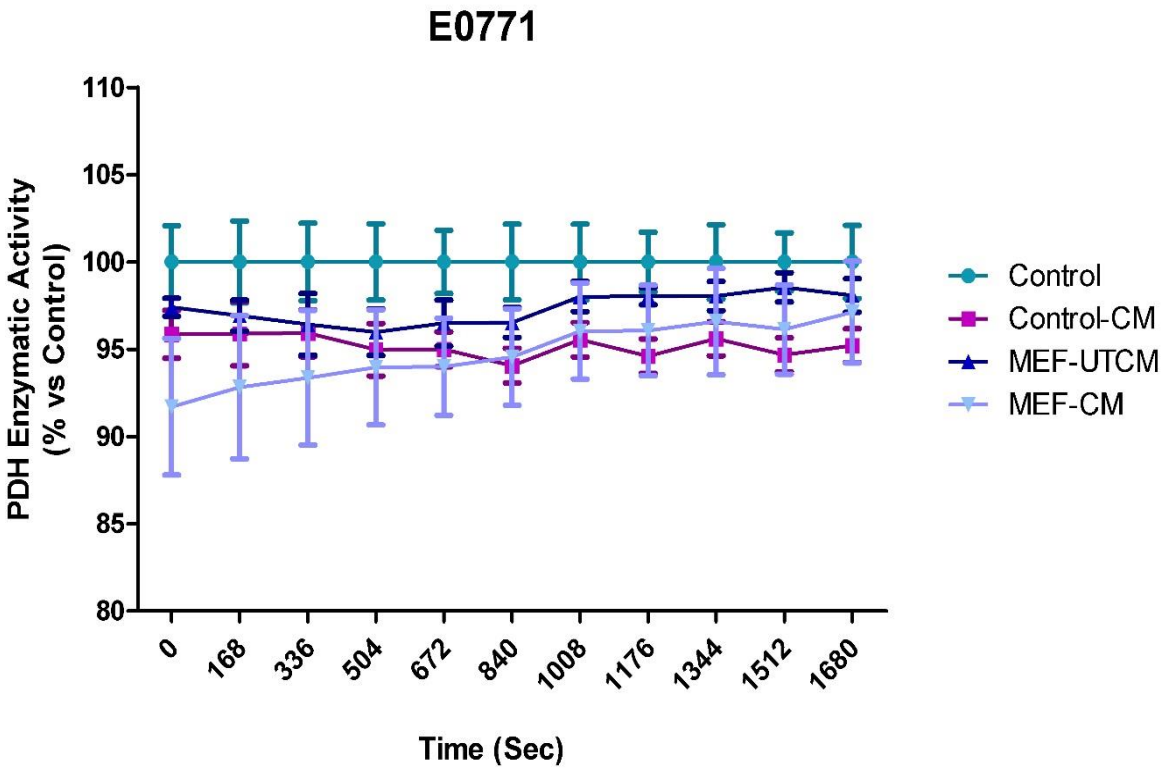

Figure 3.49: Determination of the effects of MEF conditioned media on the enzymatic activity of PDH in E0771 murine breast cancer cells. Subsequent to 12 hours of glucose deprivation (0 mM glucose DMEM), E0771 cells were subjected to (1) Control, (2) Control conditioned media (Control-CM), (3) Untreated MEF conditioned media (MEF-UTCM) and (4) E0771 treated MEF conditioned media (MEF-CM) for 24 hours. Statistical analysis: Two-way ANOVA with Bonferroni post hoc correction. All results are presented as mean ± SEM (n=3).

3.5.8. Mitomycin C Concentration Response

In order to establish a concentration of Mitomycin C that results in the effective inhibition of proliferation, E0771 cells were treated with various concentrations of Mitomycin C for a period of 24 hours. Nuclear counts were performed by manually counting intact nuclei following Hoechst 33342 staining. When compared to control (0 hr), a significant increase in the number of nuclei present was observed after 24 hours of no treatment (Control 24 hrs) (251.5 ± 21.79 vs 147.9 ± 7.161, $p<0.0001$), this was taken as the total proliferative capacity of E0771 cells in a 24 hour period. Treatment with both 5.0 µg/ml (167.5 ± 12.58 vs 251.5 ± 21.79, $p<0.01$) and 10 µg/ml (143.5 ± 8.738 vs 251.5 ± 21.79, $p<0.0001$) of Mitomycin C resulted in a significant decrease in the number of nuclei after 24 hours when compared to Control (24 hrs).

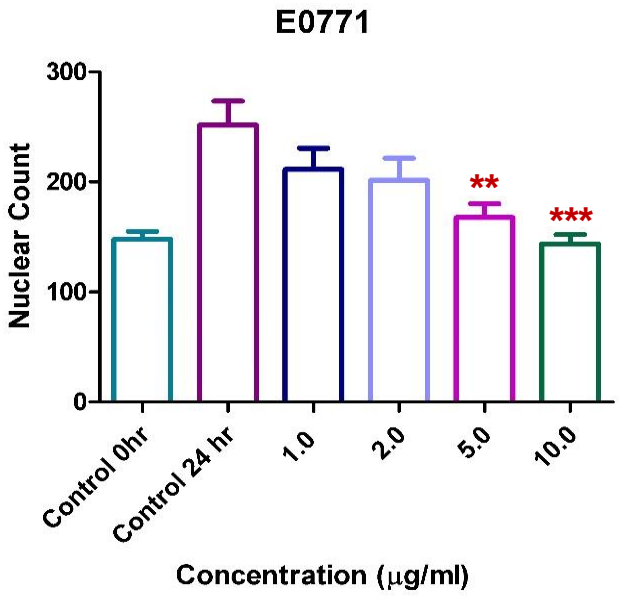

Figure 3.50: Determining the effects of Mitomycin C on the proliferative capabilities of E0771 murine breast cancer cells. Under standard cellular conditions nuclear counts were performed on E0771 cells subjected to (1) Control (0 hrs), (2) Control (24 hrs), (3) 1.0 µg/ml (4) 2.0 µg/ml (5) 1.0 µg/ml, and (6) 10 µg/ml Mitomycin C for 24 hours. Nuclear counts were assessed following Hoechst 33342 staining by manually counting intact nuclei. Statistical analysis: One way ANOVA with Bonferroni post hoc correction. All results are presented as mean ± SEM (n=3). ** = $p<0.01$ vs control and *** = $p<0.0001$ vs control (24 hrs).

Based on the Mitomycin C concentration response obtained, treatment with 10 µg/ml Mitomycin C for a period of 24 hours lead to a significant reduction in the nuclear count of the E0771 murine breast cancer cells compared to the 24 hour control. The reduction observed was comparable to the nuclear counts obtained for the baseline control (0 hrs), therefore this concentration was chosen for all subsequent experiments.

3.5.9. Migration (Scratch) Assay

Migration (scratch) assays were performed in E0771 cancer cells following MEF-CM treatment for 24 hrs. Images of wound areas were acquired at time points 6, 12, 18 and 24 hours during the 24 hour MEF-CM treatment period. Statistical analyses by means of two-way ANOVAs (with Bonferroni post hoc) were performed separately for each time point. Collective graphs showing the statistical results and representative images for each separate time point are included below. Proliferation control groups (cells not treated with Mitomycin C) showed significantly greater wound closure when compared to other treatment groups. This is as expected, as wound closure can be attributed to the fact that both cellular migration and proliferation contribute to wound closure.

When compared to control groups, a significant reduction in the percentage of wound closure was observed at the 6 hour and 12 hour time points in control-CM (6 hr: 7.871% ± 1.181% vs 26.430% ± 4.523%, $p<0.0001$ and 12 hr: 31.806% ± 3.695% vs 45.289% ± 3.596%, $p<0.01$), MEF-UTCM (6 hr: 8.712% ± 2.151% vs 26.430% ± 4.523%, $p<0.0001$ and 12 hr: 21.399% ± 1.675% vs 45.289% ± 3.596%, $p<0.0001$), and MEF-CM (6 hr: 8.340% ± 2.013% vs 26.430% ± 4.523%, $p<0.0001$ and 12 hr: 30.576% ± 4.498% vs 45.289% ± 3.596%, $p<0.0001$) groups. No significant differences were observed for any of the groups at the 18 hour time points. At the 24 hour time point only the MEF-UTCM

treatment group showed a significant reduction in percentage wound closure when compared to the control group (72.892% ± 2.540% vs 83.422% ± 2.104%, p<0.05).

However, when compared to the control-CM groups no significant changes in the percentage of wound closure was observed for either the MEF-UTCM or MEF-CM groups across all time points.

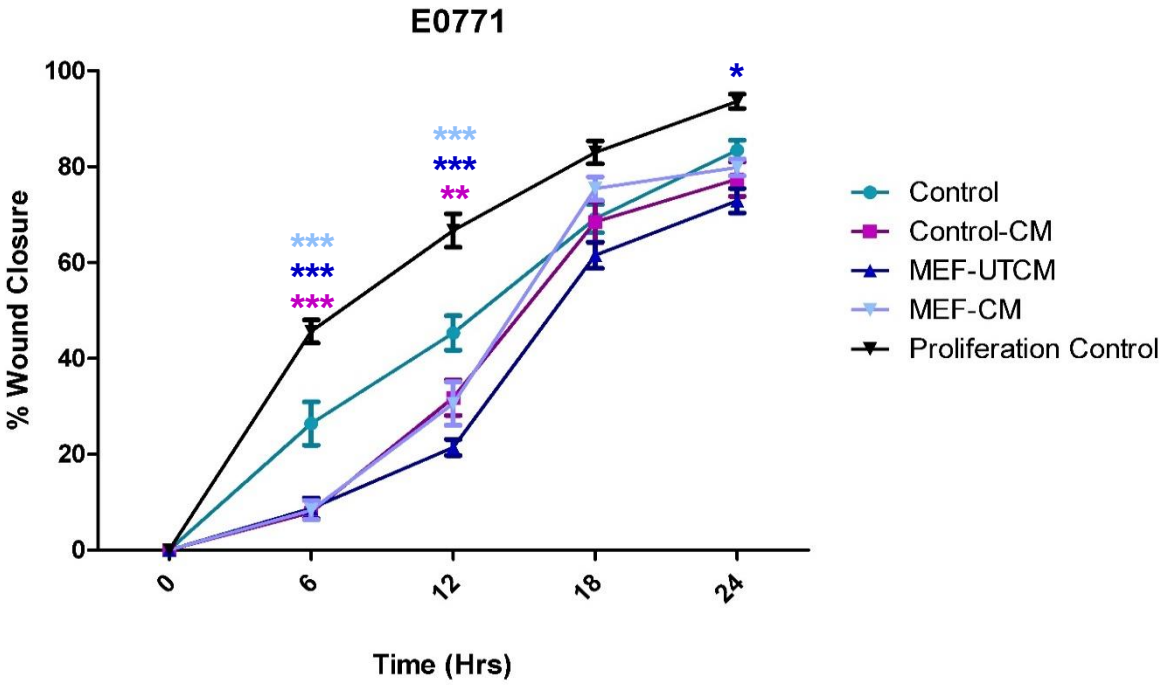

Figure 3.51: Determining the effects of MEF conditioned media on the migratory capacity of E0771 murine breast cancer cells. Subsequent to 12 hours of glucose deprivation (0 mM glucose DMEM), E0771 cells were subjected to (1) Control, (2) Control conditioned media (Control-CM), (3) Untreated MEF conditioned media (MEF-UTCM) and (4) E0771 treated MEF conditioned media (MEF-CM) for 24 hours. Migratory capacity following treatment was assessed by means of a wound healing (Scratch) assay. Statistical analysis: Two-way ANOVA with Bonferroni post hoc correction. All results are presented as mean ± SEM (n=9). * = p<0.05 vs control, ** = p<0.01 vs control and *** = p<0.0001 vs control.

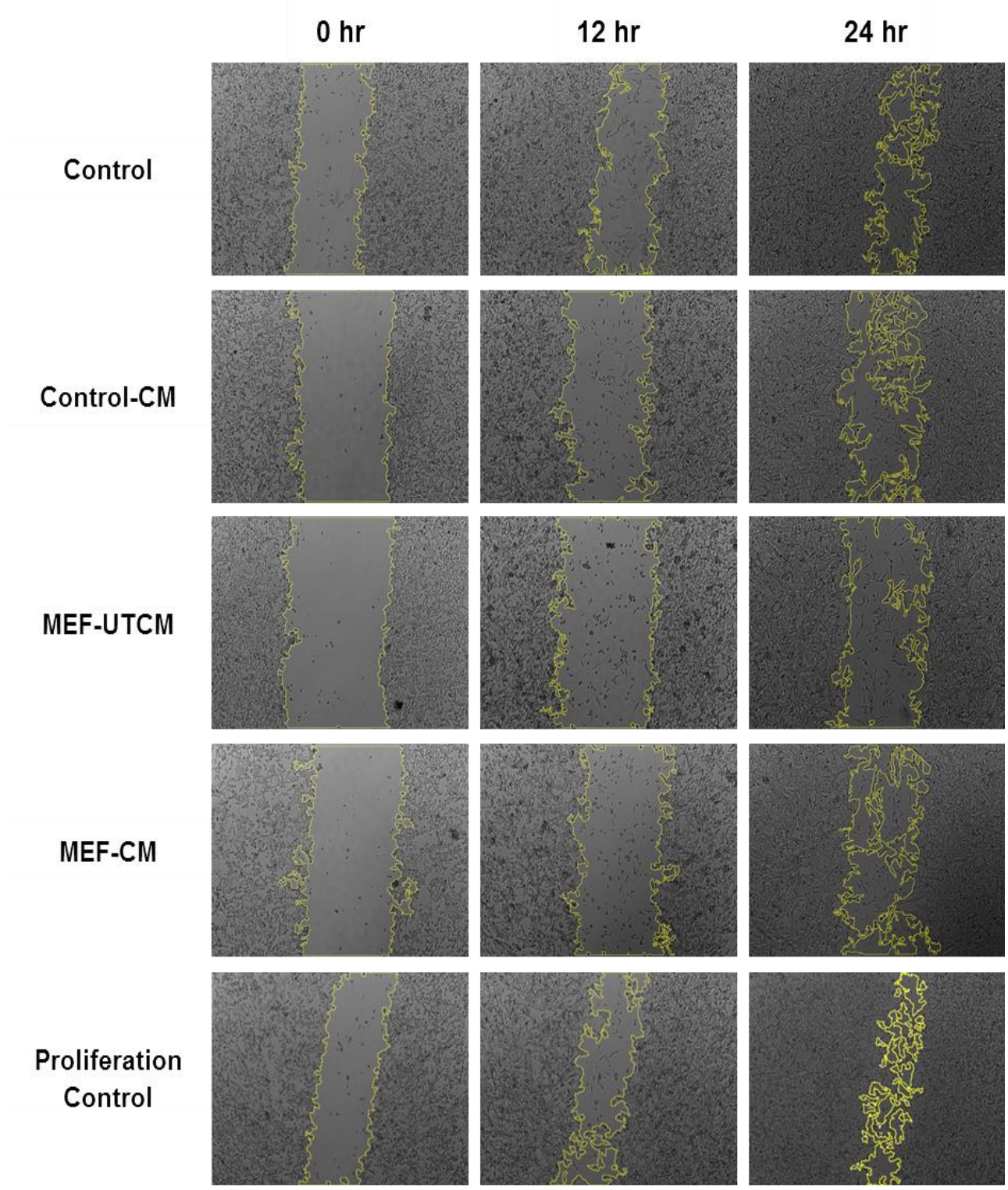

Figure 3.52: Representative time point images of the migration (scratch) assay performed on E0771 murine breast cancer cells following MEF conditioned media treatment. Subsequent to 12 hours of glucose deprivation (0 mM glucose DMEM), E0771 cells were subjected to (1) Control, (2) Control conditioned media, (3) Untreated MEF conditioned media and (3) E0771 treated MEF conditioned media for 24 hours. Image analysis performed in ImageJ using an MRI_wound_healing plugin, and images displayed are for the 0, 12 and 24 hour time points only.

Based on the fact that no statistical differences were obtained with the analysis of the percentage wound closure at the 18 hour time point, the slopes of the regression lines (Figure 3.49) for each separate time point were analysed to determine whether treatment with MEF-CM has an effect on the rate of change at which E0771 cells migrate into the wound area between each time point. Significantly lower slopes were seen in control-CM (1.312 ± 0.1968% vs 4.405% ± 0.7538%, $p<0.01$), MEF-UTCM (1.452% ± 0.3584% vs 4.405% ± 0.7538%, $p<0.01$) and MEF-CM (1.390% ± 0.3355% vs 4.405% ± 0.7538%, $p<0.01$) treatment groups in comparison to control between the 0-6 hr time points. A significant increase in the slope was seen following MEF-CM treatment in comparison to control (7.476 ± 0.8522% vs 3.983% ± 0.7789%, $p<0.05$) between the 12-18 hr time points.

Table 3.1: Determining the effects of MEF conditioned media on the rate of change (slope) of migration of E0771 murine breast cancer cells.

		Proliferation Control	Control	Control-CM	MEF-UTCM	MEF-CM
0-6 hrs	Slope	7.605 ± 0.3984	4.405 ± 0.7538	1.312 ± 0.1968	1.452 ± 0.3584	1.390 ± 0.3355
	p-value	< 0.0001	< 0.0001	< 0.0001	0.0009	0.0008
6-12 hrs	Slope	3.510 ± 0.7022	3.143 ± 0.9630	3.989 ± 0.6464	2.114 ± 0.4543	3.706 ± 0.8213
	p-value	0.0001	0.0049	< 0.0001	0.0003	0.0004
12-18 hrs	Slope	2.717 ± 0.7010	3.983 ± 0.7789	6.116 ± 0.9433	6.689 ± 0.5344	7.476 ± 0.8522
	p-value	0.0013	0.0001	< 0.0001	< 0.0001	< 0.0001
18-24 hrs	Slope	1.775 ± 0.4680	2.372 ± 0.6085	1.487 ± 0.9333	1.893 ± 0.6219	0.7352 ± 0.4980
	p-value	0.0016	0.0013	0.1306	0.0077	0.1593

*p-values indicate slopes which are significantly non-zero

Furthermore, in order to determine whether treatment with MEF-CM has an effect on migratory rate of E0771 cancer cells, the rate of wound closure was assessed by determining the percentage wound closure over time. A significant reduction in the rate of wound closure was seen at both the 6 hour and 12 hour time points for the control-CM (6 hr: 131.191% ± 19.675% vs 440.498% ± 75.379%, $p<0.0001$ and 12 hr: 265.049 ±

30.788% vs 377.409% ± 29.969%, p<0.05), MEF-UTCM (6 hr: 145.202% ± 35.843% vs 440.498% ± 75.379%, p<0.0001 and 12 hr: 178.323 ± 13.958% vs 377.409% ± 29.969%, p<0.0001) and MEF-CM (6 hr: 138.995% ± 33.546% vs 440.498% ± 75.379%, p<0.0001 and 12 hr: 254.798% ± 37.482% vs 377.409% ± 29.969%, p<0.01) treatment groups when compared to control. However, only the MEF-UTCM (512.781% ± 22.784% vs 380.561% ± 23.820%, p<0.01) showed a significant increase in the rate of E0771 cell migration at the 18 hour time point when compared to control.

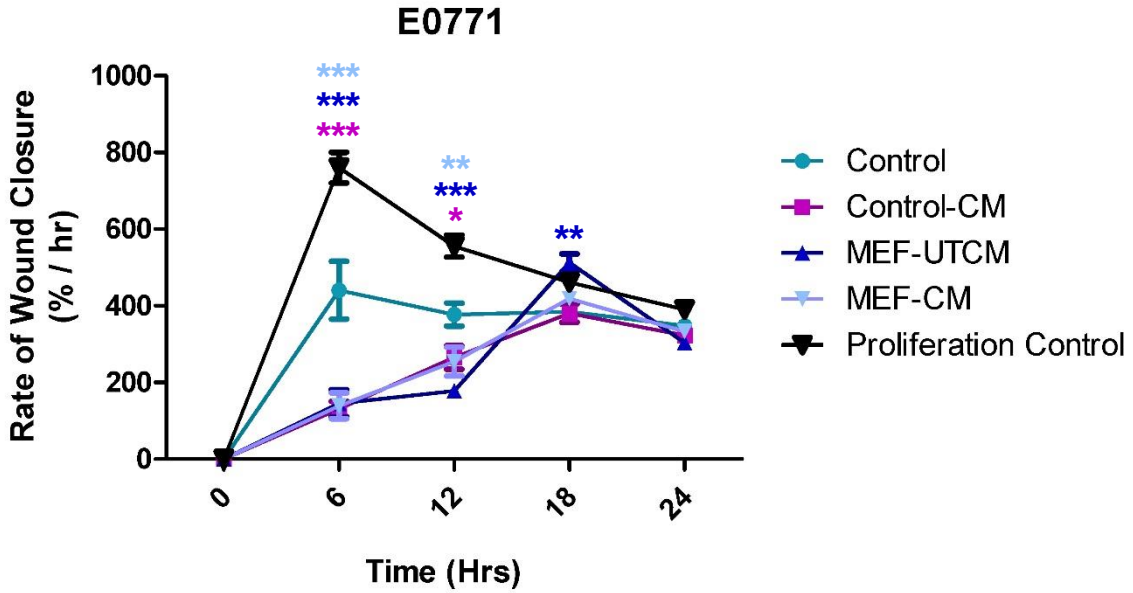

Figure 3.53: Determining the effects of MEF conditioned media on the rate of migration of E0771 murine breast cancer cells. Subsequent to 12 hours of glucose deprivation (0 mM glucose DMEM), E0771 cells were subjected to (1) Control, (2) Control conditioned media (Control-CM), (3) Untreated MEF conditioned media (MEF-UTCM) and (4) E0771 treated MEF conditioned media (MEF-CM) for 24 hours. Rate of wound closure (% / hr) was calculated by dividing the % wound closure at each time point by the number of hours passed. Statistical analysis: Two-way ANOVA with Bonferroni post hoc correction. All results are presented as mean ± SEM (n=9). * = p<0.05 vs control, ** = p<0.01 vs control and *** = p<0.0001 vs control.

Again, in order to determine if MEF-CM affects the change in the rate of wound closure of E0771 cancer cells between each time point, the slopes of the regression lines (Figure

3.51) between each time point were analysed separately. Significantly lower slopes were seen in control-CM (21.87% ± 3.279% vs 73.42% ± 12.56%, p<0.0001), MEF-UTCM (24.20% ± 5.974% vs 73.42% ± 12.56%, p<0.0001) and MEF-CM (23.17% ± 5.591% vs 73.42% ± 12.56%, p<0.0001) treatment groups in comparison to control between the 0-6 hr time points. Of interest to note is that the rate of migration decreases rapidly (represented by a change from a positive to negative slope) as early as the 6-12 hour time points in both the proliferation control (-34.12% ± 8.205%) and the control groups (-10.51% ± 13.52%). However, the rate of migration is only seen to decrease between 18-24 hour time points in the control-CM (-9.660% ± 4.692%), MEF-UTCM (-34.84% ± 4.187%) and MEF-CM (-14.40% ± 2.554%).

Table 3.2: Determining the effects of MEF conditioned media on the change in the rate (slope) of wound closure of E0771 cancer cells.

		Proliferation Control	Control	Control-CM	MEF-UTCM	MEF-CM
0-6 hrs	Slope	126.7 ± 6.640	73.42 ± 12.56	21.87 ± 3.279	24.20 ± 5.974	23.17 ± 5.591
	p-value	< 0.0001	< 0.0001	< 0.0001	0,0009	0,0008
6-12 hrs	Slope	-34.12 ± 8.205	-10.51 ± 13.52	22.31 ± 6.090	5.520 ± 6.411	19.30 ± 8.384
	p-value	0,0007	0,4481	0,0021	0,4019	0,0351
12-18 hrs	Slope	-15.78 ± 5.298	1.161 ± 5.708	19.25 ± 6.488	55.74 ± 4.453	27.38 ± 6.641
	p-value	0,0089	0,8414	0,0091	< 0.0001	0,0008
18-24 hrs	Slope	-11.82 ± 2.433	-6.131 ± 3.126	-9.660 ± 4.692	-34.84 ± 4.187	-14.40 ± 2.554
	p-value	0,0002	0,0675	0,0562	< 0.0001	< 0.0001

*p-values indicate slopes which are significantly non-zero

3.5.10. EMT Assessment

In order to determine whether epithelial-to-mesenchymal transition plays a role in the migratory capacity of E0771 following treatment with MEF-CM. Western blotting analysis was employed to assess the relative protein expression of the mesenchymal markers; α-smooth muscle actin (α-SMA), platelet derived growth factor receptor α (PDGFRα) and vimentin as well as the epithelial cell surface marker E-cadherin.

3.5.10.1. α-SMA and PDGFRα

When compared to the control group, we observed a significant increase in the relative protein expression levels of α-SMA in E0771 breast cancer cells that had been treated with MEF-CM (141.1% ± 9.479% vs 100% ± 11.42%, p=0.0323). However, when PDGFRα protein expression levels were assessed no statistically significant differences were observed across all treatment groups when compared to control.

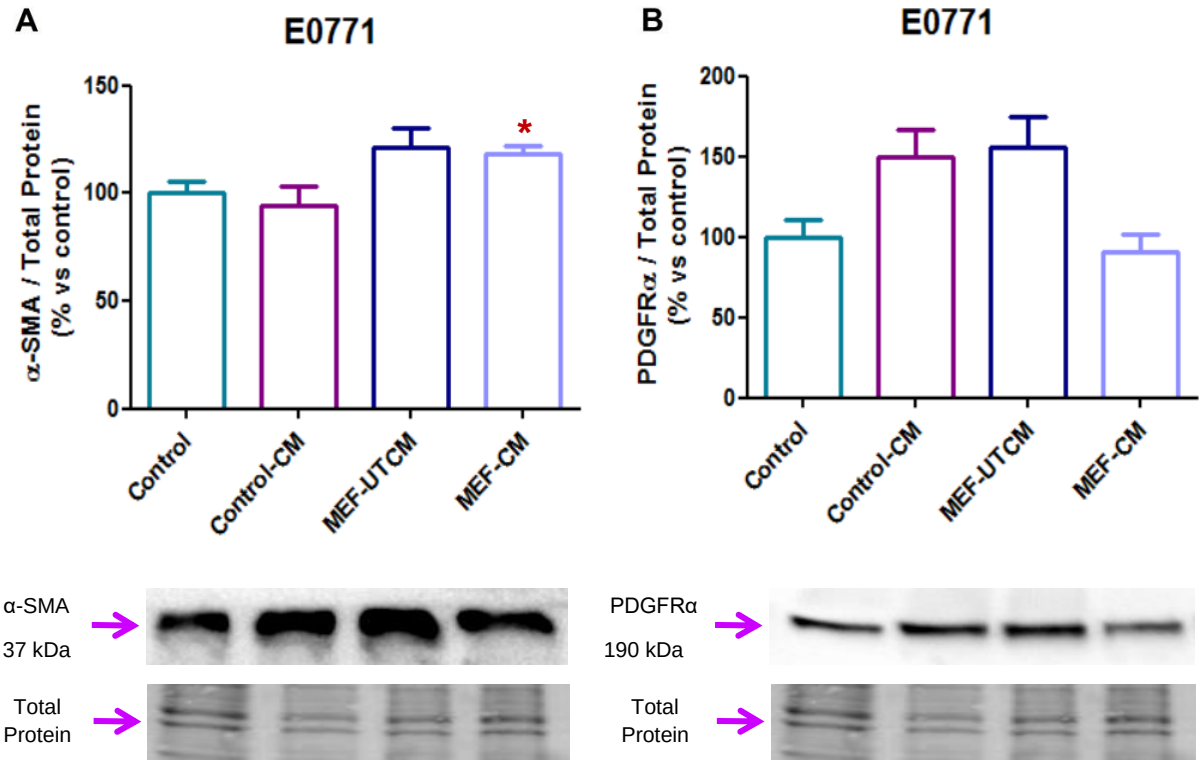

Figure 3.54: Western blot analysis of α-SMA and PDGFRα in E0771 breast cancer cells following MEF conditioned media treatment. Subsequent to 12 hours of glucose deprivation (0 mM glucose DMEM), E0771 cells were subjected to (1) Control, (2) Control conditioned media (Control-CM), (3) Untreated MEF conditioned media (MEF-UTCM) and (4) E0771 treated MEF conditioned media (MEF-CM) for 24 hours. Statistical analysis: One way ANOVA with Bonferroni post hoc correction. All results are presented as mean ± SEM (n=3). * = p<0.05 vs control.

3.5.10.2. Vimentin and E-cadherin

Assessment of vimentin showed a significant increase in relative protein expression levels in E0771 breast cancer cells following treatment with MEF-CM (188.0% ± 5.651% vs 100% ± 13.12%, p=0.0010) in comparison to the control group. We also observed a significant decrease in the protein expression of the epithelial marker E-cadherin following treatment with both MEF-UTCM (55.79% ± 9.842% vs 100% ± 11.09%, p=0.0098) and MEF-CM (38.06% ± 9.317% vs 100% ± 11.09%, p=0.0006) in comparison to the control group.

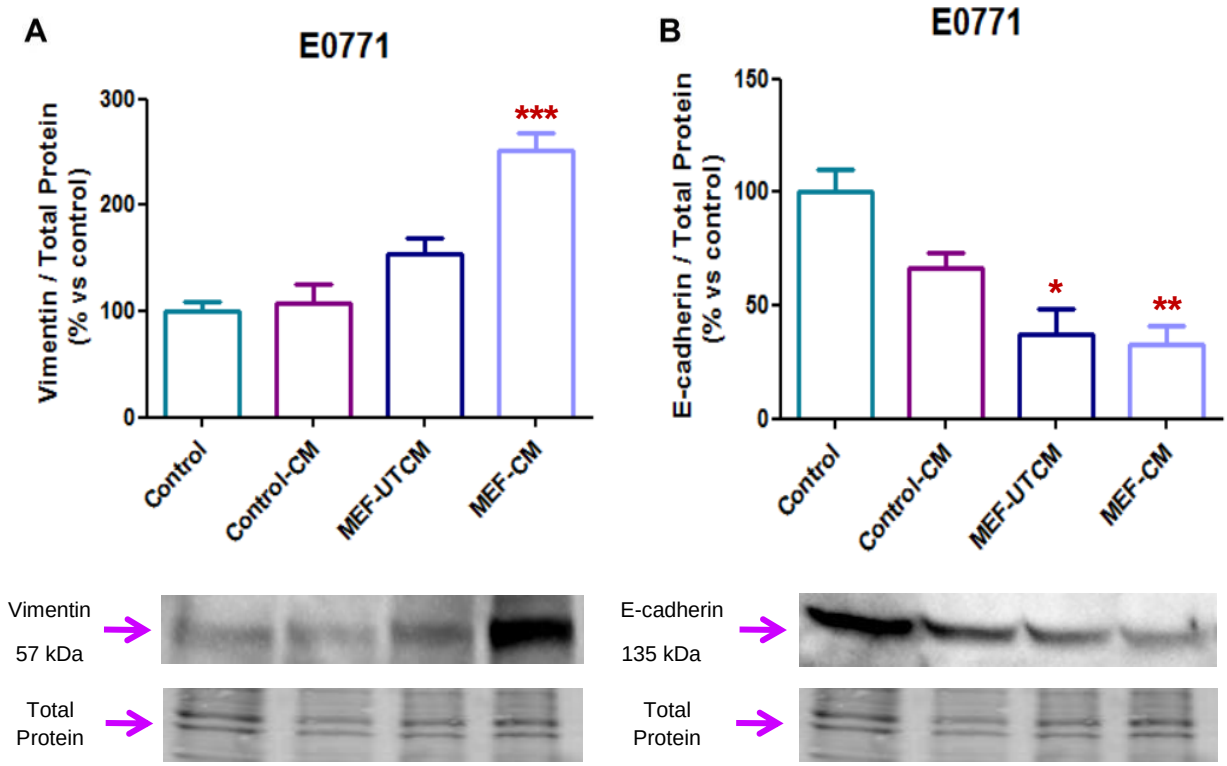

Figure 3.55: Western blot analysis of vimentin and E-cadherin in E0771 breast cancer cells following MEF conditioned media treatment. Subsequent to 12 hours of glucose deprivation (0 mM glucose DMEM), E0771 cells were subjected to (1) Control, (2) Control conditioned media (Control-CM), (3) Untreated MEF conditioned media (MEF-UTCM) and (4) E0771 treated MEF conditioned media (MEF-CM) for 24 hours. Statistical analysis: One way ANOVA with Bonferroni post hoc correction. All results are presented as mean ± SEM (n=3). * = p<0.05 vs control, ** = p<0.01 vs control and *** = p<0.0001 vs control.

3.6: Effects of MEF Conditioned Media on Doxorubicin Resistance and Cell Migration in E0771 Breast Cancer Cells

3.6. Effects of MEF Conditioned Media on Doxorubicin Resistance and Cell Migration in E0771 Breast Cancer Cells

In addition to the role that CAFs play in mediating cell migration and cancer metastasis, it has become increasingly evident that CAFs also play a role in the chemotherapeutic resistance of tumours (Kojima *et al*., 2010, Yang *et al*., 2010, Müerköster *et al*., 2008). Based on this, the next section of this study focuses on elucidating the influences that the combination of MEF conditioned media and doxorubicin treatment have on E0771 breast cancer cell metabolism and cell migration.

3.6.1. Doxorubicin Dose Response

In order to establish a dose of doxorubicin that produces the least significant percentage of cell death in the doxorubicin resistant E0771 murine breast cancer cells. E0771 cells were treated with various concentrations of doxorubicin for a period of 24 hours. MTT cell viability assays were carried out to determine the relative percentage cell death. When compared to control, neither 0.1, or 1.0 μM doxorubicin resulted in a decrease in the MTT reductive capacity (0.1 μM:98.52% ± 2.802% vs 100% ± 3.434% and 1.0 μM: 92.60% ± 2.698% vs 100% ± 3.434%), however when subjected to either 2.5, 5.0, or 10.0 μM of doxorubicin for a period of 24 hours a significant reduction in MTT reductive capacity (2.5 μM: 73.31% ± 2.588% vs 100% ± 3.434%, $p<0.0001$. 5.0 μM: 69.13% ± 2.442% vs 100% ± 3.434%, $p<0.0001$ and 10.0 μM: 68.46% ± 3.104% vs 100% ± 3.434%, $p<0.0001$) when compared to control.

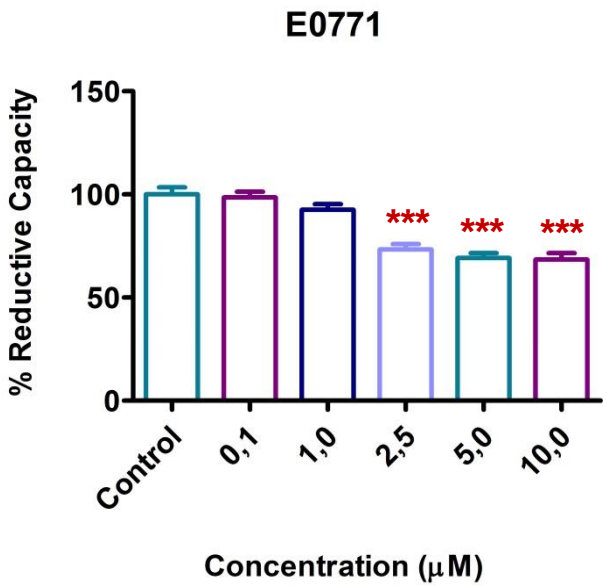

Figure 3.56: The effect of various concentrations of Doxorubicin on the viability of E0771 murine breast cancer cells. E0771 cells were incubated in 0 (Control), 0.1, 1.0 2.5, 5.0 and 10.0 µM doxorubicin for 24 hours. Cell viability was assessed using the MTT assay. Values are expressed as a percentage of the control and presented as mean ± SEM (n=3). *** = $p<0.0001$ vs control.

Based on initial doxorubicin dose responses, treatment with 2.5 µM doxorubicin over a period of 24 hours lead to a significant reduction in cell viability of the E0771 murine breast cancer cells, therefore this concentration was chosen for all further experiments. As we aimed to assess the effects of MEF conditioned media on doxorubicin resistance, E0771 cells were first glucose starved for 12 hours as previously described and then treated with MEF-CM in combination with 2.5 µM doxorubicin for 24 hours. Therefore, the following treatment groups were used for this section of the study (1) control; (2) control conditioned media (Control-CM); (3) MEF untreated conditioned media (MEF-UTCM), (4) MEF conditioned media (MEF-CM), (5) 2.5 µM Doxorubicin, (6) 2.5 µM Doxorubicin + control conditioned media (Dox + Control-CM), (7) 2.5 µM Doxorubicin + MEF untreated conditioned media (Dox + MEF-UTCM) and (8) 2.5 µM Doxorubicin + MEF conditioned media (Dox + MEF-CM).

3.6.2. Cell Viability

MTT cell viability assays were carried out to assess the viability of E0771 murine cancer cells following treatments. E0771 cells showed a significant reduction in MTT reductive capacity following 2.5 µM doxorubicin treatment when compared to control (77.21% ± 1.776% vs 100% ± 2.630%, $p<0.0001$), However, when glucose deprived E0771 cells were treated with doxorubicin in combination with MEF-CM a significant increase in mitochondrial reductive capacity was observed when compared to doxorubicin treatment alone (91.39% ± 3.870% vs 77.21% ± 1.776%, $p<0.05$).

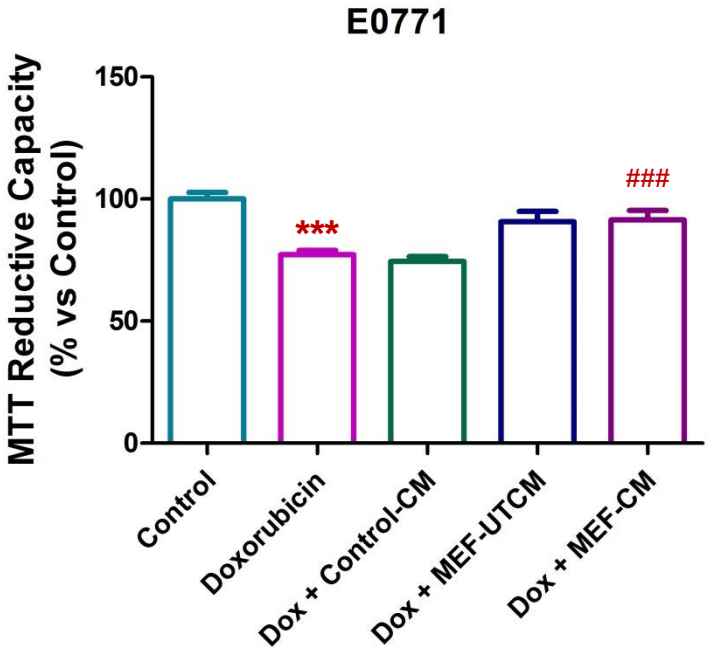

Figure 3.57: Determining the effects of MEF conditioned media in combination with doxorubicin on the viability of glucose deprived E0771 murine breast cancer cells. Subsequent to 12 hours of glucose deprivation (0 mM glucose DMEM), E0771 cells were subjected to (1) Control, (2) Doxorubicin, (3) Doxorubicin + control conditioned media (Dox + Control-CM), (4) Doxorubicin + MEF untreated conditioned media (Dox + MEF-UTCM) and (5) Doxorubicin + MEF conditioned media (Dox + MEF-CM) for 24 hours. Cell viability was assessed using the MTT assay. Statistical analysis: One way ANOVA with Bonferroni post hoc correction. All results are presented as mean ± SEM (n=3). *** = $p<0.0001$ vs Control, ### = $p<0.0001$ vs Doxorubicin.

3.6.3. Cell Death Assessment (Hoechst + PI)

As previously described, cell death analysis by means of flow cytometry, following doxorubicin treatment in conjunction with MEF conditioned media was conducted in order to further validate the results obtained for the MTT cell viability assay. A significant decrease in E0771 live cell population was observed following MEF-CM treatment in combination with 2.5 µM doxorubicin in comparison to the control group (70.03% ± 0.4356% vs 85.40% ± 1.044%, $p<0.0001$). A concomitant increase in the dead cell population of E0771 cancer cells treated with the combination of MEF-CM and doxorubicin was also observed when compared to control (30.18% ± 0.4294% vs 10.40% ± 0.8983%, $p<0.0001$).

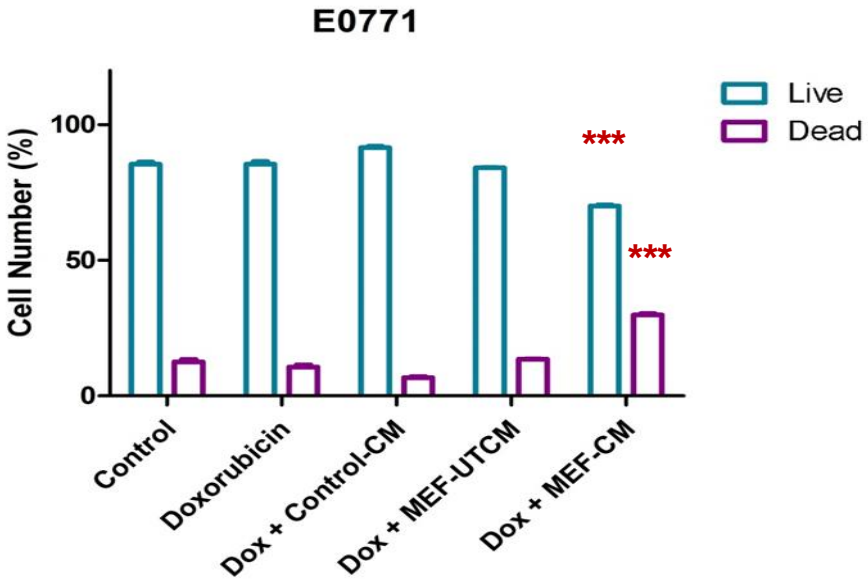

Figure 3.58: Determination of the effects of MEF conditioned media in combination with doxorubicin on cell death in glucose deprived E0771 murine breast cancer cells. Subsequent to 12 hours of glucose deprivation (0 mM glucose DMEM), E0771 cells were subjected to (1) Control, (2) Doxorubicin, (3) Doxorubicin + Control conditioned media, (4) Doxorubicin + Untreated MEF conditioned media (Dox + MEF-UTCM) and (5) Doxorubicin + E0771 treated MEF conditioned media (Dox + MEF-CM) for 24 hours. Live / Dead cell populations were determined by means of flow cytometry following Hoechst 33342 and PI staining. Statistical analysis: One way ANOVA with Bonferroni post hoc correction. All results are presented as mean ± SEM (n=3). *** = $p<0.0001$ vs Doxorubicin.

3.6.4. MCT1/4 transporter expression

When compared to both doxorubicin (Dox) and Dox + control-CM, no significant differences in either MCT-1 (monocarboxylate importer) or MCT-4 (monocarboxylate exporter) protein expression levels were observed across all treatment groups.

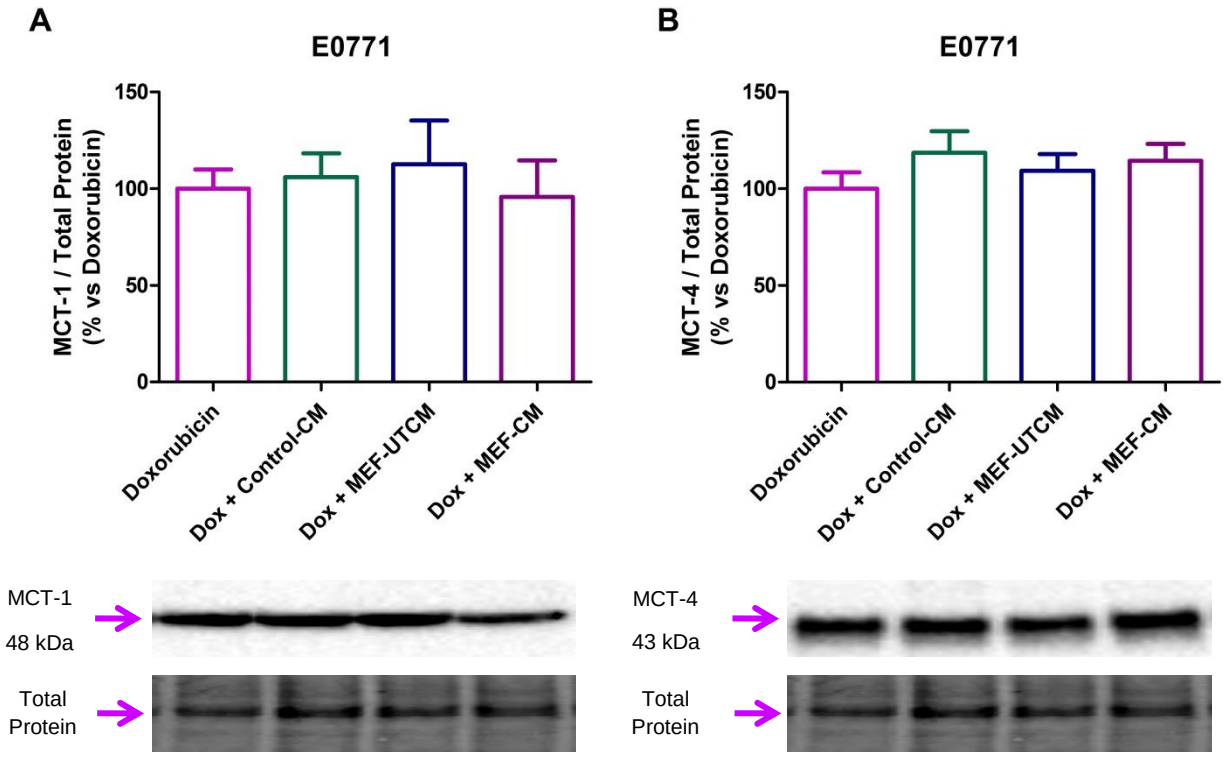

Figure 3.59: Western Blot analysis of MCT-1 and MCT-4 protein expression in E0771 breast cancer cells treated with doxorubicin and MEF conditioned media. Subsequent to 12 hours of glucose deprivation (0 mM glucose DMEM), E0771 cells were subjected to (1) Doxorubicin (Dox), (2) Dox + Control conditioned media, (3) Dox + Untreated MEF conditioned media (MEF-UTCM) and (3) Dox + E0771 treated MEF conditioned media (MEF-CM) for 24 hours. Statistical analysis: One way ANOVA with Bonferroni post hoc correction. All results are presented as mean ± SEM (n=3).

3.6.5. L-Lactate Assay

As previously described, L-lactate concentrations were assessed following treatment of glucose deprived E0771 cells with MEF conditioned media in combination with 2.5 µM

doxorubicin by means of a commercially available colorimetric assay. A significant increase in L-lactate concentration was observed in E0771 breast cancer cells following doxorubicin treatment in combination with MEF-CM (211.1% ± 21.75% vs 111.5% ± 13.49%, p=0.0176) when compared to doxorubicin alone.

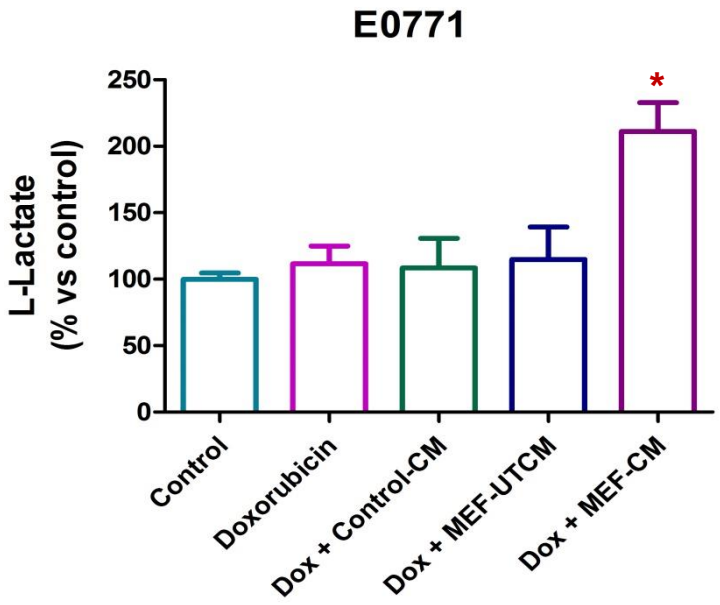

Figure 3.60: Determination of the effects of MEF conditioned media on L-lactate concentrations in E0771 murine breast cancer cells. Subsequent to 12 hours of glucose deprivation (0 mM glucose DMEM), E0771 cells were subjected to (1) Control, (2) Doxorubicin, (3) Doxorubicin + Control conditioned media, (4) Doxorubicin + Untreated MEF conditioned media (Dox + MEF-UTCM) and (5) Doxorubicin + E0771 treated MEF conditioned media (Dox + MEF-CM) for 24 hours. Statistical analysis: One way ANOVA with Bonferroni post hoc correction. All results are presented as mean ± SEM (n=3). * = $p<0.05$ vs Doxorubicin.

3.6.6. ATP Production Assay

Determination of relative ATP production in glucose deprived E0771 breast cancer cells treated with Doxorubicin in combination with MEF conditioned media, demonstrated a significant increase in ATP production following Dox + MEF-UTCM (30.03 ± 1.420 vs 17.79 ± 0.7905, p=0.0079) and Dox + MEF-CM (42.54 ± 2.188 vs 17.79 ± 0.7905, p=0.0087) when compared to doxorubicin alone. Additionally, when compared to Dox +

control-CM, a significant increase in ATP production was also observed following doxorubicin treatment in combination with MEF-UTCM (30.03 ± 1.420 vs 16.32 ± 3.004, p=0.0145) and MEF-CM (42.54 ± 2.188 vs 16.32 ± 3.004%, p=0.0083).

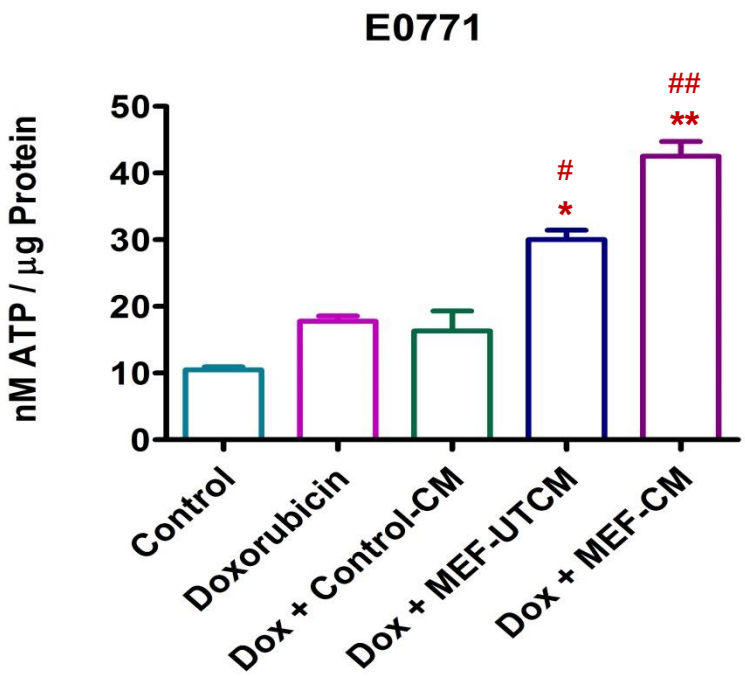

Figure 3.61: Determining the effects of MEF conditioned media in combination with doxorubicin on ATP production in E0771 murine breast cancer cells. Subsequent to 12 hours of glucose deprivation (0 mM glucose DMEM), E0771 cells were subjected to (1) Control, (2) Doxorubicin, (3) Doxorubicin + Control conditioned media, (4) Doxorubicin + Untreated MEF conditioned media (Dox + MEF-UTCM) and (5) Doxorubicin + E0771 treated MEF conditioned media (Dox + MEF-CM) for 24 hours. Statistical analysis: One way ANOVA with Bonferroni post hoc correction. All results are presented as mean ± SEM (n=3). ** = p<0.01 vs Doxorubicin, # = p<0.05 vs Dox + control-CM and ## = p<0.01 vs Dox + control-CM.

3.6.7. Pyruvate dehydrogenase (PDH) Assay

We observed a significant increase in total amount of PDH present in E0771 cells that had been treated with doxorubicin in combination with MEF-CM at the 1680 second time point (129.5% ± 8.204% vs 97.29% ± 6.791%, p<0.05) alone when compared to the doxorubicin group. Additionally, when compared to the dox + control-CM group a significant increase

in PDH, from the 840 second time point (111.0% ± 2.282% vs 79.58% ± 9.696%, p<0.05) onwards was observed in the following dox + MEF-CM treatment.

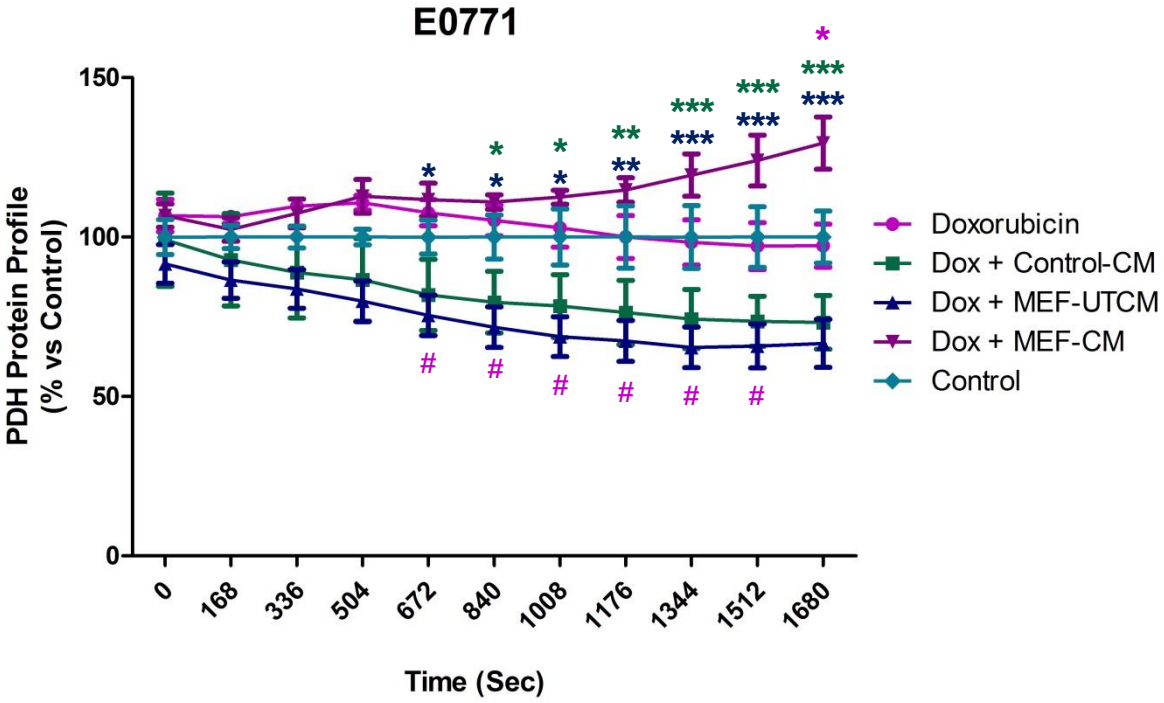

Figure 3.62: Determination of the effects of doxorubicin in combination with MEF conditioned media on the protein profile of PDH in E0771 murine breast cancer cells. Subsequent to 12 hours of glucose deprivation (0 mM glucose DMEM), E0771 cells were subjected to (1) Control, (2) Doxorubicin, (3) Doxorubicin + Control conditioned media, (4) Doxorubicin + Untreated MEF conditioned media (Dox + MEF-UTCM) and (5) Doxorubicin + E0771 treated MEF conditioned media (Dox + MEF-CM) for 24 hours. Statistical analysis: Two-way ANOVA with Bonferroni post hoc correction. All results are presented as mean ± SEM (n=3). * represent statistically significant results for the dox + MEF-CM group and # represent statistically significant results for the dox + MEF-UTCM group. The colour of the symbol denotes the comparison group.

Furthermore, when compared to the dox + MEF-UTCM treatment group a statistically significant increase was seen from the 504 second time point (112.8% ± 5.327% vs 79.87% ± 6.402%, p<0.05). Of interest to note is that while the total PDH amount significantly increases over time in the dox + MEF-CM group when compared to control, significant decreases over time in the total PDH amount is seen in the dox + MEF-UTCM

group, from the 672 second time point (75.44% ± 6.326% vs 107.6% ± 4.094%, $p<0.05$) up to the 1680 second time point in comparison to control.

3.6.8. PDH Enzyme Activity Assay

Again, when the enzymatic activity of PDH was assessed over time, no significant differences were observed for all treatment groups across all time points when compared to the doxorubicin only group.

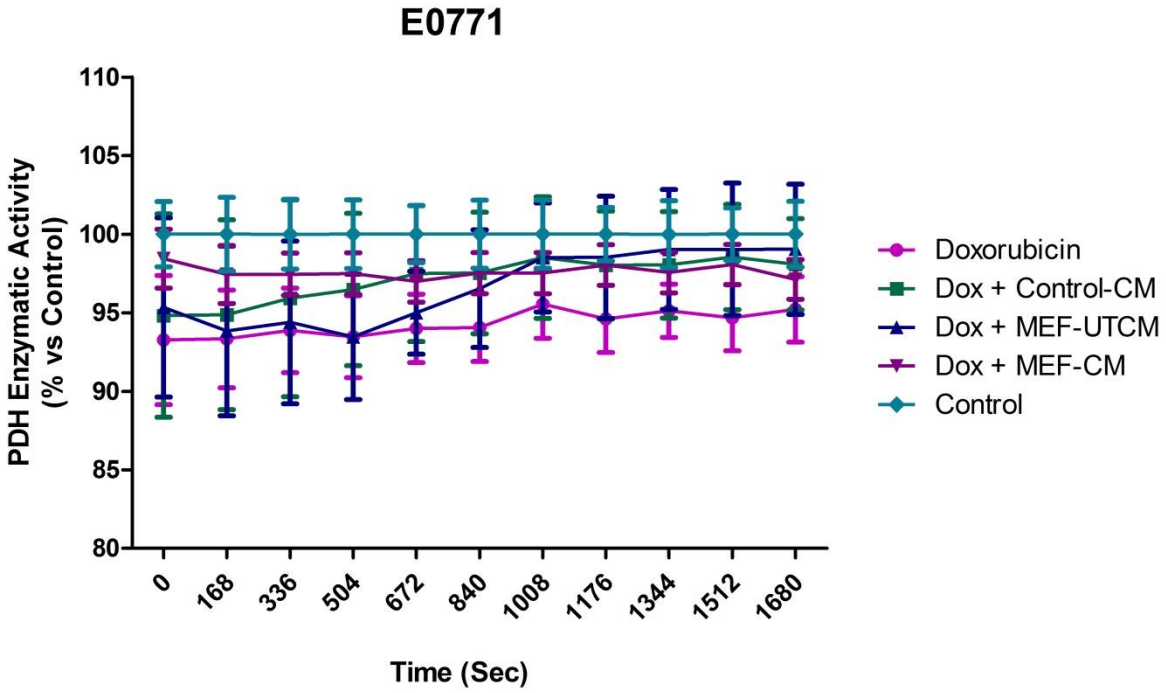

Figure 3.63: Determination of the effects of doxorubicin in combination with MEF conditioned media on the enzymatic activity of PDH in E0771 murine breast cancer cells. Subsequent to 12 hours of glucose deprivation (0 mM glucose DMEM), E0771 cells were subjected to (1) Control, (2) Doxorubicin, (3) Doxorubicin + Control conditioned media, (4) Doxorubicin + Untreated MEF conditioned media (Dox + MEF-UTCM) and (5) Doxorubicin + E0771 treated MEF conditioned media (Dox + MEF-CM) for 24 hours. Statistical analysis: Two-way ANOVA with Bonferroni post hoc correction. All results are presented as mean ± SEM (n=3).

3.6.9. Migration (Scratch) Assay

Subsequent to metabolic assessment of E0771 breast cancer cells following combined treatment with doxorubicin and MEF-CM, cell migration was assessed with the use of a migration (scratch) assay, as previously described (see section 3.5.9). A significant reduction in wound closure was observed at the 6 hour time point in the Dox + control-CM (14.99% ± 1.964% vs 34.18% ± 5.720%, $p<0.01$), Dox + MEF-UTCM (6.043% ± 7.048% vs 34.18% ± 5.720%, $p<0.0001$), and Dox + MEF-CM (13.00% ± 6.647% vs 34.18% ± 5.720%, $p<0.0001$) groups, compared to doxorubicin. Furthermore, a significant reduction in % wound closure was seen at the 12, 18 and 24 hour time points only for the dox + MEF-UTCM (12 hour: 19.97% ± 5.918% vs 43.22% ± 5.160%, $p<0.0001$, 18 hour: 41.32% ± 6.128% vs 61.33% ± 4.519%, $p<0.01$ and 24 hour: 48.78% ± 4.939% vs 68.13% ± 3.044%, $p<0.01$) group when compared to doxorubicin alone.

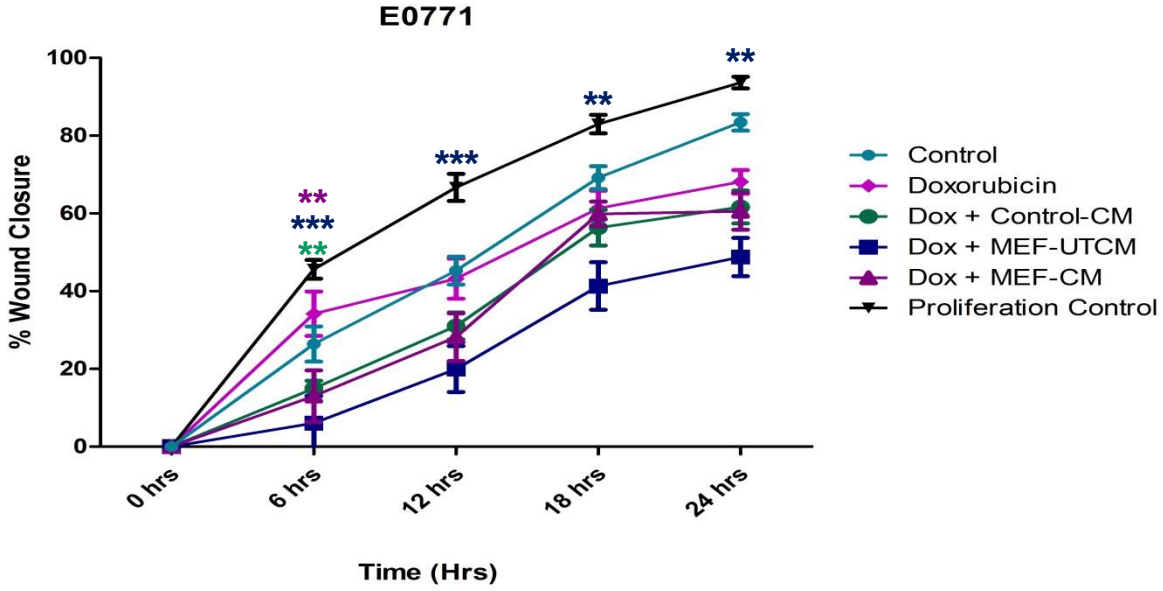

Figure 3.64: Determining the effects of MEF conditioned media in combination with doxorubicin on the migratory capacity of E0771 murine breast cancer cells. Subsequent to 12 hours of glucose deprivation (0 mM glucose DMEM), E0771 cells were subjected to (1) Doxorubicin, (2) Doxorubicin + Control conditioned media, (3) Doxorubicin + Untreated MEF conditioned media (MEF-UTCM) and (4) Doxorubicin + E0771 treated MEF conditioned media (MEF-CM) for 24 hours. Statistical analysis: Two-way ANOVA with Bonferroni post hoc correction. All results are presented as mean ± SEM (n=9). ** = $p<0.01$ vs Doxorubicin and *** = $p<0.0001$ vs Doxorubicin

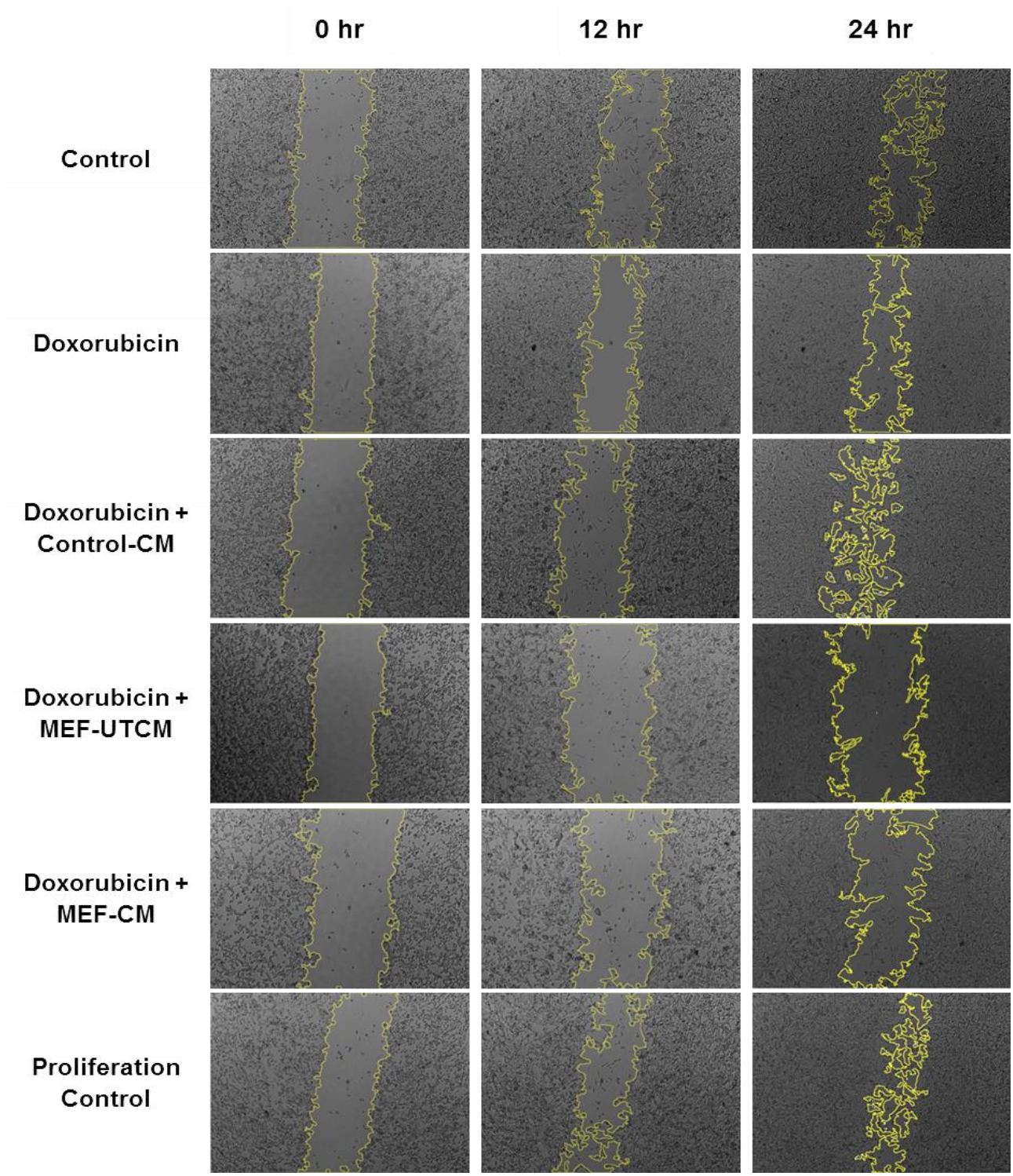

Figure 3.65: Representative time point images of the migration (scratch) assay performed on E0771 murine breast cancer cells following doxorubicin and MEF conditioned media treatment. Subsequent to 12 hours of glucose deprivation (0 mM glucose DMEM), E0771 cells were subjected to (1) Doxorubicin, (2) Dox + Control conditioned media, (3) Dox + Untreated MEF conditioned media and (4) Dox + E0771 treated MEF conditioned media for 24 hours. Image analysis performed in ImageJ using an MRI_wound_healing plugin, and images displayed are for the 0, 12 and 24 hour time points only.

Again, the slopes of the regression lines (Figure 3.64) for each separate time point were analysed to determine whether treatment with the combined effects of doxorubicin and MEF-CM have an effect on the rate of change of migration of E0771 cancer cells. Significantly lower slopes were seen following doxorubicin + control-CM (2.498 ± 0.3274% vs 5.697% ± 0.9533%, $p<0.01$) in comparison to control between the 0-6 hr time points. However, no statistically significant differences in the slopes, for any of the treatment groups, were observed between the 6-12 hr, 12-18 hr and 18-24 hr time points.

Table 3.3: Determining the effects of doxorubicin and MEF conditioned media on the rate of change (slope) of migration of E0771 murine breast cancer cells.

		Proliferation Control	Control	Doxorubicin	Dox + Control-CM	Dox + MEF-UTCM	Dox + MEF-CM
0-6 hrs	Slope	7.605 ± 0.3984	4.405 ± 0.7538	5.697 ± 0.9533	2.498 ± 0.3274	1.007 ± 1.175	2.167 ± 1.108
	p-value	< 0.0001	<0.0001	< 0.0001	< 0.0001	0.4039	0.0681
6-12 hrs	Slope	3.510 ± 0.7022	3.143 ± 0.9630	1.506 ± 1.284	2.678 ± 0.6632	2.320 ± 1.534	2.529 ± 1.505
	p-value	0.0001	0.0049	0.2579	0.001	0.1499	0.1124
12-18 hrs	Slope	2.717 ± 0.7010	3.983 ± 0.7789	3.018 ± 1.143	4.211 ± 0.9599	3.559 ± 1.420	5.282 ± 1.148
	p-value	0.0013	0.0001	0.0178	0.0005	0.0234	0.0003
18-24 hrs	Slope	1.775 ± 0.4680	2.372 ± 0.6085	1.134 ± 0.9081	0.8882 ± 1.043	1.243 ± 1.312	0.1122 ± 0.9534
	p-value	0.0016	0.0013	0.2298	0.4071	0.3573	0.9078

*p-values indicate slopes which are significantly non-zero

As previously described, the rate of wound closure was assessed by determining the percentage wound closure over time. Again, significant reduction in the rate of wound closure was seen only at the 6 hour for the dox + control-CM (249.8% ± 32.74% vs 569.7% ± 95.33%, $p<0.0001$), dox + MEF-UTCM (234.2% ± 90.63% vs 569.7% ± 95.33%%, $p<0.0001$) and dox + MEF-CM (216.7% ± 110.8% vs 569.7% ± 95.33%%, $p<0.0001$) treatment groups when compared to control. Additionally, only the dox + MEF-UTCM group (204.3% ± 25.96% vs 360.2% ± 43.00%, $p<0.05$) showed a significant decrease in the rate of wound closure at the 12 hour time point when compared to doxorubicin alone.

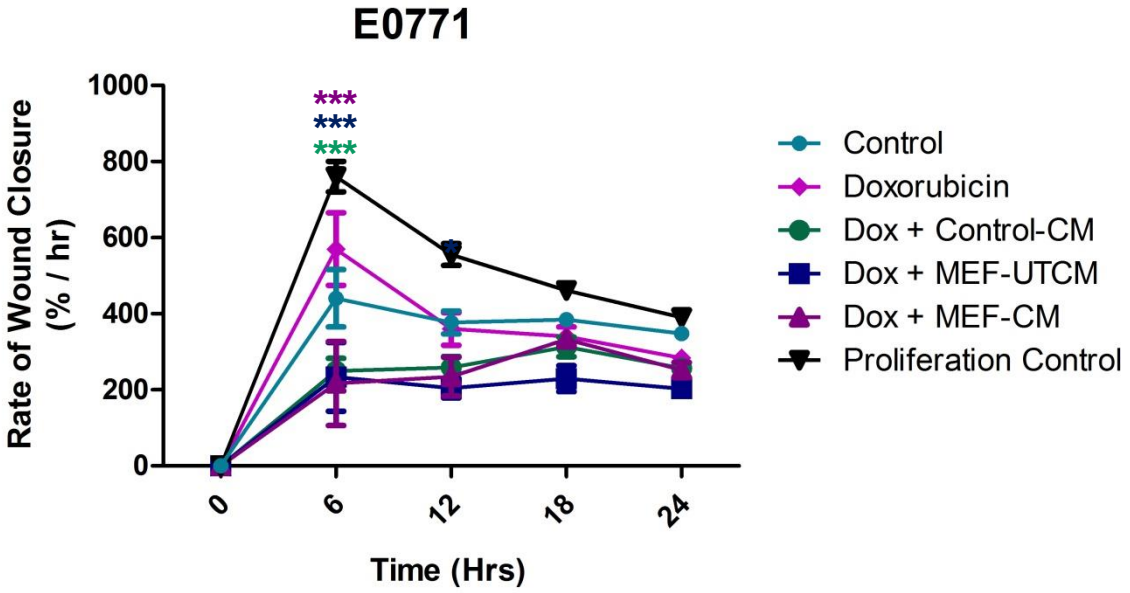

Figure 3.66: Determining the effects of doxorubicin and MEF conditioned media on the rate of migration of E0771 murine breast cancer cells. Subsequent to 12 hours of glucose deprivation (0 mM glucose DMEM), E0771 cells were subjected to (1) Doxorubicin, (2) Doxorubicin + Control conditioned media, (3) Doxorubicin + Untreated MEF conditioned media (Dox + MEF-UTCM) and (4) Doxorubicin + E0771 treated MEF conditioned media (Dox + MEF-CM) for 24 hours. Rate of wound closure (% / hr) was calculated by dividing the % wound closure at each time point by the number of hours passed. Statistical analysis: Two-way ANOVA with Bonferroni post hoc correction. All results are presented as mean ± SEM (n=9). * = $p<0.05$ vs doxorubicin and *** = $p<0.0001$ vs doxorubicin.

Assessment of the slopes of the regression lines (Figure 3.66) between each time point were again analysed separately. Significantly lower slopes were seen in the Dox + MEF-UTCM (39.03% ± 15.11% vs 94.95% ± 15.89%, $p<0.05$) and Dox + MEF-CM (35.12% ± 18.46% vs 94.95% ± 15.89%, $p<0.05$) treatment groups in comparison to doxorubicin between the 0-6 hr time points. Again, the rate of migration decreases rapidly (represented by a change from a positive to negative slope) as early as the 6-12 hour time points in both the proliferation control (-34.12% ± 8.205%), doxorubicin only (-34.93% ± 17.43%) and the Dox + MEF-UTCM (-4.973% ± 15.71%) groups. However, the rate of migration is only seen to decrease between 18-24 hour time points in the Dox + control-CM (-9.336% ± 5.181%) and the Dox + MEF-CM (-13.39% ± 4.420%) groups. Of interest to note is that

the MEF-UTCM experiences a second burst in the rate of migration (evident by a change from a negative to a positive slope) between the 12-18 hour time points (4.207% ± 7.136%) which rapidly decreases again between the 18-24 hour time points.

Table 3.4: Determining the effects of doxorubicin and MEF conditioned media on the rate of change (slope) of migration of E0771 murine breast cancer cells.

		Proliferation Control	Control	Doxorubicin	Dox + Control-CM	Dox + MEF-UTCM	Dox + MEF-CM
0-6 hrs	Slope	126.7 ± 6.640	73.49 ± 12.56	94.95 ± 15.89	41.64 ± 5.456	39.03 ± 15.11	36.12 ± 18.46
	p-value	< 0.0001	<0.0001	< 0.0001	< 0.0001	0.0200	0.0681
6-12 hrs	Slope	-34.12 ± 8.205	-10.51 ± 13.52	-34.93 ± 17.43	1.493 ± 7.271	-4.973 ± 15.71	3.018 ± 20.32
	p-value	0.0007	0.4481	0.0623	0.8399	0.7557	0.8838
12-18 hrs	Slope	-15.78 ± 5.298	1.161 ± 5.708	-3.242 ± 8.298	9.014 ± 6.424	4.207 ± 7.136	16.30 ± 8.985
	p-value	0.0089	0.8414	0.7012	0.1797	0.5637	0.0884
18-24 hrs	Slope	-11.82 ± 2.433	-6.131 ± 3.126	-9.472 ± 4.688	-9.336 ± 5.181	-4.384 ± 6.630	-13.39 ± 4.420
	p-value	0.0002	0.0675	0.0604	0.0904	0.5178	0.0080

*p-values indicate slopes which are significantly non-zero

3.6.10. Epithelial-to-Mesenchymal Transition (EMT) Assessment

In order to determine whether the combined treatment effects of doxorubicin and MEF-CM result in the induction of EMT, as well as to determine the role of EMT in E0771 cancer cell migration in the presence of both chemotherapy and “activated” fibroblast conditioned media, we assessed the relative protein expression of several key markers of EMT, namely; α-SMA, PDGFRα, vimentin and E-cadherin by means of Western blot analysis.

3.6.10.1. α-SMA and PDGFRα

Our results showed a significant decrease in the protein expression of α-SMA following both Dox + MEF-UTCM (33.40% ± 3.141% vs 100% ± 5.790%, p<0.0001) and Dox + MEF-CM (26.82% ± 6.837% vs 100% ± 5.790%, p=0.0002) treatment in comparison to doxorubicin treatment alone. When compared to Dox + control-CM a significant decrease in α-SMA expression was also observed for the MEF-UTCM (33.40% ± 3.141% vs 114.5% ± 16.99%, p=0.0033) and MEF-CM (26.82% ± 6.837% vs 114.5% ± 16.99%, p=0.0030)

treatment groups. Additionally, we observed a significant decrease in PDGFRα protein expression levels in the Dox + control-CM (42.88% ± 12.47% vs 100% ± 2.904%, p=0.0043), Dox + MEF-UTCM (25.67% ± 5.881% vs 100% ± 2.904%, p<0.0001) and Dox + MEF-CM (25.15% ± 4.550% vs 100% ± 2.904%, p<0.0001) treatment groups when compared to doxorubicin alone.

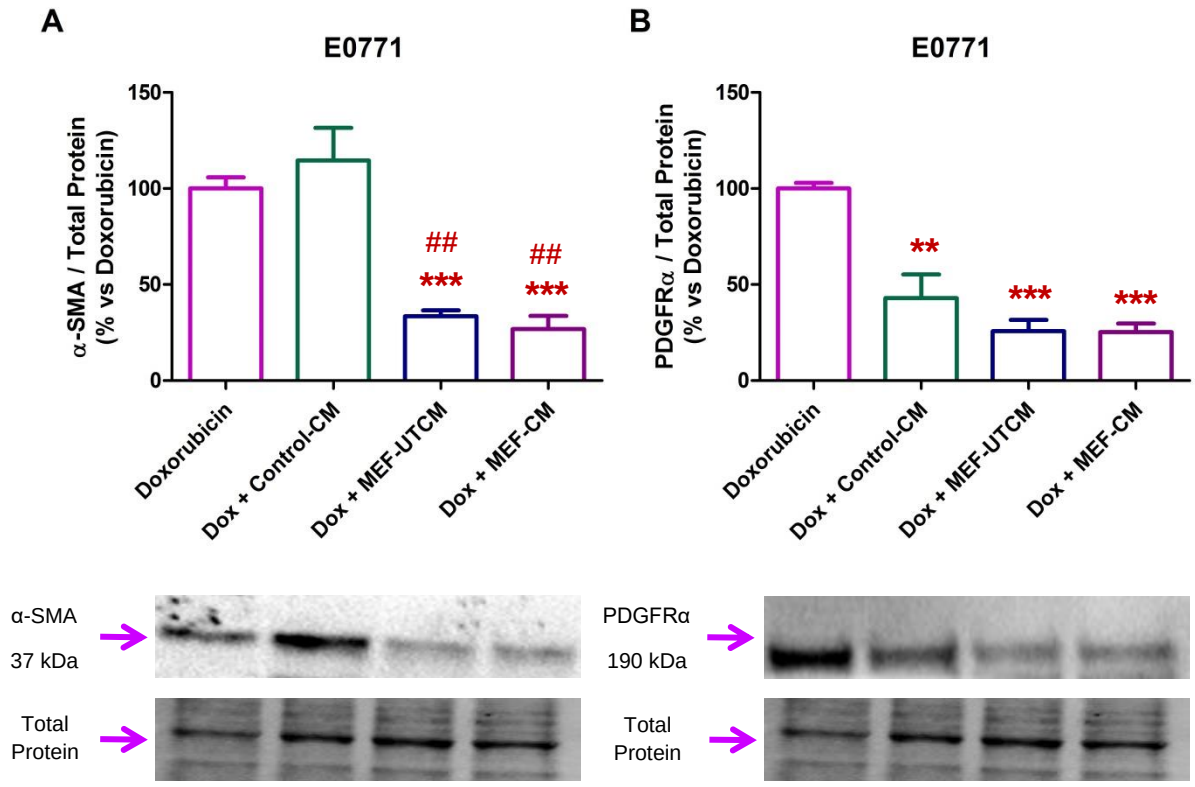

Figure 3.67: Western Blot analysis of α-SMA and PDGFRα protein expression in E0771 breast cancer cells following combined doxorubicin and MEF conditioned media treatment. Subsequent to 12 hours of glucose deprivation (0 mM glucose DMEM), E0771 cells were subjected to (1) Doxorubicin, (2) Doxorubicin + Control conditioned media, (3) Doxorubicin + Untreated MEF conditioned media (Dox + MEF-UTCM) and (4) Doxorubicin + E0771 treated MEF conditioned media (Dox + MEF-CM) for 24 hours. Statistical analysis: One way ANOVA with Bonferroni post hoc correction. All results are presented as mean ± SEM (n=3). ** = p<0.01 vs Doxorubicin, *** = p<0.0001 vs Doxorubicin and ## = p<0.01 vs Doxorubicin + Control-CM.

3.6.10.2. Vimentin and E-cadherin

Assessment of vimentin revealed a significant increase in relative protein expression levels in E0771 breast cancer cells following treatment with Dox + MEF-UTCM (302.8% ± 45.03% vs 100% ± 10.62%, p=0.0037) and Dox + MEF-CM (361.7% ± 53.55% vs 100% ± 10.62%, p=0.0025) when compared to doxorubicin treatment alone. Additionally, we observed a significant increase in E-cadherin protein expression following treatment with Dox + control-CM (213.1% ± 21.71% vs 100% ± 11.04%, p=0.0035), Dox + MEF-UTCM (195.5% ± 17.73% vs 100% ± 11.04%, p=0.0038) and Dox + MEF-CM (191.4% ± 30.43% vs 100% ± 11.04%, p=0.0302) in comparison to the doxorubicin only treated group.

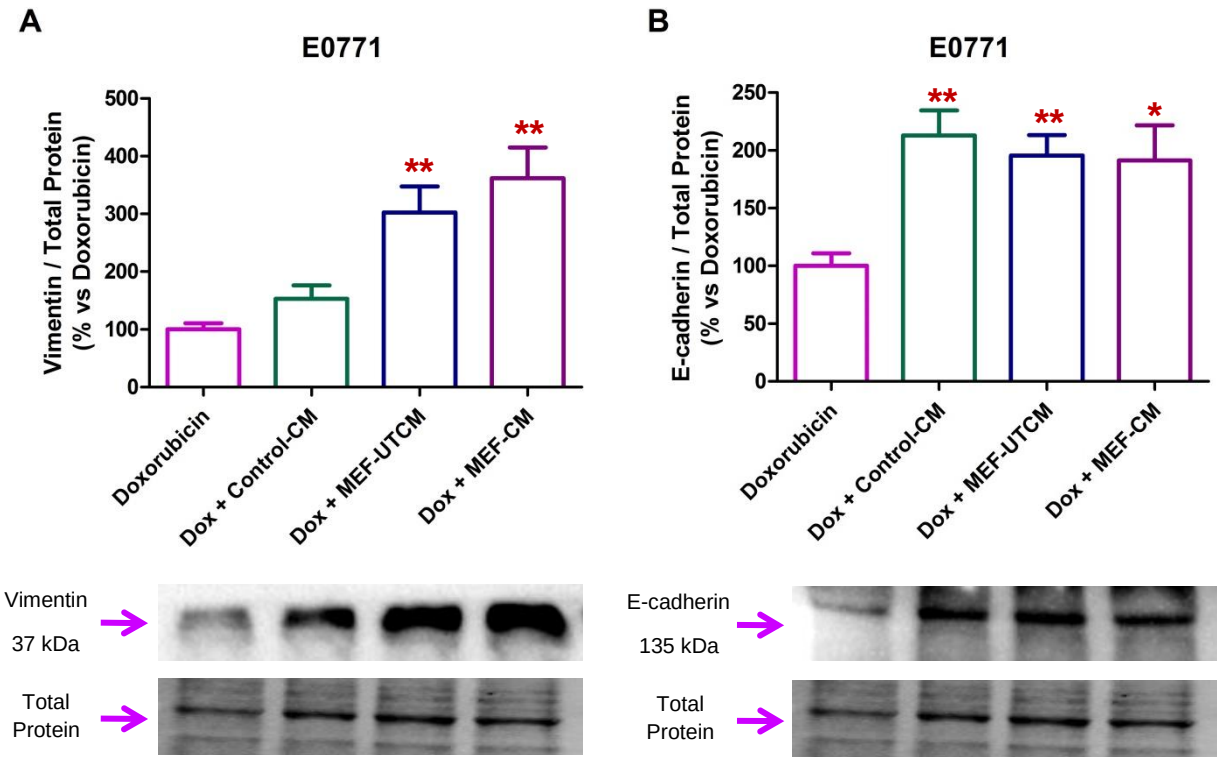

Figure 3.68: Western Blot analysis of α-SMA and PDGFRα protein expression in E0771 breast cancer cells following MEF conditioned media treatment. Subsequent to 12 hours of glucose deprivation (0 mM glucose DMEM), E0771 cells were subjected to (1) Doxorubicin, (2) Doxorubicin + Control conditioned media, (3) Doxorubicin + Untreated MEF conditioned media (Dox + MEF-UTCM) and (4) Doxorubicin + E0771 treated MEF conditioned media (Dox + MEF-CM) for 24 hours. Statistical analysis: One way ANOVA with Bonferroni post hoc correction. All results are presented as mean ± SEM (n=3). * = $p<0.05$ vs Doxorubicin and ** = $p<0.01$ vs Doxorubicin.

3.7: The Effects of Autophagic Manipulation in CAFs on the Migration Capacity of E0771 Breast Cancer Cells

3.7. The Effects of Autophagic Manipulation in CAFs on the Migration Capacity of E0771 Breast Cancer Cells

The induction of autophagy is thought be a central component of metabolic reprogramming in CAFs, and it is thought that the generation of metabolic intermediates through autophagy plays a central role in promoting epithelial cancer cell survival and metastasis (Wang *et al*., 2017). Therefore, this section of the study was aimed at partially elucidating the role of autophagic manipulation in CAFs on cancer cell migration.

3.7.1. Verification of Atg5 Knockdown in MEF Cells

Knockdown of Atg5 in MEF cells was confirmed with the use of Western blotting, after MEF cells were electroporated using 500 ng of esiRNA targeted against Atg5 for a period of 96 hours.

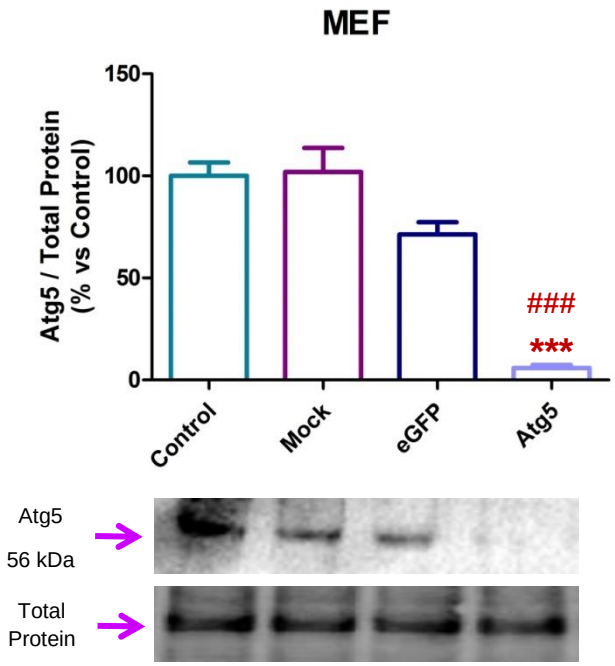

Figure 3.69: Verification of Atg5 knockdown. MEF cells were electroporated with 500 ng esiRNA and the following groups established (1) Control, (2) Mock (no esiRNA), (3) eGFP and (4) Atg5. Statistical analysis: One way ANOVA with Bonferroni post hoc correction. All results are presented as mean ± SEM (n=3). *** = $p<0.0001$ vs control and ### = $p<0.0001$ vs eGFP.

We observed a significant reduction in Atg5 protein expression levels was observed following 96 hours of 500 ng esiRNA treatment when compared to both control (5.890% ± 1.597% vs 100% ± 6.608%, $p<0.0001$), and the negative (eGFP) esiRNA control cells (5.890% ± 1.597% vs 71.26% ± 6.067%, $p<0.0001$), indicating an approximate 94% silencing efficiency in the MEF cells.

3.7.2. Cell Viability

Subsequent to the verification of Atg5 knockdown, esiRNA containing media was removed and conditioned media was generated (as previously described, see section 2.3) from Atg5 knockdown MEFs. E0771 cells were then treated with Atg5 knockdown MEF conditioned media (Atg5 MEF-CM) for 24 hours and cell viability assays were performed.

A significant reduction in MTT reductive capacity of E0771 cancer cells following treatment with Atg5 MEF-CM when compared to control (62.42% ± 6.372% vs 100% ± 3.613%,

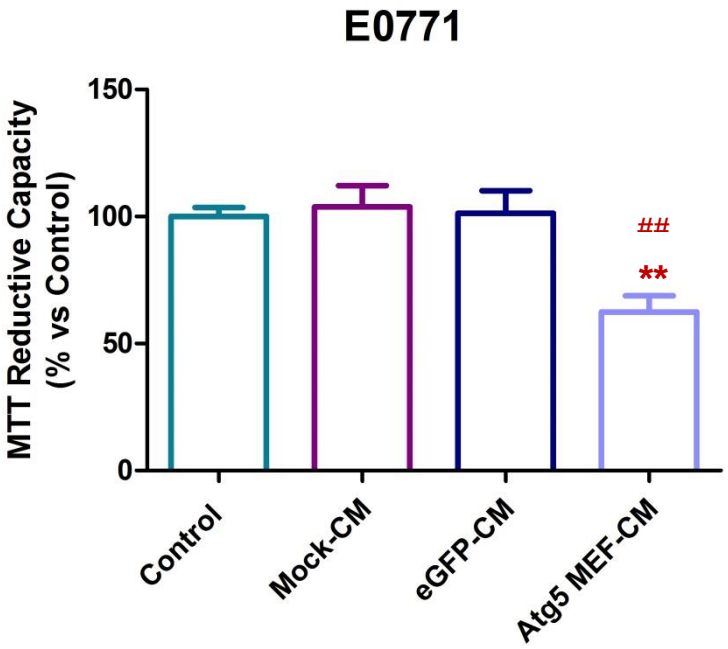

Figure 3.70: Cell viability of E0771 breast cancer cells following Atg5 MEF-CM treatment. E0771 cells were subjected to (1) Control, (2) Mock-CM, (3) eGFP-CM and (4) Atg5 MEF-CM. Statistical analysis: One way ANOVA with Bonferroni post hoc correction. All results are presented as mean ± SEM (n=3). ** = $p<0.01$ vs control and ## = $p<0.01$ vs eGFP.

p=0.0002) and the negative control eGFP group (62.42% ± 6.372% vs 101.3% ± 8.944%, p<0.01) was observed.

3.7.3. Migration (Scratch) Assay

Following the successful knockdown of Atg5 in “activated” MEFs, conditioned media was generated and used to treat E0771 breast cancer cells. Migration (scratch) assays were performed in E0771 cancer cells following Atg5 MEF-CM treatment for 24 hrs. Image acquisition and analysis was performed as previously described (see section 3.5.9).

When compared to the control group, a significant reduction in the percentage of wound closure was observed at the 12, 18 and 24 hour time points in Mock-CM (12 hr: 15.21% ± 4.864% vs 36.05% ± 4.514%, p<0.01, 18 hr: 22.24% ± 4.052% vs 52.23% ± 4.578%, p<0.0001 and 24 hr: 34.48% ± 3.778% vs 57.67% ± 2.354%, p<0.0001), eGFP-CM (12 hr: 18.30% ± 2.246% vs 36.05% ± 4.514%, p<0.05, 18 hr: 20.84% ± 1.833% vs 52.23% ± 4.578%, p<0.0001 and 24 hr: 27.72% ± 2.326% vs 57.67% ± 2.354%, p<0.0001) and Atg5 MEF-CM (12 hr: 14.96% ± 8.066% vs 36.05% ± 4.514%, p<0.01, 18 hr: 28.26% ± 5.813% vs 52.23% ± 4.578%, p<0.0001 and 24 hr: 36.61% ± 7.787% vs 57.67% ± 2.354%, p<0.01) groups.

However, when compared to the Mock-CM group no significant changes in the percentage of wound closure were observed for Atg5 MEF-CM group across all time points.

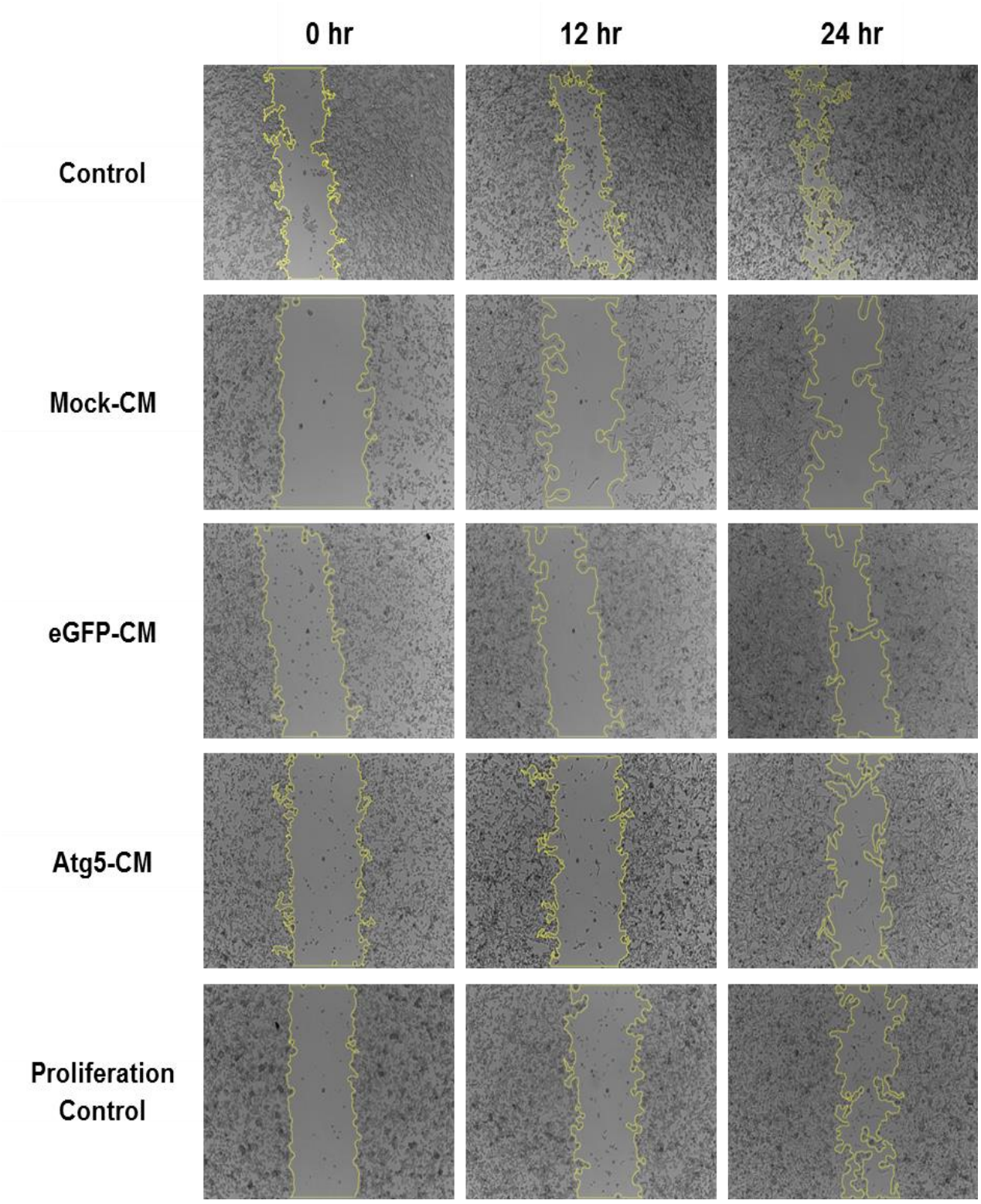

Figure 3.71: Representative time point images of the migration (scratch) assay performed on E0771 murine breast cancer cells following treatment with Atg5 knockdown MEF-CM. E0771 cells were subjected to (1) Control (Dox), (2) Mock-CM (no esiRNA), (3) eGFP-CM (- ve control) and (4) Atg5 MEF-CM for 24 hours. Image analysis performed in ImageJ using an MRI_wound_healing plugin, and images displayed are for the 0, 12 and 24 hour time points only.

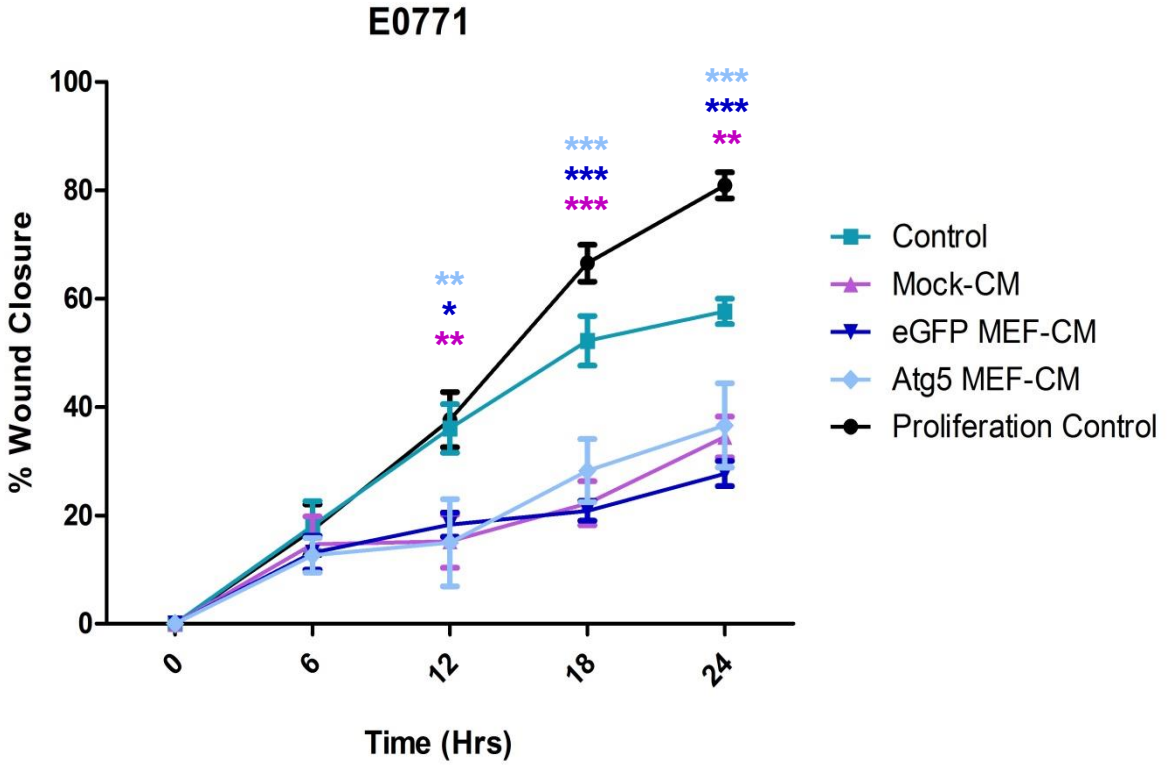

Figure 3.72: Determining the effects of MEF conditioned media on the migratory capacity of E0771 murine breast cancer cells. Subsequent to 12 hours of glucose deprivation (0 mM glucose DMEM), E0771 cells were subjected to (1) Control, (2) Control conditioned media, (3) Untreated MEF conditioned media (MEF-UTCM) and (3) E0771 treated MEF conditioned media (MEF-CM) for 24 hours. Migratory capacity following treatment was assessed by means of a wound healing (Scratch) assay. Statistical analysis: Two-way ANOVA with Bonferroni post hoc correction. All results are presented as mean ± SEM (n=9). * = $p<0.05$ vs control, ** = $p<0.01$ vs control and *** = $p<0.01$ vs control.

As we failed to see any statistically significant differences when comparisons against the mock-CM group were performed, the slopes of the regression lines (Figure 3.69) for each separate time point were again analysed. However, this provided no new insights into the rate of change at which E0771 cells migrate into the wound when subjected to Atg5 knockdown MEF-CM, as we observed no statistically significant differences in the slopes of the regression lines for all treatment groups, across all time points.

Table 3.5: Determining the effects of Atg5 knockdown MEF conditioned media on the rate of change (slope) of migration of E0771 murine breast cancer cells.

		Proliferation Control	Control	Mock-CM	eGFP-CM	Atg5 MEF-CM
0-6 hrs	Slope	2.892 ± 0.7775	3.011 ± 0.7608	2.441 ± 0.8560	2.185 ± 0.5212	2.108 ± 0.5311
	p-value	0.0019	0.0011	0.0115	0.0007	0.0011
6-12 hrs	Slope	3.387 ± 1.151	2.998 ± 1.070	0.09423 ± 1.179	0.8657 ± 0.6418	0.3847 ± 1.445
	p-value	0.0096	0.0128	0.9373	0.1961	0.7935
12-18 hrs	Slope	4.815 ± 1.021	2.697 ± 1.072	1.170 ± 1.055	0.4231 ± 0.4832	2.217 ± 1.657
	p-value	0.0002	0.0229	0.2836	0.3942	0.1996
18-24 hrs	Slope	2.396 ± 0.6966	0.9054 ± 0.8579	2.040 ± 0.9233	1.147 ± 0.4936	1.392 ± 1.620
	p-value	0.0034	0.3069	0.0420	0.0336	0.4027

*p-values indicate slopes which are significantly non-zero

Furthermore, the assessment of the rate of wound closure of E0771 breast cancer cells following treatment with Atg5 knockdown MEF conditioned media, revealed significantly decreased rates of migration at the 12 and 18 hour time points for the mock-CM (12 hr: 126.8% ± 40.53% vs 300.4% ± 37.62%, $p<0.05$ and 18 hr: 123.5% ± 22.51% vs 290.2% ± 25.43%, $p<0.05$) and eGFP-CM (12 hr: 152.5% ± 18.72% vs 300.4% ± 37.62%, $p<0.05$ and 18 hr: 115.8% ± 10.18% vs 290.2% ± 25.43%, $p<0.01$) treatment groups when compared to control. A significantly decreased migration rate in the Atg5 treatment group was only observed at the 12 hour time point when compared to control (124.6% ± 67.22% vs 300.4% ± 37.62%, $p<0.01$). Again, when compared to both the mock-CM and eGFP-CM control groups no statistically significant differences in the rate of E0771 cell migration was observed following treatment with Atg5 knockdown MEF-CM across all time points.

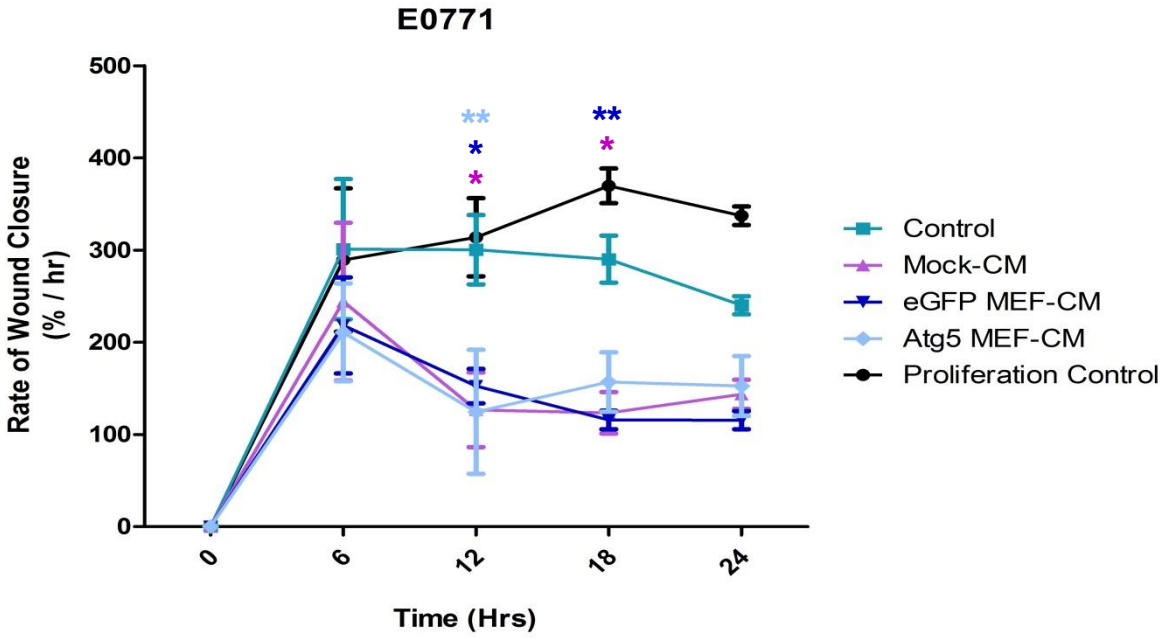

Figure 3.73: Determining the effects of Atg5 knockdown MEF conditioned media on the rate of migration of E0771 murine breast cancer cells. E0771 cells were subjected to (1) Control, (2) Mock-CM (no esiRNA), (3) eGFP-CM (negative control) and (4) Atg5 MEF-CM for 24 hours. Rate of wound closure (% / hr) was calculated by dividing the % wound closure at each time point by the number of hours passed. Statistical analysis: Two-way ANOVA with Bonferroni post hoc correction. All results are presented as mean ± SEM (n=9). * = $p<0.05$ vs control and ** = $p<0.01$ vs control.

Analysis of the slopes of each regression line for the rate of wound closure (Figure 3.70) again revealed no significant differences across all time points for all treatment groups.

Table 3.6: Determining the effects of Atg5 knockdown MEF conditioned media on the rate of change (slope) of migration of E0771 murine breast cancer cells.

		Proliferation Control	Control	Mock-CM	eGFP-CM	Atg5 MEF-CM
0-6 hrs	Slope	48.20 ± 12.96	50.18 ± 12.68	40.69 ± 14.27	36.41 ± 8.687	35.14 ± 8.851
	p-value	0.0019	0.0011	0.0115	0.0007	0.0011
6-12 hrs	Slope	4.124 ± 14.76	-0.1045 ± 14.15	-19.56 ± 15.78	-10.99 ± 9.230	-14.36 ± 14.28
	p-value	0.7835	0.9942	0.2331	0.2511	0.3294
12-18 hrs	Slope	9.308 ± 7.745	-1.707 ± 7.568	-0.5409 ± 7.727	-6.123 ± 3.552	5.394 ± 12.43
	p-value	0.2469	0.8244	0.9451	0.1040	0.6701
18-24 hrs	Slope	-5.426 ± 3.574	-8.318 ± 4.543	3.355 ± 4.578	-0.04404 ± 2.343	-0.7417 ± 7.630
	p-value	0.1485	0.0858	0.4743	0.9852	0.9238

*p-values indicate slopes which are significantly non-zero

3.7.4. Epithelial-to-Mesenchymal Transition Assessment

In order to determine if the migratory capacity of E0771 breast cancer cells subjected to treatment with Atg5 knockdown MEF conditioned media is influenced by a transition of these cells away from a metastatic phenotype, several key markers of epithelial-to-mesenchymal transition were assessed using Western blot analysis. A significant reduction in α-SMA protein expression was seen following mock-CM treatment (9.798% ± 1.144% vs 100% ± 10.39%, p=0.0044) in comparison to the control group. However, treatment with Atg5 MEF-CM resulted in a significant increase in α-SMA expression (139.0% ± 17.48% vs 9.798% ± 1.144%, p<0.0001) when compared to the mock-CM group.

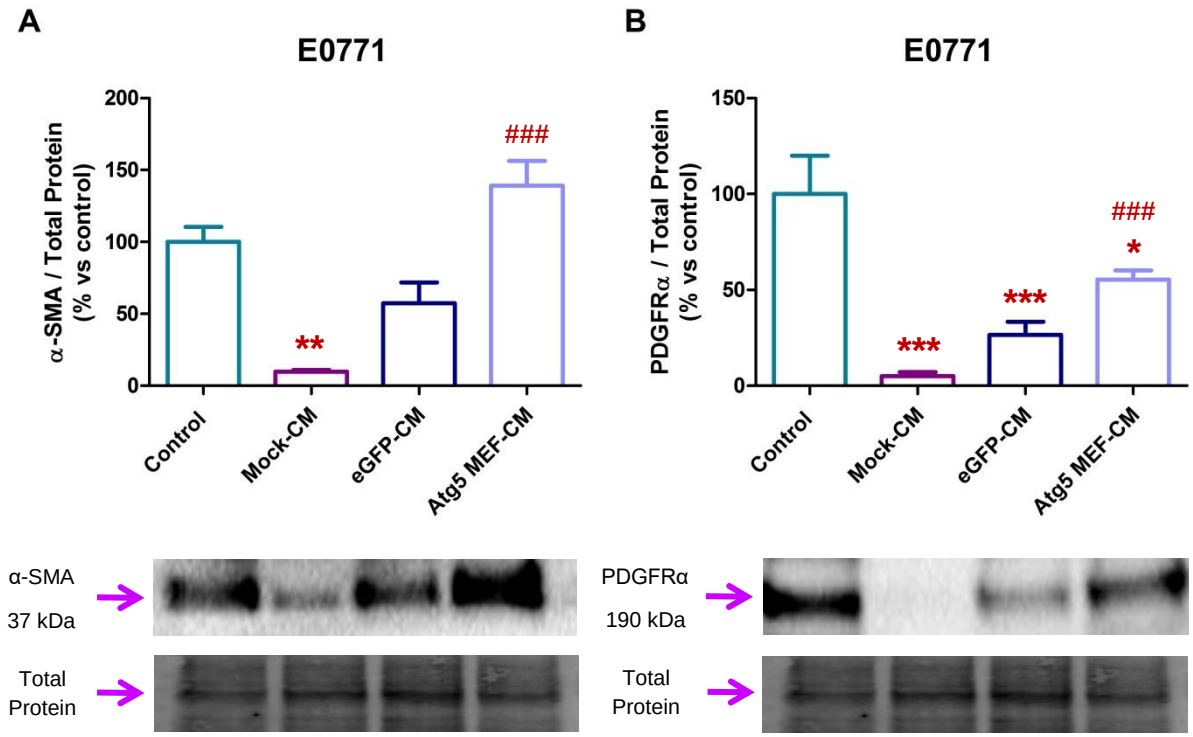

Figure 3.74: Western blot analysis of α-SMA and PDGFRα protein expression in E0771 breast cancer cells following treatment with Atg5 knockdown MEF conditioned media. E0771 cells were subjected to (1) Control, (2) Mock-CM (no esiRNA), (3) eGFP-CM (negative control) and (4) Atg5 MEF-CM for 24 hours. Statistical analysis: One way ANOVA with Bonferroni post hoc correction. All results are presented as mean ± SEM (n=3). * = p<0.05 vs control, ** = p<0.01 vs control *** = p<0.0001 and ### = p<0.0001 vs mock-CM.

We observed a significant reduction in PDGFRα protein expression was observed in the mock-CM (5.034% ± 2.210% vs 100% ± 19.98%, p<0.0001), eGFP-CM (26.57% ± 6.828% vs 100% ± 19.98%, p<0.0001), and Atg5 MEF-CM (55.48% ± 4.670% vs 100% ± 19.98%, p=0.0477) treatment groups when compared to control. When compared to the mock-CM control group a significant increase in PDGFRα protein expression was seen in the Atg5 MEF-CM group (55.48% ± 4.670% vs 5.034% ± 2.210%, p<0.05).

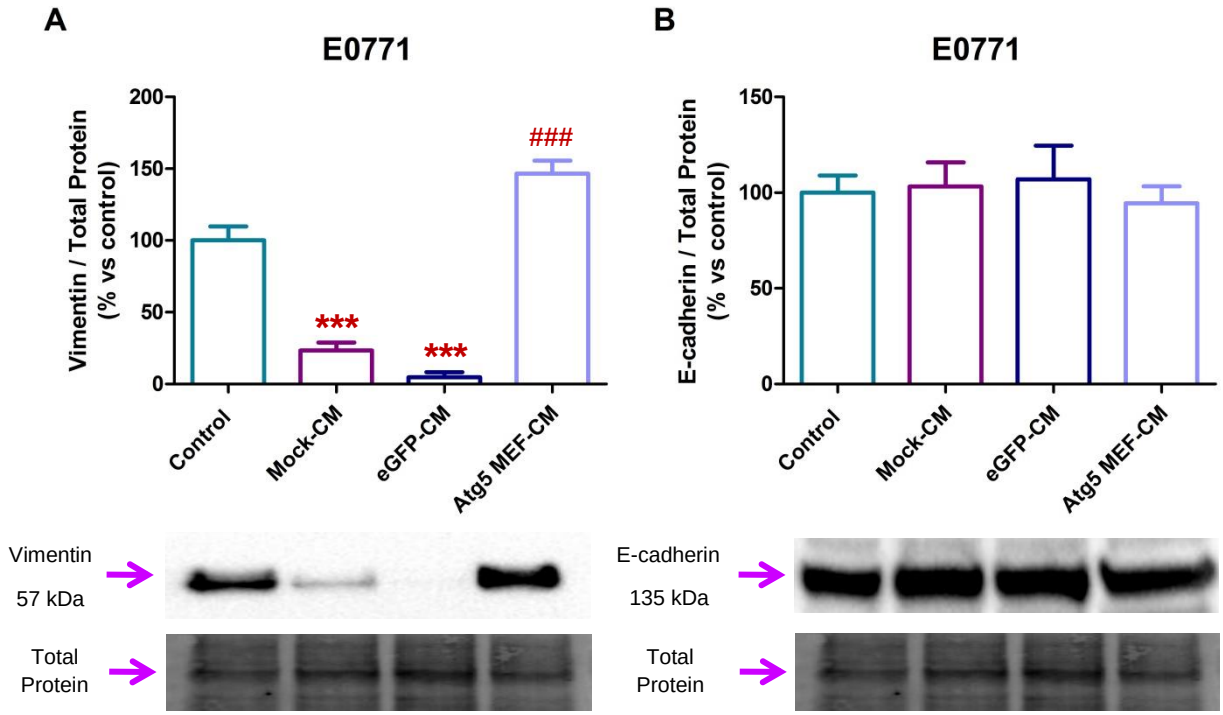

Figure 3.75: Western blot analysis of vimentin and E-cadherin protein expression in E0771 breast cancer cells following treatment with Atg5 knockdown MEF conditioned media. E0771 cells were subjected to (1) Control, (2) Mock-CM (no esiRNA), (3) eGFP-CM (negative control) and (4) Atg5 MEF-CM for 24 hours. Statistical analysis: One way ANOVA with Bonferroni post hoc correction. All results are presented as mean ± SEM (n=3). *** = p<0.0001 and ### = p<0.0001 vs mock-CM.

When assessing vimentin expression in E0771 cancer cells a similar trend was observed, where we noted a significant reduction in vimentin expression following treatment with mock- CM (26.68% ± 6.932% vs 100% ± 15.79%, p=0.0008) and eGFP-CM (8.726% ± 5.179% vs 100% ± 15.79%, p<0.0001) when compared to control. Additionally, when

compared to the mock-CM group a significant increase in vimentin protein expression was seen following Atg5 MEF-CM treatment (143.3% ± 21.11% vs 26.68% ± 6.932%, p=0.0001). However no significant differences in the protein expression levels of the epithelial marker E-cadherin were observed across all treatment groups when compared to the control.

3.8: *In vivo* tumour-bearing C57BL/6 mouse model

3.8. *In vivo* tumour-bearing C57BL/6 mouse model

While the use of conventional *in vitro* cell culture models provide valuable insight into a wide variety of pathological disease states, the use of these models fall severely short when it comes to the study of the tumour microenvironment and cell-cell interactions that promote tumour progression, metastasis and chemotherapeutic resistance. We therefore, employed a tumour-bearing C57BL/6 mouse model in order to better recapitulate the tumour microenvironment.

3.8.1. The Effects of *in vivo* Doxorubicin Administration on Body Weight, Tumour Volume and Survival

A total of 40 female C57BL/6 mice aged 8-weeks were randomly divided into four groups, and following one week of acclimatization, mice were inoculated into the fourth mammary fat pad with the syngeneic E0771 breast cancer cell line, whilst control animals received HBSS inoculations. Upon the appearance of palpable tumours, doxorubicin administration commenced as previously described (see section 2.17) with animals receiving a cumulative dose of 12 mg/kg over the course of the study design. Tumours were palpable as early as day nine following E0771 cell inoculations and by day fourteen all 20 tumour-bearing animals had measurable tumours. Body weight and tumour volume measurements were recorded every second day.

Assessment of body weights over the duration of the study showed no significant differences (Figure 3.76), although a trend to increase was observed in the tumour control and tumour + doxorubicin groups, indicative of an increase in tumour burden.

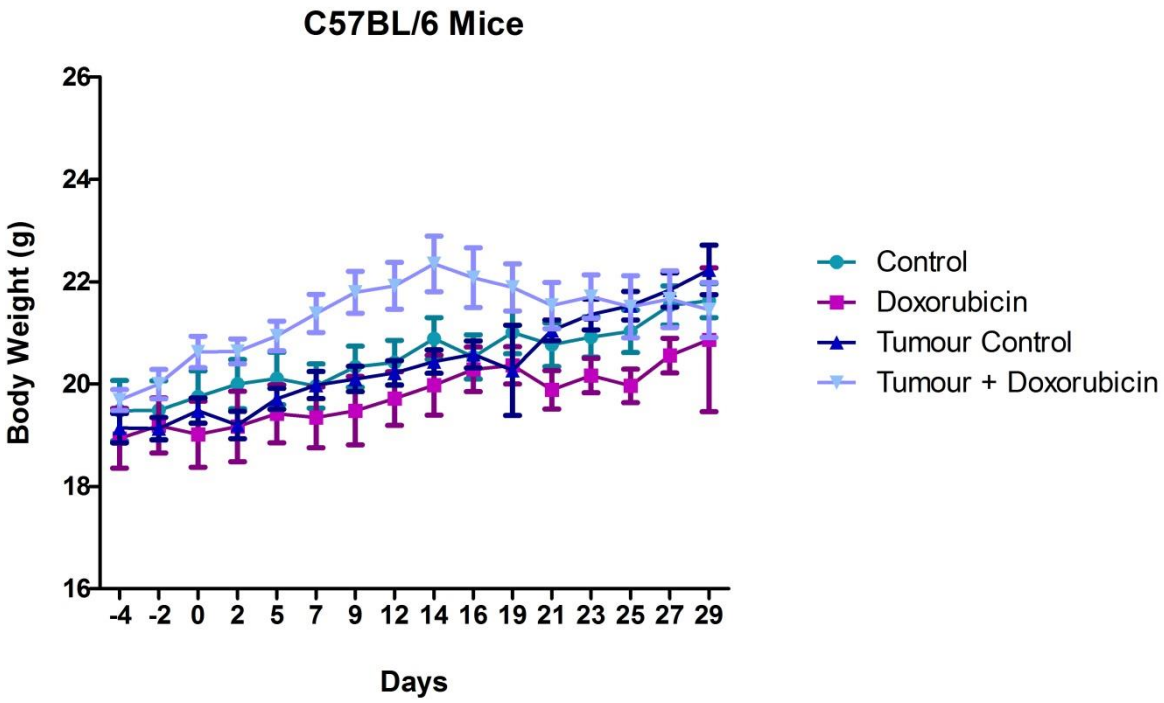

Figure 3.76: Average body weight of mice throughout the duration of study. Female C57BL/6 mice were randomised into four groups (1) Control, (2) Doxorubicin, (3) Tumour Control and (4) Tumour + Doxorubicin. All results are presented as mean ± SEM (n=10 per group).

Assessment of tumour volume revealed a rapid increase in tumour burden in both the tumour control and tumour + doxorubicin groups (Figure 3.77). Despite the administration of doxorubicin, tumour volume increased at a rate comparable to that of control animals who did not receive doxorubicin.

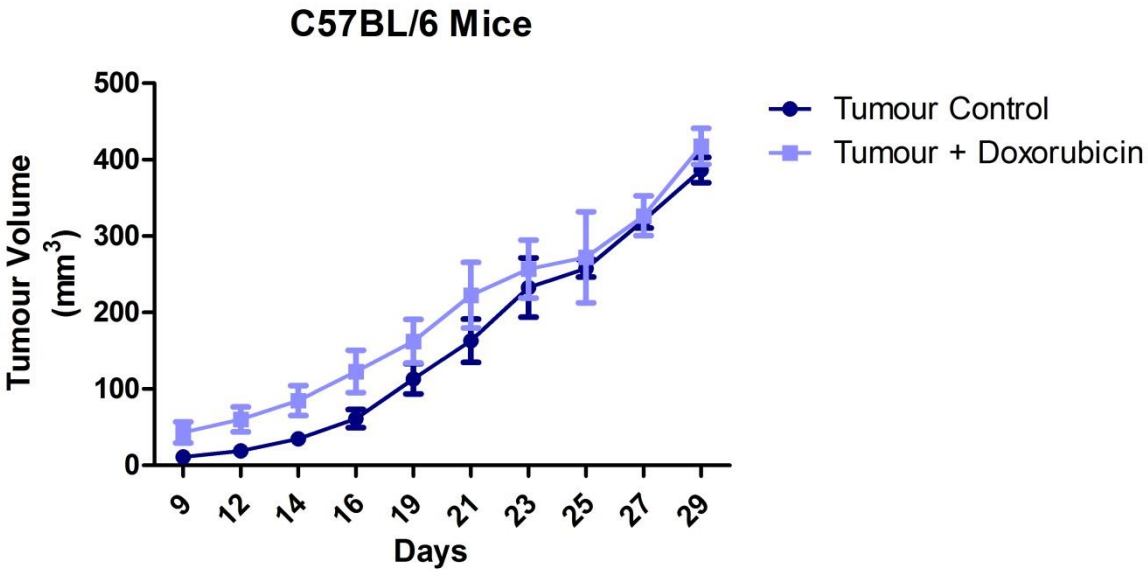

Figure 3.77: Average tumour volume of mice throughout the duration of study. Female C57BL/6 mice were randomised into four groups (1) Control, (2) Doxorubicin, (3) Tumour Control and (4) Tumour + Doxorubicin. Only Tumour control and Tumour + Doxorubicin grouped animals received inoculation with carcinogenic E0771 murine breast cancer cells. Control animals received an isovolumetric inoculation with HBSS. All results are presented as mean ± SEM (n=10 per group).

Furthermore, a Kaplan-Meier survival analysis was performed in order to determine if any significant differences exist in the time taken to reach desired tumour volume (~400 mm^3) between groups. Due to the development of bleeding ulcers at the site of doxorubicin injection humane endpoints were enforced for two mice (one from each the doxorubicin control and tumour + doxorubicin groups), and mice were thus sacrificed before the required tumour volume / end of the study period was reached. Although a separation of the curves of the tumour-bearing groups from non-tumour-bearing groups was observed to occur towards the end of the study (Figure 3.78), no statistically significant differences were observed between the groups ($p=0.7125$).

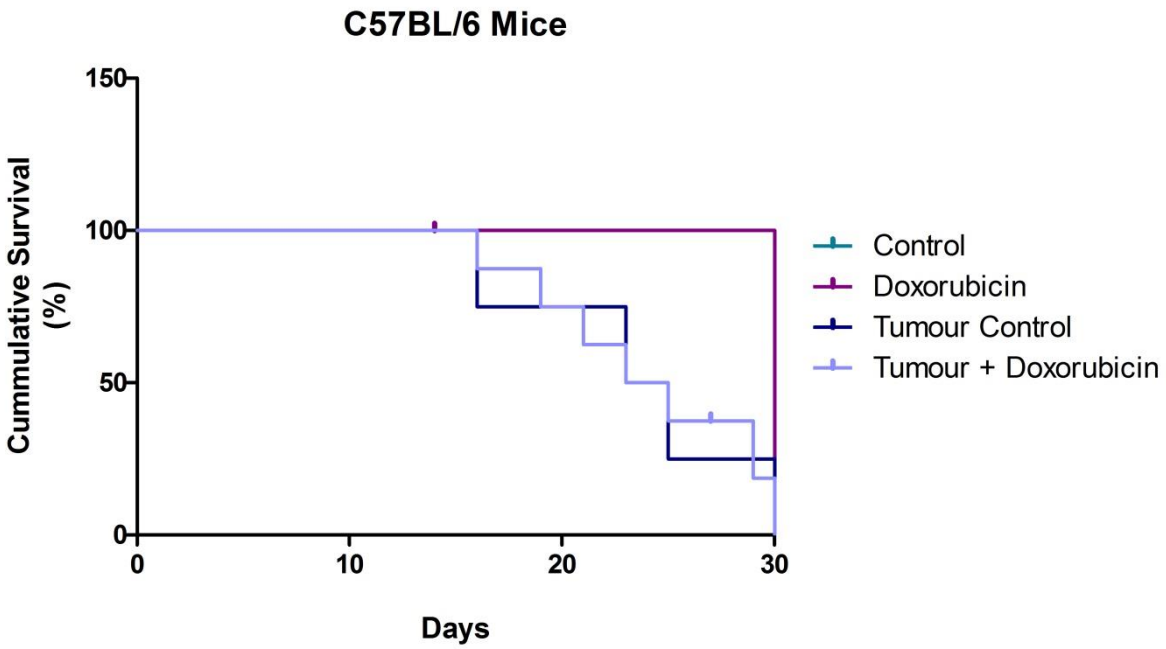

Figure 3.78: Kaplan-Meier survival analysis showing the cumulative survival percentage of C57BL/6 mice throughout the course of the study. Female C57BL/6 mice were randomised into four groups (1) Control, (2) Doxorubicin, (3) Tumour Control and (4) Tumour + Doxorubicin. All results are presented as mean ± SEM (n=10 per group). ı = censored animal (humane endpoint enforced).

Upon sacrifice, tumours and mammary fat pads were harvested from mice and processed appropriately for further analysis as described previously (see section 2.17.3). Briefly, tumours and mammary fat pads were divided into three sections for histological / immunofluorescence, Western blotting analysis (n=6 per group) as well as for primary epithelial organoid isolation (n=4 per group).

3.8.2. Histology – Ultrastructure and Fibrosis Assessment

Mammary fat pads were harvested from animals and served as non-carcinogenic control samples. Wherever possible, mammary fat pads from all four groups were analysed alongside the tumour samples harvested from tumour-bearing mice. Ultrastructure was assessed with the use of conventional haematoxylin and eosin (H&E) staining.

Ultrastructural Assessment of Mammary Fat Pads

Qualitative assessment of mammary fat pad ultrastructure showed no major ultrastructural changes between any of the groups, although it was noted that mammary fat pads harvested from tumour + doxorubicin animals showed more intense H&E staining.

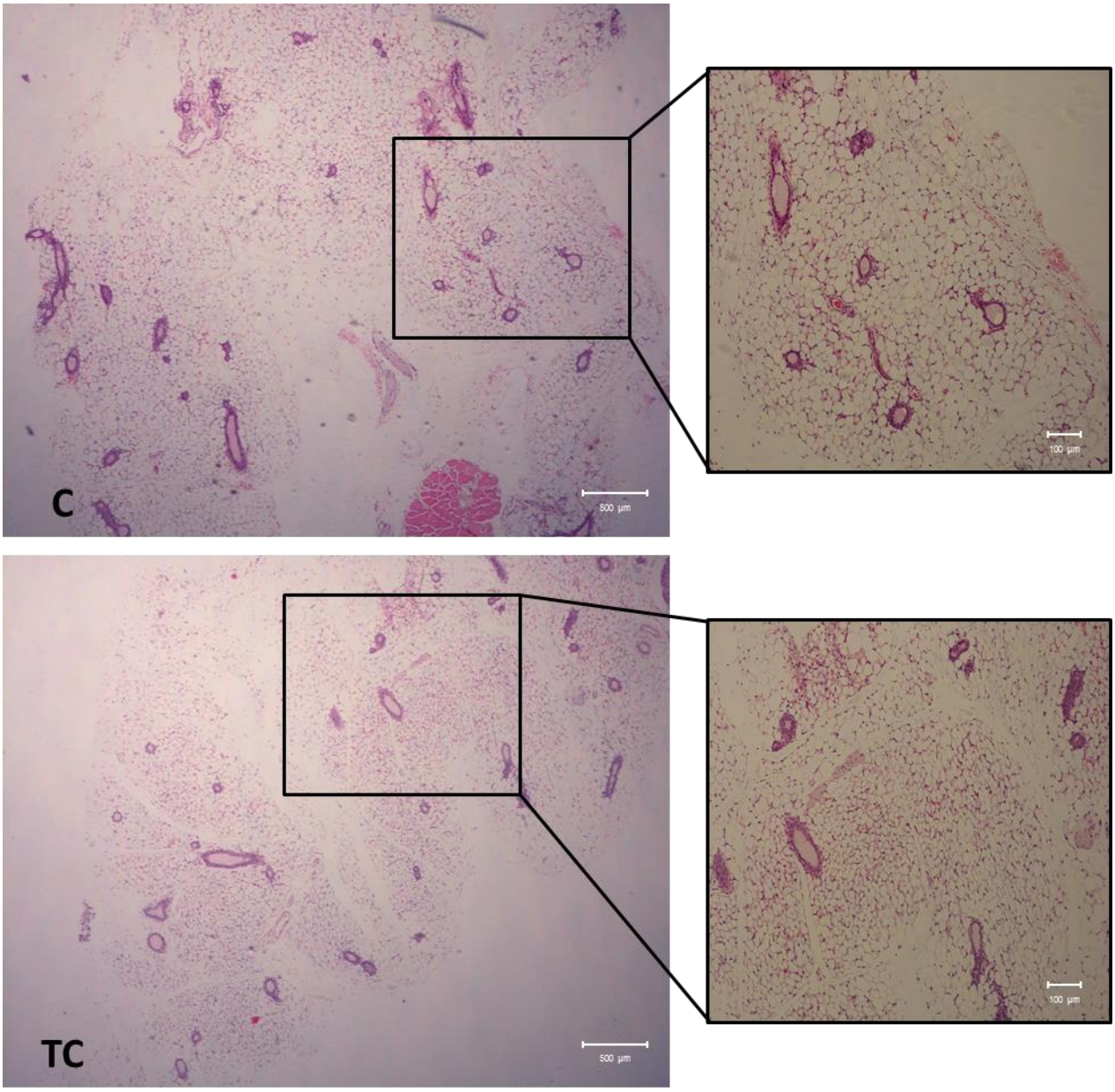

Figure 3.79: Representative ultrastructural (H&E) images of mammary fat pads harvested from C57BL/6 mice. Fourth mammary fat pads (left and right) were harvested from female C57BL/6 mice. Representative images displayed are from Control (C) and Tumour Control (TC) groups. Magnification at 4x and 10x.

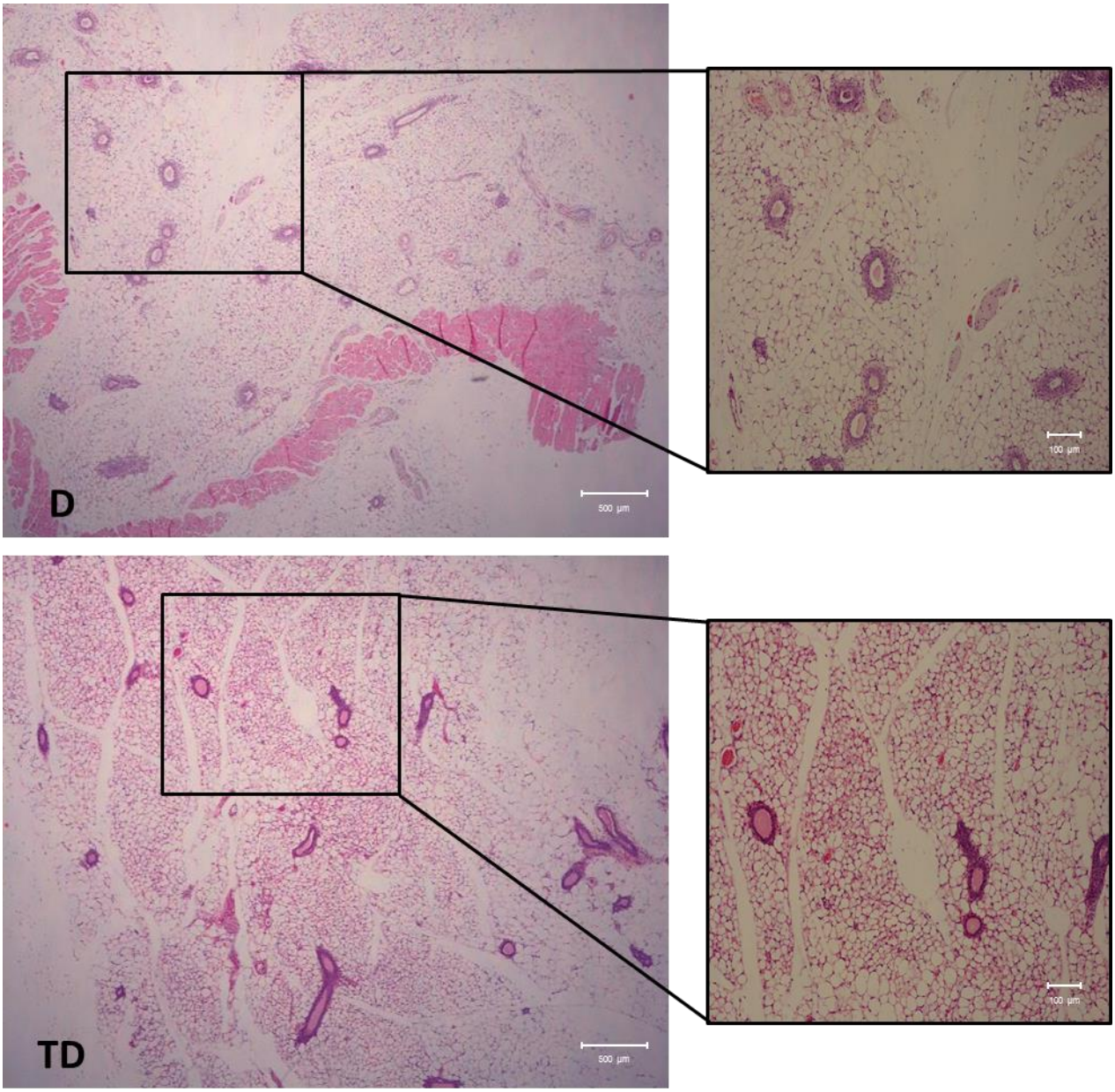

Figure 3.80: Representative ultrastructural (H&E) images of mammary fat pads harvested from C57BL/6 mice. Fourth mammary fat pads (left and right) were harvested from female C57BL/6 mice. Representative images displayed are from Doxorubicin (D) and Tumour + Doxorubicin (TD) groups. Magnification at 4x and 10x.

Ultrastructural Assessment of Tumours

Ultrastructural assessment of tumours revealed three distinct regions, an outer peripheral section which is densely compacted and stains strongly for nuclear material (purple staining), a middle region which appears less compact and stains less heavily for nuclear

material and finally an inner region located towards the centre of the tumour where nuclear staining is drastically diminished (pink staining). These regions were observed in both the tumour control and tumour + doxorubicin groups.

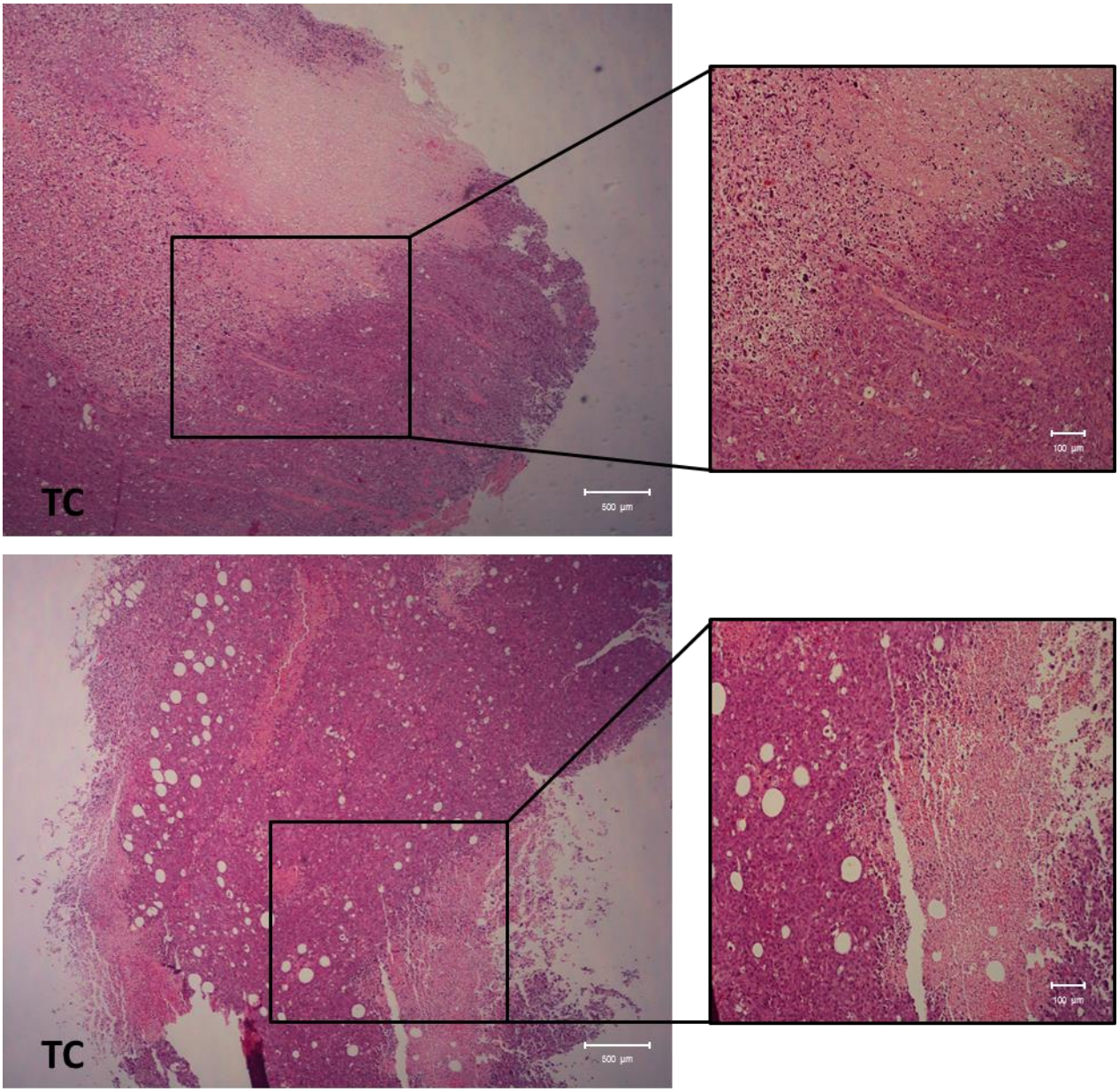

Figure 3.81: Representative ultrastructural (H&E) images of tumours harvested from C57BL/6 mice. Tumours were harvested from female C57BL/6 mice. Representative images displayed are from Tumour Control (TC) and Tumour + Doxorubicin (TD) groups. Magnification at 4x and 10x.

Additionally, of interest we noted in both the tumour control and tumour + doxorubicin groups an increase in fat cell accumulation into the tumour site as well as the formation of neo-angiogenic blood vessels within the tumour mass.

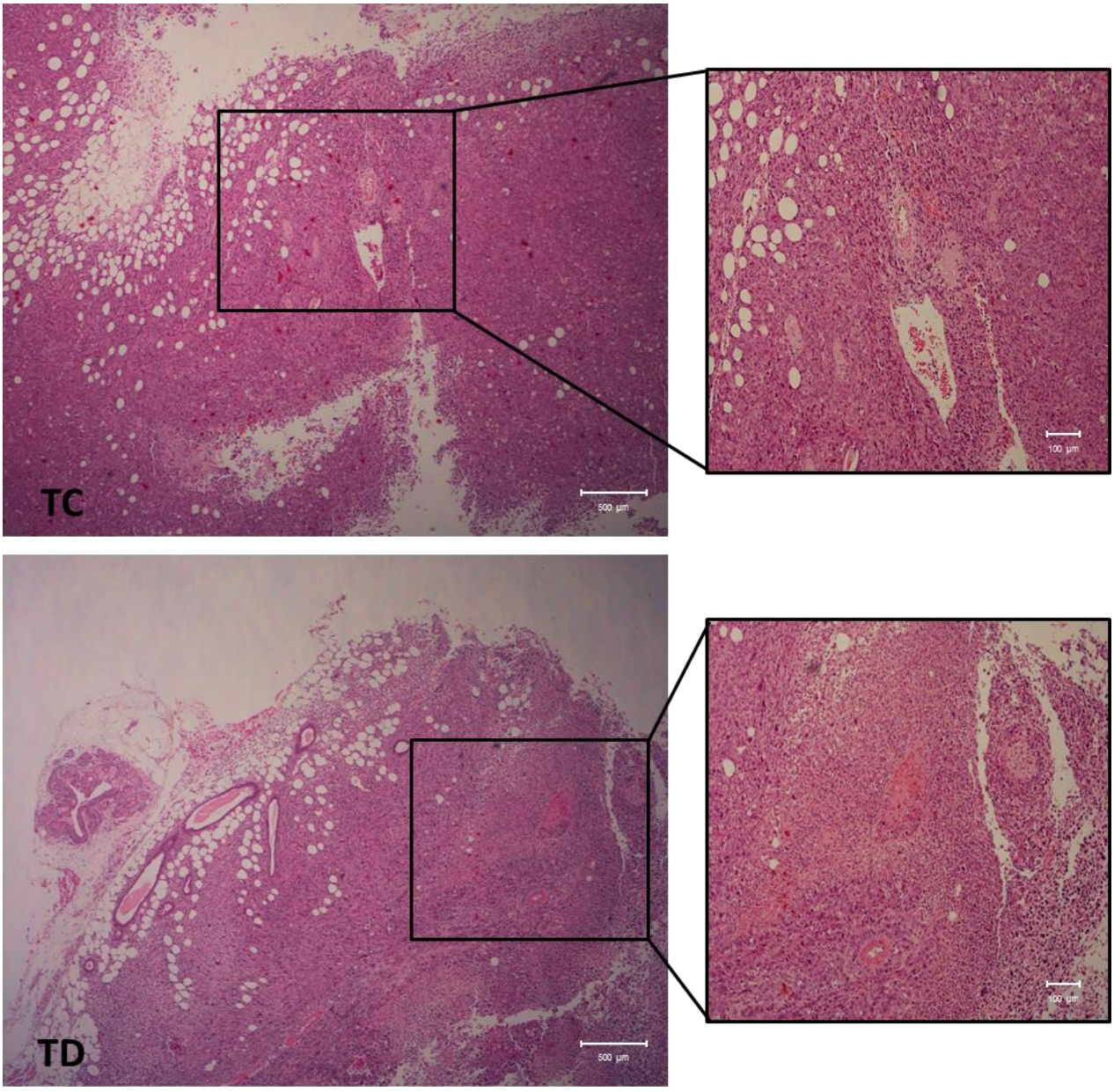

Figure 3.82: Representative ultrastructural (H&E) images of tumours harvested from C57BL/6 mice. Tumours were harvested from female C57BL/6 mice. Representative images displayed are from Tumour Control (TC) and Tumour + Doxorubicin (TD) groups. Magnification at 4x and 10x.

Furthermore, as CAFs are known to result in extensive remodelling of the extracellular matrix leading to increased collagen deposition, we next assessed the extent of fibrosis in both mammary fat pads and tumours in response to tumour burden and doxorubicin treatment.

Assessment of Fibrosis in Mammary Fat Pads

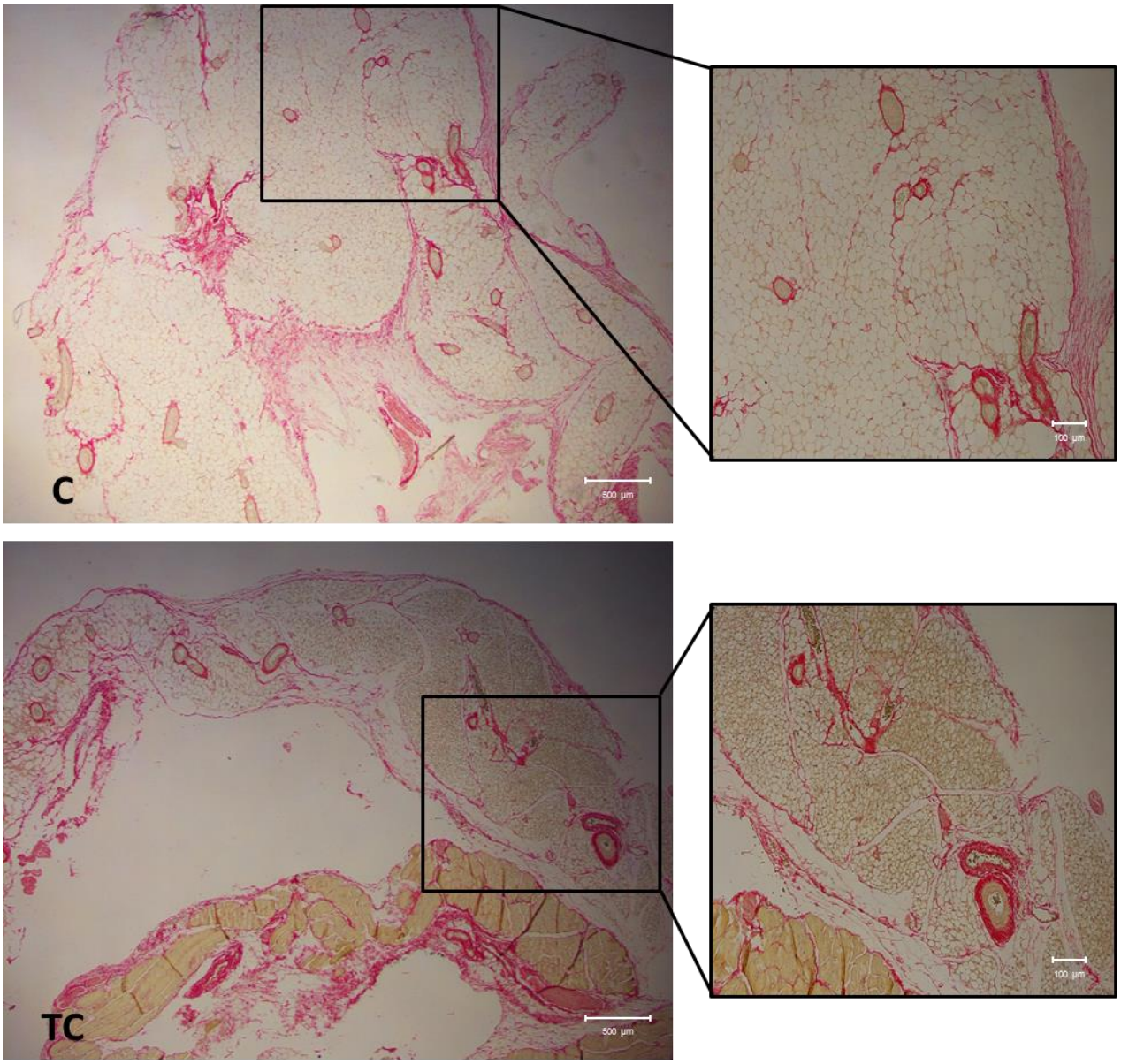

Figure 3.83: Representative Picrosirius Red images of mammary fat pads harvested from C57BL/6 mice. Fourth mammary fat pads (left and right) were harvested from female C57BL/6 mice. Representative images displayed are from Control (C) and Tumour Control (TC) groups. Magnification at 4x and 10x.

Extensive collagen deposition was observed surrounding blood vessels and between lobules. Qualitatively no obvious differences in fibrosis were observed between the control, tumour control and doxorubicin samples. However, a clear reduction in collagen deposition (signified by decreased red staining) was observed in the mammary fat pads of tumour-bearing mice who were treated with doxorubicin (tumour + doxorubicin).

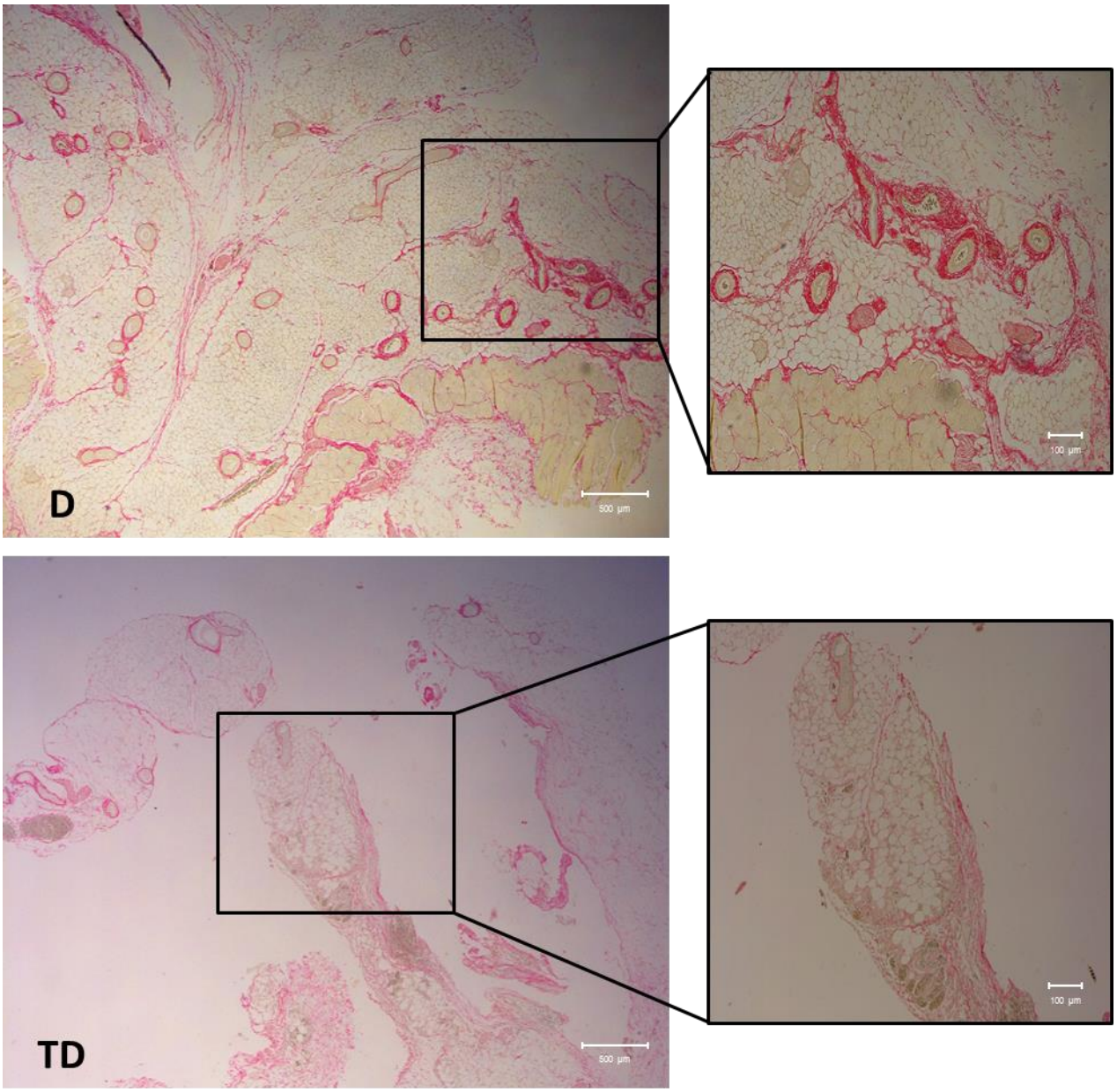

Figure 3.84: Representative Picrosirius Red images of mammary fat pads harvested from C57BL/6 mice. Fourth mammary fat pads (left and right) were harvested from female C57BL/6 mice. Representative images displayed are from Doxorubicin (D) and Tumour + Doxorubicin (TD) groups. Magnification at 4x and 10x.

Assessment of Fibrosis in Tumours

Again, as seen in the mammary fat pads we observed strong collagen staining surrounding neo-angiogenic blood vessels within the tumours. However, fibrosis was also seen to occur within the tumour itself and a significantly greater staining intensity was observed in tumour + doxorubicin in comparison to tumour control samples.

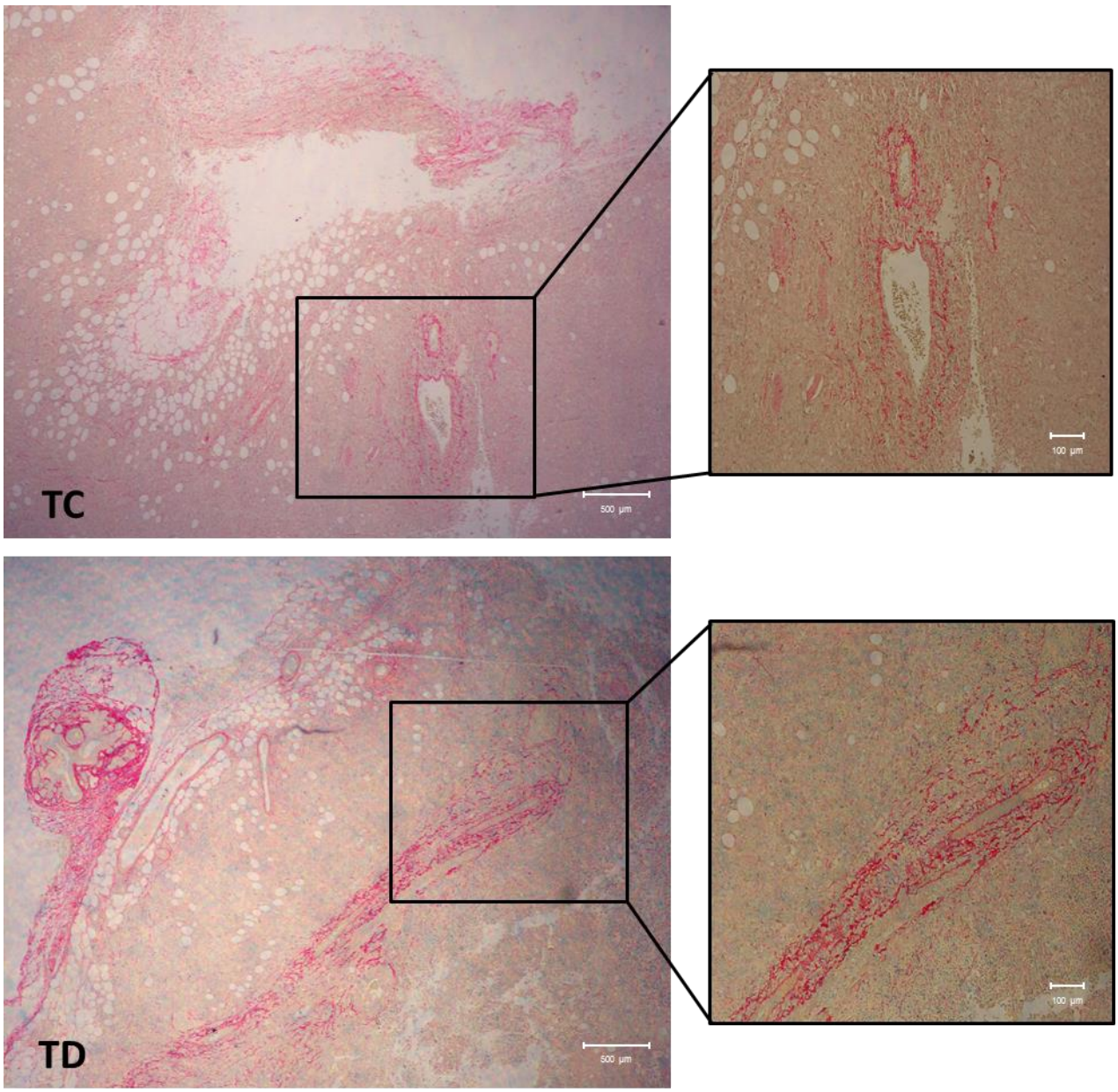

Figure 3.85: Representative Picrosirius Red images of tumours harvested from C57BL/6 mice. Tumours were harvested from female C57BL/6 mice. Representative images displayed are from Tumour Control (TC) and Tumour + Doxorubicin (TD) groups. Magnification at 4x and 10x.

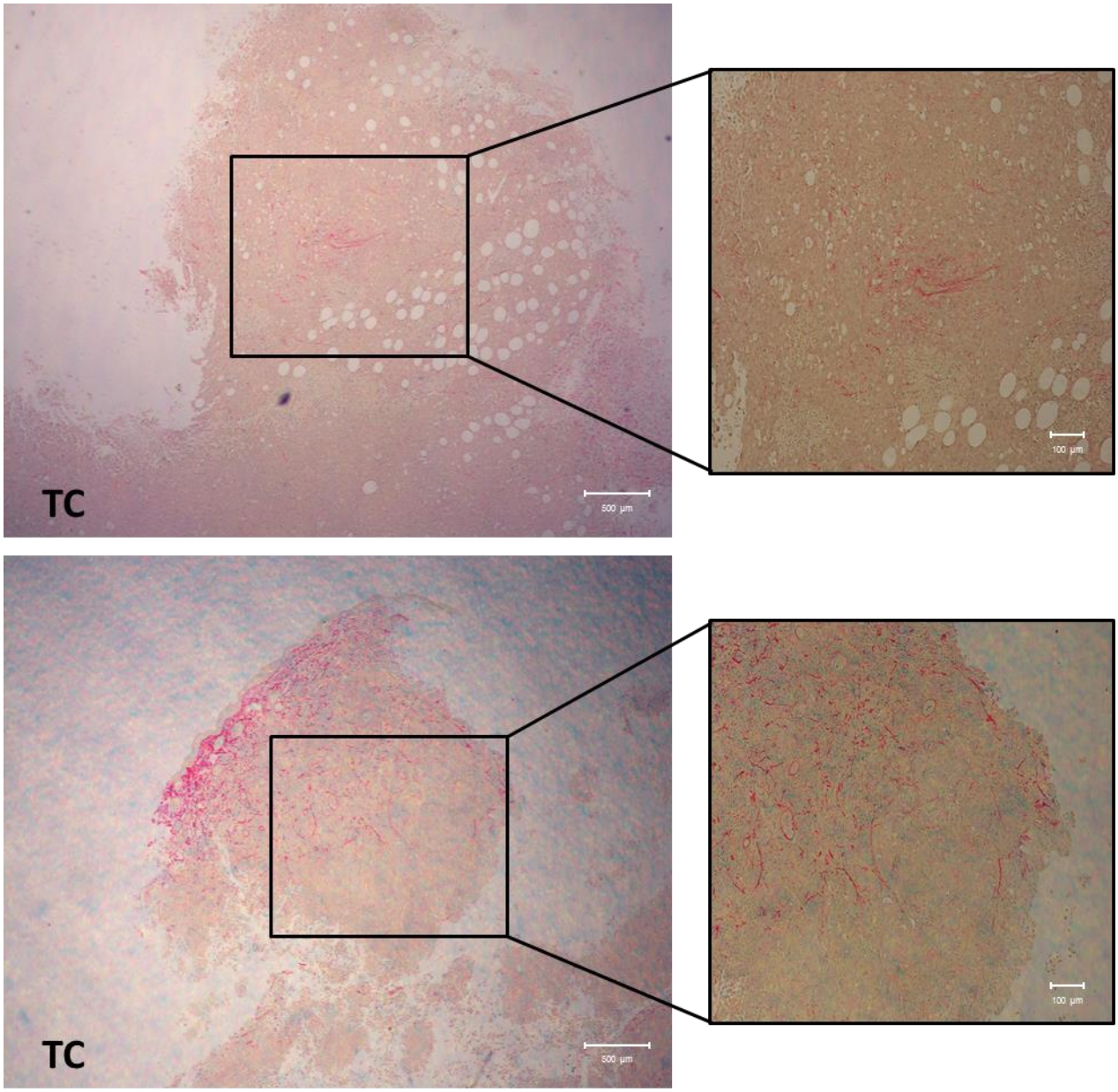

Figure 3.86: Representative Picrosirius Red images of tumours harvested from C57BL/6 mice. Tumours were harvested from female C57BL/6 mice. Representative images displayed are from Tumour Control (TC) and Tumour + Doxorubicin (TD) groups. Magnification at 4x and 10x.

3.8.3. Assessing the Effects of *in* vivo Doxorubicin administration on Tumour Cell Proliferation and Fibroblast Infiltration

Based on the observation that tumours display three distinct regions evident in the H&E ultrastructure assessment, we aimed to determine if these regions are representative of a

hypoxic / nutrient deprived gradient present within the tumour core. Therefore, immunofluorescence staining for proliferation in tumour samples only was performed using Ki67, a marker exclusive to cell proliferation.

We observed clear regions of cell proliferation, evident by an increase in the mean fluorescent intensity, in both the tumour control and tumour + doxorubicin groups. However, only the tumour + doxorubicin group showed the distinctive proliferative regions corresponding to the H&E staining performed, a radial pattern of cell proliferation was observed instead in the tumour control group. Additionally, it was noted that the tumour + doxorubicin group also displays a larger region of highly proliferative cells in comparison to the tumour control group.

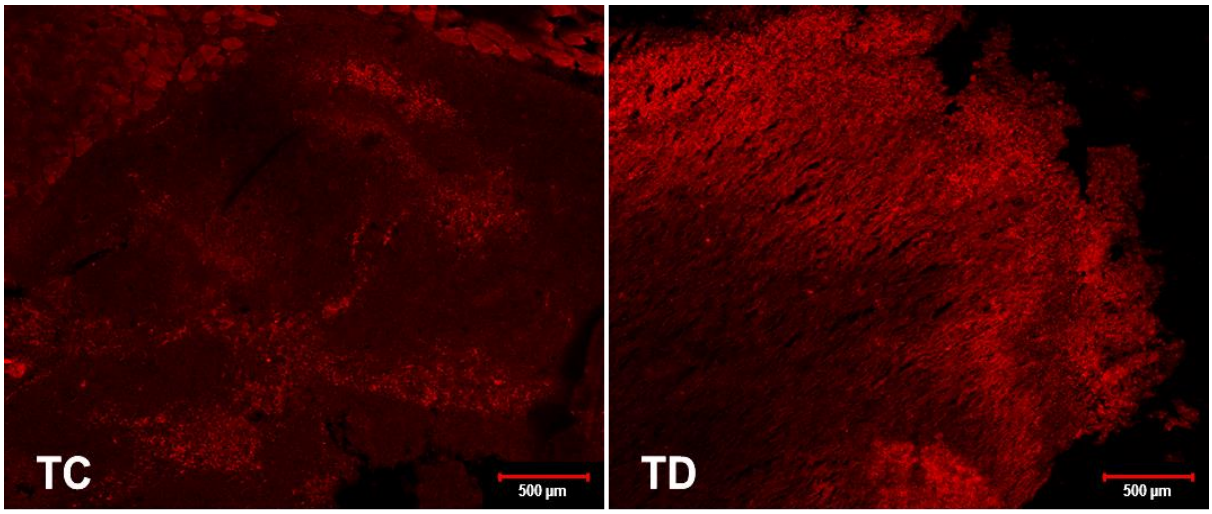

Figure 3.87: Representative immunofluorescent images of tumours harvested from C57BL/6 mice. Tumours were harvested from female C57BL/6 mice and confocal microscopy was performed following staining for Ki67. Representative images displayed are from Tumour Control (TC) and Tumour + Doxorubicin (TD) groups. Magnification at 10x.

Furthermore, as collagen deposition was observed to occur within tumour masses, and this was seen to increase with exposure to doxorubicin, we next aimed to determine whether an infiltration and “activation” of cancer-associated fibroblasts into the tumour stroma could account for the increased fibrosis we observed.

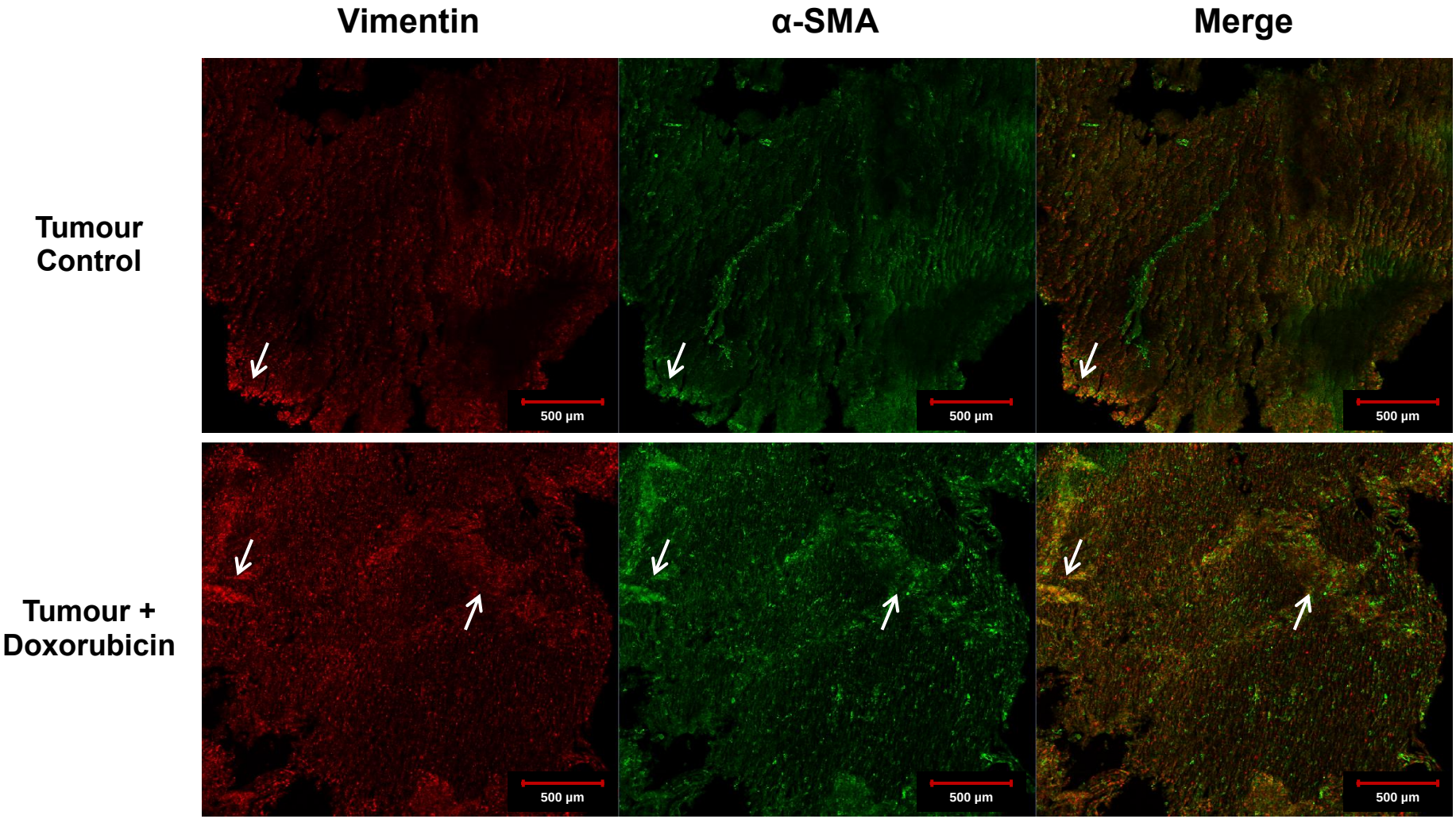

Figure 3.88: Representative immunofluorescent images of tumours harvested from C57BL/6 mice. Tumours were harvested from female C57BL/6 mice and confocal microscopy was performed following staining for α-SMA and vimentin. Representative images displayed are from Tumour Control (TC) and Tumour + Doxorubicin (TD) groups. Magnification at 10x.

Immunofluorescent imaging of α-SMA and vimentin expression in tumours revealed areas of co-localization of α-SMA with vimentin in both the tumour control and tumour + doxorubicin groups. However, increased regions of co-localization between α-SMA and vimentin were observed in the tumour + doxorubicin group when compared to the tumour control group.

3.8.4. Determining the Effects of Exogenous MEF-CM on the Invasive Capacity of Isolated Primary Epithelial Organoids

In order to better understand the influences that CAFs have on enhancing the migratory and invasive capacity of epithelial cancer cells within the context of an *in vivo* tumour setting, epithelial organoids were isolated from both mammary fat pads and tumours and were then subjected to treatment with/out MEF conditioned media (MEF-CM) that was generated in the *in vitro* cell culture model, and subjected to a 3D branching morphogenesis assay. Briefly, mammary fat pads and tumours were dissociated and isolated epithelial organoids were plated in Matrigel® in order to maintain their 3D structure and prevent contact with the cell culture plastic ware. Organoids were then treated with MEF-CM and phase-contrast time-lapse images of primary epithelial cell invasion out of the organoid mass were acquired every 12 hours for a period of 60 hours.

Based on the fact that tumours were inoculated into the fourth mammary fat pad, the separation of mammary fat pad epithelial organoids from tumour epithelial organoids is impossible. Additionally, epithelial cells form one of the smallest cell components of mammary fat tissue and only a few viable epithelial organoids can be isolated from a single mammary fat pad. As such, mammary fat pad epithelial organoids were only isolated from control and doxorubicin animals and utilized as non-cancerous controls.

Control (C) Group

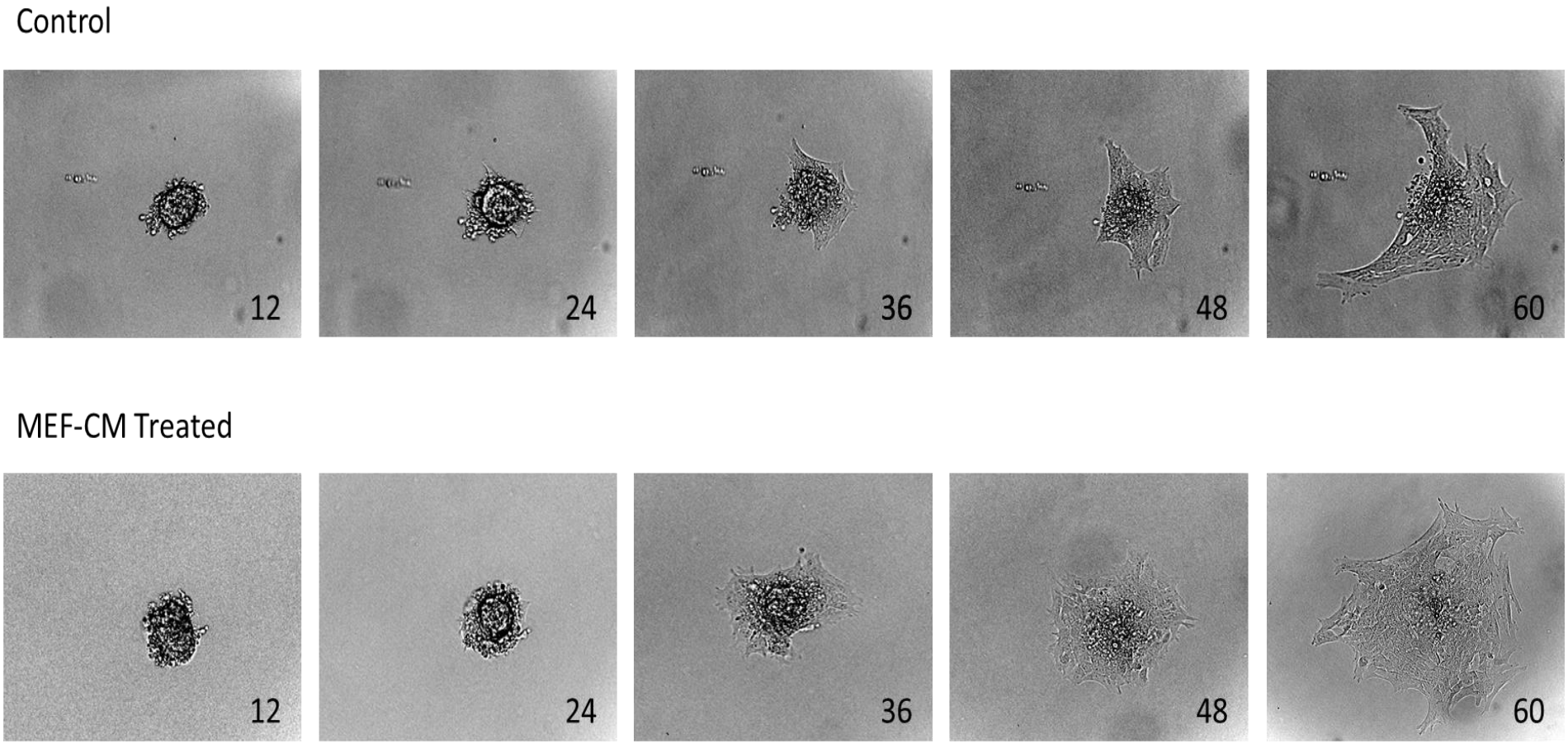

Figure 3.89: Representative phase contrast time-lapse images of epithelial organoids harvested from C57BL/6 mice. Primary epithelial organoids were isolated from dissociated mammary fat pads. Organoids were plated in Matrigel® and representative images displayed are from the Control (C) group of animals where organoids were subjected to treatment with either control media or MEF-CM. Magnification at 4x

Doxorubicin (D) Group

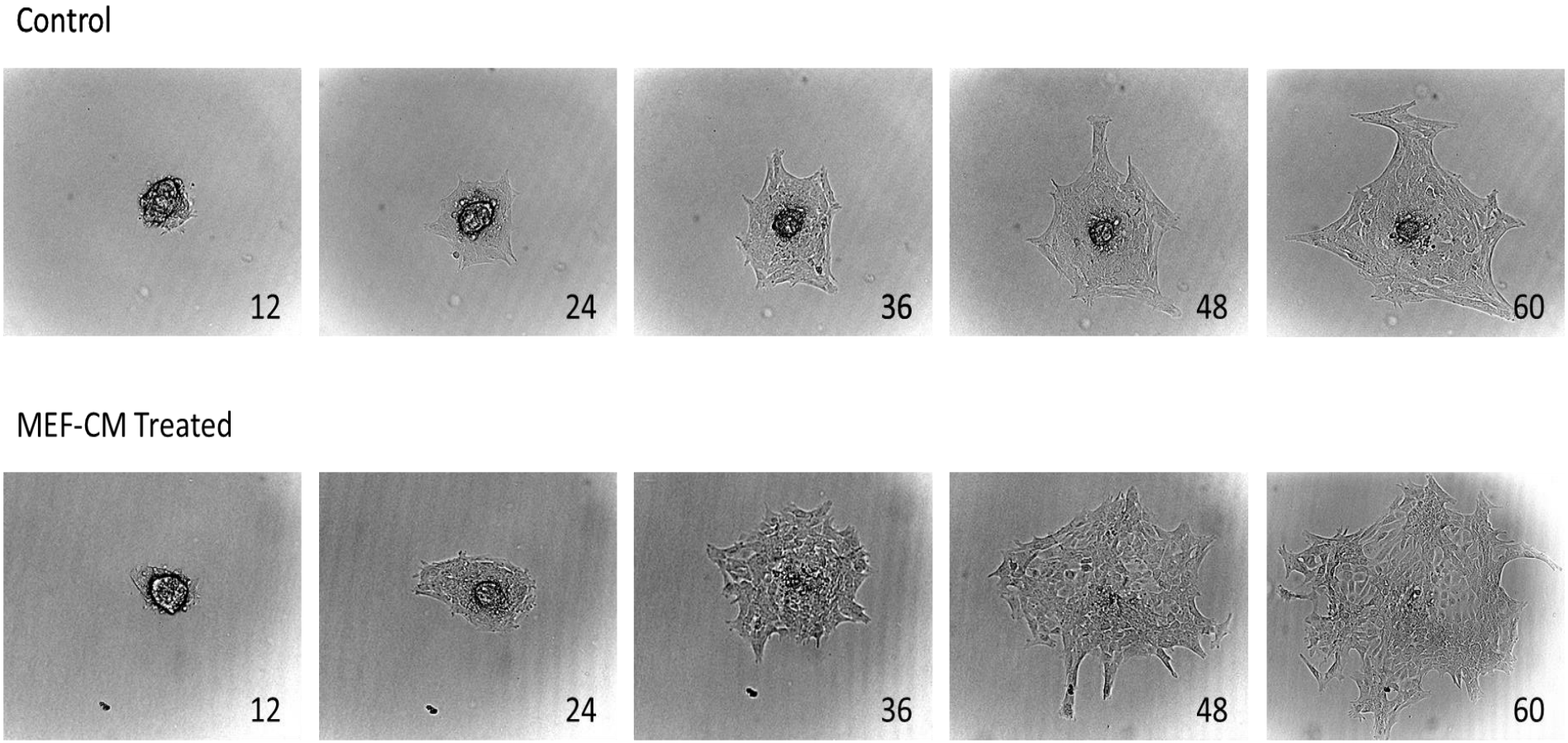

Figure 3.90: Representative phase contrast time-lapse images of epithelial organoids harvested from C57BL/6 mice. Primary epithelial organoids were isolated from dissociated mammary fat pads. Organoids were plated in Matrigel® and representative images displayed are from the Doxorubicin (D) group of animals where organoids were subjected to treatment with either control media or MEF-CM. Magnification at 4x

Tumour Control (TC) Group

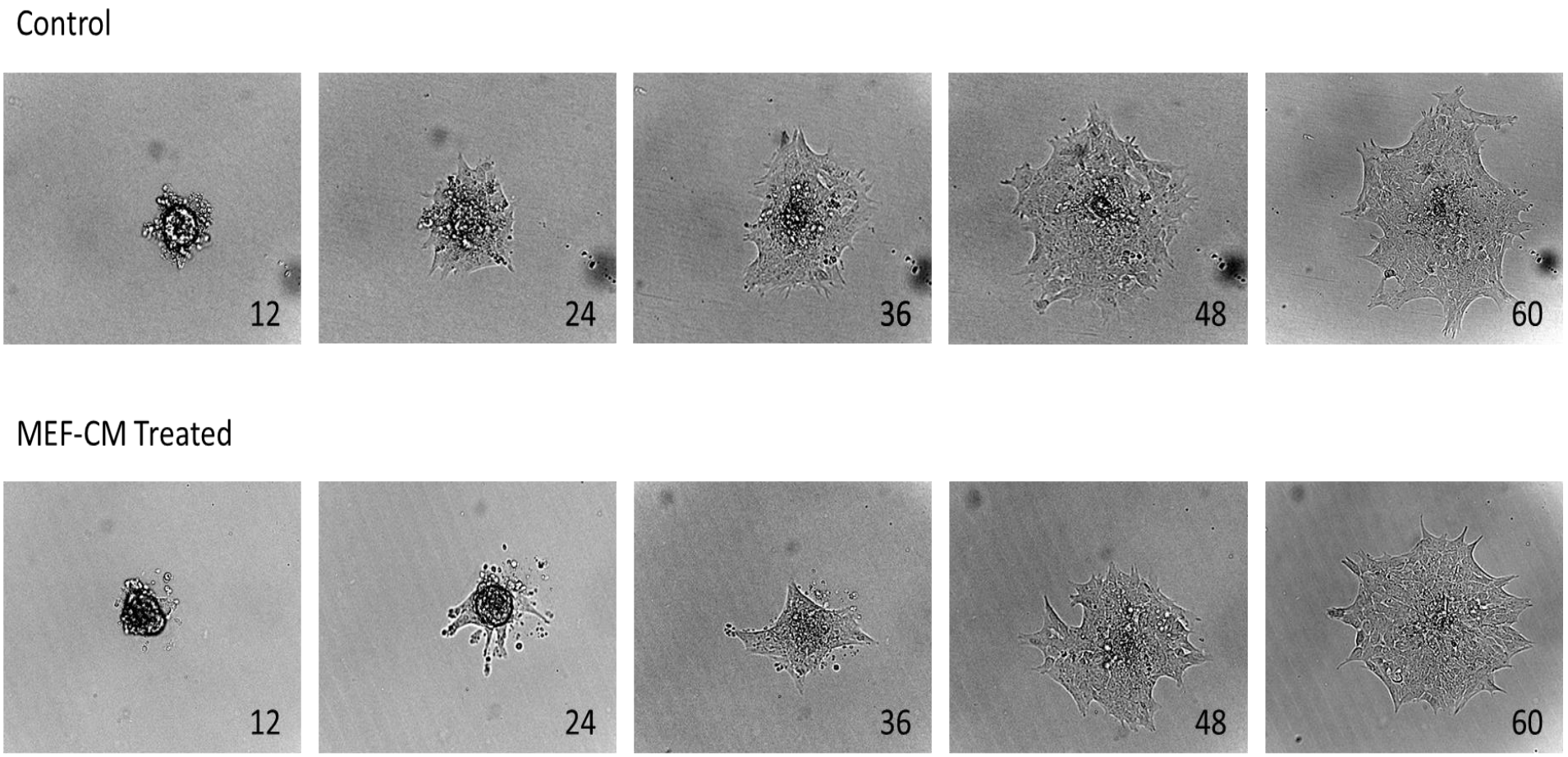

Figure 3.91: Representative phase contrast time-lapse images of epithelial organoids harvested from C57BL/6 mice. Primary epithelial organoids were isolated from dissociated mammary fat pads. Organoids were plated in Matrigel® and representative images displayed are from the Tumour Control (TC) group of animals where organoids were subjected to treatment with either control media or MEF-CM. Magnification at 4x

Tumour + Doxorubicin (TD) Group

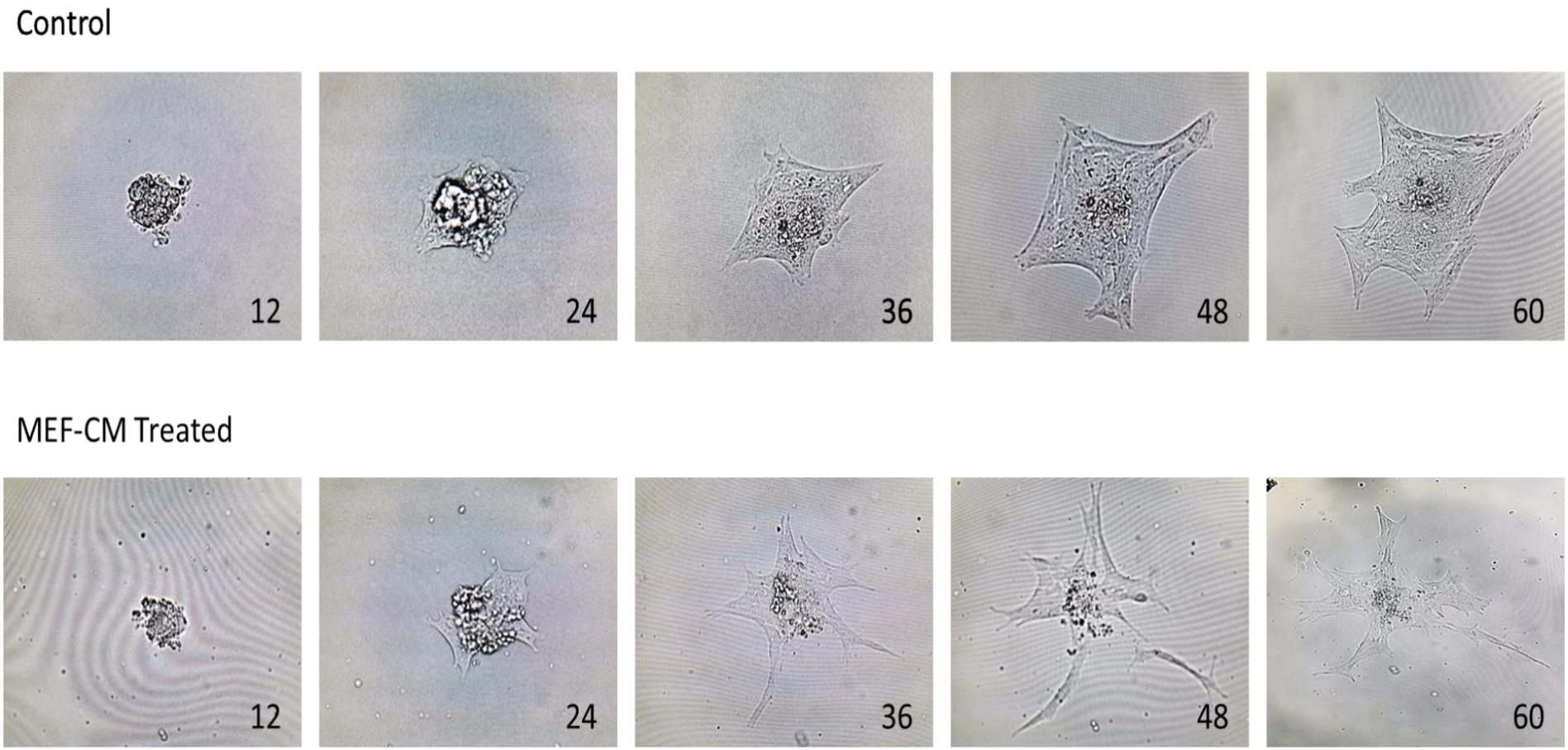

Figure 3.92: Representative phase contrast time-lapse images of epithelial organoids harvested from C57BL/6 mice. Primary epithelial organoids were isolated from dissociated mammary fat pads. Organoids were plated in Matrigel® and representative images displayed are from the Tumour + Doxorubicin (TD) group of animals where organoids were subjected to treatment with either control media or MEF-CM. Magnification at 4x

Results from our 3D branching morphogenesis assay showed that organoids isolated from all groups of mice successfully lead to the invasion of primary epithelial cells into the Matrigel®. Enhanced invasion was observed following doxorubicin administration in animals, as we observed an increased migratory distance of leader edges from the organoid “mass” in the control media group when compared to that of organoids isolated from control animals. Furthermore, the treatment of organoids from the control, doxorubicin and tumour + doxorubicin groups with MEF-CM resulted in increased migration of epithelial cells into the Matrigel®. This was evident by either an increase in total “surface area”, seen in the control and doxorubicin groups, or an increase in the distance of the leader front (length) from the organoid “mass”. Of interest to note, is that in addition to the increased distance leader edges migrated in organoids isolated from the tumour + doxorubicin group, treatment with MEF-CM also resulted in epithelial cells detaching from their leader edge at the 48 hour time point. A subsequent “catch-up effect” of the leader edge was then observed in this group at the 60 hour time point.

3.8.5. Determining the Role of Epithelial-to-Mesenchymal Transition in Response to *in vivo* Doxorubicin Administration

Finally, we aimed to determine whether *in vivo* doxorubicin administration leads to alterations in epithelial-to-mesenchymal transition (EMT) in whole mammary fat pads and tumours of C57BL/6 mice. We therefore employed Western blot analysis for several key markers of EMT, namely; α-SMA, PDGFRα, vimentin and E-cadherin.

3.8.5.1. α-SMA and PDGFRα

Analysis of α-SMA of mammary fat pads harvested from C57BL/6 mice revealed a significant reduction in α-SMA protein expression in the tumour + doxorubicin group when compared to control (51.58% ± 12.39% vs 100% ± 7.336%, p=0.0072), doxorubicin (51.58% ± 12.39% vs 104.0% ± 9.319%, p=0.0069), and tumour control (51.58% ± 12.39% vs 112.3% ± 15.21%, p=0.0113) groups.

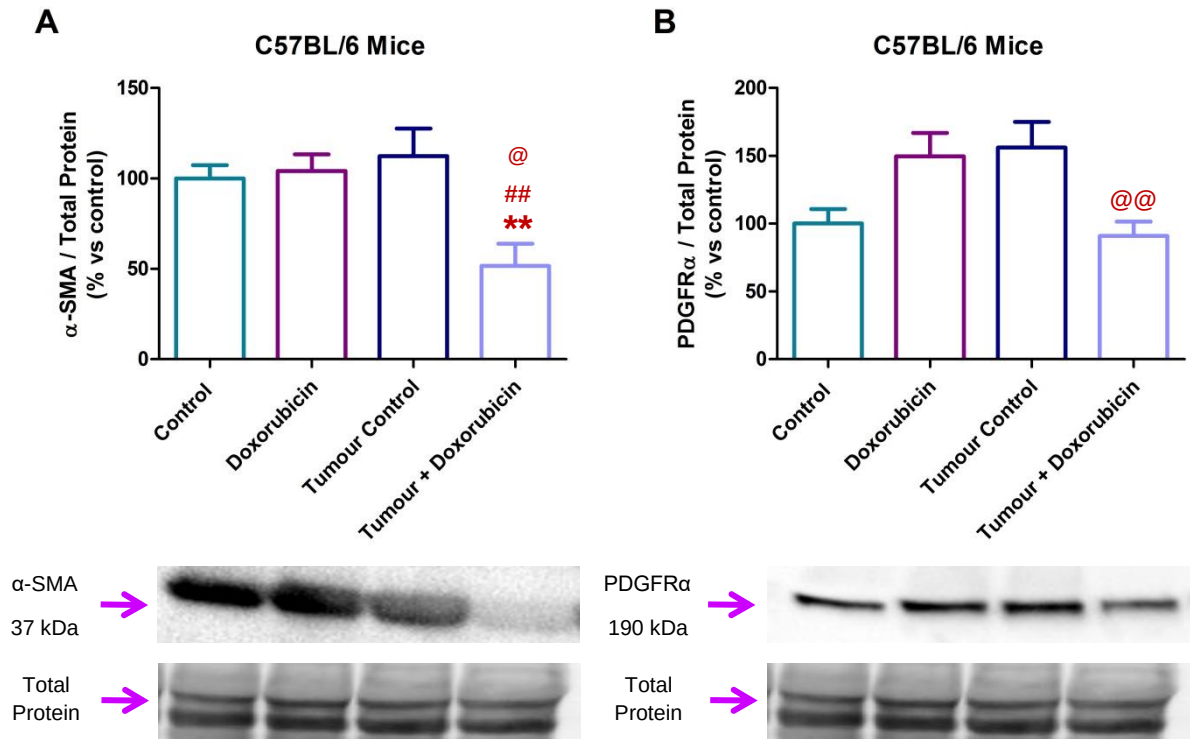

Figure 3.93: Western blot analysis of α-SMA and PDGFRα protein expression in mammary fat pads of female C57BL/6 mice. Statistical analysis: One way ANOVA with Bonferroni post hoc correction. All results are presented as mean ± SEM (n=6). ** = p<0.01 vs Control, ## = p<0.01 vs Doxorubicin and @@ = p<0.01 vs Tumour Control.

Although a trend to increased PDGFRα protein expression was observed in the doxorubicin and tumour control groups of the mammary fat pads, this was not statistically significant when compared to control. A significant reduction in PDGFRα protein

expression was however observed in the tumour + doxorubicin group when compared to the tumour control group (90.91% ± 10.49% vs 156.1% ± 18.83%, p=0.0091).

Whole tumour Western blot analysis of α-SMA protein expression showed no significant differences in the expression of α-SMA in the tumour + doxorubicin group compared to that of the tumour control (p=0.1095). A significant reduction in PDGFRα protein expression was however observed in the tumour + doxorubicin group compared to the tumour control group (65.63% ± 5.950% vs 100% ± 4.069%, p=0.0008).

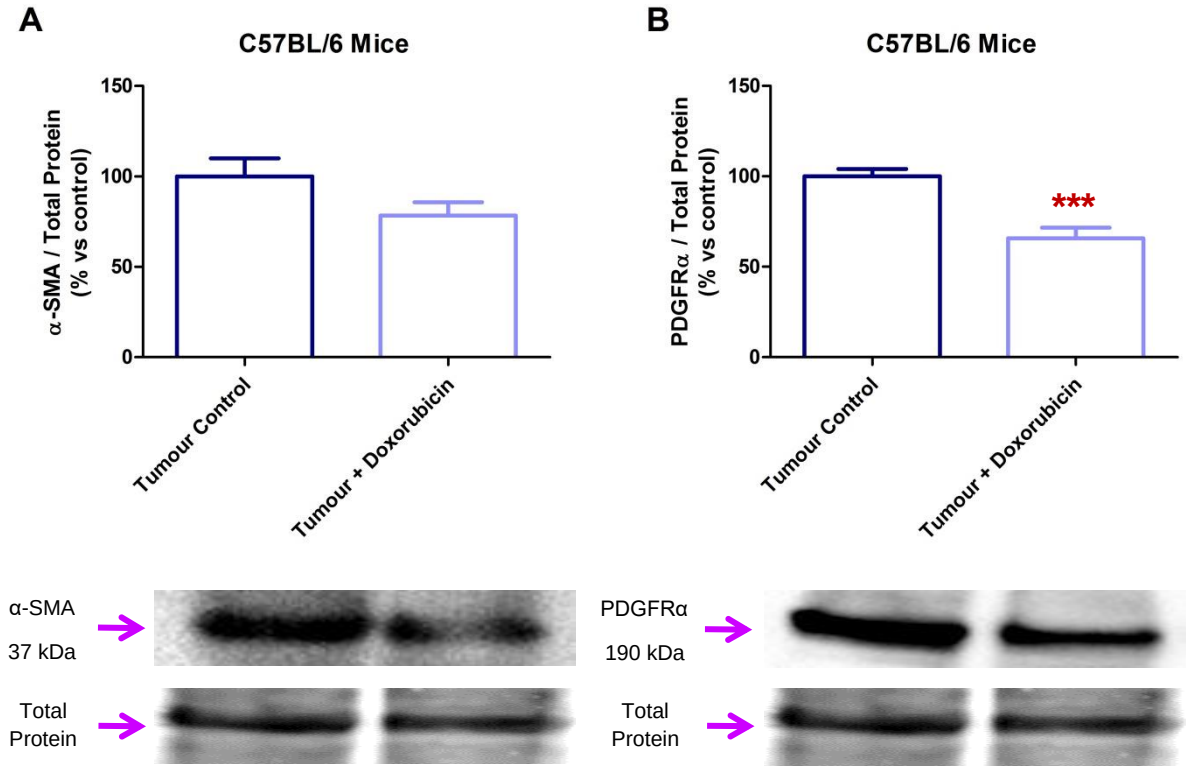

Figure 3.94: Western blot analysis of α-SMA and PDGFRα protein expression tumours of female C57BL/6 mice. Statistical analysis: One way ANOVA with Bonferroni post hoc correction. All results are presented as mean ± SEM (n=6). ***= p<0.0001 vs Tumour Control.

3.8.5.2. Vimentin and E-cadherin

Western blot analysis of vimentin and E-cadherin protein expression in the mammary fat pads of mice showed a significant increase in vimentin expression in the tumour control group (8068% ± 1903% vs 100% ± 71.80%, p=0.0058) when compared to the control and doxorubicin (8068% ± 1903% vs 2441% ± 547.3%, p=0.0295) groups. Additionally, a significant decrease in vimentin protein expression was observed in the tumour + doxorubicin group (8068% ± 1903% vs 1769% ± 169.1%, p=0.0165) when compared to the tumour control group. Furthermore, a significant increase in E-cadherin expression levels in the tumour control group (222.5% ± 37.29% vs 100% ± 9.570%, p=0.0191) was observed when compared to the control group.

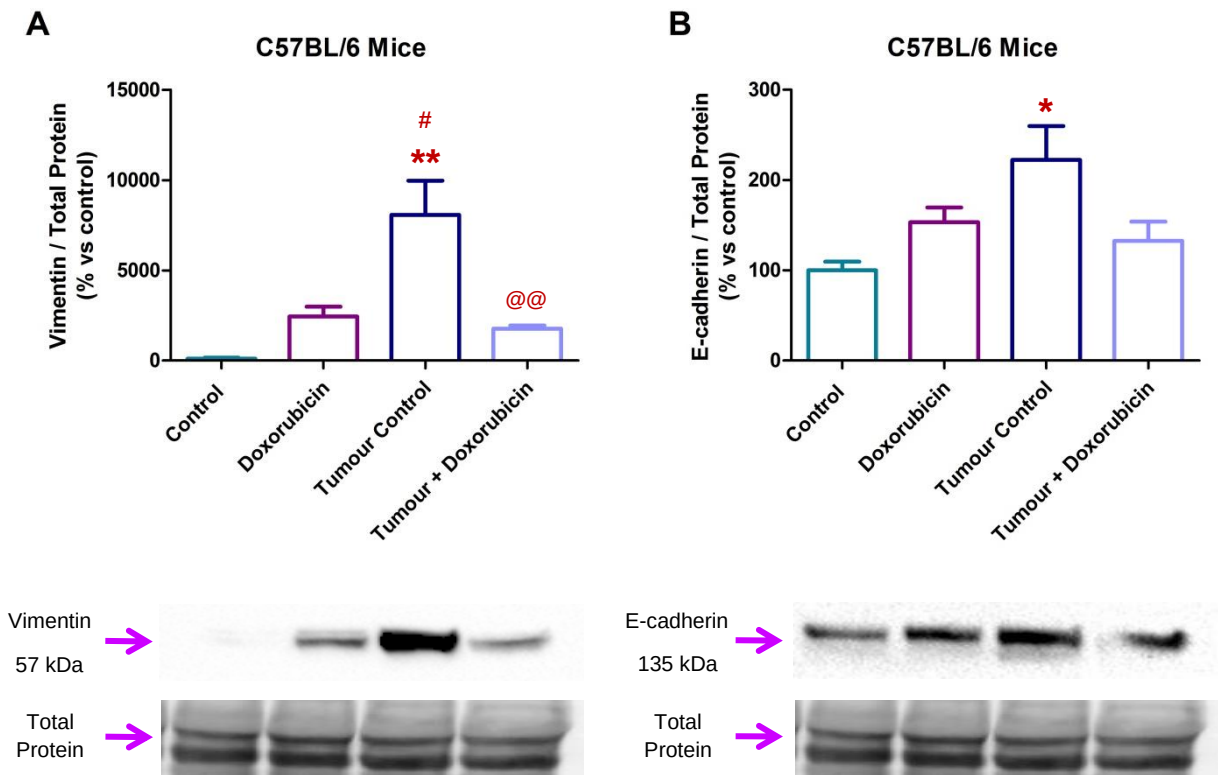

Figure 3.95: Western blot analysis of vimentin and E-cadherin protein expression in mammary fat pads of female C57BL/6 mice. Statistical analysis: One way ANOVA with Bonferroni post hoc correction. All results are presented as mean ± SEM (n=6). *** = p<0.0001 vs Control, # = p<0.05 vs Doxorubicin, @ = p<0.05 vs Tumour Control and @@ = p<0.01 vs Tumour Control.

Tumour analysis of vimentin and E-cadherin protein expression showed a significant reduction in vimentin expression in the tumour + doxorubicin group (62.54% ± 6.853% vs 100% ± 11.04%, p=0.0163) in comparison to the tumour control. Whereas, significantly increased in E-cadherin expression was observed in the tumour + doxorubicin group (173.0% ± 17.07% vs 100% ± 10.96%, p=0.0048) when compared to the control group.

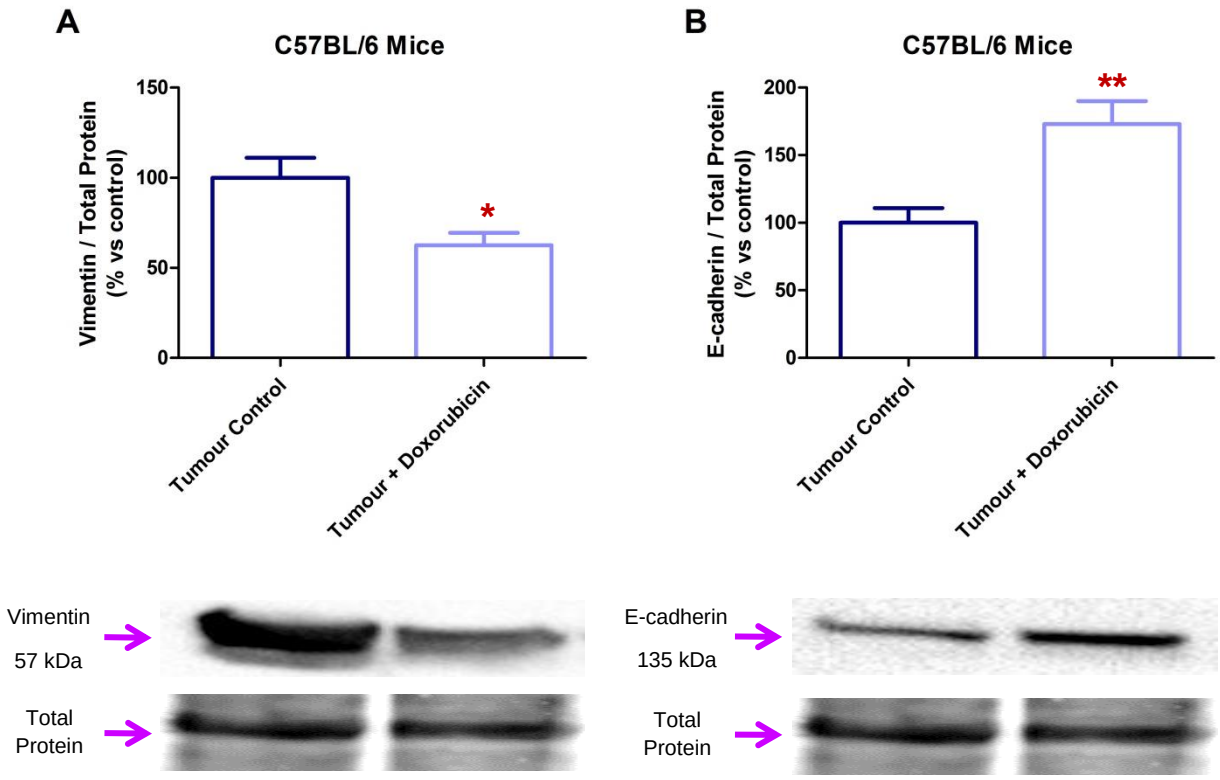

Figure 3.96: Western blot analysis of vimentin and E-cadherin protein expression in tumours of female C57BL/6 mice. Statistical analysis: One way ANOVA with Bonferroni post hoc correction. All results are presented as mean ± SEM (n=6). * = p<0.05 vs Tumour Control, ** = p<0.01 vs Tumour Control.

Chapter 4: Discussion

4.1. Introduction

Tumours are now recognized as being highly complex tissues, with the stromal cell compartment (containing most notably, fibroblasts and endothelial cells) contributing significantly to the pro-tumourigenic and metastatic capabilities of cancerous epithelial cells. Previously, this contribution of stromal cells, in particular cancer-associated fibroblasts (CAFs), to the tumourigenic process has been largely underestimated.

Cancer is a global concern, and the burden of this disease is rapidly on the rise in both developed and developing countries. Currently, the resistance of cancer cells to chemotherapeutic agents, like doxorubicin, is an ongoing and complex issue faced by both oncologists and patients alike. Increasing evidence implicates the molecular stromal-tumour interactions in the enhancement and progression of chemo-resistance. Furthermore, many preclinical models fail to accurately represent the influence of the tumour microenvironment (Singh et al., 2010) on cancer cell survival and progression towards a metastatic phenotype. As such there is a critical need for the development of novel treatment strategies which interfere with the metabolic capacity of the tumour microenvironment.

4.2. Induction of Oxidative Stress without Cell Death in E0771 Breast Cancer Cells

According to the 'reverse Warburg effect', nutrient/oxygen deprived epithelial cancer cells have the propensity to "educate" surrounding stromal cells to increase aerobic glycolysis and autophagy, resulting in the enhanced production of metabolites which can be utilized by epithelial cancer cells to sustain tumour growth and metastasis (Pavlides *et al*., 2009). Therefore, in this part of the study we aimed to establish a time course of glucose deprivation in murine E0771 breast cancer cells, which induces significant oxidative stress while still maintaining cell viability. We have demonstrated a compensatory mechanism in these cells to glucose deprivation, where a significant reduction in MTT reductive capacity was observed following 4, 8, 24, 48 and 72 hours of glucose deprivation. However, no significant decrease was seen following 12 hours of treatment with glucose deprived DMEM **(Figure 3.1)**. These results are in accordance with data we obtained for four other human breast cancer cell lines **(Figure 3.2 and Figure 3.3)**, as well as other studies where glucose deprivation in PC12 rat pheochromocytoma cells resulted in the rapid reduction in MTT reductive capacity immediately following glucose deprivation, with a slight increase occurring after 3 hours, where after MTT reductive capacity rapidly decreased over time (Liu *et al*., 2003).

As glucose is the predominant substrate in neoplastic cells with high glycolytic rates, this could account for the rapid decrease in MTT reductive capacity we observed following 4 and 8 hours of glucose deprivation in the E0771 cancer cells. The increased reductive capacity we observed after 12 hours of glucose deprivation could be a result of a compensatory mechanism, whereby E0771 cancer cells are able to switch their substrate utilization. This has been reported in several studies, whereby other substrates (such as amino acids and glutamine) present in culture media can be utilized for survival

(Tsun and Possemato, 2015, Tardito *et al*., 2015) in the absence of glucose. This could also explain the significant decrease in reductive capacity we observed with longer deprivation times, as the depletion of these utilized substrates would result in a second bout of metabolite starvation, and thus a rapid decrease in cell viability ensues.

The inactivation of tumour suppressors and concomitant hyper-activation of oncogenes, has long been associated with the susceptibility of mammalian cells to proliferation (Pedraza-Fariña, 2006). Moreover, changes in cellular metabolism has been shown to be tightly coupled with cell proliferation (Matoba *et al*., 2006), and many of the tumour suppressor genes and oncogenes governing cell cycle arrest and proliferation are also known to regulate glucose uptake and utilization (Schwartzenberg-Bar-Yoseph *et* al., 2004, Gao *et al*., 2009). This is not surprising, as during cellular proliferation cells are required to increase the availability of biomolecules and metabolites at a rate which is sufficient to meet the increased demand. In order to maintain sustained proliferative capabilities, cancer cells are required to fundamentally alter many of the pathways involved in nutrient utilization and energy metabolism to cope with the increased metabolic demands of proliferation, a “hallmark of cancer” proposed by Hanahan and Weinberg (2011).

As cell proliferation is metabolically demanding, during the initial stages of inadequate nutrient supply, cellular metabolism is drastically reduced and cells resort to cell cycle arrest, favouring quiescence in order to promote survival. However, under conditions of prolonged nutrient deprivation, basal cellular metabolism cannot be maintained and the induction of apoptotic cell death ensues (Altman and Rathmell, 2012). Based on this knowledge, we assessed key protein markers of DNA damage (PARP) and apoptosis induction (caspase-3 and cleaved caspase-3) in parallel with oxidative stress (cytosolic H_2O_2 and mitochondrial $O_2^{\bullet-}$), in order to determine a time point where E0771 cancer

cells display increased oxidative stress in response to glucose deprivation without significantly inducing apoptotic cell death.

Western blot analysis of the E0771 murine breast cancer cells in response to short term (4-12 hours) glucose deprivation, showed a slight, non-significant increase in PARP **(Figure 3.4)** and cleaved caspase-3 **(Figure 3.5)** expression following 8 hours of glucose deprivation. As the cleavage of caspase-3 results in its activation and the commitment of cells to apoptotic cell death (Elmore, 2007), the ratio of cleaved caspase-3 to total caspase-3 expression provides further insight into the commitment of these E0771 cancer cells to apoptotic cell death following glucose deprivation. Our results showed that the ratio of caspase-3 to total caspase-3 was significantly increased following both 4 and 8 hours of glucose deprivation, but returned to control levels at the 12 hour time point **(Figure 3.5)**. A significant increase in mitochondrial superoxide ($O_2^{\bullet-}$) levels was also observed after 12 hours of glucose deprivation in the E0771 cancer cells **(Figure 3.6b)**. However, no significant changes in cytoplasmic hydrogen peroxide (H_2O_2) levels were observed across all time points **(Figure 3.6a)**. This may be explained by the fact that the antioxidant capacity of these cells was able to quickly neutralise any H_2O_2 that may have been produced as a result of glucose deprivation induced stress. Taken together these results suggest that following complete glucose deprivation, a rapid induction of cell death occurs with a concomitant decrease in mitochondrial reductive capacity. However, as cancer cells have the propensity to easily switch their substrate utilization to suit the availability of metabolites, glucose deprived E0771 cancer cells were able to survive despite having increased mitochondrial oxidative stress after 12 hours of glucose deprivation.

4.3. The Effects of Glucose Deprivation on the Proteome Secreted from E0771 Breast Cancer Cells

It is widely accepted that the secretion of proteins plays a role in various aspects of cell signalling including cell-cell communication and migration. Over the last decade proteomic analysis of secreted proteins has facilitated the understanding of the molecular mechanisms underlying cell-cell communication and has fast become a viable approach in the identification of possible diagnostic and prognostic biomarkers in cancer (Patel, 2014). The understanding of the cellular “language” involved in the metabolic reprogramming of CAFs by epithelial cancer cells will thus have profound effects on future chemotherapeutic strategies, targeted to the tumour microenvironment. Therefore, in this section of the study, we aimed to utilize a bioinformatics approach to assess the protein composition of conditioned media generated from E0771 breast cancer cells following 12 hours of glucose deprivation, in order to determine possible candidate proteins involved in the metabolic reprogramming of MEFs. Our analysis of the proteome of E0771 conditioned media revealed a total of 61 protein elements exclusively present in glucose deprived E0771 conditioned media (E0771_GD), and a total of 41 protein elements were observed exclusively in control E0771 conditioned media (E0771_C) **(Figure 3.7)**. Submission of the upregulated GO terms of E0771_GD into REVIGO resulted in a collapse of these proteins into several biological processes, many of which were shown to be involved in cell migration, cell-cell adhesion and glucose metabolism **(Figure 3.9)**.

We observed a significant clustering of proteins involved in gluconeogenesis and glycolysis in glucose deprived E0771 conditioned media (E0771_GD) **(Figure 3.11)**. Most notably, we observed the upregulation of the glycolytic enzymes glucose-6-phosphate dehydrogenase (G6PD), enolase (ENO) 1/3 and pyruvate kinase, muscle (PKM), this was initially surprising as glucose deprivation in E0771 breast cancer cells is

expected to result in a downregulation in glycolytic flux. However, functional annotation clustering (FAC) analysis in DAVID revealed a significant upregulation in in both protein catabolism and protein polyubiquitination **(Figure 3.13)**. These data suggest that an increase in protein polyubiquitination and catabolism occur in response to glucose deprivation in E0771 breast cancer cells. The breakdown of these proteins could provide metabolic intermediates, resulting in an upregulation of glycolysis, and thereby serving as an essential energy source for E0771 breast cancer cell survival.

Additionally, exosome-like vesicles isolated from breast and prostate tumour cells have been shown to contain proteins including, annexins (A1 and A2), actin, pyruvate kinase (M1 and M2), heat shock protein (HSP 90α), AHNAK and histone (H4) (Hosseini-Beheshti *et al*., 2012, Kruger *et al*., 2014). All of which we observed to be significantly upregulated in glucose deprived E0771 conditioned media. Recently, the nucleoprotein AHNAK was shown to be highly expressed in human breast tumour samples and is critical for the production of extracellular vesicles, including exosomes, as well as the targeted directionality of these vesicles towards stromal fibroblasts, resulting in increased fibroblast migration (Silva *et al.,* 2016). Based on this evidence, we postulate that the upregulation of AHNAK and other exosome-associated proteins in glucose deprived E0771 conditioned media might be as a result of enhanced exosomal release from these nutrient deprived cancer cells, and that this serves as a possible survival strategy utilized by epithelial cancer cells in response to decreased nutrient availability.

Moreover, significant upregulation of the 14-3-3 protein domain was observed to occur in glucose deprived E0771 conditioned media **(Figure 3.12)**. Increased 14-3-3 protein expression has been shown to contribute to a wide variety of tumour promoting processes in metastatic cancers (Wilker and Yaffe, 2004, Morrison, 2009, Aitken, 2011), and the overexpression of several 14-3-3 isoforms are associated with poor clinical outcomes and increased metastatic risk in patients with hepatocellular carcinoma (Liu *et*

al., 2011, Ko *et al*., 2011). In recent years the epsilon isoform of the 14-3-3 protein (14-3-3ε) has been implicated in the regulation of cancer cell epithelial-to-mesenchymal transition (EMT), invasion and metastasis (Liu *et al*., 2013), and the overexpression of 14-3-3ε contributes to EMT progression in hepatocellular carcinoma, by increasing vimentin and N-cadherin expression while also decreasing E-cadherin protein expression. Furthermore, the delta isoform 14-3-3δ, heterogeneous nuclear ribonucleoprotein K (HNRNPK) **(Figure 3.12)** and Annexin A1 have all been implicated in enhanced EMT and metastatic progression in cancer (Chaundhury *et al*., 2010, Ge *et* al., 2012, Sobral-Leite *et al*., 2015, Raychaudhuri *et al*., 2016), which we have shown are also significantly upregulated in glucose deprived E0771 conditioned media **(Figure 3.10 and Figure 3.12)**. Furthermore, as 14-3-3 has been shown to be secreted on extracellular vesicles, like exosomes, it is conceivable that the upregulation of the 14-3-3 protein domain in glucose deprived E0771 conditioned media is further indicative of the presence of exosome release in response to glucose deprivation and that 14-3-3 positive exosomes could play a role in the activation of EMT.

Finally, the pro-metastatic and EMT inducing results we obtained were further corroborated by the observation that significant clustering of proteins involved in the canonical Wnt signalling pathway **(Figure 3.9 and Figure 3.13)** were seen using both REVIGO and DAVID. Classically, canonical Wnt signalling is β-catenin dependent and is well characterized for the role it plays in cancer progression and metastasis (Planutis *et al*., 2013, Lemieux *et al*., 2015). In mammalian cells, Wnt signalling is involved in the regulation of cell survival, adhesion, migration and invasion (Chen *et al*., 2001, Kurayoshi *et al*., 2006), and has also been implicated in EMT induction and progression (Vincan and Barker, 2008, Kahlert *et al*., 2012). The exosomal secretion of active Wnt ligands has been shown to exhibit functional signal-inducing activity upon their uptake in recipient cells. Furthermore, the recruitment and “activation” of CAFs in the tumour

microenvironment by the Wnt ligand Wnt7a is mediated by both canonical Wnt signalling as well as TGFβ receptor signalling (Avgustinova *et al*., 2016). Therefore, we further propose that the upregulation of proteins involved in Wnt signalling in glucose deprived E0771 conditioned media may additionally be secreted on exosomes and that this will exhibit functionality in recipient cells, leading to enhanced EMT and cell migration.

As CAFs characteristically display signs of smooth muscle differentiation during their activation, which entails the acquisition of an enhanced mesenchymal phenotype (Busch *et al*., 2017), our results from the proteomics analysis of glucose deprived E0771 conditioned media collectively suggest that 14-3-3 and other pro-metastatic proteins are secreted in exosomes, in response to 12 hours of glucose deprivation. Indeed, if this is the case the secretion of these exosomes, containing pro-EMT and plausibly metabolic cargo, could serve as a potential mechanism whereby E0771 breast cancer cells “activate” and metabolically reprogram stromal CAFs to promote their own survival. However, in order to validate this, conditioned media would need to be separated into different fractions and extensive research on the exosomal fraction would need to be conducted in order to; firstly, identify the presence of E0771 secreted exosomes and secondly, to determine the exact proteomic composition of these exosomes and how their cargo is altered in response to glucose deprivation.

4.4. Effects of E0771 Conditioned Media on Cancer-Associated Fibroblast Metabolism

Within the tumour stroma CAFs are large spindle-shaped mesenchymal cells with well-defined fibronexi and stress fibres (De Wever *et al*., 2008). The identification of CAFs within the tumour microenvironment relies on the concomitant expression of several key protein markers such as alpha smooth muscle actin (α-SMA), platelet derived growth factor receptor α/β (PDGFR α/β), vimentin, and several others (Hinz *et al*., 2007). Furthermore, in several cases CAFs have very low to negative expression of epithelial cell markers such as E-cadherin and CD31. In particular, cancerous regions present in invasive ductal carcinoma of the breast display increased α-SMA$^+$ expressing myofibroblasts with decreasing CD34$^+$ fibrocytes (Catteau *et al*., 2013). The increased expression of α-SMA in the tumour stroma has been shown to contribute to cytoskeletal organization and to inhibit fibroblast migration, thereby increasing the contractile ability of CAFs (Ronnov-Jessen *et al*., 1996). Additionally, the abundant infiltration of α-SMA positive CAFs has been shown to occur in metastatic 4T1 and 410.4 mouse mammary carcinomas, but fails to occur in less aggressive 4T07 tumours (Avgustinova *et al*., 2016).

Based on this evidence, we aimed to firstly determine whether normal mouse embryonic fibroblasts (MEFs) could be “activated” into a cancer-associated fibroblast phenotype. As such we made use of Western blotting analysis and confocal microscopy to assess the expression levels of several CAF-associated mesenchymal protein markers, namely; α-SMA, PDGFRα and vimentin as well as the epithelial protein marker, E-cadherin. We observed a significant increase in the expression of α-SMA in MEF cells treated with glucose deprived E0771 conditioned media when compared to both control and control conditioned media **(Figure 3.14 and Figure 3.15a).** A significant increase in vimentin

(Figure 3.14 and Figure 3.16a) expression was also seen in both untreated and glucose deprived E0771 conditioned media. These results are in agreement with literature where the recruitment of mesenchymal stem cells (MSCs) into prostate tumours has been shown to induce CAF activation, evident by the increased acquisition of both α-SMA and vimentin expression (Jung *et al*., 2013). Furthermore, the "activation" of CAFs is additionally associated with the decrease and/or loss of the epithelial marker E-cadherin. This was indeed observed in response to glucose deprived E0771 conditioned media in our Western blot analysis of E-cadherin protein expression **(Figure 3.16b)**. We observed no statistical differences in the protein expression of PDGFRα across all of the treatment groups **(Figure 3.15b)**. Although PDGFRα is a known protein marker of CAFs (Erez *et al*., 2010) the fact that we did not observe a statistically significant increase in protein expression in response to glucose deprived E0771 conditioned media was slightly unexpected. However, as PDGFRα expression is also a marker of the capacity of cells to undergo EMT (Zhang *et al.,* 2016, Yang *et al*., 2017), the non-significant increase we observed following both untreated E0771 and glucose deprived E0771 conditioned media treatment **(Figure 3.15b)** indicates that these cells have the capacity to undergo transition to a more mesenchymal phenotype. Therefore, when taken collectively our results suggest that MEF cells are indeed "activated" to a CAF phenotype in response to E0771 conditioned media and more so when these E0771 cancer cells have been starved of glucose for 12 hours (E0771-CM).

Subsequent to the verification that MEF cells are able to "activate" a CAF phenotype when exposed to glucose deprived E0771 conditioned media, we set out to determine the effects that E0771 conditioned media has on the metabolic profile of "activated" CAFs. Our results show that glucose deprived E0771-CM lead to a significant increase in MTT reductive capacity of "activated" CAFs **(Figure 3.17)**. This result was unexpected as it is thought that during the "reverse Warburg effect" the activation of CAFs by the

transfer of oxidative stress from cancer cells induces mitochondrial dysfunction in CAFs (Martinez-Outschoorn *et al*., 2010). However, our result may be explained by the fact that in response to induced stress, mitochondria initially undergo a respiratory burst in a compensatory attempt to promote cell survival, resulting in a rapid increase in MTT reduction (Pruett and Loftis, 1990). It is thus conceivable that we could have observed a decrease in MTT reductive capacity following a longer treatment time.

Martinez-Outschoorn and colleagues (2010) demonstrated that, within a co-culture system, MCF-7 human breast cancer cells can induce oxidative stress in adjacent hTERT immortalized fibroblasts. Based on this, we aimed to assess whether conditioned media derived from glucose deprived E0771 cancer cells would elicit the same response and induce oxidative stress in "activated" MEFs. We observed a significant increase in the mean fluorescent intensity of both DCF (cytosolic H_2O_2) and MitoSOX (mitochondrial $O_2^{\bullet}$-) in MEF cells that were treated with glucose deprived E0771-CM alone **(Figure 3.18)**. Our results are thus in accordance with those obtained by Martinez-Outschoorn and colleagues (2010).

Hypoxia-inducible factor α (HIF-1α) is an essential component in the cellular adaptive response to hypoxia. The stabilization of HIF-1α has been shown to occur in response to both hypoxic and non-hypoxic stimuli (Richard *et al*., 2000). Although reactive oxygen species (ROS), including H_2O_2 and $O_2^{\bullet}$-, have been associated with the induction of HIF-1α (Jung *et al*., 2008), the mechanisms underlying the induction and stabilization of HIF-1α by ROS remains to be fully elucidated; it has however been proposed that under conditions of limited oxygen supply, the stabilization of HIF-1α is linked to the oxygen sensor capacity of ROS (Richard *et al*., 2000, Görlach *et al*., 2001). In addition to the regulatory role of ROS in HIF-1α stabilization, under both hypoxic and non-hypoxic conditions, nutrient sensing by adenosine monophosphate-activated protein kinase

(AMPK) activity also plays a critical role in regulating HIF-1α transcriptional activity during hypoxic conditions in a variety of cancer types (Lee *et al*., 2003). Our Western blot analysis of HIF-1α protein expression showed a significant increase following treatment with both untreated E0771 and glucose deprived E0771 conditioned media, suggesting that the stabilization of HIF-1α in "activated" MEFs by epithelial cancer cells occurs independently of nutrient deprivation **(Figure 3.19)**. A possible explanation for the increased expression of HIF-1α we observed in the untreated E0771 conditioned media treatment group could be as a result of the ability of mitochondrial ROS to stabilize HIF-1α (Comito *et al*., 2011), although we did not observe a statistically significant increase in either MitoSox **(Figure 3.18b)** or DCF **(Figure 3.18a)** in MEF cells following untreated E0771 conditioned media treatment, the increase in mitochondrial superoxide levels seen may have become significant following a longer treatment period.

The activation of HIF-1α has several critical functions, which include the maintenance of cellular redox and energy homeostasis. Most notably in the context of this study, HIF-1α stabilization plays an essential role in the induction of autophagy in several cancer cell types and in MEFs (Tracy *et al.,* 2007, Bellot *et al*., 2009). The removal of ROS-transformed mitochondria by the process of autophagy (more specifically, mitophagy) during hypoxic and nutrient deprived conditions, has been shown to reduce intracellular oxidative stress and promote cell survival (Scherz-Shouval *et al*., 2007, Chen *et al*., 2009). The mammalian Target of Rapamycin (mTOR) functions as a critical sensor of intracellular nutrient availability. As such mTOR serves as a potent negative regulator of autophagic activity and a decrease in its activity leads to the induction autophagy through the activation of Atg13 and Unc-51-like kinase (ULK1), two of the main initiators of phagophore formation (Lozy et al., 2012). We observed a significant decrease in both mTOR (Ser^{2448}) phosphorylation and total mTOR protein expression **(Figure 3.20)**

following the treatment of MEF cells with both E0771 untreated conditioned media and E0771 conditioned media, suggestive of the induction of autophagy. The induction of autophagy by decreased mTOR activity is accompanied by the increased expression of the autophagic marker LC3 II (Kimura *et al*., 2009). As such, we assessed LC3 II expression in MEF cells following E0771 conditioned media treatment and observed no significant changes in LC3 II protein expression across all treatment groups **(Figure 3.21a)**, which may suggest that autophagic flux has not been increased in response to E0771 conditioned media treatment. This result was unexpected as it has been proposed previously that autophagy is induced in stromal cells in response to increased oxidative stress (Pavlides *et al*., 2012, Maes *et al*., 2013) to provide glycolytic intermediates resulting in the enhanced production of L-lactate. In order to obtain a better understanding of the role of autophagy in MEF cells following E0771 conditioned media treatment, we assessed the protein expression of the autophagy receptor p62/SQSTM1 (p62). A significant increase in p62 protein expression was seen in MEFs following treatment with both untreated E0771 and glucose deprived E0771 conditioned media **(Figure 3.21b)**. p62 recognises and binds to proteins tagged by ubiquitin, targeting them for degradation (Komatsu *et al*., 2007), and during the process of autophagosome formation, p62 associates with LC3 II sequestered to the inner surface of the phagophore (Mizushima *et al*., 2008). Autophagosomal cargo is subsequently delivered to lysosomes (Rabinowitz *et al.*, 2010) where the release of lysosomal digestive enzymes results in the degradation of p62 as well as sequestered cellular constituents. As such, the accumulation of p62 we observed following E0771-CM might indicate impaired autophagosomal clearance. As mentioned previously, p62 is also an adaptor protein which plays a role in various other pathways, including the ubiquitin proteasome system (UPS) (Babu *et al*., 2005). Based on this, the increase in p62 protein expression we observed, might be attributed to enhanced activity of the UPS system in

MEFs when treated with E0771 conditioned media. The UPS also plays a critical role in proteasomal degradation and has been shown to play a role in the regulation of metabolic genes (Maneix *et al*., 2016). It is conceivable that enhanced UPS activity may play a role in regulating glycolysis in our treatment conditions, and could serve as an additional source (i.e. amino acids) of metabolic intermediates.

Additionally, HIF-1α results in increased glycolytic flux by activating the transcription of genes regulating glucose transporters and glycolysis (Iyer *et al*., 1998, Seagroves *et al.,* 2001, Lum *et al*., 2007). Based on this, we assessed glucose uptake in MEF cells following treatment with E0771-derived conditioned media by utilizing the fluorescent deoxyglucose analog, 2-NBDG. We observed a significant increase in glucose uptake in MEF cells that were treated with conditioned media derived from glucose deprived E0771 cancer cells **(Figure 3.22)**. We have also shown that this increase in glucose uptake is in part mediated by the glucose transporter, GLUT4 **(Figure 3.23)**. The increased translocation of GLUT4 to the plasma membrane in response to glucose deprived E0771 conditioned can be explained by the fact that in insulin-sensitive tissues, the translocation of both the GLUT3 and GLUT4 transporters is stimulated by the presence of the growth factor insulin-like growth factor 1 (IGF-1) (Bryant *et al.,* 2002). The role of GLUT4 mediated glucose uptake in MEF cells in response to treatment with E0771-CM is further substantiated by our proteomics data as an increase in IGF-1 was observed in the conditioned media derived from glucose deprived E0771 cancer cells **(Figure 3.12)**. Collectively, our data suggest that in response to conditioned media derived from glucose deprived E0771 breast cancer cells, ROS-induced increased HIF-1α leads to an increase in IGF-1 mediated GLUT4 translocation, thus increasing glucose uptake in “activated” MEF cells.

Under normal cellular conditions the end product of glycolysis, pyruvate is converted to acetyl-CoA, by the enzyme pyruvate dehydrogenase (PDH). Acetyl-CoA then enters the tricarboxylic acid (TCA) cycle resulting in an increase in energy production via oxidative phosphorylation. However, HIF-1α stabilization during conditions of increased cellular stress leads to the inhibition of PDH with the accumulation of intracellular pyruvate. As the inhibition of PDH prevents the conversion of pyruvate to acetyl-CoA, it is converted to lactate, allowing for continuous flux through glycolysis (Kim *et al*., 2006, Papandreou *et al*., 2006). Based on the theory that the "reverse Warburg effect" is a prominent feature within the tumour microenvironment, HIF-1α mediated inhibition of PDH is recognized as being a central component of the "reverse Warburg effect". The increased glycolytic flux induced in CAFs, therefore leads to the enhanced production of metabolites such as lactate, which may be shunted to and utilized by oxygen and nutrient deprived epithelial cancer cells. Our aim was to determine whether HIF-1α activation results in the inhibition of PDH in MEF cells following treatment with E0771 conditioned media. Our results showed a significant increase in the amount of PDH in MEFs in response to treatment with glucose deprived E0771 conditioned media **(Figure 3.24)**. However, the assessment of PDH activity showed no significant differences following treatment with E0771 conditioned media **(Figure 3.25)**. This result was unexpected, however, the increase in the amount of PDH we observed in MEF cells following treatment with glucose deprived E0771 conditioned media could be as a result of a compensatory mechanism in an attempt to overcome an increase in glycolytic flux. The fact that we did not see an accompanying increase in PDH activity suggests that HIF-1α may indeed be influencing PDH activity, where the indirect inhibition of PDH by HIF-1α occurs via the direct induction of pyruvate dehydrogenase kinase (PDK). Therefore it is plausible that the induction of PDK by HIF-1α, may be time dependent

and as a result, a decrease in PDH activity would only be seen following longer treatment periods.

We also set out to determine whether the enhanced glucose uptake we observed in MEF cells treated with E0771 conditioned media increases glycolytic flux with subsequent lactate production in these cells. We observed a significant increase in L-lactate concentrations in MEFs cells following treatment with either untreated E0771 conditioned media or glucose deprived E0771 conditioned media. However, no significant differences in L-lactate concentrations were observed in MEF cells treated with glucose deprived E0771-CM in comparison to untreated E0771 conditioned media **(Figure 3.26)**. This might suggest that the ability of E0771 cancer cells to enhance L-lactate production occurs independently of glucose concentrations. Nutrient deprived / hypoxic cancer cells are assumed to enhance the “reverse Warburg effect” in CAFs in comparison to normoxic cancer cells which receive adequate nutrients. However, due to the metabolic plasticity of epithelial cancer cells, oxygenated cancer cells have equal propensity to undergo metabolic symbiosis in order to satisfy their bioenergetics demands (Kennedy *et al*., 2010).

The adaptability of cancer cell metabolism favours continuous tumour growth during periods of fluctuating glucose and oxygen tension within the changing tumour microenvironment. The monocarboxylate transporters (MCT) -1 and -4 are critical role players in the metabolic adaptability of cancer cells, which mediate the transport of several monocarboxylic acids, such as pyruvate and L-lactate across the plasma membrane (Pavlides *et al*., 2009). The existence of what has been termed the stromal-epithelial “lactate shuttle” within the tumour allows for the transfer of L-lactate, produced by stromal CAFs, to epithelial cancer cells; thus allowing for increased flux through oxidative phosphorylation in epithelial cancer cells (Whitaker-Menezes *et al*., 2011). An

increase in the expression of the monocarboxylate exporter MCT-4, could signify an increase in the export of L-lactate we observed in MEFs treated with E0771 conditioned media. We therefore, assessed MCT-1 and MCT-4 protein expression in MEFs following E0771 conditioned media treatment. We observed a significant decrease in the expression of MCT-1, responsible for lactate import **(Figure 3.27a)**. This result further supports the notion that E0771 conditioned media induces an increase in endogenous L-lactate production in MEFs. However, when MCT-4 protein expression was assessed we observed no significant changes across all treatment groups **(Figure 3.27b)**. This suggests that the increased L-lactate production in MEFs treated with E0771 conditioned media is not exported out of the cell. However, as MCT-1 and MCT-4 are not the only monocarboxylate transporters present in fibroblasts, it is conceivable that the enhanced L-lactate we observed could be exported out of MEFs via MCT-2. Furthermore, as MEFs were treated with E0771 conditioned media for 24 hours, this treatment time may have been sufficient to induce an increase in L-lactate production but not long enough to induce MCT-4 receptor expression.

4.5. The Effects of E0771 Conditioned Media on the Proteome Secreted from Mouse Embryonic Fibroblast Cells

As previously described, proteomic analysis of secreted proteins provides invaluable insight into the potential mechanisms underlying the cell-cell communications governing metabolic reprogramming within the tumour microenvironment. Therefore, in order to determine candidate proteins which could possibly be involved in promoting E0771 breast cancer cell survival and migration, we again aimed to utilize a bioinformatics approach to assess the protein composition of conditioned media generated from MEF cells previously treated with E0771 conditioned media. Broad assessment of protein elements which were differentially regulated between groups revealed a total of 7 protein elements exclusively present in conditioned media generated from MEF cells treated with E0771 untreated conditioned media (MEF_EUM) and a total of 23 protein elements exclusively to the conditioned media generated from MEF cells treated with glucose deprived E0771 conditioned media (MEF_ECM). Additionally a total of 32 elements were observed exclusively in control MEF conditioned media (MEF_C). Furthermore, we observed a total of 9 elements to be common to both MEF_C and MEF_ECM, 17 common elements to MEF_C and MEF_EUM, and a total of 24 protein elements were found to be present in all three conditions **(Figure 3.28)**.

Interestingly, when GO terms and protein lists for both MEF_UTCM and MEF_CM were submitted in REVIGO and DAVID and collapsed into biological processes, we noted that several biological processes were observed to be significantly downregulated in MEF_UTCM **(Figure 3.29)** but were upregulated in MEF_ECM **(Figure 3.36)**. Of these biological processes, Wnt signalling, protein polyubiquitination, glycolysis, gluconeogenesis and cell-cell adhesion were observed to be differentially regulated between MEF_UTCM and MEF_ECM. These results suggest that glucose deprived

E0771 breast cancer cells elicit differential metabolic reprogramming of MEF cells, resulting in the secretion of a pro-metastatic and glycolytic proteome, thereby highlighting the capacity of nutrient deprived breast cancer cells to reprogram the tumour microenvironment to suit their metabolic demands; thus promoting cancer cell survival and metastasis.

In addition to the scatterplots, REVIGO also allows for the visualization and assessment of interactive graphs, which provides further insight into the hierarchical interactions between biological processes. Of interest, we observed a highly significant interaction between the tumour necrosis factor-mediated and the positive regulation of canonical Wnt signalling pathways. Aberrant tumour necrosis factor α (TNFα) signalling has been shown to promote cell migration thereby enhancing the metastatic dissemination of cancer cells (Karin and Greten, 2005, Kitakata *et al*., 2002, Li *et al*., 2012). Additionally the production of TNFα by stromal cells contributes significantly to tumour progression and is associated with poor clinical outcomes (Balkwill, 2002). However, the mechanisms whereby TNFα exerts these pro-metastatic effects in the tumour microenvironment remains to be fully elucidated. One mechanism that has been described involves the activation of Akt by TNFα, leading to the stimulation of NF-κβ and the upregulation of Snail (Julien *et al*., 2007).

The zinc-finger protein Snail is a critical transcriptional repressor of E-cadherin, therefore the induction of Snail plays a fundamental role in epithelial-to-mesenchymal transition (EMT) and subsequent promotion of metastasis (Wu and Zhou, 2010). As such, TNFα is recognized as a being a profound role player in EMT-induced cancer cell migration and metastasis via the induction of NF-κβ/Snail signalling (Wu *et al*., 2009). TNFα has also been shown to induce Wnt/β-catenin signalling through the suppression of GSK-3β activity (Oguma *et al*., 2008). The activation of the Wnt signalling pathway in cancer further contributes to the induction of EMT through the upregulation of Snail (Yook *et al*.,

2006). Moreover, exosomes released from synovial fibroblasts have been shown to contain a membrane bound form of TNFα (Zhang *et al*., 2006). Based on the knowledge that both Wnt ligands and TNFα are secreted in exosomes, we therefore speculate that the upregulation of proteins involved in both Wnt and TNF-mediated signalling observed in MEF_ECM **(Figure 3.37)** serves as a potential signalling mechanism whereby CAFs can promote cancer metastasis.

In order to corroborate this, we analysed the functional annotation clustering (FAC) data obtained in DAVID for potential proteins associated with exosomes. Again, we observed a significant upregulation in the proteins annexins (A1 and A2), heat shock protein (HSP 90α), S100 calcium binding protein A11 (S100A11) and charged multivesicular body protein 4B (CHMP4B), all of which are known to be secreted in exosome-like vesicles or endosomes (Wang *et al*., 2012, Greening *et al*., 2016). The upregulation of these exosome associated proteins in MEF_ECM indicates that exosomes may indeed be critical mediators in cell-cell communications within the tumour microenvironment.

In addition to the hierarchical interactions observed between TNF and Wnt signalling, we also noted significant interactions between the MAPK cascade, proteolysis, glycolysis and protein polyubiquitination **(Figure 3.38)**. Abnormalities in the mitogen-activated protein kinase (MAPK) cascade play a critical role in cancer progression (Sui *et al*., 2014). Classically, the MAPK signalling pathway consists of the c-jun N-terminal kinase (JNK), the extracellular-signal-regulated kinase (ERK) and p38 MAPK (Hommes *et al*., 2003). Upon activation, the MAPK signalling pathway exerts several cellular responses ranging from proliferation to apoptotic cell death (Dhillion *et al*., 2007). Recently, it has been proposed that in response to genotoxic stress, p38 MAPK and JNK are critical role players in the crosstalk between apoptosis and autophagy (Sui *et al*., 2014). The molecular mechanisms underlying p38 MAPK induced autophagy remain to be fully elucidated, however, it is thought that the phosphorylation of glycogen synthase 3β

(GSK3β) by p38 MAPK signalling results in autophagy-mediated cell survival (Choi *et al*., 2012); whereas, JNK mediated autophagic induction occurs via the dissociation of Beclin-1 from Bcl-2/Bcl-xL (Zhou *et al*., 2011). Moreover, the activation of both PI3K/Akt/mTOR and Ras/MAPK signalling cascades are associated with more aggressive cancer phenotypes, and poor clinical outcomes (Calvisi *et al*., 2011). In recent years, the molecular mechanisms underlying the functional cross-talk between PI3K/Akt/mTOR and Ras/MAPK signalling in cancer has gained widespread interest as a potential therapeutic target. mTORC1 has been shown to play a critical role in PI3K/Akt/mTOR and Ras/MAPK crosstalk, as the inhibition of mTORC1 results in the activation of both MAPK signalling (Carracedo *et al*., 2008) and autophagy (Wong *et al*., 2015). Regardless of the molecular mechanisms underlying the interaction between MAPK signalling and autophagy, it is clear that the induction of these signalling pathways have wide spread consequences for the survival and progression of cancer.

In addition to the interaction between autophagy and MAPK signalling in the promotion of cancer cell survival, cellular homeostasis is maintained through the tight regulation of both autophagy and ubiquitin proteasome system (UPS) mediated protein degradation (Lilienbaum, 2013). The careful orchestration between these two cellular degradative pathways is mediated by the cytosolic adapter protein p62/SQSTM1 (p62) (Puissant *et al*., 2012). As previously described the interaction between LC3 II and p62 is critical for autophagic protein degradation (Pankiv *et al*., 2007), however, p62 also influences UPS-mediated protein degradation as the ubiquitin binding domain of p62 allows for the binding of ubiquitinated lysine residues, thus facilitating the delivery of ubiquitinated proteins to the proteasome system for degradation (Matsumoto *et al*., 2011).

These results might suggest that in the context of our study, treatment of MEF cells with conditioned media generated from glucose deprived E0771 breast cancer cells result in enhanced protein catabolism through the induction of the ubiquitin proteasome system

(UPS) and possibly MAPK mediated autophagy. Increased protein catabolism in MEF cells could lead to the production of glycolytic intermediates which may be utilized by E0771 breast cancer cells for survival. These results combined with the enhanced glucose uptake **(Figure 3.22)** and L-lactate production **(Figure 3.26)** we observed with the molecular analysis of MEF cells following treatment with glucose deprived E0771 conditioned media are suggestive of the induction of the “reverse Warburg effect”. However, further analysis on the role of the ubiquitin proteasome system and MAPK-mediated autophagy in the induction of the “reverse Warburg effect” still needs to be assessed.

4.6. Effects of MEF Conditioned Media on E0771 Breast Cancer Cell Metabolism and Migration

Signalling via the PI3K/Akt pathway in cancer contributes significantly to the promotion of cancer cell survival and tumour progression. The activation of the PI3K/Akt signalling pathway through both integrin and chemokine signalling has been well characterized (Datta *et al*., 1997). As cancer-associated fibroblasts are known to enhance tumour desmoplasia, the increased expression of integrins and chemokines during ECM remodelling leads to enhanced PI3K/Akt signalling (Lu and Kang, 2010). Our proteomics analyses of conditioned media obtained from MEF cells which had been treated with glucose deprived E0771-CM (MEF-CM) showed a significant increase in collagen type IV alpha 1 chain (COL4A1) **(Figure 3.41)**. COL4A1 is an essential mediator of focal adhesion signalling and results in the activation of PI3K by focal adhesion kinase (FAK) (Chen *et al.,* 1994). Furthermore, we also observed an increase in IGF-1 **(Figure 3.41)**, an additional activator of PI3K/Akt signalling in cancer. Enhanced PI3K/Akt signalling in cancer cells has a wide variety of effects, the most prominent, within the context of this study, being the sustained proliferative signalling of epithelial cancer cells (Stemke-Hale *et al*., 2008) and epithelial-to-mesenchymal induced cancer cell migration (Fu *et al*., 2015). Based on this, we assessed the cell viability of glucose deprived E0771 breast cancer cells following treatment with both treated and untreated MEF conditioned media. A significant increase in mitochondrial reductive capacity was seen following both MEF untreated conditioned media (MEF-UTCM) and MEF conditioned media (MEF-CM) when compared to control conditioned media (control-CM) **(Figure 3.43)**. This is suggestive of either increased cell proliferation or mitochondrial stress, leading to a respiratory burst. In the context of our study, enhanced cell proliferation is unlikely to be occurring as we have shown that 12 hours of glucose deprivation in E0771 murine breast cancer cells

leads to a switch in substrate utilization **(Figure 3.1)**, with an increase in mitochondrial oxidative stress **(Figure 3.6b)**. It is therefore, more likely that the increase in MTT reductive capacity we observed when glucose deprived E0771 cancer cells are treated with MEF conditioned media, is as a result of increased mitochondrial stress and not enhanced cell proliferation. Additionally, when cell death was assessed by means of flow cytometry, we observed no significant changes in either live cell or dead cell populations across all treatment groups **(Figure 3.44)**. This suggests that the activation of PI3K signalling within the context of this study is not involved in the induction of apoptotic cell death or cell proliferation but rather favours the survival of glucose deprived E0771 cancer cells.

As mentioned previously, MCT-1 is a critical role player in the metabolic adaptability of cancer cells, allowing for the import of L-lactate, produced by CAFs, into epithelial cancer cells (Whitaker-Menezes *et al*., 2011). As the increased expression of MCT-1 in epithelial cancer cells will allow for the enhanced uptake of L-lactate, we employed Western blot analysis to determine changes in the protein expression of both MCT-1 (L-lactate import) and MCT-4 (L-lactate export). A significant increase in protein expression of MCT-1 with a concomitant decrease in the expression of the exporter MCT-4 was observed in glucose deprived E0771 breast cancer cells that were subjected to MEF-CM treatment in comparison to control **(Figure 3.45b)**. Additionally, we observed a significant 2-fold increase in L-lactate concentrations in E0771 cells subjected to MEF-CM treatment in comparison to control **(Figure 3.46)**. Taken together, this data allows us to infer to a degree that L-lactate imported into E0771 cancer cells contributes to the increased L-lactate concentrations we observed.

The concept of metabolic symbiosis implies that enhanced L-lactate concentrations within the tumour microenvironment leads to the net flux of L-lactate into epithelial

cancer cells where the conversion of L-lactate to pyruvate leads to enhanced oxidative phosphorylation and energy production (Sotgia *et al*., 2012). As such, ATP production was assessed in E0771 breast cancer cells following MEF conditioned media treatment. We observed a significant increase in ATP concentrations in E0771 breast cancer cells following MEF-CM treatment alone in comparison to both the control and control-CM groups **(Figure 3.47)**, supporting the notion that metabolites derived from metabolically reprogrammed CAFs are utilized by epithelial cancer cells for energy production and subsequent enhanced cell survival. Based on this and the fact that cancer cells have the propensity to utilize oxidative phosphorylation as an additional energy source during periods of increased metabolic demand ("reverse Warburg effect") (Ward *et al*., 2012), the enhanced ATP concentrations we observed following MEF-CM treatment may be indicative of an increase in the flux of metabolites through oxidative phosphorylation.

Pyruvate dehydrogenase forms part of a multi-subunit complex, termed the pyruvate dehydrogenase complex (PDC), which catalyzes the irreversible rate-limiting decarboxylation of pyruvate to acetyl-CoA. The availability of pyruvate entering oxidative phosphorylation is therefore entirely dependent on the enzymatic activity of the PDC, and therefore represents a critical regulatory step in glucose metabolism (McFate *et al*., 2008). Therefore, for this study we carried out a pyruvate dehydrogenase (PDH) enzymatic activity assay in conjunction with a protein profile assay as a determinant of the oxidative phosphorylation capacity of E0771 breast cancer cells subjected to treatment with MEF conditioned media. Our results showed no significant differences in either the protein profile of PDH **(Figure 3.48)** or the enzymatic activity of PDH **(Figure 3.49)** in E0771 murine breast cancer cells across all treatment groups. Although we did not observe an increase in PDH activity in response to MEF-CM treatment, we cannot conclusively state that the overall flux of oxidative phosphorylation remains unchanged. Due to the complex nature of cancer cell metabolism coupled with the propensity of

cancer cells to switch substrate utilization due to metabolic plasticity; it is therefore plausible that increased oxidative phosphorylation could still take place in E0771 breast cancer cells following treatment with MEF-CM, where TCA intermediates are generated and shunted into oxidative phosphorylation bypassing PDH. For instance, it is known that enhanced reductive carboxylation of glutamine-derived acetyl-CoA often occurs in cancer cells with diminished mitochondrial activity (Wise *et al*., 2011, Metallo *et al*., 2012). Based on this, additional metabolic assessments on E0771 breast cancer cells treated with MEF conditioned media will need to be conducted in order to fully elucidate whether the ”reverse Warburg effect” is indeed playing a role in maintaining E0771 breast cancer cell survival.

Furthermore, increased expression of pyruvate dehydrogenase kinase -1 (PDK-1), a potent antagonizer of PDH, plays a critical role in mediating the metastatic potential (Du *et al*., 2015) and regulation of metabolic reprogramming (Battello *et al*., 2016) in breast cancer cells which preferentially disseminate to the liver. Dupuy and colleagues (2015) also demonstrated that PDK-1 is essential for the effective dissemination and formation of liver metastases, evident by a reduction in both metastatic lesion number and size in Balb/c mice receiving splenic injection of cells expressing PDK-1 targeted shRNA (shPDK1) in comparison to control shRNA (shLUC) expressing cells (Dupuy *et al*., 2015).

When this is considered, in conjunction with the increased clustering of proteins involved in cell migration and metastasis from our proteomic analysis of MEF_ECM **(Figure 3.36 and Figure 3.37)**, it becomes clearer and more likely that treatment of E0771 breast cancer cells with MEF_ECM is involved more prominently in enhancing the metastatic phenotype of these E0771 cells. As such, the next aim of this study was therefore to determine the effects of MEF conditioned media in mediating E0771 cell migration and progression to a metastatic phenotype. We therefore made use of a migration (scratch)

assay to monitor and assess the capacity and rate of E0771 cancer cell migration in response to treatment with MEF conditioned media.

An interesting observation noted for both the untreated MEF conditioned media (MEF-UTCM) and MEF-CM treated groups was a steep increase in the slopes of the generated curves between 12 and 18 hours of conditioned media treatment, signifying an increase in the migratory speed (rate of change) of E0771 breast cancer cells in response to treatment with MEF conditioned media. Therefore, in order to determine if the speed at which E0771 cells treated with MEF conditioned media migrate is significant when compared to control, separate linear regression lines were generated between each time point. Between 12 - 18 hour treatment points a significant increase in in the slope of the linear regression line (migratory speed) was observed in MEF-UTCM and MEF-CM treated E0771 cancer cells **(Table 3.1)**. Collectively, these results are in accordance with those obtained by Hu and colleagues (2013) where an increase in the transverse migratory capacity of SGC-7901 gastric cancer cells was observed following 24 hours of exposure to CAF conditioned media (Hu *et al*., 2013).

During the process of metastatic dissemination, epithelial cancer cells are obligated to acquire the ability to invade through the basement membrane, disseminate through the circulatory system and then proliferate at distant metastatic sites (Egeblad *et al*., 2008, Fein and Egeblad, 2013). The ability of cancer cells to invade is dependent on their acquisition of a more migratory phenotype, characterized by an increase in mesenchymal cell markers, such as vimentin, α-SMA and PDGFRα and others (Wei *et al*., 2008, Lee *et al*., 2013, MacDonald *et al*., 2001). Therefore, in order to determine whether the enhanced speed of migration observed in E0771 breast cancer cells following treatment with MEF conditioned media, we employed Western blotting analyses for four key markers of epithelial-to-mesenchymal transition (EMT). Our results showed a significant increase in the mesenchymal markers α-SMA **(Figure 3.54a)** and

vimentin **(Figure 3.55a)** in E0771 breast cancer cells in response to MEF-CM treatment alone. In order to more accurately determine whether E0771 cancer cells have acquired a more migratory capacity, an increase in mesenchymal markers needs to be accompanied by a loss or decrease in epithelial cell markers. As E-cadherin constitutes the prominent cell-adhesion molecule responsible for maintaining tight epithelial cell-cell adhesion, the downregulation of E-cadherin in cancer is associated with EMT induction and enhanced tumour invasion (Von Burstin *et al*., 2009). Therefore, E-cadherin is often utilized as an essential marker of EMT in cancer cells. Our results showed a significant reduction in E-cadherin protein expression in E0771 breast cancer cells following treatment with MEF-UTCM as well as with MEF-CM in comparison to control **(Figure 3.55b)**. Collectively, this data suggests that treatment of E0771 breast cancer cells with MEF conditioned media does indeed result in the acquisition of a more mesenchymal phenotype. This is consistent with several studies where CAF-mediated EMT induction in PC3 cells results in the enhanced motility and the acquisition of a stem-like behaviour (Giannoni *et al*., 2011, Xiao *et al*., 2014, Guan *et al*., 2014, Lau *et al*., 2016).

4.7. Effects of MEF Conditioned Media on Doxorubicin resistance in E0771 Breast Cancer Cells

Anthracyclines, such as doxorubicin, are considered as some of the most effective chemotherapeutic agents for the treatment of breast cancer (Barrett-Lee *et al*., 2009). Unfortunately, anthracyclines are also cytotoxic and affect a wide variety of physiological systems. Aside from the severe cumulative dose-dependent side effects, resistance of cancer cells to chemotherapeutic strategies (chemo-resistance) has become an ongoing complex issue faced by many cancer patients. Tumours may become resistant to a wide range of chemotherapies, during the process of acquiring resistance, this ultimately leads to an approximate 90% failure rate seen with the treatment of metastatic breast cancer (MBC) (Coley *et al*., 2008). Furthermore, the majority of patients diagnosed with breast cancer will at some point have a recurrence of the disease, resulting in a poorer clinical outcome. It is widely accepted that cancer cell response to chemotherapeutic agents, including doxorubicin, is strongly influenced by signals derived from stromal cells present within the tumour microenvironment (Velaei *et al*., 2016).

In the past, the tumour microenvironment and the influence of stromal cells in advancing tumour progression and metastasis has been largely underestimated, as such research into understanding the influence of the tumour microenvironment in conferring chemotherapeutic resistance to epithelial cancer cells has gained increasing attention. The next part of this study, was therefore established in order to elucidate the effects that MEF-CM in combination with doxorubicin has on E0771 breast cancer cell metabolism and migration. We first set out to determine a lower, clinically relevant dose of doxorubicin which leads to significant cell death in the chemotherapy resistant E0771 murine breast cancer cells **(Figure 3.56)**. Our results demonstrate that 2.5 µM doxorubicin lead to a significant reduction in MTT reductive capacity of E0771 cancer cells. The combination of MEF-CM with doxorubicin treatment resulted in a significant

increase in the mitochondrial reductive capacity of E0771 breast cancer cells **(Figure 3.57)**. This result is similar to those obtained in the previous section where MEF-CM alone resulted in a significant increase in MTT reductive capacity of E0771 cells. As described previously, this increase in mitochondrial reductive capacity likely demonstrates a mitochondrial respiratory burst (van de Loosdrecht *et al*., 1994, Stephanenko and Dmitrenko, 2015) and not increased cell proliferation. Assessment of cell death by means of flow cytometry showed a significant increase in the dead cell population with a concomitant decrease in the live cell population of E0771 cells treated with MEF-CM and doxorubicin **(Figure 3.58)**, suggesting that MEF-CM was able to overcome doxorubicin resistance in E0771 breast cancer cells. However, in order to accurately determine the mode of cell death that occurs in E0771 breast cancer cells in response to MEF-CM in addition to doxorubicin treatment, additional assays to assess autophagy, apoptosis and necrosis would need to be performed.

In order to determine the role that doxorubicin plays in the induction of the "reverse Warburg effect" in E0771 cancer cells treated with MEF conditioned media, we again assessed the protein expression of the L-lactate transporters, MCT-1 and MCT-4. We observed a significant increase in the expression of the exporter MCT-4 following MEF-CM treatment in combination with doxorubicin treatment when compared to the doxorubicin control group **(Figure 3.59b)**. A significant increase in the concentration of L-lactate was observed in E0771 cancer cells treated with the combination of doxorubicin and MEF-CM **(Figure 3.60)**, indicating that this L-lactate can be shunted into oxidative phosphorylation and utilized by E0771 breast cancer cells, contributing to the enhanced ATP production we observed **(Figure 3.61)**.

Doxorubicin is a weak basic chemotherapeutic agent which has an acid dissociation constant of 7.5 - 9.5, as such the cellular uptake of doxorubicin is significantly reduced in tumours where increased interstitial lactate results in a lowered pH (Gerweck *et al*.,

2006, Mellor *et al*., 2011). Therefore, a further explanation for the increased expression of MCT-4 and significant increases in L-lactate we observed in E0771 breast cancer cells treated with MEF-CM in combination with doxorubicin, might be that the enhanced export of L-lactate out of E0771 cancer cells results in an increased acidification of the surrounding cellular environment, in an attempt to significantly reduce doxorubicin uptake.

As described previously, PDH catalyzes the conversion of pyruvate to acetyl-CoA thereby governing the metabolic transition of glycolysis to oxidative phosphorylation (Golias *et al*., 2016). Our results showed a significant increase in the protein profile of PDH in E0771 cancer cells treated with MEF-CM in combination with doxorubicin in comparison to all other treatment groups **(Figure 3.62)**, this result was promising with regards to the induction of the "reverse Warburg effect", however, when we assessed PDH enzymatic activity in these cells, no significant differences were observed across all treatment groups in comparison to control **(Figure 3.63)**. This suggests that although overall PDH protein expression is upregulated following 24 hours of MEF-CM plus doxorubicin treatment, the activation of PDH remains the same and therefore the enzymatic conversion rate of pyruvate to acetyl-CoA remains constant. When the non-significant increase in L-lactate levels we observed is taken into account with an enhanced PDH expression, it becomes plausible that the induction of the "reverse Warburg effect" could be occurring in E0771 cancer cells treated with MEF-CM in conjunction with doxorubicin. However, additional metabolic assessment using isotopically labelled metabolic substrates (such as ^{13}C-glucose) need to be performed in order to fully elucidate the contribution of the "reverse Warburg effect" to E0771 breast cancer metabolism, within the context of this study.

The systemic use of chemotherapeutic agents for the treatment of cancer has been shown to effectively eradicate cancer cells, however, more and more commonly

increased resistance to chemotherapeutic agents and enhanced metastases has been reported (Li *et* al., 2015, Daenen *et al*., 2011). Based on this we set out to determine the combined effects of doxorubicin and MEF-CM treatment on E0771 breast cancer cell migration and the induction of EMT. Our results showed a significant reduction in the migratory capacity of E0771 breast cancer cells in response to the combined treatments of doxorubicin with MEF-UTCM across all time points **(Figure 3.64)**, suggesting that fibroblasts that have not been activated to a CAF phenotype lead to a reduction in the metastatic capacity of epithelial breast cancer cells. Similar to the results obtained for the treatment of E0771 cells with MEF-CM alone **(Figure 3.52)**, we noted a significant increase in the slopes of the generated curves between 12 and 18 hours of the combined treatment using MEF-CM and doxorubicin, again signifying an increase in the migratory speed (rate of change) of E0771 breast cancer cells. Similarly, separate linear regression lines were generated between each time point in order to determine if the speed at which E0771 cells migrate was significant when compared to doxorubicin alone **(Table 3.3)**. Between 12 - 18 hour treatment points, a significant increase in in the slope of the linear regression line (migratory speed) was observed in Doxorubicin and MEF-CM combination treated E0771 group.

The induction of epithelial-to-mesenchymal (EMT) has been suggested to confer both chemoresistance and metastatic properties in breast cancer cells (Kurrey *et al*., 2009, Hollier *et al*., 2009). Furthermore, in addition to its' therapeutic effects, doxorubicin has also been implicated in enhanced malignancy through the induction of EMT. Both β-catenin and TGFβ-signalling are critical for the process of doxorubicin-induced EMT in a variety of human cancer types, including gastric and breast cancer (Han *et al*., 2013). Therefore, we assessed the protein expression levels of several key markers of EMT to determine the effects of doxorubicin in combination with MEF conditioned media on EMT induction. Our results showed a significant reduction in α-SMA and PDGFRα protein

expression **(Figure 3.67)** following doxorubicin treatment in combination with both MEF-UTCM and MEF-CM in E0771 breast cancer cells. Additionally, we noted a significant increase in both vimentin and E-cadherin protein expression **(Figure 3.68)** following the combined treatments of doxorubicin with MEF-UTCM or MEF-CM. The significant reduction in PDGFRα expression we observed suggests an overall decrease in EMT in E0771 breast cancer cells, despite the increase in vimentin expression we observed. However, in doxorubicin resistance breast cancer cells, vimentin expression serves as a critical marker of metastatic capacity (Pan *et al*., 2012, Tezcan and Gündüz, 2014), evident by the fact that silencing of vimentin is associated with a drastic reduction in both metastasis and invasiveness (McInroy and Määttä, 2007). Based on this evidence, the increase in vimentin expression we observed, suggests that an increase in the metastatic ability of E0771 breast cancer cells occurs as a result of doxorubicin treatment alone and more so when combined with MEF conditioned media. Our results are consistent with several other studies which have demonstrated a significant increase in vimentin expression following long term doxorubicin treatment (Li *et al*., 2015).

EMT is a dynamic and relatively fluid process, wherein the conversion of epithelial cells into a mesenchymal state is not necessarily an irreversible commitment (Zheng *et al*., 2015). In tumours, the presence of cells which have converted fully to a mesenchymal state is rare, and most commonly quasi-mesenchymal phenotypes are observed, wherein partial EMT has occurred. Furthermore, recent evidence suggests that the equal co-expression of both epithelial (E) and mesenchymal (M) signatures, defined as an E/M state, is associated with increased plasticity, self-renewal and stemness (Grosse-Wilde *et al*., 2015) which indicates a more metastatic phenotype. As such it is conceivable that with the combination of doxorubicin and MEF-CM treatment, E0771 breast cancer cells undergo partial EMT, and therefore the increased co-expression of vimentin and E-cadherin represents a quasi-mesenchymal state.

4.8. The Effects of Autophagic Manipulation in CAFs on the Migration Capacity of E0771 Breast Cancer Cells

The autophagic process plays a critical role in maintaining cellular homeostasis and biogenesis during periods of nutrient deprivation / hypoxia (Pavlides *et al*., 2012). During tumourigenesis, autophagy provides a pro-survival advantage to cancer cells (Tóth *et al*., 2002). In the context of the tumour microenvironment, the induction of stromal autophagy in addition to enhanced nutrient import by cancer cells allows for the recycling of nutrients, thus supporting tumour growth and proliferation (Katheder *et al*., 2017)

Based on this knowledge, we used Atg5 as a molecular target to assess the role of autophagy in CAFs on the migratory capacity of E0771 breast cancer cells. Therefore, we made use of an endoribonuclease-prepared siRNA (esiRNA) against the murine Atg5 gene to effectively silence Atg5 protein expression in MEFs. Prior to assessing the effects of conditioned media generated from Atg5 knockdown MEFs, we verified the silencing of Atg5 in MEF cells using Western blot analysis. Our results, show that we were able to achieve a silencing efficiency of 94% using 500 ng of Atg5 esiRNA for a period of 96 hours **(Figure 3.69)**, we therefore made use of this concentration and time point for all subsequent transfections done to generate Atg5 knockdown MEF conditioned media (Atg5 MEF-CM).

In order to determine whether autophagic manipulation in CAFs can counteract the survival effects we observed in E0771 breast cancer cells following treatment with MEF conditioned media **(Figure 3.43 and Figure 3.44)**, we carried out MTT viability assays on E0771 cancer cells following treatment with Atg5 knockdown conditioned media (Atg5 MEF-CM). Our results show that Atg5 MEF-CM effectively reduces the MTT

reductive capacity of E0771 breast cancer cells when compared to untreated E0771 cells (control) as well those that had been treated with mock-CM (no esiRNA). This suggests that the decrease in MTT reductive capacity, and therefore a decrease in cell viability, is as a direct result of Atg5 silencing in MEFs and not due to the transfection procedure itself. This result is a promising indication that the inhibition of autophagy in stromal CAFs could serves as a potential therapeutic target for the treatment of breast cancer. However, this avenue would need more extensive research, in order to elucidate whether the targeting of CAF autophagy could potentially sensitize epithelial breast cancer cells to the cytotoxic effects of chemotherapeutic drugs, like doxorubicin.

The role of autophagy in cancer metastasis is another “double-edged sword” as during the initial stages of metastatic dissemination, autophagy inhibits invasion of cancer cells by restricting necrosis-induced inflammation and inducing cell death (DeNardo *et al*., 2009, Mukhopadhyay *et al*., 2014). However, during advanced stages of metastasis, enhanced survival of ECM-detached cancer cells, autophagy serves as a pro-metastatic process protecting cancer cells from cellular stressors encountered at distant metastatic tumour sites (Han *et al*., 2008, Herrero-Martín *et al*., 2009). Furthermore, the production of pro-migratory and invasive factors through autophagy has been shown to promote Ras-driven invasion and migration of cancer cells (Lock *et al*., 2014).

In addition to the pro-survival role that autophagy in CAFs has been proposed to play in cancer cell survival (Wang *et al*., 2017b), enhanced autophagy in surrounding stromal CAFs is thought to also promote metastatic dissemination of epithelial cancer cells. This is thought to occur as a result of the secretion of circulating chemokines and pro-metastatic factors, including matrix metalloprotease-9 (MMP-9) and lysyl oxidase (LOX) (Erler *et al*., 2009). Additionally, Wang and colleagues recently demonstrated that conditioned media derived from isolated CAFs with enhanced autophagy not only enhanced survival, but also resulted in the promotion of EMT in triple negative breast

cancer cells when compared to conditioned media derived from normal fibroblasts (Wang *et al*., 2017a). However, it is currently not clear whether the processes of autophagy and EMT act in concert with each other to promote cancer cell invasion and metastasis or if EMT is independent of autophagy. Furthermore, the extent on which cancer cells rely on enhanced autophagy in stromal cells has yet to be fully elucidated. Therefore, in this section of the study, as proof of concept we set out to determine whether the manipulation of autophagy in MEFs could lead to altered EMT and migratory capacity of E0771 breast cancer cells.

We observed a significant reduction in the migratory capacity of E0771 breast cancer cells following treatment with Atg5 MEF-CM **(Figure 3.72)**, however, we also observed a similar reduction in E0771 migration with the treatment with both the mock-CM and eGFP-CM. Therefore, the results we observed are as a direct result of the electroporation and not an effect of Atg5 silencing in MEFs. The effects of electroporation on cell migration were made more evident when EMT was assessed by means of Western blotting, where a significant reduction in α-SMA, PDGFRα **(Figure 3.74)** and vimentin **(Figure 3.75a)** protein expression was observed in E0771 cells that treated with conditioned media derived from MEF cells which had been electroporated without any esiRNA (mock-CM). These results may be explained by the fact that electroporation involves the permeabilization of the plasma membrane with the use of a high energy electrical current in order to allow the entry of siRNA into the cell. While this had no effect on the viability it may have resulted in potent effects on cell-cell adhesion and cytoskeletal structure of MEF cells. Based on the significant clustering of proteins involved in cell-cell adhesion and migration we observed with the proteomics analysis of MEF conditioned media (see section 3.4) it is conceivable that electroporation of MEF cells could lead to significant alterations in the proteome of MEF conditioned media and thus could account for the significant loss in expression of the mesenchymal protein

markers, α-SMA, PDGFRα and vimentin that we observed in E0771 breast cancer cells following treatment with mock-CM. This is further corroborated by the fact that electroporation with voltages of 200 – 1000 V has previously been shown to result in a disruption of the actin cytoskeleton in 3T3 fibroblasts and also lead to alterations in cell adhesiveness of MDA-MB-231 breast cancer cells (Pehlivanova *et al*., 2012). Our transfection protocol made use of a single 1350 V pulse, as this falls past the extreme end of that used by Pehlivanova and colleagues, our results suggests that this could indeed have resulted in actin cytoskeleton reorganization in MEFs thereby affecting EMT in the E0771 breast cancer cells.

Although we observed a significant reduction in α-SMA, PDGFRα and vimentin protein expression as a result of the electroporation process, we also noted that E0771 breast cancer cells that were treated with the Atg5 knockdown MEF conditioned media (MEF-CM) showed a significant increase in all three mesenchymal markers, α-SMA, PDGFRα and vimentin **(Figure 3.74 and Figure 3.75)**, when compared to the mock-CM treated control group. This suggests that the knockdown of Atg5 in MEFs rescues the loss of mesenchymal markers due to the electroporation process we observed in E0771 breast cancer cells. Although these results are suggestive of a mild recovery of a mesenchymal phenotype in E0771 breast cancer cells, we are unable to effectively conclude what the role of autophagic manipulation in CAFs has on the migratory capacity of E0771 breast cancer cells. In order to effectively determine this, these experiments would need to be repeated using a different transfection protocol which does not result in drastic alterations in cell-cell adhesion and migration processes of MEFs. Additionally, it would be of great interest to assess the proteome of conditioned media generated from electroporated MEFs in order to determine the specific alterations that occur in response to the electroporation procedure.

4.9. In vivo Tumour-Bearing C57BL/6 Mouse Model

In vitro cancer models are extensively used to study the molecular mechanisms underlying cancer progression, chemoresistance and metastasis (Katt *et al*., 2016), and while these models provide invaluable insight for the development of novel chemotherapeutic strategies, they often fail to effectively represent the complexity of the 3D tumour microenvironment. Furthermore, the influences of the stromal compartment of tumours have been largely underestimated and as such many pre-clinical models have resulted in the clinical failure of chemotherapeutic strategies (Singh *et al*., 2010). Therefore, in order to gain a better understanding into the systemic influences exerted on epithelial cancer cells and the effects that this has on tumour growth, chemoresistance and metastatic capacity, we employed a physiologically relevant *in vivo* tumour-bearing mouse model.

Briefly, 40 eight week old female C57BL/6 mice were utilized for this section of the study. Mice were inoculated with syngeneic E0771 breast cancer cells into the right fourth mammary fat pad, and following the appearance of palpable tumours, mice received a cumulative dose of 12 mg/kg doxorubicin. We observed no significant differences in the body weights of mice across all treatment groups when compared to controls **(Figure 3.76)**. Additionally, doxorubicin administration had no effect on tumour growth over the course of the study **(Figure 3.77).** Our *in* vitro results indicate that the E0771 breast cancer cells are resistant to the cytotoxic effects of doxorubicin, as the viability of E0771 cells is maintained (at approximately 80%) following concentrations which exceed clinically relevant concentrations (10.0 µM) of doxorubicin **(Figure 3.56)**. Clinically the administration of doxorubicin involves doses which range between 15 and 90 mg/m^2, which results in plasma concentrations ranging from 0.3 – 5 µM (Gewirtz, 1999). Therefore, as the dosage of doxorubicin we chose for the *in vivo* tumour-bearing mouse model was calculated to fall within the clinically relevant dosages of doxorubicin

administration (12 mg/kg is equivalent to 36 mg/m^2 in mice) (Reagan-Shaw *et al*., 2007), the fact that we did not see any differences in the tumour volumes of mice treated with doxorubicin confirm the resistant nature of these cells. These results were further supported when Kaplan-Meier survival analyses were performed, as no statistically significant differences were observed in the time taken to reach the desired tumour volume **(Figure 3.78)**.

Once tumours reached a desired volume of 400 mm^3, mice were sacrificed and tumours as well as mammary fat pads were harvested and processed for further analysis. Histological assessment of mammary fat pads qualitatively showed no major ultrastructural changes between the groups **(Figure 3.79 and Figure 3.80)**. Additionally, significant collagen deposition was observed surrounding blood vessel and between lobules in all groups **(Figure 3.83 and Figure 3.84)**. However, a significant decrease in the intensity of collagen staining was observed in the mammary fat pads of tumour-bearing mice that were treated with doxorubicin. This may have resulted from a slight difference in staining times between samples; however, the effects of doxorubicin on normal mammary tissue cannot be excluded, as it is widely accepted that doxorubicin has profound cytotoxic effects on normal tissue.

Histologically, we observed three distinct regions of nuclear staining within tumour sections from tumour control and tumour + doxorubicin animals **(Figure 3.81 and Figure 3.82)**. In order to determine whether these regions can be associated with hypoxia / nutrient deprivation, immunofluorescent staining for the proliferation marker Ki67 was performed on tumour sections **(Figure 3.87)**. Again in tumour sections from animals that had been treated with doxorubicin we observed distinctive regions of cell proliferation, where the outer region of tumour sections stained more intensely (indicated by an increase in the mean fluorescent intensity) than the inner region. Based on these results, we were able to conclude that the inner regions observed in our H&E stains occur as a

result of decreased cell proliferation, which is most likely associated with an oxygen / nutrient gradient that is established as tumour volume increases.

Interestingly, we also observed significant fat cell infiltration in addition to the formation of new blood vessels (neo-angiogenesis) within tumour sites in both tumour control and tumour + doxorubicin animals **(Figure 3.82)**. The infiltration of non-tumourigenic cells into the tumour site, highlight the importance of stromal cells within the tumour microenvironment. Additionally, when compared to the highly organized and well defined blood vessels seen in the mammary fat pads, we noted that newly formed blood vessels within the tumour are significantly larger and more chaotic, these results are not surprising as it is well-known that new vasculature within tumours are structurally and functionally abnormal in comparison to those observed in normal tissue (Nagy *et al*., 2009). Furthermore, unlike that seen in normal tissue, tumour blood vessels have detached or absent pericytes (Inai *et al*., 2004) in some cases the diameter of the blood vessel is smaller and they exhibit increased permeability to large molecules (Izumi *et al*., 2002, Winkler *et al*., 2004, Tong *et al*., 2004).

Picosirius Red staining for fibrosis in tumours, similarly showed an increase in collagen deposition around newly formed blood vessels within tumours **(Figure 3.85)** as seen in mammary fat pads. However, we also noted an increase in collagen deposition within the tumour mass itself which was not surrounding any visible blood vessels **(Figure 3.86)**. In order to determine whether the increased fibrosis observed within the tumour mass occurred as a result of increased fibroblast infiltration, and subsequent CAF “activation”, into the tumour mass we performed immunofluorescent staining against both α-SMA and vimentin. While both tumour control and tumour + doxorubicin sections stained heavily for both α-SMA and vimentin **(Figure 3.88)**, we noted several regions of increased co-localization in the tumour + doxorubicin group. These regions are suggestive of the presence of CAFs within the tumour mass. However, in order to

definitively state that these are CAF specific regions, additional imaging would need to be performed, wherein additional markers of CAFs are utilized. For instance, it would be of great benefit to perform a four colour stain where samples are stained for additional CAF markers namely; E-cadherin and PDGFRα, in addition to α-SMA and vimentin.

As mentioned previously, tumours are recognized as being highly complex organs, and this highly structured environment plays a critical role in the survival and progression of cancerous epithelial cells within the tumour (Tanner and Gottesman, 2015). In recent years, research into the influence of the tumour microenvironment on epithelial cancer cells has become critical, as it has become increasingly evident that the interactions between stromal and epithelial cancer cells plays a role in tumour progression and metastasis. Additionally, the three dimensional (3D) nature of tumours results in differential effects on epithelial cancer cells that cannot be recapitulated using traditional two dimensional (2D) *in vitro* cell culture models (Yoshii *et al*., 2015). Therefore, in order to gain a better understanding of the influence of CAFs on epithelial cell invasion and thus their metastatic capacity, we employed the 3D branching morphogenesis assay using epithelial organoids isolated from both the mammary fat pads and tumours of C57BL/6 mice, and subjected isolated organoids to treatment with MEF conditioned media.

Interestingly, we observed that the treatment of epithelial organoids isolated from control **(Figure 3.89)** and tumour-control **(Figure 3.91)** animals with MEF conditioned media, showed no significant differences in the degree of invasion of epithelial cells into Matrigel® compared to control media treated organoids. However, organoids that were isolated from animals which received the *in vivo* administration of doxorubicin, showed enhanced invasion and migratory capacity when subjected to MEF conditioned media treatment. This was observed in organoids isolated from both doxorubicin control **(Figure 3.90)** and tumour + doxorubicin **(Figure 3.92)** animals, suggesting that

doxorubicin results in the enhanced invasive capacity of primary mammary epithelial organoids regardless of whether these were isolated from normal tissue or from tumours. Additionally, we also noted that when tumour + doxorubicin isolated organoids were treated with MEF conditioned media, epithelial cells migrate quickly out of the central organoid “mass”, and detach from their leader edge **(Figure 3.92)**. This result suggests that tumour epithelial organoids acquire an enhanced metastatic capacity when exposed to both doxorubicin and MEF-CM.

In recent years, it has become increasingly evident that the *in* vivo administration of doxorubicin induces pro-metastatic changes within the microenvironment of primary breast tumours (Karagiannis *et al*., 2017). This has been attributed to what has been termed, the tumour microenvironment of metastasis (TMEM) which consists of the direct contact of an epithelial cancer cell with both an endothelial cell and a macrophage (Rohan *et al*., 2014). The interaction of these cells within the tumour microenvironment has been associated with enhanced metastasis in human breast cancers (Robinson *et al*., 2009), and chemotherapeutic agents, including doxorubicin, elicits TMEM-mediated pro-metastatic changes within the breast tumour microenvironment. Moreover, the clustering of pro-migratory proteins we observed with the proteomic analysis of MEF conditioned media, could further explain the enhanced migratory capacity of epithelial organoids we observed. We therefore propose that CAFs elicit pro-metastatic changes in the tumour microenvironment of mammary tumours though the secretion of pro-migratory factors which result in similar effects to those mediated by TMEM.

We further, set out to determine whether epithelial-to-mesenchymal transition (EMT) in tumours affects their metastatic capacity. Therefore, Western blot analysis of whole tumours and mammary fat pads was employed to assess the relative protein expression levels of α-SMA, PDGFRα, vimentin and E-cadherin. In tumours a significant reduction in the protein expression levels of both PDGFRα **(Figure 3.94b)** and vimentin **(Figure**

3.96a) was observed in tumour + doxorubicin mice. Additionally, this was associated with a significant increase in E-cadherin expression **(Figure 3.96b)**. Collectively, these results suggest that in mammary tumours, doxorubicin results in decreased EMT, which would often be associated with decreased metastatic capacity of tumour cells. Despite this, the results we obtained for the 3D branching morphogenesis assay suggest an increase in epithelial cell migration. Conventionally, invasion and metastasis can be defined as the migration of single cells, groups of cells or as elongated strands of connected cancer cells (Leighton *et al*., 1960). With the dissemination of collective strands of epithelial cells, cell-cell adhesions remain intact (Friedl *et al*., 2012), and therefore would not be associated with the loss of E-cadherin, or the subsequent induction of EMT. Based on this, we speculate that the enhanced migratory capacity we observed in epithelial organoids isolated from tumour-bearing mice treated with doxorubicin occurs as a result of collective cell migration that is not associated with the induction of EMT. However, as the Western blot analysis was performed on tumour samples that were not subjected to MEF conditioned media treatment, we cannot rule out the induction of EMT in epithelial organoids as this may have occurred as a result of pro-migratory factors present in MEF conditioned media. Moreover, as whole tumours were utilized for Western blot analysis, the EMT results we obtained are representative of the tumour microenvironment as a whole; therefore it is possible that we may have observed an increase in EMT using Western blot analysis on isolated epithelial cells in addition to the whole tumour samples.

Finally, to assess the effects of doxorubicin on the migratory capacity of non-tumourigenic mammary tissue, we assessed markers of EMT using Western blot analysis. A significant decrease in the protein expression levels of α-SMA **(Figure 3.93a)** in the mammary fat pads harvested from tumour-bearing mice treated with doxorubicin when compared to both control and tumour control mice were observed. Additionally,

when compared to tumour control mice, only a significant reduction in both PDGFRα **(Figure 3.93b)** protein expression was observed in the mammary fat pads of tumour + doxorubicin mice. A significant increase in vimentin protein expression was seen in the mammary fat pads of tumour control mice when compared to control (no tumours) **(Figure 3.95a)**, however, this decreased significantly with doxorubicin administration in tumour-bearing mice. Similarly, E-cadherin protein expression was significantly increased in tumour control animals when compared to control **(Figure 3.95b)**, however, no significant difference was observed in the tumour + doxorubicin treated group when compared to both control and tumour control groups. Collectively, this data suggests that an increase in E/M phenotype is seen in the mammary fat pads of tumour control mice. However, treatment with doxorubicin causes this phenotype to return to that of control animals. Mammary tissue is comprised predominantly of adipocytes supported by connective tissue interspersed with stromal, endothelial cell and macrophages (Kim *et al*., 2013). As adipose tissue constitutes the most abundant stromal compartment of mammary tissue, the close proximity of primary breast tumours to adipocytes suggests that adipose tissue contributes significantly to the development and progression of breast cancer (Dumitrescu and Cotarla, 2005). The presence of mesenchymal stem cells (MSC) within the tumour microenvironment, derived either from bone marrow or from the breast tissue itself, have been described for their ability to promote tumour growth, angiogenesis and metastasis (Walter *et al*., 2009, Muehlberg *et al*., 2009, Pinilla *et al*., 2009). In fact, the recruitment of MSCs into the tumour microenvironment and their subsequent differentiation has been shown to give rise to CAFs (Zhao *et al*., 2010). Therefore, our results **(Figure 3.93 and Figure 3.95)** could likely reflect the propensity of normal mammary tissue to generate mesenchymal stem-like cells, which may disseminate to the tumour site and support tumour growth and metastasis. Additionally, doxorubicin treatment could reverse the E/M phenotype seen in tumour-bearing mice.

Chapter 5: Final Conclusions

The highly complex nature of the tumour microenvironment combined with the influences that surrounding stromal cells have on cancerous epithelial cells contribute significantly to tumour growth and progression. Although extensive progress over the last decade has been made in an attempt to elucidate the role of the tumour microenvironment in tumour progression, the molecular mechanisms underlying this interaction as well as the involvement of CAFs in epithelial cancer cell migration and metastasis remain largely underestimated. Therefore, in order to gain a better understanding of the stromal-epithelial interactions within the tumour microenvironment we employed a well-defined *in vitro* model as well as a physiologically relevant *in vivo* tumour-bearing mouse model of breast cancer. We also utilized a bioinformatics approach in order to assess the secreted proteome from both epithelial cancer cells and “activated” fibroblasts to determine the molecular mechanisms underlying the contribution of each cell type to the metabolic reprogramming of the tumour microenvironment.

We observed several differences in the ability of glucose deprived E0771 breast cancer cells to metabolically reprogram MEF cells, most notably differential effects in the secreted proteome of MEF cells was observed following treatment with glucose deprived E0771 conditioned media in comparison to control E0771 conditioned media. This likely reflects the propensity of epithelial cancer cells to selectively reprogram stromal cell metabolism depending on their bioenergetic demands, and thus highlights the plasticity of epithelial cancer cells and their ability to extensively manipulate the surrounding microenvironment for survival and subsequently their metastatic dissemination.

This study provides convincing evidence which illustrates the important role that the induced metabolic reprogramming of stromal fibroblasts has on the survival of nutrient deprived breast cancer cells. Additionally, we show that nutrient deprivation of E0771

cancer cells results in the secretion of a differential proteome from MEF cells, resulting in enhanced proteolysis and glucose metabolism, and thereby increasing the production of metabolites, such as L-lactate, which can be utilized by nutrient deprived E0771 breast cancer cells for ATP production and cell survival. Furthermore, we also provide evidence that “activated” CAFs confer pro-metastatic abilities to E0771 breast cancer cells, via the induction of epithelial-to-mesenchymal transition (EMT) and induce an increased rate of migration. The results obtained from the tumour-bearing mouse model reflect the enhanced metastatic capacity conferred to by MEF conditioned media. It also highlighted the synergistic effects that pro-migratory factors secreted by “activated” CAFs and doxorubicin elicit on the enhanced migration and invasiveness of isolated primary epithelial organoids. Most importantly, as the majority of patients with metastatic breast cancer relapse and ultimately develop tumours which have become more resistant to chemotherapeutic agents like doxorubicin, our results contribute significantly to the development of new therapeutic strategies to overcome these obstacles.

During the course of this study we experienced a few limitations. Most importantly, we were unable to determine the effects of autophagic manipulation in CAFs on the migratory capacity of epithelial breast cancer cells due to the potent effects that electroporation has on cell-cell adhesion and epithelial-to-mesenchymal transition (EMT). Therefore, the use of an alternative transfection protocol, such as the use lipofectamine 3000, which does not influence cell adhesion junctions and EMT, would be of great benefit in elucidating the role of stromal autophagy on the metastatic capacity of epithelial cancer cells. Although we assessed the protein profile as well as the enzymatic activity of pyruvate dehydrogenase (PDH) as an indicator of the ability of MEF and E0771 cells to undergo oxidative phosphorylation in response to conditioned media treatment, we were unable to definitively determine the oxidative phosphorylation capacity of these cells as metabolic intermediates may be shunted into the tricarboxylic

acid (TCA) cycle independently of PDH. Therefore, the use of more in depth metabolic analysis of both glycolysis and oxidative phosphorylation may have provided better insight into the metabolic reprogramming of MEFs and the subsequent pro-survival effects conferred to epithelial cancer cells.

Based on the significant role that cancer-associated fibroblasts (CAFs) play in tumour progression, chemoresistance and metastasis, it is recommended that additional co-culture models are performed, particularly ones utilizing a 3D approach, wherein epithelial cancer cells are cultured together with CAFs. The use of such a 3D co-culture model could provide insight into the effects that direct contact with stromal cells has on the survival and metastatic capacity of epithelial cancer cells. Furthermore, it is well established that standard 2D cell culture models greatly affect the phenotype of cells therefore the use of a 3D model could better recapitulate the *in* vivo tumour microenvironment and as such provide invaluable information into the effects of cell-cell adhesions on tumour growth and survival.

In conclusion, we have demonstrated that “activated” mouse embryonic fibroblast (MEF) cells contribute significantly to the pro-survival and pro-metastatic abilities of glucose deprived E0771 breast cancer cells. Furthermore, this study has contributed significantly to the understanding of the molecular mechanisms underlying the stromal-epithelial interactions within the tumour microenvironment. However, extensive research still needs to be conducted in order to exploit these interactions for the development of novel therapeutic strategies for the treatment of metastatic breast cancer.

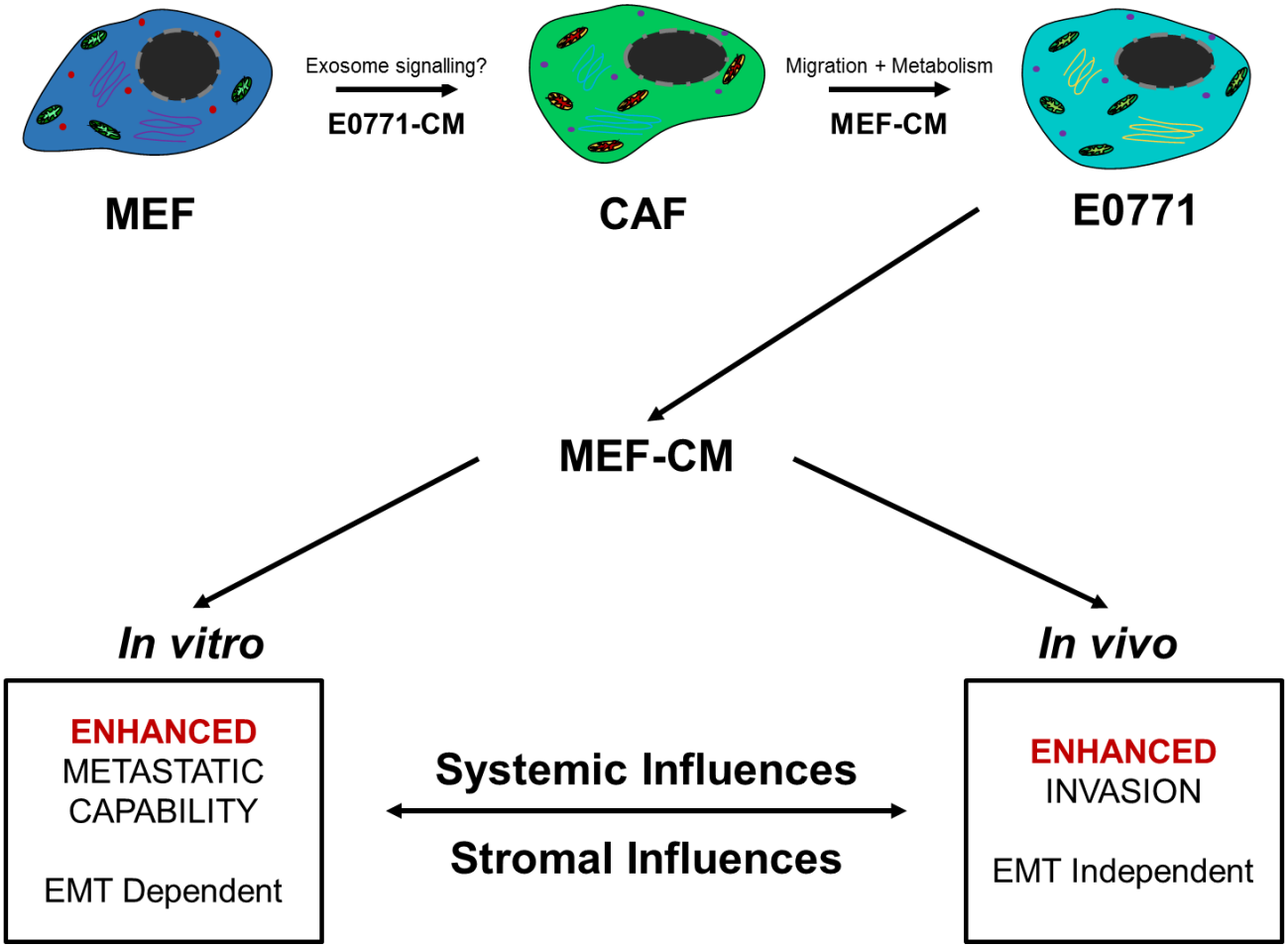

Figure 5.1: Summary of main findings. We have demonstrated that glucose deprived E0771 breast cancer cells successfully "activate" to a cancer-associated fibroblast (CAF) phenotype in normal mouse embryonic fibroblast (MEF) cells. This is most likely due to the release of exosomes which result in the acquisition of an enhanced mesenchymal phenotype. We have also demonstrated that treatment with MEF conditioned media elicits differential responses *in vitro* and *in vivo*. *In vitro* treatment of glucose deprived E0771 breast cancer cells with MEF conditioned media resulted in an enhanced metastatic capability that was dependent on epithelial-to-mesenchymal transition. Whereas, *in vivo* MEF conditioned media promoted enhanced invasiveness of epithelial organoids which was independent of epithelial-to-mesenchymal transition induction.

Chapter 6: References

- Abramsson, A., Lindblom, P., Betsholtz. (2003). Endothelial and nonendothelial sources of PDGF-B regulate pericyte recruitment and influence vascular pattern formation in tumors. *J. Clin. Invest*. 112, 1142–1151.
- Aitken, A. (2011). Post-translational modification of 14-3-3 isoforms and regulation of cellular function. *Seminars in Cell & Developmental Biology*. 22, 673-680. doi: 10.1016/j.semcdb.2011.08.003.
- Akashi, T., Koizumi, K., Tsuneyama, K., Saiki, I., Takano, Y., Fuse, H. (2008). Chemokine receptor CXCR4 expression and prognosis in patients with metastatic prostate cancer. *Cancer Sci*. 99(3), 539-542.
- Altman, B.J., Rathmell, J.C. (2012). Metabolic stress in autophagy and cell death pathways. *Cold Spring Harb Perspect Biol*. 4, a008763. Doi: 10.1101/cshperspect.a008763.
- Amano, H., Hiyashi, I., Endo, H., Kitsato, H., Yamashina, S., Maruyama, T., *et al*. (2003). Host prostaglandin e2-ep3 signaling regulates tumor-associated angiogenesis and tumor growth. *J Exp Med*. 197(2), 221-32.
- An, Q., Han, C., Zhou, Y., Li, F., Li, D., Zhang, X., Yu, Z., Duan, Z., Kan, Q. (2015). In vitro effects of mitomycin C on the proliferation of the non-small-cell lung cancer line A549. *Int J Clin Exp Med*. 8(11), 20516-20523.
- Anderberg, C., Li, H., Fredriksson, L., Andrae, J., Betsholtz, C., Li, X., Eriksson, U., Pietras, K., (2009). Paracrine signaling by Platelet Derived Growth Factor-CC promotes tumor growth by recruitment of cancer-associated fibroblasts. *Cancer Res*. 69(1), 369–378. doi: 10.1158/0008-5472.CAN-08-2724.

- Ao, M., Brewer, B.M., Yang, L., Franco Coronel, O.E., Hayward, S.W., Webb, D.J., Li, D. (2015). Stretching fibroblasts remodels fibronectin and alters cancer cell migration. *Scientific Reports*. 5(8334), doi: 10.1038/srep08334.
- Ao, Z., Shah, S.H., Machlin, L.M., Parajuli, R., Miller, P.C., Rawal, S., *et al.* (2015). Identification of cancer-associated fibroblasts in circulating blood from patients with metastatic breast cancer. *Cancer Res*. 75(22), 4681-4687.
- Augsten, M., Hägglöf, C., Olsson, E., Stolz, C., Tsagozis, P., Levchenko, T., Frederick, M.J., Borg, A., Micke, P., Egevad, L., Östman, A. (2009). CXCL14 is an autocrine growth factor for fibroblasts and acts as a multi-modal stimulator of prostate tumor growth. *Proc. Natl. Acad. Sci. USA*. 106, 3414–3419.
- Avgustinova, A., Iravani, M., Robertson, D., Fearns, A., Gao, Q., Klingbeil, P., *et al*. (2016). Tumour cell-derived Wnt7a recruits and activates fibroblasts to promote tumour aggressiveness. *Nature Communications*. 7, 10305. doi: 10.1038/ncomms10305.
- Babu, J.R., Geetha, T., Wooten, M.W. (2005). Sequestosome 1/p62 shuttles polyubiquitinated tau for proteasomal degradation. *Journal of Neurochemistry*. 94, 192-203. doi:10.1111/j.1471-4159.2005.03181.x.
- Baixauli, F., López-Otin, C., Mittelbrunn, M. (2014). Exosomes and autophagy: coordinated mechanisms for the maintenance of cellular fitness. *Frontiers in Immunology.* 5, 403. doi: 10.3389/fimmu.2014.00403
- Balkwill, F. (2002). TNF-α in promotion and progression of cancer. *Cancer and Metastasis Reviews.* 25, 409-416. doi: 10.1007/s10555-006-9005-3.
- Balkwill, F. (2006). TNF-α in promotion and progression of cancer. *Cancer Metastasis Rev*. 25, 409-416. doi: 10.1007/s10555-006-9005-3.
- Bar, J., Feniger-Barish, R., Lukashchuk, N., Shaham, H., Moskovits, N., Goldfinger, N., *et al*. (2009). Cancer cells supress p53 in adjacent fibroblasts. *Oncogene*. 28, 933-936. doi: 10.1038/onc.2008.445

- Barrett-Lee, P.J., Dixon, J.M., Farrell, C., Jones, A., Leonard, R., Murray, N., *et al*. (2009). Expert opinion on the use of anthracyclines in patients with advanced breast cancer at cardiac risk. *Ann Oncol*. 20(5), 816-27.
- Battello, N., Zimmer, A.D., Goebel, C., Dong, X., Behrmann, I., Haan, C., Hiler, K., Wegner, A. (2016). The role of HIF-1 in oncostatin M-dependent metabolic reprogramming of hepatic cells. *Cancer & Metabolism*. 4(3), 1-14. doi: 10.1186/s40170-016-0141-0.
- Baumann, F., Leukel, P., Doerfelt, A., Beier, C.P., Dettmer, K., Oefner, P.J., *et al*. (2009). Lactate promotes glioma migration by TGF-beta2-dependent regulation of matrix metalloproteinase-2. *Neuro Oncol*. 11, 368–80.
- Belda-Iniesta, C., Pernía, O., Simó, R. (2011). Metformin: a new option in cancer treatment. *Clinical & Translational Oncology*. 13, 363–367.
- Bellot, G., Garcia-Medina, R., Gounon, P., Chiche, J., Roux, D., Pouysségur, J., Mazure, N.M. (2009). Hypoxia-induced autophagy is mediated through hypoxia-inducible factor induction of BNIP3 and BNIP3L via their BH3 domains. *Molecular and Cellular Biology*. 29(10), 2570-2581. doi:10.1128/MCB.00166-09.
- Bhowmick, N.A., Ghiassi, M., Bakin, A., Aakre, M., Lundquist, C.A., Engel, M.E., Arteaga, C.L., Moses, H.L. (2001). Transforming growth factor-β1 mediates epithelial to mesenchymal transdifferentiation through a RhoA-dependent mechanism. *Molecular Biology of the Cell*. 12, 27-36.
- Bhowmick, N.A., Neilson, E.G., Moses, H.L. (2004). Stromal fibroblasts in cancer initiation and progression. *Nature*. 432, 332–337.
- Bhowmick, N.A., Zentt, R., Ghiassi, M., McDonnell, M., Moses, H.I. (2001). Integrin β1 signalling is necessary for transforming growth factor-β activation of p38MAPK and

epithelial plasticity. *Journal of Biological Chemistry*. 276(50). 46707-46713. doi: 10.1074/jbc.M106176200.

- Bierie, B., Moses, H.L. (2006). TGFβ: The molecular Jekyll and Hyde of cancer. *Nat Rev Cancer*. 6, 506-520. doi:10.1038/nrc1926.
- Birchmeier, W., Behrens, J. (1994). Cadherin expression in carcinomas: role in the formation of cell junctions and the prevention of invasiveness. *Biochimica et Biophysica Acta.* 1198(1994), 11-26.
- Bissell, M.J., Radisky, D.C., Rizki, A. (2002). The organizing principle: microenvironmental influences in the normal and malignant breast. *Differentiation.* 70, 537-546.
- Blanco, M.J., Moreno-Bueno, G., Sarrio, D., Locascio, A., Cano, A., Palacios, J., Nieto, M.A. (2002). Correlation of Snail expression with histological grade and lymph node status in breast carcinomas. *Oncogene*. 21, 3241-3246. doi: 10.1038/sj/onc/1205416.
- Bonuccelli, G., Tsirigos, A., Whitaker-Menezes, D., Pavlides, S., Pestell, R.G., Chiavarina, B., *et al*. (2010). Ketones and lactate "fuel" tumour growth and metastasis. *Cell Cycle*. 9(17), 3506-3514. doi: 10.4161/cc.9.17.12731.
- Boulares, a. H. (1999). Role of poly(ADP-ribose) polymerase (PARP) cleavage in apoptosis. Caspase 3-resistant PARP mutant increases rates of apoptosis in transfected cells. *Journal of Biological Chemistry*. 274(33), 22932–22940.
- Brooks, G.A. (2009). Cell–cell and intracellular lactate shuttles. *J Physiol*. 587(23), 5591–5600. doi: 10.1113/jphysiol.2009.178350
- Bryant, N.J., Govers, R., James, D.E. (2002). Regulated transport of the glucose transporter GLUT4. *Mol Cell Biol*. 3, 267-277. doi: 10.1038/nrm782.
- Burger, J.A., Tsukada, N., Burger, M., Zvaifler, N.J., Dell'Aquila, M., Kipps, T. (2000). Blood-derived nurse-like cells protect chronic lymphocytic leukemia B cells from spontaneous apoptosis through stromal cell-derived factor-1. *Blood*. 96(8), 2655-2663.

- Busch, S., Andersson, D., Bom, E., Walsh, C., Ståhlberg, A., Landberg, G. (2017). Cellular organization and molecular differentiation model of breast cancer-associated fibroblasts. *Molecular Cancer*. 16(1):73. doi: 10.1186/s12943-017-0642-7.
- Cai, W-J., Li, M.B., Wu, X., Wu, S., Zhu, W., Chen, D., *et al*. (2009). Activation of the integrins α5β1 and αvβ3 and focal adhesion kinase (FAK) during arteriogoenesis. *Mol Cell Biochem*. 322, 161-169.
- Calvisi *et al*., 2011). Inactivation of Ras GTPase-activating proteins promotes unrestrained activity of wild-type Ras in human liver cancer. *Journal of Hepatology*. 54(2), 311-319. doi: 10.1016/j.jhep.2010.06.036.
- Calvo, F., Sahai, E. (2011). Cell communication networks in cancer invasion. *Current Opinion in Cell Biology*. 23, 621–629. doi: 10.1016/j.ceb.2011.04.010
- Camenisch, G., Pisabarro, M.T., Sherman, D., Kowalski, J., Nagel, M., Hass, P., *et al.* (2002). ANGPTL3 stimulates endothelial cell adhesion and migration via integrin αvβ3 and induces blood vessel formation *in vivo*. *J Biol Chem*. 277(19), 17281-17290.
- Campbell, I.D., Humphries, M.J. (2011). Integrin structure, activation, and interactions. *Cold Spring Harb Perspect Biol*. doi: 10.1101/cshperspect.a004994.
- Camps, J.L., Chang, S-M., Hsu, T.C., Freeman, M.R., Hong, S-J., Zhau, H.E., Von Eschenbach, A.C., Chung, L.W.K. (1990). Fibroblast-mediated acceleration of human epithelial tumor growth in vivo. *Proc Natl Acad Sci U S A*. 87, 75–79.
- Capparelli, C., Guido, C., Witaker-Menezes, D., Bonuccelli, G., Balliet, R., Pestell, T.G., *et al*. (2012). Autophagy and senescence in cancer-associated fibroblasts metabolically supports tumor growth and metastasis, via glycolysis and ketone production. *Cell Cycle*. 11(12), 2285-2302. doi: 10.4161/cc.20718.
- Carpenter, L., Halestrap, A.P. (1994). The kinetics, substrate and inhibitor specificity of the lactate transporter of Ehrlich–Lettre tumor cells studied with the intracellular pH indicator BCECF. *Biochem. J*. 304, 751–760.

- Carracedo, A., Ma, L., Teruya-Feldstein, J., Rojo, F., Salmena, L., Alimonti, A., *et al*. (2008). Inhibition of mTORC1 leads to MAPK pathway activation through a PI3K-dependent feedback loop in human cancer. *J Clin Invest*. 118(9), 3065-3074. doi: 10.1172/JCI34739.
- Carrer, A., Wellen, K.E. (2015). Metabolism and epigenetics: a link cancer cells exploit. *Curr Opin Biotech*. 34, 23-29.
- Catteau, X., Simon, P., Noël, J-C. (2016). Stromal expression of matrix metalloproteinase 2 in cancer-associated fibrobasts is strongly related to human epidermal growth factor receptor 2 status in invasive breast carcinoma. *Mol Clin Oncol*. 4, 375-378.
- Catteau, X., Simon, P., Vanhaeverbeek, M., Nöel, J-C. (2013). Variable stromal periductular expression of CD34 and smooth muscle actin (SMA) in intraductal carcinoma of the breast. *PLOS One*. 8(3), e57773. doi: 10.1371/journal.pone.005777.
- Chaundhury, A., Hussey, G.S., Ray, P.S., Jin, G., Fox, P.L., Howe, P.H. (2010). Transforming growth factor-β (TGFβ)-mediated phosphorylation of hnRNP E1 induces EMT via transcript selective translational induction of Dab2 and ILEI. *Nat Cell Biol*. 13(3), 286-293. doi: 10.1038/ncb2029.
- Cheeti, S., Warrier, B.K., Lee, C.H. (2006). The role of monocarboxylate transporters in uptake of lactic acid in HeLa cells. *International Journal of Pharmaceutics*. 325, 48-54.
- Chen, H., Yang, W-W., Wen, Q-T., Xu, L., Chen, M. (2009). TGF-β-induced fibroblast activation protein expression, fibroblast activation protein expression increases the proliferation, adhesion, and migration of H0-8910PM. *Experimental and Molecular Pathology*. 87, 189-194. doi:10.1016/j.yexmp.2009.09.001.
- Chen, H-C., Guan, J-L. (1994). Stimulation of phosphatidylinositol 3'-kinase association with focal adhesion kinase by platelet-derived growth factor. *The Journal of Biological Chemistry*. 269(49), 31229-31233.

- Chen, S., Guttridge, D.C., You, Z., Zhang, Z., Fribley, A., Mayo, M.W., Kitajewski, J., Wang, C-Y. (2001). Wnt-1 signaling inhibits apoptosis by activating β-catenin/T cell factor-mediated transcription. *The Journal of Cell Biology*. 152(1), 87-96.
- Chen, W-X., Liu, X-M., Lv, M-M., Chen, L., Zhao, J-H., Zhong, S-L., *et al*. (2014). Exosomes from drug-resistant breast cancer cells transmit chemoresistance by horizontal transfer of microRNAs. *PLOS One*. 9(4). doi:10.1371/journal.pone.0095240.
- Chen, Y., McMillan-Ward, E., Kong, J., Isreals, S.J., Gibson, S.B. (2008). Oxidative stress induces autophagic cell death independent of apoptosis in transformed and cancer cells. *Cell Death Differ*. 15, 171-182.
- Childs, B.G., Baker, D.J., Kirkland, J.L., Campisi, J., Van Deursen, J.M. (2014). Senescence and apoptosis: dueling or complementary cell fates? *EMBO Reports.* 15(11), 1139–1153. doi: 10.15252/embr.201439245.
- Choi, C-H., Lee, B-H., Ahn, S-G., Oh, S-H. (2012). Proteasome inhibition-induced p38 MAPK/ERK signaling regulates autophagy and apoptosis through the dual phosphorylation of glycogen synthase kinase 3β. *Biochemical and Biophysical Research Communications*. 418(4), 759-764. doi: 10.1016/j.bbrc.2012.01.095.
- Ciravolo, V., Huber, V., Ghedini, G.C., Venturelli, E., Bianchi, F., Campiglio, M., *et al*. (2011). Potential role of HER2-overexpressing exosomes in countering Trastuzumab-based therapy. *J Cell Physiol*. 227, 658-667.
- Coley, H.M. (2008). Mechanisms and strategies to overcome chemotherapy resistance in metastatic breast cancer. *Cancer Treat Rev*. 34(4), 378–90.
- Comijn, J., Berx, G., Vermassen, P., Verschueren, K., van Grunsven, L., Bruyneel, E., Mareel, M., Huylebroeck, D., van Roy, D. (2001). The two-handed E box binding zinc finger protein SIP1 downregulates E-cadherin and induces invasion. *Molecular Cell*. 7, 1267–1278.

- Comito, G., Calvani, M., Giannoni, E., Bianchini, F., Calorini, L., Torre, E., Migliore, C., Giordano, S., Chiarugi, P. (2011). HIF-1α stabilization by mitochondrial ROS promotes Met-dependent invasive growth and vasculogenic mimicry in melanoma cells. *Free Radical Biology & Medicine*. 51, 893-904. doi: 10.1016/j.freeradbiomed.2011.05.042.
- Conacci-Sorrell, M., Zhurinsky, J., Ben-Ze'ev, A. (2002). The cadherin-catenin adhesion system in signaling and cancer. *J. Clin. Invest*. 109, 987–991. doi: 10.1172/JCI200215429.
- Cui, W., Fowlis, D.J., Bryson, S., Duffie, E., Ireland, H., Balmain, A., Akhurst, R.J. (1996). TGFβ1 inhibits the formation of benign skin tumors, but enhances progression to invasive spindle carcinomas in transgenic mice. *Cell*. 86, 531-542.
- Daenen, L.G.M., Roodhart, J.M.L., van Amersfoort, M., Dehnad, M., Roessingh, W., Ulfman, L.H., Derksen, P.W.B., Voest, E.E. (2011). Chemotherapy enhances metastasis formation via VEGFR-1-expressing endothelial cells. *Cancer Res.* 71(22), 6976-6985. doi: 10.1158/0008-5472.CAN-11-0627.
- Datta, S.R., Dudek, H., Tao, X., Masters, S., Fu, H., Gotoh, Y., *et al*. (1997). Akt phosphorylation of BAD couples survival signals to the cell-intrinsic death machinery. *Cell*. 91, 231-241.
- De Boeck, A., Hendrix, A., Maynard, D., Van Bockstal, M., Daniëls, A., Pauwels, P., *et al*. (2013). Differential secretome analysis of cancer-associated fibroblasts and bone marrow-derived precursors to identify microenvironmental regulators of colon cancer progression. *Proteomics*. 13, 379-388. doi: 10.1002/pmic.201200179.
- De Boeck, A., Pauwels, P., Hensen, K., Rummens, J.L., Westbroek, W., Hendrix, A., *et al*. (2012). Bone marrow-derived mesenchymal stem cells promote colorectal cancer progression through paracrine neuregulin 1/HER3 signalling. *Gut*. 62, 550-560. doi:10.1136/gutjnl-2011-301393.

- De Jong, O.G., Verhaar, M.C., Chen, Y., Vader, P., Gremmels, H., Posthuma, G., *et al*. (2012). Cellular stress conditions are reflected in the protein and RNA content of endothelial cell-derived exosomes. *J Extracell Vesicles*. doi: 10.3402/jev.v1i0.18396.
- De Wever, O., Demetter, P., Mareel, M., Bracke, M. (2008). Stromal myofibroblasts are drivers of invasive cancer growth. *Int J Cancer*. 123, 2229-2238. doi: 10.1002/ijc.23925.
- De Wever, O., Mareel, M. (2002). Role of myofibroblasts at the invasion front. *Biol Chem*. 383, 55-67.
- De Wever, O., Nguyen, Q-D., Van Hoorde, L., Bracke, M., Bruyneel, E., Gespach, C., Mareel, M. (2004). Tenascin-C and SF/HGF produced by myofibroblasts in vitro provide convergent proinvasive signals to human colon cancer cells through RhoA and Rac. *FASEB*. 18, 1016-1018. doi: 10.1096/fj.03-1110fje.
- DeBerardinis, R.J. (2008). Is cancer a disease of abnormal cellular metabolism? New angles on an old idea. *Genet Med*. 10(11), 767–777. doi:10.1097/GIM.0b013e31818b0d9b
- Degenhardt, K., Mathew, R., Beaudoin, B., Bray, K., Anderson, D., Chen, G., *et al*. (2006). Autophagy promotes tumor cell survival and restricts necrosis, inflammation, and tumorigenesis. *Cancer Cell*. 10(1), 51-64.
- DeNardo, D.G., Barreto, J.B., Andreu, P., Vasquez, L., Tawfik, D., Kolhetkar, N., Coussens, L.M. (2009). $CD4^+$ T cells regulate pulmonary metastasis of mammary carcinomas by enhancing protumor properties of macrophages. *Cancer Cell*. 16(2), 91-102. doi:10.1016/j.ccr.2009.06.018.
- Denef, N., Chen, Y., Weeks, S.D., Barcelo, G.., Schüpbach, T. (2008). Crag regulates epithelial architecture and polarized deposition of basement membrane proteins in Drosophila. *Developmental Cell*. 14, 354-364. doi: 10.1016/j.devcel.2007.12.012.
- Dernyck, R., Akhurst, R.J. (2007). Differentiation plasticity regulated by TGF-β family proteins in development and disease. *Nature Cell Biology*. 9(9), 1000-1004.

- Dhillion, A.S., Hagan, S., Rath, O., Kolch, W. (2007). MAP kinase signalling pathways in cancer. *Oncogene*. 26, 3279-3290. doi: 10.1038/sj.onc.1210421.
- Dimmer, K-S., Friedrich, B., Lang, F., Deitmer, J.W. Bröer, S. (2000). The low-affinity monocarboxylate transporter MCT4 is adapted to the export of lactate in highly glycolytic cells. *Biochem J*. 350(1), 219-27.
- Doherty, J.R., Cleveland, J.L. (2013). Targeting lactate metabolism for cancer therapeutics. *J Clin Invest*. 123(9), 3685–3692. doi: 10.1172/JCI69741
- Du, J., Yang, M., Chen, S., Li, D., Chang, Z., Dong, Z. (2015).\ PDK1 promotes tumour growth and metastasis in a spontaneous breast cancer model. *Oncogene*. 1-10. doi: 10.1038/onc.2015.393.
- Duda, D.G., Duyverman, A.M.M.J., Kohno, M., Snuderl, M., Steller, E.J.A., Fukumura, D., *et al.* (2010). Malignant cells facilitate lung metastasis by bringing their own soil. *PNAS*. 107(50), 21677-21682.
- Duluc, C., Moatassim-Billah, S., Chalabi-Dchar, M., Perraud, A., Samain, R., Breibach, F., *et al*. (2015). Pharmacological targeting of the protein synthesis mTOR/4E-BP1 pathway in cancer-associated fibroblasts abrogates pancreatic tumour chemoresistance. *EMBO Mol Med*. 7, 735-753.
- Dumitrescu, R.G., Cotarla, I. (2005). Understanding breast cancer risk - where do we stand in 2005? *J Cell Mol Med*. 9(1), 208-221. doi: 10.1111/j.1582-4934.2005.tb00350.x.
- Dupuy, F., Tabariès, S., Andrzejewski, S., Dong, Z., Blagih, J., Annis, M.G., *et* al. (2015). PDK1-dependent metabolic reprogramming dictates metastatic potential in breast cancer. *Cell Metabolism*. 22, 577-589. doi: 10.1016/j/cmet.2015.08.007.
- Eagle, H. (1955). Nutrition needs of mammalian cells in tissue culture. Science. 122(3168), 501-504.
- Egeblad, M., Ewald, A.J., Askautrud, H.A., Truitt, M.L., Welm, B.E., Bainbridge, E., Peeters, G., Krummel, M.F., Werb, Z. (2008). Visualizing stromal cell dynamics in

different tumor microenvironments by spinning disk confocal microscopy. *Disease Models & Mechanisms*. 1, 155-167. doi:10.1242/dmm.000596.

- Egeblad, M., Werb, Z. (2002). New functions for the matrix metalloproteinases in cancer progression. *Nat. Rev. Cancer*. 2, 161-174.
- Eger, A., Aigner, K., Sondregger, S., Dampier, B., Oehler, S., Schreiber, M., Berx, G., Cano, A., Beug, H., Foisner, R. (2005). DeltaEF1 is a transcriptional repressor of E-cadherin and regulates epithelial plasticity in breast cancer cells. *Oncogene*. 24, 2375-2395. doi:10.1038/sj.onc.1208429.
- Eger, A., Stockinger, A., Park, J., Lamgkopf, E., Mikula, M., Gotzmann, J., Mikulits, W., Beug, H., Foisner, R. (2004). β-Catenin and TGFβ signalling cooperate to maintain a mesenchymal phenotype after FosER-induced epithelial to mesenchymal transition. *Oncogene*. 23, 2672–2680. doi:10.1038/sj.onc.1207416.
- Eisinger-Mathason, T.S., Zhang, M., Qiu, Q., Skuli, N., Nakazawa, M.S., Karakasheva, T., *et al*. (2013). Hypoxia-Dependent Modification of Collagen Networks Promotes Sarcoma Metastasis. *Cancer Discovery*. 3(10), 1190-1205. doi: 10.1158/2159-8290.CD-13-0118.
- Elmore, S. (2007). Apoptosis: A review of programmed cell death. *Toxicol Pathol*. 35(4), 495-516.
- Erez, N., Glanz, S., Raz, Y., Avivi, C., Barshack, I. (2013) Cancer associated fibroblasts express pro-inflammatory factors in human breast and ovarian tumours. *Biochem Bioph Res Co*. 437, 397-402.
- Erez, N., Truitt, M., Olson, P., Hanahan, D. (2010). Cancer-associated fibroblasts are activated in incipient neoplasia to orchestrate tumor-promoting inflammation in an NF-κβ-dependent manner. *Cancer Cell*. 17, 135-147. doi: 10.1016/j.ccr.2009.12.041.
- Erler, J.T., Bennewith, K.L., Cox, T.R., Lang, G., Bird, D., Koong, A., Le, Q-T., Giaccia, A.J. (2009). Hypoxia-induced lysyl oxidase is a critical mediator of bone marrow cell

recruitment to form the pre-metastatic niche. *Cancer Cell*. 15(1), 35-44. doi:10.1016/j.ccr.2008.11.012.

- Farrelly, N., Lee, Y-J., Oliver, J., Dive, C., Streuli, C.H. (1999). Extracellular matrix regulates apoptosis in mammary epithelium through a control on insulin signalling. *J Cell Biol*. 144(6), 1337-1347.
- Fein, M.R. Egeblad, M. (2013). Caught in the act: revealing the metastatic process by live imaging. *Disease Models & Mechanisms*. 6, 580-593. doi: 10.1242/dmm.009282.
- Février, B., Raposo, G. (2004). Exosomes: endosomal-derived vesicles shipping extracellular messages. *Curr Opin Cell Biol*. 16, 415-421.
- Fischer, K., Hoffmann, P., Voelkl, S., Medenbauer, N., Ammer, J., Edinger, M., *et al*. (2007). Inhibitory effect of tumor cell-derived lactic acid on human T cells. *Blood*. 109(9), 3812-3819.
- Friedl, P., Locker, J., Sahai, E., Segall, J.E. (2012). Classifying collective cancer cell invasion. *Nat Cell Biol*. 14(8), 777-783.
- Fu, Q-F., Liu, Y., Fan, Y., Hua, S-N., Qu, H-Y., Dong, S-W. (2015). Alpha-enolase promotes cell glycolysis, growth, migration, and invasion in non-small cell lung cancer through FAK-mediated P13K/AKT pathway. *Journal of Haematology & Oncology*. 8(22), 1-13. doi: 10.1186/s13045-015-0117-5.
- Fukumura, D., Xavier, R., Sugiura, T., Chen, Y., Park, E-C., Lu, N., Selig, M., Nielsen, G., Taksir, T., Jain, R.K., Seed, B. (1998). Tumor induction of vegf promoter activity in stromal cells. *Cell*. 94, 715-725.
- Furuhashi, M., Sjöblom, T., Abramsson, A., *et al*. (2004). Platelet-derived growth factor production by B16 melanoma cells leads to increased pericyte abundance in tumors and an associated increase in tumor growth rate. *Cancer Res*. 64, 2725–2733.

- Gao, P., Tchernyshyov, I., Chang, T-C., Lee, Y-S., Kita, K., Ochi, T., *et al*. (2009). c-Myc suppression of miR-23 enhances mitochondrial glutaminase and glutamine metabolism. *Nature*. 458(7239). 762-765. doi: 10.1038/nature07823.
- Ge, S., Mao, Y., Yi, Y., Xie, D., Chen, Z., Xiao, Z. (2012). Comparative proteomic analysis of secreted proteins from nasopharyngeal carcinoma-associated stromal fibroblasts and normal fibroblasts. *Experimental and Therapeutic Medicine*. 3, 857-860. doi: 10.3892/etm.2012.483.
- Gerweck, L.E., Vijayappa, S., Kozin, S. (2006). Tumor pH controls the *in vivo* efficacy of weak acid and base chemotherapeutics. *Mol Cancer Ther*. 5(5), 1275-1279. doi:10.1158/1535-7163.MCT-06-0024.
- Gewirtz, D.A. (1999). A critical evaluation of the mechanisms of action proposed for the antitumor effects of the anthracycline antibiotics Adriamycin and Daunorubicin. *Biochemical Pharmacology*. 57(7), 727-741.
- Gheldof, A., Berx, G. (2013). Cadherins and epithelial-to-mesenchymal transition. *Prog Mol Biol Transl Sci*. 116, 317-336. doi: 10.1016/B978-0-12-394311-8.00014-5.
- Giannoni, (2010). Reciprocal activation of prostate cancer cells and cancer-associated fibroblasts stimulates epithelial-mesenchymal transition and cancer stemness. *Cancer Res*. 70(17), 6945-6956. doi: 10.1158/0008-5472.CAN-10-0785.
- Giannoni, E., Bianchini, F., Calorini, L., Chiarugi, P. (2011). Cancer associated fibroblasts exploit reactive oxygen species through a proinflammatory signature leading to epithelial mesenchymal transition and stemness. *Antioxidants & Redox Signaling*. 14(12), 2361-2371.
- Gilbert, J., Baker, S.D., Bowling, M.K., Grochow, L., Fig, W. D., Zabelina, Y., *et al*. (2001). A phase I dose escalation and bioavailability study of oral sodium phenylbutyrate in patients with refractory solid tumor malignancies. *Clin Cancer Res*. 7, 2292-2300.

- Gilkes, D.M., Semenza, G.L. (2013). Role of hypoxia-inducible factors in breast cancer metastasis. *Future Oncol*. 9(11), 1623-1636. doi:10.2217/fon.13.92.
- Gladden, L.B. (2008). A “lactatic” perspective on metabolism. *Medicine & Science in Sports & Exercise*. 40(3), 477-485. doi: 10.1249/MSS.0b013e31815fa580
- Goetze, K., Walenta, S., Ksiazkiewicz, M., Kunz-Schughart, L., Mueller-Klieser, W. (2011). Lactate enhances motility of tumor cells and inhibits monocyte migration and cytokine release. *International Journal of Oncology*. 39, 453-463. doi: 10.3892/ijo.2011.1055
- Görlach, A., Diebold, I., Schini-Kerth, U., Berchner-Pfannschmidt, U., Roth, U., Brandes, R.P., Kietzmann, T., Busse, R. (2001). Thrombin activates the hypoxia-inducible factor-1 signalling pathway in vascular smooth muscle cells: Role of the $p22^{phox}$-containing NADPH oxidase. *Circ Res*. 89, 47-54.
- Gottardi, C.J., Wong, E., Gumbiner, B.M. (2001). E-Cadherin suppresses cellular transformation by inhibiting β-catenin signaling in an adhesion-independent manner. *The Journal of Cell Biology*. 153(5), 1049–1059.
- Gotzmann, J., Huber, H., Thallinger, C., Wolschek, M., Jansen, B., Schulte-Hermann, R., Beug, H., Mikulits, W. (2002). Hepatocytes convert to a fibroblastoid phenotype through the cooperation of TGF-β1 and Ha-Ras: steps towards invasiveness. *Journal of Cell Science*. 115, 1189-1202.
- Grasso, S., Menéndez-Gutiérrez, M. P., Carrasco-García, E., Mayor-López, L., Tristante, E., Rocamora-Reverte, L., *et al.* (2012). Cell death and cancer, novel therapeutic strategies. *Apoptosis and Medicine*. 67-110. doi: 10.5772/51285.
- Greening, D.W., Ji, H., Chen, M., Robinson, B.W.S., Dick, I.M., Creaney, J., Simpson, R.J. (2016). Secreted primary human malignant mesothelioma exosome signature reflects oncogenic cargo. *Scientific Reports*. 6,32643. doi: 10.1038/srep32643.

- Gregory, P.A., Bert, A.G., Paterson, E.L., Barry, S.C., Tsykin, A., Farshid, G., Vadas, M.A., Khew-Goodall, Y., Goodall, G.J. (2008). The miR-200 family and miR-205 regulate epithelial to mesenchymal transition by targeting ZEB1 and SIP1. *Nature Cell Biology*. 10, 593 – 601. doi:10.1038/ncb1722.
- Grosse-Wilde, A., d'Herouël, A.F., McIntosh, E., Ertaylan, G., Skuoin, A., Kuestner, R.E., del Sol, A., Walters, K-A., Huang, S. (2015). Stemness of the hybrid epithelial/mesenchymal state in breast cancer and its association with poor survival. *PLOS One*. 10(5), e0126522. doi: 10.1371/journal.pone.0126522.
- Grünert, S., Jechlinger, M., Beug, H. (2003). Diverse cellular and molecular mechanisms contribute to epithelial plasticity and metastasis. *Mol Cell Biol*. 4, 657-665.
- Guan, J., Zhang, H., Wen, Z., Gu, Y., Cheng, Y., Sun, Y., Zhang, T., Jia, C., Lu, Z., Chen, J. (2014). Retinoic acid inhibits pancreatic cancer cell migration and EMT through the downregulation of IL-6 in cancer associated fibroblast cells. *Cancer Letters*. 345, 132-139. doi: 10.1016/j.canlet.2013.12.006.
- Guillaumond, F., Leca, J., Olivares, O., Lauaut, M-N., Vidal, N., Berthezène, P., *et al.* (2013). Strengthened glycolysis under hypoxia supports tumor symbiosis and hexosamine biosynthesis in pancreatic adenocarcinoma. *PNAS*. 110(10), 3919-3924.
- Hall, C.N., Klein-Flügge. M.C., Howarth, C., Attwell, D. (2012). Oxidative phosphorylation, not glycolysis, powers pre- and postsynaptic mechanisms underlying brain information processing. *J Neurosci*. 32(26), 8940–8951. doi: 10.1523/JNEUROSCI.0026-12.2012
- Han, J., Hou, W., Goldstein, L.A., Lu, C., Stolz, D.B., Yin, X-M., Rabinowich, H. (2008). Involvement of protective autophagy in TRAIL resistance of apoptosis-defective tumor cells. *The Journal of Biological Chemistry*. 283(28), 19665-19677. doi: 10.1074/jbc.M710169200.

- Han, R., Xiong, J., Xiao, R., Altaf, E., Wang, J., Liu, Y., Xu, H., Ding, Q., Zhang, Q. (2013). Activation of β-catenin signalling is critical for doxorubicin-induced epithelial-mesenchymal transition in BGC-823 gastric cancer cell line. *Tumor Biol.* 34, 277-284. doi: 10.1007/s13277-012-0548-3.
- Hanada, T., Noda, N.N., Satomi, Y., Ichimura, Y., Fulioka, Y., Takao, T., *et al*. (2007). The Atg12-Atg5 conjugate has a novel E3-like activity for protein lipidation in autophagy. *J Biol Chem*. 282(52), 37298-37302.
- Hanahan D., Weinberg RS. (2000). The hallmarks of cancer. *Cell*. 100, 57-70.
- Hanahan D., Weinberg RS. (2011) Hallmarks of cancer: The next generation. *Cell*. 144(5), 646-674.
- Hashimoto, O., Yoshida, M., Koma, Y-I., Yanai, T., Hasegawa, D., Kosaka, Y., *et al.* (2016). Collaboration of cancer-associated fibroblasts and tumour-associated macrophages for neuroblastoma development. *J Pathol*. 240, 211-223.
- Hembruff, S.L., Jokar, I., Yang, L., Cheng, N. (2010). Loss of transforming growth factor-beta signalling in mammary fibroblasts enhances CCL2 secretion to promote mammary tumour progression through macrophage-dependent and –independent mechanisms. *Neoplasia*. 12(5), 425-433.
- Herrero-Martín, G., Høyer-Hansen, M., Garcia-Garcia, C., Fumarola, C., Farkas, T., López-Rivas, A., Jäättelä, M. (2009). TAK1 activates AMPK-dependent cytoprotective autophagy in TRAIL-treated epithelial cells. *The EMBO Journal*. 28(6), 677-685. doi: 10.1038/ emboj.2009.8.
- Hill. R.P., Marie-Egyptienne, D.T., Hedley, D.W. (2009). Cancer stem cells, hypoxia and metastasis. *Semin Radiat Oncol*. 19, 106-111.
- Hinz, B., Phan, S.H., Thannickal, V.J., Galli, A., Bochaton-Piallat, M-L., Gabbiani, G. (2007). The myofibroblast: One function, multiple origins. *The American Journal of Pathology*. 170(6), 1807-1816. doi: 10.2353/ajpath.2007.070112.

- Hippert, M.M., O'Toole, P.S., Thorburn, A. (2006). Autophagy in cancer: good, bad, or both? *Cancer Research*. 66(19), 9349–51. doi:10.1158/0008-5472.CAN-06-1597
- Hiraki, K., Kimura, I. (1963) .Studies on the treatment of malignant tumors with fibroblast-inhibiting agent II. Effects of chloroquine on animal tumors. *Acta Med Okayama*. 17, 239-252.
- Hiraki, K., Kimura, I. (1964a). Studies on the treatment of malignant tumors with fibroblast-inhibiting agent IV. Effects of chloroquine on malignant lymphomas. *Acta Med Okayama*. 18, 87-92.
- Hiraki, K., Kimura, I. (1964b). Studies on the treatment of malignant tumors with fibroblast-inhibiting agent III. Effects of chloroquine on human cancers. *Acta Med Okayama*. 18, 71-85.
- Hoffman, R.M. (2013). Stromal-cell and cancer-cell exosomes leading to the metastatic exodus for the promised niche. *Breast Cancer Res*. 15(310), doi: 10.1186/bcr3426.
- Hollier, B.G., Evans, K., Mani, S.A. (2009). The epithelial-to-mesenchymal transition and cancer stem cells: A coalition against cancer therapies. *J Mammary Gland Biol Neoplasia*. 14, 29-43. doi: 10.1007/s10911-009-9110-3.
- Hommes, D.W., Peppelenbosch, M.P., Deventer, S.J.H. (2003). Mitogen activated protein (MAP) kinase signal transduction pathways and novel anti-inflammatory targets. *Gut*. 52(1), 144-151.
- Hoshino, A., Costa-Silva, B., Shen, T-L., Rodrigues, G., Hashimoto, A., Mark, M. T., *et al*. (2015). Tumour exosome integrins determine organotropic metastasis. *Nature*. 527, 329–335.
- Hosseini-Beheshti, E., Pham, S., Adomat, H., Li, N., Tomlison Guns, E.S. (2012). Exosomes as biomarker enriched microvesicles: Characterization of exosomal proteins derived from a panel of prostate cell lines with distinct AR phenotypes. *Molecular & Cellular Proteomifcs*. 11(10), 863-885. doi: 10.1074/mcp.M111.014845.

- Hu, C., Wang, Z., Zhai, L., Yang, M., Shan, L., Chai, C., Liu, M., Wang, L. (2013). Effects of cancer-associated fibroblasts on the migration and invasion abilities of SGC-7901 gastric cancer cells. *Oncology Letters*. 5, 609-612. doi: 10.3892/ol.2012.1023.
- Hu, Y., Yan, C., Mu, L., Huang, K., Li, X., Tao, D., *et al.* (2015). Fibroblast-derived exosomes contribute to chemoresistance through priming cancer stem cells in colorectal cancer. *PLOS One*. 10(5), doi:10.1371/journal.pone.0125625.
- Husain, Z., Seth, P., Sukhatme, V. (2013). Tumor-derived lactate and myeloid-derived suppressor cells: linking metabolism to cancer immunology. *Oncoimmunology*. 2(11), e26383.
- Ikeda, Y., Hayashi, I., Kamoshita, E., Yamazaki, A., Endo, H., Ishihara, K., *et al*. (2000). Host stromal bradykinin B2 receptor signaling facilitates tumor-associated angiogenesis and tumor growth. *Cancer Res*. 64, 5178-5185.
- Inai, T., Mancuso, M., Hashizume, H., Baffert, F., Haskell, A., Baluk, P., *et al*. (2004). Inhibition of Vascular Endothelial Growth Factor (VEGF) Signaling in Cancer Causes Loss of Endothelial Fenestrations, Regression of Tumor Vessels, and Appearance of Basement Membrane Ghosts. *American Journal of Pathology*, 165(1), 35-52.
- Infante, J.R., Matsubayashi, H., Sato, N., Tonacia, J., Klein, A.P.., Riall, T.A., *et al.* (2007). Peritumoral fibroblast SPARC expression and patient outcome with resectable pancreatic adenocarcinoma, *J. Clin. Oncol*. 25, 319–325.
- Iyer, N.V., Kotch, L.E., Agani, F., Leung, S.W., Laughner, E., Wenger, R.H., *et al*. (1998). Cellular and developmental control of O_2 homeostasis by hypoxia-inducible factor 1α. *Genes & Development*. 12, 149-162.
- Izumi, D., Ishimoto, T., Miyake, K., Sugihara, H., Eto, K., Sawayama, H., *et al*. (2016). CXCL12/CXCR4 activation by cancer-associated fibroblasts promotes integrin β1 clustering and invasiveness in gastric cancer. *Int J Cancer*. 138, 1207-1219.

- Izumi, Y., Xu, L., di Tomaso, E., Fukumura, D., Jain, R.K. (2002).Herceptin acts as an anti-angiogenic cocktail. *Nature.* 416, 279-280.
- Janda, E., Lehmann, K., Killisch, I., Jechlinger, M., Herzig, M., Downward, J., Beug, H., Grünert, S. (2002). Ras and TGFβ cooperatively regulate epithelial cell plasticity and metastasis: dissection of Ras signalling pathways. *Journal of Cell Biology*. 156(2), 299-313. doi: 10.1083/jcb.200109037.
- Jechlinger, M., Grünert, S., Beug, H. (2002). Mechanisms in epithelial plasticity and metastasis: insights from 3D cultures and expression profililng. *Journal of Mammary Gland Biology and Neoplasia*. 7(4), 415-432.
- Joyce, J.A., Pollard, J.W. (2009). Microenvironmental regulation of metastasis, Nat. Rev. Cancer. 9, 239–252.
- Julien, S., Puig, I., Caretti, E., Bonavanture, J., Nelles, L., van Roy, F., Dargemont, C., de Herreros, A.G., Bellacosa, A., Larue, L. (2007). Activation of NF-kappaB by Akt upregulates Snail expression and induces epithelium mesenchyme transition. *Oncogene*. 26(53), 7445-56. doi: 10.1038/sj.onc.1210546.
- Jung, S.N., Yang, W.K., Kim, J., Kim, H.S., Yun, H., Park, H., Kim, S.S., Choe, W., Kang, I., Ha, J. (2008). Reactive oxygen species stabilize hypoxia-inducible factor-1 alpha protein and stimulate transcriptional activity via AMP-activated protein kinase in DU145 human prostate cancer cells. *Carcinogenesis*. 29(4), 713-721. doi: 10.1093/carcin/bgn032.
- Jung, Y., Kim, J.K., Shiozawa, Y., Wang, J., Mishra, A., Joseph, J., *et* al. (2013). Recruitment of mesenchymal stem cells into prostate tumors promotes metastasis. *Nat Commun*. 4, 1795. doi: 10.1038/ncomms2766.
- Kahlert, U.D., Maciaczyk, D., Doostkam, S., Orr, B.A., Simons, B., Bogiel, T., *et al*. (2012). Activation of canonical Wnt/β-catenin signalling enhances *in vitro* motility of

glioblastoma cells by activation of ZEB1 and other activators of epithelial-to-mesenchymal transition. *Cancer Letters*. 325, 42-53. doi: 10.1016/j.canlet.2012.05.024.

- Kalluri, R., Weinberg, R.A. (2009). The basics of epithelial-mesenchymal transition. *J Clin Invest*. 119(6), 1420-1428. doi:10.1172/JCI39104.
- Kanda, M., Shimizu, D., Tanaka, H., Shibata, M., Iwata, N., Hayashi, M., *et al*. (2016). Metastatic pathway-specific transcriptome analysis identifies MFSD4 as a putative tumor suppressor and biomarker for hepatic metastasis in patients with gastric cancer. *Oncotarget*. 7(12), 13667-13679. doi: 10.18632/oncotarget.7269.
- Karagiannis, G.S., Pastoriza, J.M., Wang, Y., Harney, A.S., Entenberg, D., Pignatelli, J., *et al*. (2017). Neoadjuvant chemotherapy induces breast cancer metastasis through a TMEM-mediated mechanism. *Sci Transl Med*. 9(397). doi:10.1126/scitranslmed.aan0026.
- Karin, M., Greten, F.R. (2005). NF-κβ: linking inflammation and immunity to cancer development and progression. *Nature Reviews Immunology*. 5, 749-759. doi:10.1038/nri1703.
- Karna, P., Zughaier, S., Pannu, V., Simmons, R., Narayan, S., Aneja, R. (2010). Induction of reactive oxygen species-mediated autophagy by a novel microtubule-modulating agent. *J Biol Chem*. 285(24), 18737-18748.
- Karnoub, A.E., Dash, A.B., Vo, A.P., Sullivan, A., Brooks, M.W., Bell, G.W., Richardson, A.L., Polyak, K., Tubo, R., Weinberg, R.A. (2007). Mesenchymal stem cells within tumour stroma promote breast cancer metastasis. *Nature*. 449, 557-563.
- Katheder, N.S., Khezri, R., O'Farrell, F., Schultz, S.W., Jian, A., Rahman, M.M., *et* al. (2017). Microenvironmental autophagy promotes tumor growth. *Nature*. 541, 417-420. doi: 10.1038/nature20815.

- Katt, M.E., Placone, A.L., Wong, A.D., Xu, Z.S., Searson, P.C. (2016). *In vitro* tumor models: Advantages, disadvantages, variables, and selecting the right platform. *Frontiers in Bioengineering and Biotechnology*. 4(12). doi: 10.3389/fbioe.2016.00012.
- Kauppila, S., Stenbäck, F., Risteli, J., Jukkola, A., Risteli, L. (1998). Aberrant type I and type III collagen gene expression in human breast cancer *in vivo*. *J Pathol*. 186, 262-268.
- Kennedy, K.M., Dewhirst, M.W. (2010). Tumor metabolism of lactate: The influence and therapeutic potential for MCT and CD147 regulation. *Future Oncol*. 6(1), 127. doi:10.2217/fon.09.145.
- Kim, J., Escalante, L.E., Dollar, B.A., Hanson, S.E., Hematti, P. (2013). Comparison of breast and abdominal adipose tissue mesenchymal stromal/stem cells in support of proliferation of breast cancer cells. *Cancer Investigation*. 31, 550–554. doi: 10.3109/07357907.2013.830737.
- Kim, J-W., Tchemshyov, I., Semenza, G.L., Dang, C.V. (2006). HIF-1-mediated expression of pyruvate dehydrogenase kinase: A metabolic switch required for cellular adaptation to hypoxia. *Cell Metabolism*. 3, 177-185. doi: 10.1016/j.cmet.2006.02.002.
- Kim, Y.T., Choi, E.K., Kim, J.W., Kim, D.K., Kim, S.H., Yang, W.I. (2002). Expression of E-cadherin and α-, β-, γ-catenin proteins in endometrial carcinoma. *Yosei Medical Journal*. 43(6), 701-711.
- Kimura, S., Fujita, N., Noda, T., Yoshimori, T. (2009). Monitoring autophagy in mammalian cultured cells through the dynamics of LC3. *Methods in Enzymology*. 452. doi: 10.1016/S0076-6879(08)03601-X.
- Kitakata, H., Nemoto-Sasaki, Y., Takahashi, Y., Kondo, T., Mai, M., Mukaida, N. (2002). Essential roles of tumor necrosis factor receptor p55 in liver metastasis of intrasplenic administration of colon 26 cells. *Cancer Research*. 62(22), 6682-6687.

- Klein, C.A. (2003). The systemic progression of human cancer: a focus on the individual disseminated cancer cell--the unit of selection. *Adv Cancer Res*. 89, 35-67.
- Ko, B-S., Lai, I-R., Chang, T-C., Liu, T-A., Chen, S-C., Wang, J., Jan, Y-J., Liou, J-Y. (2011). Involvement of 14-3-3γ overexpression in extrahepatic metastasis of hepatocellular carcinoma. *Human Pathology*. 42, 129-135. doi:10.1016/j.humpath.2010.01.028.
- Kojima, Y., Acar, A., Eaton, E.N., Mellody, K. T., Scheel, C., Ben-Porath, I., *et al*. (2010). Autocrine TGF-β and stromal cell-derived factor-1 (SDF-1) signalling drives the evolution of tumour-promoting mammary stromal myofibroblasts. *P Natl Acad Sci USA*. 107(46), 20009-20014.
- Kokudo, T., Suzuki, Y., Yoshimatsu, Y., Yamazaki, T., Watabe, T., Miyazono, K. (2008). Snail is required for TGFβ-induced endothelial mesenchymal transition of embryonic stem cell derived endothelial cells. *Journal of Cell Science*. 121, 3317-3324. doi: 10.1242/jcs.028282.
- Komatsu, M., Waguri, S., Koike, M., Sou, Y.-S., Ueno, T., Hara, T., *et al.* (2007). Homeostatic levels of p62 control cytoplasmic inclusion body formation in autophagy-deficient mice. *Cell*. 131(6), 1149–63.
- Kondo, Y., Kanzawa, T., Sawaya, R., & Kondo, S. (2005). The role of autophagy in cancer development and response to therapy. *Nature Reviews Cancer*. 5(9), 726–34.
- Kops, G.J.P.L., Medema, R.H., Glassford, J., Essers, M. A. G., Dijkers, P. F., Coffer, P. J., *et al*. (2002). Control of cell cycle exit and entry by protein kinase B-regulated forkhead transcription factors. *Mol Cell Biol*. 22(7), 2025-2036.
- Korpal, M., Lee, E.S., Hu, G., Kang, Y. (2008). The miR-200 family inhibits epithelial-mesenchymal transition and cancer cell migration by direct targeting of E-cadherin

transcriptional repressors ZEB1 and ZEB2. *J Biol Chem*. 283(22), 14910–14914. doi: 10.1074/jbc.C800074200.

- Kosaka, N., Iguchi, H., Yoshioka, Y., Takeshita, F., Matsuki, Y., Ochiya, T. (2010). Secretory mechanisms and intracellular transfer of microRNAs in living cells. *J Biol Chem*. 285(23), 17442-17452.
- Koukourakis, M.I., Giatromanolaki, A., Sivridis, E., Gatter, K.C., Harris, A.L. (2005). Pyruvate dehydrogenase and pyruvate dehydrogenase kinase expression in non small cell lung cancer and tumour-associated stroma. *Neoplasia*. 7(1), 1-6. doi: 10.1593/neo.04373.
- Kruger, S., Abd Elmageed, Z.Y., Hawke, D.H., Wömer, P.M., Abdel-Mageed, A.B., Alt, E.U., Izadpanah, R. (2014). Molecular characterization of exosome-like vesicles from breast cancer cells. *BMC Cancer*. 14(44).
- Kurayoshi, M., Oue, N., Yamamoto, H., Kishida, M., Inoue, A., Asahara, T., Yasui, W., Kikuchi, A. (2006). Expression of Wnt-5a is correlated with aggressiveness of gastric cancer by stimulating cell migration and invasion. *Cancer Res*. 66, 10439-10448. doi:10.1158/0008-5472.CAN-06-2359.
- Kurrey *et al*., 2009). Snail and Slug mediate radioresistance and chemoresistance by antagonizing p53-mediated apoptosis and acquiring a stem-like phenotype in ovarian cancer cells. *Stem Cells.* 27, 2059-2068. doi: 10.1002/stem.154.
- Lau, E.Y.T., Lo, J., Cheng, B.Y.L., Ma, M.K.F., Lee, J.M.F., Ng, Y.J.Y., *et al*. (2016). Cancer-associated fibroblasts regulate tumor-initiating cell plasticity in hepatocellular carcinoma through c-Met/FRA1/HEY1 signaling. *Cell Reports*. 15, 1175-1189. doi: 10.1016/j.celrep.2016.04.019.
- LeBedis, C., Chen, K., Fallavollita, L., Boutros, T., Brodt, P. (2002). Peripheral lymph node stromal cells can promote growth and tumorigenicity of breast carcinoma cells through the release of IGF-1 and EGF. *Int.J.Cancer*. 100, 2-8. doi: 10.1002/ijc.10481

- Lee, H.W., Park, Y.M., Lee, S.J., Cho, H.J., Kim, D-H., Lee, J-I., *et al.* (2013). Alpha-smooth muscle actin (ACTA2) is required for metastatic potential of human lung adenocarcinoma. *Clin Cancer Res*, 19(21), 5879-5889. doi: 10.1158/1078-0432.CCR-13-1181.
- Lee, M., Hwang, J-T., Lee, H-J., Jung, S-N., Kang, I., Chil, S-G., Kim, S-S., Ha, J. (2003). AMP-activated Protein Kinase Activity Is Critical for Hypoxia-inducible Factor-1 Transcriptional Activity and Its Target Gene Expression under Hypoxic Conditions in DU145 Cells. *Journal of Biological Chemistry*. 278(41), 39653-39661. doi: 10.1074/jbc.M306104200.
- Lee, M., Yoon, J-H, (2015). Metabolic interplay between glycolysis and mitochondrial oxidation: The reverse Warburg effect and its therapeutic implication. *World J Biol Chem*. 6(3), 148-161. doi: 10.4331/wjbc.v6.i3.148.
- Leighton, J., Kalla, R.L., Turner, J.M., Fennell, R.H. (1960). Pathogenesis of tumor invasion. *Cancer Res.* 20(5), 575-586.
- Lemieux, E., Cagnol, S., Beaudry, K., Carrier, J., Rivard, N. (2015). Oncogenic KRAS signalling promotes the Wnt/β-catenin pathway through LRP6 in colorectal cancer. *Oncogene*. 34, 4914-4927. doi:10.1038/onc.2014.416.
- Leventhal, K.R., Yu, H., Kass, L., Lakins, J.N., Egeblad, M., Erler, J.T., *et al*. (2009). Matrix crosslinking forces tumor progression by enhancing integrin signalling. *Cell*. 139(5), 891–906. doi:10.1016/j.cell.2009.10.027.
- Levine, A.J., Puzio-Kuter, A.M. (2010). The control of the metabolic switch in cancers by oncogenes and tumor suppressor genes. *Science Metabolism*. 330, 1340-1344.
- Levine, B. (2007). Autophagy and cancer. *Nature*. 446, 745 – 747.
- Li, C.W., Xia, W., Huo, L., Lim, S.O., Wu, Y., Hsu, J.L., *et al*. (2012). Epithelial-mesenchyme transition induced by TNF-α requires NF-κB-mediated transcriptional

upregulation of Twist1. *Cancer Res*. 72(5), 1290–1300. doi: 10.1158/0008-5472.CAN-11-3123.

- Li, H., Zhang, J., Chen, S-W., Liu, L-L., Gao, F., Zhuang, S-M., *et al*. (2015). Cancer-associated fibroblasts provide a suitable microenvironment for tumor development and progression in oral tongue squamous cancer. *J Transl Med*. 13(1), 198.
- Li, J., Liu, H., Yu, J., Yu, H. (2015). Chemoresistance to doxorubicin induces epithelial-mesenchymal transition via upregulation of transforming growth factor β signalling in HCT116 colon cancer cells. *Molecular Medicine Reports*. 12, 192-198. doi: 10.3892/mmr.2015.3356.
- Li, M., Li, M., Yin, T., Shi, H., Wen, Y., Zhang, B., *et al*. (2016). Targeting of cancer-associated fibroblasts enhances the efficacy of cancer chemotherapy by regulating the tumour microenvironment. *Mol Med Rep*. 13, 2476-2484.
- Lilienbaum, A. (2013). Relationship between the proteasomal system and autophagy. *Int J Biochem Mol Biol*. 4(1), 1–26.
- Liu, T-A., Jan, Y-J., Ko, B-S., Chen, S-C., Liang, S-M., Hung, Y-L., *et al*. (2011). Increased expression of 14-3-3β promotes tumor progression and predicts extrahepatic metastasis and worse survival in hepatocellular carcinoma. *The American Journal of Pathology*. 179(6), 2698-2708. doi: 10.1016/j.ajpath.2011.08.010.
- Liu, T-A., Jan, Y-J., Ko, B-S., Liang, S-M., Chen, S-C., Wang, J., Hsu, C., Wu, Y-M., Liou, J-Y. (2013). 14-3-3ε overexpression contributes to epithelial-mesenchymal transition of hepatocellular carcinoma. *PLOS One*. 8(3), e57968. doi:10.1371/journal.pone.0057968.
- Liu, Y., Song, X-D., Liu, W., Zhang, T-Y., Zuo, J. (2003). Glucose deprivation induces mitochondrial dysfunction and oxidative stress in PC12 cell line. *J Cell Mol Med.* 7(1) 49-56.

- Lock, R., Kenific, C.M., Leidal, A.M., Salas, E., Debnath, J. (2014). Autophagy-dependent production of secreted factors facilitates oncogenic RAS-driven invasion. *Cancer Discovery*. 4(4), 466-479. doi: 10.1158/2159-8290.CD-13-0841.
- Lock, R., Roy, S., Kenific, C.M., Su, J.S., Salas, E., Ronen, S.M., Debnath, J. (2010). Autophagy facilitates glycolysis during Ras-mediated oncogenic transformation. *Mol. Biol. Cell.* 22(2), 165-168. doi: 10.1091/mbc.E10-06-0500.
- Loeffler, M., Krüger, J.A., Niethammer, A.G., Reisfeld, R.A. (2006). Targeting tumour-associated fibroblasts improves cancer chemotherapy by increasing intratumoral drug uptake. *J Clin Invest*. 116(7), 1955-1962.
- Lozy, F., Karantza, V. (2012). Autophagy and cancer cell metabolism. *Seminars in Cell & Developmental Biology*. 23(4), 395–401.
- Lu, H., Forbes, R.A., Verma, A. (2002). Hypoxia-inducible factor 1 activation by aerobic glycolysis implicates the Warburg effect in carcinogenesis. *The journal of biological chemistry*. 277(26), 23111–23115.
- Lu, X., Kang, Y. (2010). Hypoxia and hypoxia-inducible factors: master regulators of metastasis. *Clin Cancer Res*. 16(24). doi: 10.1158/1078-0432.CCR-10-1360.
- Lu, Y., Azad, N., Wang, L., Iyer, A.K.V., Castranova, V., Jian, B-H., Rojanaskakul, Y. (2010). Phosphatidylinositol-3-Kinase/Akt regulates Bleomycin-induced fibroblast proliferation and collagen production. *Am J Respir Cell Mol Biol*. 42, 432-441.
- Luga, V., Wrana, J.L. (2013). Tumor–stroma interaction: revealing fibroblast-secreted exosomes as potent regulators of wnt-planar cell polarity signaling in cancer metastasis. *Cancer Res*. 73, 6843-6847.
- Luga, V., Zhang, L., Viloria-Petit, A.M., Ogunjima, A. A., Inanlou, M. R., Chiu, E., *et al*. (2012). Exosomes mediate stromal mobilization of autocrine Wnt-PCP signalling in breast cancer cell migration. *Cell*. 151, 1542-1556.

- Lum, J.J., Bui, T., Gruber, M., Gordan, J.D., DeBererdinis, R.J., Covello, K.L., Simon, M.C., Thompson, C.B. (2007). The transcription factor HIF-1α plays a critical role in the growth factor-dependent regulation of both aerobic and anaerobic glycolysis. *Genes & Development*. 21, 1037-1049. doi: 10.1101/gad.1529107.
- Löhr. M., Schmidt, C., Ringel, J., Kluth, M., Müller, P., Nizze, H. *et al.* (2001). Transforming growth factor-β1 induces desmoplasia in an experimental model of human pancreatic carcinoma. *Cancer Res*. 61, 550-555.
- MacDonald, T.J., Brown, K.M., LaFleur, B., Petersen, K., Lawlor, C., Chen, Y., Packer, R.J., Cogen, P., Stephen, D.A. (2001). Expression profiling of medulloblastoma: PDGRFA and the RAS/MAPK pathway as therapeutic targets for metastatic disease. *Nature Genetics*. 29, 143-152. doi: 10.1038/ng731.
- Maes, H., Rubio, N., Garg, A.D., Agostinis, P. (2013). Autophagy: shaping the tumor microenvironment and therapeutic response. *Trends in Molecular Medicine.* 19(7), 428-446. doi: 10.1016/j.molmed.2013.
- Maneix, L., Catic, A. (2016). Touch and go: Nuclear proteolysis in the regulation of metabolic genes and cancer. *FEBS Letters*. 590, 908-923. doi: 10.1002/1873-3468.12087.
- Mani, S.A., Guo, W., Liao, M.J., Eaton, E.N., Ayyanan, A., Zhou, A.Y., *et al*. (2008). The epithelial-mesenchymal transition generates cells with properties of stem cells. *Cell*. 133(4), 704-715. doi: 10.1016/j.cell.2008.03.027.
- Martin, O.J., Lee, A., McGraw, T.E. (2006). GLUT4 distribution between the plasma membrane and the intracellular compartments is maintained by an insulin-modulated bipartite dynamic mechanism. *The Journal of Biological Chemistry*. 281(1), 481-490.
- Martinez-Outschoorn, U.E., Balliet, R.M., Rivadeneira, D.B., Chiavarina, B., Pavlides, Wang, C., *et* al. (2010). Oxidative stress in cancer associated fibroblasts drives tumor-stroma co-evolution. *Cell Cycle*. 9(16), 3256-3276. Doi: 10.4161/cc9.16.12553.

- Martinez-Outschoorn, U.E., Pavlides, S., Whitaker-Menezes, D., Daumer, K. M., Milliman, J. N., Chiavarina, B., *et al*. (2010). Tumor cells induce the cancer associated fibroblast phenotype via caveolin-1 degradation: Implications for breast cancer and DCIS therapy with autophagy inhibitors. *Cell Cycle*. 9(12), 2423-2433.
- Martinez-Outschoorn, U.E., Trimmer, C., Li, Z., Whitaker-Menezes, D., Chiavarina, B., Zhou, J., *et al*. (2010). Autophagy in cancer associated fibroblasts promotes tumour cell survival: Role of hypoxia, HIF1 induction and NFkappaB activation in the tumour stromal microenvironment. *Cell Cycle*. 9(17), 3515-3533.
- Mathew, R., White, E. (2011). Autophagy in tumorigenesis and energy metabolism: friend by day, foe by night. Current Opinion in Genetics & Development. 21(1), 113–9.
- Matoba, S., Kang, J-G., Patino, W.D., Wragg, A., Boehm, M., Gavrilova, O., Hurley, P.J., Bunz, F., Hwang, P.M. (2006). p53 regulates mitochondrial respiration. *Science*. 312(5780), 1650-1653. doi: 10.1126/science.1126863.
- Matsumoto, G., Wada, K., Okuno, M., Kurosawa, M., Nukina, N. (2011). Serine 403 Phosphorylation of p62/SQSTM1 Regulates Selective Autophagic Clearance of Ubiquitinated Proteins. *Molecular Cell.* 44, 279-289. doi: 10.1016/j.molcel.2011.07.039.
- McAllister, S.S., Weinberg, R. (2010). Tumor-host interactions: A far-reaching relationship. *J Clin Oncol*. 28(26), 4022-4028.
- McAllister, S.S., Weinberg, R.A. (2014). The tumour-induced systemic environment as a critical regulator of cancer progression and metastasis. *Nature Cell Biology*. 16(8), 717-727.
- McCarty, M.F., Somcio, R.J., Stoeltzing, O., Wey, J., Fan, F., Liu, W., Bucana, C., Ellis, L.M. (2007). Overexpression of PDGF-BB decreases colorectal and pancreatic cancer growth by increasing tumor pericyte content. *J. Clin. Invest*. 117, 2114–2122.

- McFate, T., Mohyeldin, A., Lu, H., Thakar, J., Henriques, J., Halim, N.D., *et al*. (2008). Pyruvate dehydrogenase complex activity controls metabolic and malignant phenotype in cancer cells. *The Journal of Biological Chemistry*. 283(33), 22700-22708. doi: 10.1074/jbcM801765200.
- McInroy, L., Määttä, A. (2007). Down-regulation of vimentin expression inhibits carcinoma cell migration and adhesion. *Biochemical and Biophysical Research Communications*. 360, 109-114. doi:10.1016/j.bbrc.2007.06.036.
- Medema, R.H., Kops, G.J., Bos, J.L., Burgering, B.M. (2000). AFX-like forkhead transcription factors mediate cell-cycle regulation by Ras and PKB through p27Kip1. *Nature*. 404(6779), 782-787.
- Medici, D., Hay, E.D., Olsen, B.R. (2008). Snail and slug promote epithelial-mesenchymal transition through β-catenin–t-cell factor-4-dependent expression of transforming growth factor-β3. *Molecular Biology of the Cell*. 19, 4875-4887. doi: 10.1091/mbc.E08-05-0506.
- Mellor, H.R., Callaghan, R. (2011). Accumulation and distribution of doxorubicin in tumour spheroids: The influence of acidity and expression of P-glycoprotein. *Cancer Chemother Pharmacol.* 68, 1179-1190. doi: 10.1007/s00280-011-1598-8.
- Mendler, A.N., Hu, B., Prinz, P.U., Kreutz, M., Gottfried, E., Noessner, E. (2012). Tumor lactic acidosis suppresses CTL function by inhibition of p38 and JNK/c-Jun activation. *Int J Cancer*. 131, 633-640.
- Mercier, I., Casimiro, M.C., Wang, C., Rosenberg, A.L., Quong, J., Minkeu, A., *et al*. (2008). Human breast cancer-associated fibroblasts (CAFs) show caveolin-1 down-regulation and RB tumor suppressor functional inactivation: Implications for the response to hormonal therapy. *Cancer Biol Ther*. 7, 1212–1225. doi: 10.4161/cbt.7.8.6220

- Meredith, D., Bell, P., McClure, B., Wilkins, R. (2002). Functional and molecular characterisation of lactic acid transport in bovine articular chondrocytes. *Cell. Physiol. Biochem*. 12, 227–234. doi: 10.1159/000066282
- Merezhinskaya, N., Ogunwuyi, S.A., Fishbein, W.N. (2006). Expression of monocarboxylate transporter 4 in human platelets, leukocytes, and tissues assessed by antibodies raised against terminal versus pre-terminal peptides. *Molecular Genetics and Metabolism*. 87(2), 152-161. doi:10.1016/j.ymgme.2005.09.029
- Metallo, C.M., Gameiro, P.A., Bell, E.L., Mattaini, K.R., Yang, J., Hiller, K., (2012). Reductive glutamine metabolism by IDH1 mediates lipogenesis under huypoxia. *Nature*. 481(7381), 380-384. doi: 10.1038/nature10602.
- Minna, J.D., Kurie, J.M., Jacks, T. (2003). A big step in the study of small cell lung cancer. *Cancer Cell*. 4(3), 163-166. doi: 10.1016/s1535-6108(03)00221-6.
- Mitchell, M.I., Engelbrecht, A-M. (2017). Metabolic hijacking: A survival strategy cancer cells exploit? *Critical Reviews in Oncology/Hematology.* 109, 1–8. doi: 10.1016/j.critrevonc.2016.11.010.
- Miyazono, K. (2000). Positive and negative regulation of TGF-β signalling. *Journal of Cell Science*. 113, 1101-1109.
- Miyoshi, A., Kitajima, Y., Sumi, K., Sato, K., Hagiwara, A., Koga, Y., Miyazaki, K. (2004). Snail and SIP1 increase cancer invasion by upregulating MMP family in hepatocellular carcinoma cells. *British Journal of Cancer*. 90, 1265-1273. doi: 10.1038/sj.bjc.6601685.
- Mizushima, N., Levine, B., Cuervo, A. M., Klionsky, D. J. (2008). Autophagy fights disease through cellular self-digestion. *Nature.*, *451*(7182), 1069–1075.
- Modur, V., Nagarajan, R., Evers, B.M., Milbrandt, J. (2002). FOXO proteins regulate TRAIL expression: Implications for PTEN mutation in prostate cancer. *J Biol Chem*. 277, 47928–47937.

- Morrison, D.K. (2009). The 14-3-3 proteins: integrators of diverse signalling cues that impact cell fate and cancer development. *Trends Cell Biol*. 19(1), 16-23. doi: 10.1016/j.tcb.2008.10.003.
- Morselli, E., Galluzzi, L., Kepp, O., Vicencio, J.-M., Criollo, A., Maiuri, M.C., Kroemer, G. (2009). Anti- and pro-tumor functions of autophagy. *Biochimica et Biophysica Acta*. 1793(9), 1524–32.
- Muehlberg, F.L., Song, Y.H., Krohn, A., Pinilla, S.P. Droll, L.H., Leng, X., *et al*. (2009). Tissue-resident stem cells promote breast cancer growth and metastasis. *Carcinogenesis*. 30(4), 589-597. doi: 10.1093/carcin/bgp036.
- Mukhopadhyay, S., Panda, P.K., Sinha, N., Das, D.N., Bhutia, S.K. (2014). Autophagy and apoptosis: Where do they meet? *Apoptosis*. 19, 555-566. doi: 10.1007/s10495-014-0967-2
- Müller, A., Homey, B., Soto, H., Ge, N., Catron, D., Buchanan, M. E., *et al*. (2001). Involvement of chemokine receptors in breast cancer metastasis. Nature. 401, 50-56.
- Muta, H., Noguchi, M., Kanai, Y., Ochiai, A., Nawata, H., Hirohashi, S. (1996). E-cadherin gene mutations in signet ring cell carcinoma of the stomach. *Jpn J Cancer Res*. 87(8), 843-848.
- Müerköster, S.S., Werbing, V., Koch, D., Sipos, B., Ammerpohl, O., Kalthoff, H., Tsao, M-S., Fölsch, U.R., Schäfer, H. (2008). Role of myofibroblasts in innate chemoresistance of pancreatic carcinoma – Epigenetic downregulation of caspases. *Int J Cancer*. 123, 1751-1760. doi: 10.1002/ijc.23703.
- Möhle, R., Failenschmid, C., Bautz, F., Kanz, L. (1999). Overexpression of the chemokine receptor CXCR4 in B cell chronic lymphocytic leukemia is associated with increased functional response to stromal cell-derived factor-1 (SDF-1). *Leukemia*. 13, 1954-1959.

- Nagy, J.A., Chang, S-H., Dvorak, A.M., Dvorak, H.F. (2009). Why are tumour blood vessels abnormal and why is it important to know? *British Journal of Cancer.* 100, 865-869. doi:10.1038/sj.bjc.6604929.
- Nakagawa, H., Liyanarachchi, S., Davuluri, R.V., Auer, H., Martin Jr, E.W., de la Chapelle, A., Frankel, W.L. (2004). Role of cancer-associated stromal fibroblasts in metastatic colon cancer to the liver and their expression profiles. *Oncogene*. 23, 7366-7377.
- Nakamura, N., Ramaswamy, S., Vazquez, F., Signoretti, S., Loda, M., Sellers, W.R. (2000). Forkhead transcription factors are critical effectors of cell death and cell cycle arrest downstream of PTEN. *Mol Cell Biol*. 20(23), 8969-8982.
- Nawshad, A., LaGamba. D., Hay, E.D. (2004). Transforming growth factor b (TGFb) signalling in palatal growth, apoptosis and epithelial mesenchymal transformation (EMT). *Archives of Oral Biology*. 49, 675-689. doi:10.1016/j.archoralbio.2004.05.007.
- Neri, S., Hashimoto, H., Kii, H., Watanabe, H., Masutomi, K., Kuwata, T., *et al.* (2016). Cancer cell invasion driven by extracellular matrix remodelling is dependent on the properties of cancer-associated fibroblasts. *J Cancer Res Clin Oncol*. 142, 437-446.
- Nguyen, D.X., Bos, P.D., Massagué, J. (2009). Metastasis: from dissemination to organ-specific colonization. *Nature Reviews Cancer*. 9, 274-284.
- Niessen, K., Fu, Y., Chang, L., Hoodless, P., McFadden, D., Karsan, A. (2008). Slug is a direct Notch target required for initiation of cardiac cushion cellularization. *Journal of Cell Biology*. 182(2), 315-325. doi: 10.1083/jcb.200710067.
- Nieto, M.A. (2002). The Snail superfamily of zincfinger transcription factors. *Nat Rev Mol Cell Biol.* 3, 155-166. doi: 10.1038/nrm757.
- O'Brien, V., Frisch, S.M., Juliano, R.L. (1996). Expression of the integrin α5 subunit in HT29 colon carcinoma cells supresses apoptosis triggered by serum deprivation. *Exp Cell Res*. 224, 208-213.

- Oettgen, H.F., Stephenson, P.A., Schwartz, M.K., Leeper, R. D., Tallal, L., Tan, C. C., *et al*. (1970). Toxicity of E. coli L-asparaginase in man. *Cancer*. 25(2), 253-278.
- Oft, M., Heider, K-H., Beug, H. (1998). TGFβ signalling is necessary for carcinoma cell invasiveness and metastasis. *Current Biology*. 8, 1243-1252.
- Oguma, K., Oshima, H., Aoki, M., Uchio, R., Naka, K., Nakamura, S., Hirao, A., Saya, H., Taketo, M.M., Oshima, M. (2008). Activated macrophages promote Wnt signalling through tumour necrosis factor-α in gastric tumour cells. *The EMBO Journal*. 27(12), 1671-1681. doi: 10.1038/ emboj.2008.10.
- Okon, I.S., Coughlan, K.A., Zhang, M., Wang, Q., Zou, M-H. (2015). Gefitinib-mediated reactive oxygen species (ROS) instigates mitochondrial dysfunction and drug resistance in lung cancer cells. *J Biol Chem*. 290(14), 9101-9110.
- Olumi, A.F., Grossfeld, G.D., Hayward, S.W., Carroll, P.R., Tlsty, T.D., Cunha, G.R. (1999). Carcinoma-associated fibroblasts direct tumor progression of initiated human prostatic epithelium. *Cancer Res*. 59, 5002-5011.
- Orimo, A., Gupta, P.B., Sgroi, D.C., Arenzana-Seisdedos, F., Delaunay, T., Naeem, R., *et al*. (2005). Stromal fibroblasts present in invasive human breast carcinomas promote tumour growth and angiogenesis through elevated SDF-1/CXCL12 secretion. *Cell*. 121, 335-348.
- Orimo, A., Weinberg, R. (2006). Stromal fibroblasts in cancer: A novel tumor-promoting cell type. *Cell Cycle*. 5(15), 1597-1601.
- Paget, S. (1889). The distribution of secondary growths in cancer of the breast. *Lancet*. 133(3421), 571-573.
- Palmieri, F., Bisaccia, F., Capobianco, L., Dolce, V., Fiermonte, G., Iacobazzi, V., Indiveri, C., Palmieri, L. (1996). Mitochondrial metabolite transporters. *Biochim. Biophys. Acta*. 1275, 127–132.

- Pan, T-L., Wang, P-W., Huang, C-C., Yeh, C-T., Hu, T-H., Yu, J-S. (2012). Network analysis and proteomic identification of vimentin as a key regulator associated with invasion and metastasis in human hepatocellular carcinoma cells. *Journal of Proteomics*. 75, 4676-4692. doi:10.1016/j.jprot.2012.02.017.
- Pankiv, S., Clausen, T.H., Lamark, T., Brech, A., Bruun, J-A., Outzen, H., Øvervatn, A., Bjørkøy, G., Johansen, T. (2007). p62/SQSTM1 Binds Directly to Atg8/LC3 to Facilitate Degradation of Ubiquitinated Protein Aggregates by Autophagy. *The Journal of Biological Chemistry*. 282(33), 24131-24145.
- Papandreou, I., Cairns, R.A., Fontana, L., Lim, A.L., Denko, N.C. (2006). HIF-1 mediates adaptation to hypoxia by actively downregulating mitochondrial oxygen consumption. *Cell Metabolism*. 3, 187-197. doi: 10.1016/j.cmet.2006.01.012.
- Park, S-M., Gaur, A.B., Lengyel, E., Peter, M.E. (2008). The miR-200 family determines the epithelial phenotype of cancer cells by targeting the E-cadherin repressors ZEB1 and ZEB2. *Genes Dev*. 22(7), 894–907. doi: 10.1101/gad.1640608.
- Patel, S. (2014). Role of proteomics in biomarker discovery: prognosis and diagnosis of neuropsychiatric disorders. *Adv Protein Chem Struct Biol*. 94, 39-75. doi: 10.1016/B978-0-12-800168-4.00003-2.
- Paterson, E.L., Kolesnikoff, N., Gregory, P.A., Bert, A.G., Khew-Goodall, Y., Goodall, G.J. (2008). The microRNA-200 family regulates epithelial to mesenchymal transition. *The Scientific World JOURNAL*. 8, 901–904. doi: 10.1100/tsw.2008.115.
- Pavlides, S., Vera, I., Gandara, R., Sneddon, S., Pestell, R.G., Mercier, I., *et al*. (2012). Warburg meets autophagy: cancer-associated fibroblasts accelerate tumor growth and metastasis via oxidative stress, mitophagy, and aerobic glycolysis. *Antioxidants & REDOX Signalling*. 16(11), 1264-1284. doi: 10.1089/ars.2011.4243.
- Pavlides, S., Witaker-Menezes, D., Castello-Cros, R., Flomenberg, N., Witkiewics, A.K., Frank, P.G., *et al*. (2009). The reverse Warburg effect: Aerobic glycolysis in cancer

associated fibroblasts and the tumor stroma. *Cell Cycle*. 8(23), 3984-4001. doi: 10.4161/cc.8.23.10238.

- Pećina-Šlaus, N. (2003). Tumor suppressor gene E-cadherin and its role in normal and malignant cells. *Cancer Cell International.* 3(17). doi: 10.1186/1475-2867-3-17.
- Peddareddigari, V.G., Wang, D., DuBois, R.N. (2010). The tumor microenvironment in colorectal carcinogenesis. *Cancer Microenvironment*. 3, 149-166. doi: 10.1007/s12307-010-0038-3.
- Pedraza-Fariña, L.G. (2006). Mechanisms of oncogenic cooperation in cancer initiation and metastasis. *Yale Journal of Biology and Medicine*. 79, 95-103.
- Pehlivanova., V.N., Tsoneva, I.H., Tzoneva, R.D. (2012). Multiple effects of electroporation on the adhesive behaviour of breast cancer cells and fibroblasts. *Cancer Cell International*. 12(9). doi: 10.1186/1475-2867-12-9.
- Peiris-Pagès, M., Smith, D.L., Győrffy, B., Sotgia, F., Lisanti, M.P. (2015). Proteomic identification of prognostic tumour biomarkers, using chemotherapy-induced cancer-associated fibroblasts. *Aging*. 7(10), 816-838.
- Petrides, C., Neofytou, K., Agrogiannis, G., Petrou, A., Angelou, A., Kavantzas, N., *et al*. (2016). Monocarboxylate transporter 4 as a prognostic biomarker in patients with colorectal cancer and liver metastasis. *International Journal of Surgery Open*. 5, 37-43. doi: 10.1016/j.ijso.2016.10.001
- Phuphanich, S., Baker, S.D., Grossman, S.A., Carson, K. A., Gilbert, M. R., Fisher, J. D., *et al*. (2005). Oral sodium phenylbutyrate in patients with recurrent malignant gliomas: A dose escalation and pharmacologic study. *Neuro-Oncology*. 7, 177-182.
- Phypers, B., Pierce, J.M.T. (2006). Lactate physiology in health and disease. *Contin Educ Anaesth Crit Care Pain*. 6,128–32. doi: 10.1093/bjaceaccp/mkl018

- Pickard, A., Cichon, A-C., Barry, A., Kieran, D., Patel, Hamilton, P., Salto-Tellez, M., James, J., McCance, D.J. (2012). Inactivation of Rb in stromal fibroblasts promotes epithelial cell invasion. *EMBO*. 31, 3092-3103. doi: 10.1038/emboj.2012.153
- Pierre, K., Parent, A., Jayet, P-Y., Halestrap, A.P., Scherrer, U., Pellerin, L. (2007). Enhanced expression of three monocarboxylate transporter isoforms in the brain of obese mice. *J Physiol*. 583(2), 469–486. doi: 10.1113/jphysiol.2007.138594
- Pietras, K., Pahler, J., Bergers, G., Hanahan, D. (2008). Functions of paracrine PDGF signaling in the proangiogenic tumor stroma revealed by pharmacological targeting. *PLoS Med*. 5, e19.
- Pinilla, S., Alt, E., Abdul Khalek F.J., Jotzu, C., Muehlberg, F., Beckmann, C., Song, Y.H. (2009). Tissue resident stem cells produce CCL5 under the influence of cancer cells and thereby promote breast cancer cell invasion. *Cancer Lett*. 284(1), 80-85. doi: 10.1016/j.canlet.2009.04.013.
- Planutis, K., Planutiene, M., Nguyen, A.V., Moyer, M.P. Holcombe, R.F. (2013). Invasive colon cancer, but not non-invasive adenomas induce a gradient effect of Wnt pathway receptor frizzled 1 (Fz1) expression in the tumor microenvironment. *Journal of Translational Medicine*. 11(50). doi: 10.1186/1479-5876-11-50.
- Poola *et al*., (2005). Identification of MMP-1 as a putative breast cancer predictive marker by global gene expression analysis. *Nat Med*. 11, 481–483.
- Potente, M., Urbich, C., Sasaki, K-I., Hofmann, W. K., Heeschen, C., Aicher, A., *et al*. (2005). Involvement of Foxo transcription factors in angiogenesis and postnatal neovascularization. *J Clin Invest*. 115(9), 2382-2392.
- Price, N.T., Jackson, V.N., Halestrap, A.P. (1998). Cloning and sequencing of four new mammalian monocarboxylate transporter (MCT) homologues confirms the existence of a transporter family with an ancient past. *Biochem. J*. 329, 321–328.

- Puissant, A., Fenouille, N., Auberger, P. (2012). When autophagy meets cancer through p62/SQSTM1. *AM J Cancer Res.* 2(4), 397-413.
- Qian, N., Ueno, T., Kawaguchi-Sakita, N., Kawashima, M., Yoshida, N., Mikami, Y., *et al.* (2011). Prognostic significance of tumor/stromal caveolin-1 expression in breast cancer patients. *Cancer Sci*. 102(8), 1590-1596.
- Quail, D.F., Joyce J.A. (2013). Microenvironmental regulation of tumor progression and metastasis. *Nat Med.* 19(11), 1423-1437.
- Rabinowitz, J. D., White, E. (2010). Autophagy and metabolism. *Science*. 330(6009), 1344–1348.
- Rabinowitz, J.D., White, E. (2010). Autophagy and metabolism. *Science.* 330(6009), 1344–8.
- Randle, P.J. (1986). Fuel selection in animals. *Biochemical Society Transactions*. 14, 799-806.
- Rathmell, J.C., Fox, C.J., Plas, D.R., Hammerman, P.S., Cinalli, R.M., Thompson, C.B. (2003). Akt-directed glucose metabolism can prevent Bax conformation change and promote growth factor-independent survival. *Mol Cell Biol*. 23(20), 7315-7328.
- Raychaudhuri, R., Chaudhary, N., Gurjar, M., D'Souza, R., Limzerwala, J., Maddika, S., Dalal, S.N. (2016). 14-3-3δ loss leads to activation of the epithelial to mesenchymal transition due to the stabilization of c-Jun. *J Biol Chem*. 291(31), 16068-16081. doi: 10.1074/jbc.M116.723767.
- Reagan-Shaw, S., Nihal, M., Ahmad, N. (2007). Dose translation from animal to human studies revisited. *The FASEB Journal*. 22(3), 659-661. doi: 10.1096/fj.07-9574LSF.
- Redig, A.J., McAllister, S.S. (2013). Breast cancer as a systemic disease: a view of metastasis. *J Intern Med*. 274(2), 113-126. doi:10.1111/joim.12084.

- Reymond, N., Borda d'Agua, B., Ridley, A.J. (2013). Crossing the endothelial barrier during metastasis. *Nat Rev Cancer.* 13, 858-870.
- Richard, D.E., Berra, E., Pouysségur, J. (2000). Non-hypoxic pathway mediates the induction of hypoxia inducible factor 1 alpha (HIF-1α) in vascular smooth muscle cells. *J Biol Chem*. 275(35), 26765-26771. doi: 10.1074/jbc.M003325200.
- Robinson, B.D., Sica, G.L., Liu, Y-F., Rohan, T.E., Gertler, F.B., Condeelis, J.S., Jones, J.G. (2009). Tumor microenvironment of metastasis in human breast carcinoma: a potential prognostic marker linked to hematogenous dissemination. *Clin Cancer Res*. 15(7), 2433–2441. doi:10.1158/1078-0432.CCR-08-2179.
- Robinson, S.P., Ludwig, C., Paulsson, J., Östman, A. (2008). The effects of tumor-derived platelet-derived growth factor on vascular morphology and function in vivo revealed by susceptibility MRI. *Int. J. Cancer*. 122, 1548–1556.
- Rohan, T.E., Xue, X., Lin, H-M., D'Alfonso, T., Ginter, P.S., Oktay, M.H., *et al*. (2014). Tumor microenvironment of metastasis and risk of distant metastasis of breast cancer. *J Natl Cancer Inst*. 106(7), dju136. doi: 10.1093/jnci/dju136.
- Ronnov-Jessen, L., Petersen, O.W., Bissell, M.J. (1996). Cellular changes involved in conversion of normal to malignant breast: Importance of the stromal reaction. *Physiological Reviews*. 76(1), 69-125.
- Saigusa, S., Toiyama, Y., Tanaka, K., Yokoe, T., Okugawa, Y., Kawamoto, A., *et al*. (2010). Stromal CXCR4 and CXCL12 expression is associated with distant recurrence and poor prognosis in rectal cancer after chemoradiotherapy. *Ann Surg Oncol*. 17, 2051-2058.
- Saika, S., Okada, Y., Mtyamoto, T., Yamanaka, O., Ohnisht, Y., Ooshima, A., Liu, C-Y., Weng, D., Kao, W.W-Y. (2004). Role of p38 MAP kinase in regulation of cell migration and proliferation in healing corneal epithelium. *Investigative Opthalmology & Visual Science*. 45(1), 100-109. doi: 10.1167/iovs.03-0700.

- Saito, A., Kanai, Y., Maesawa, C., Ochiai, A., Torii, A., Hirohashi, S. (1999). Disruption of E-Cadherin-mediated cell adhesion systems in gastric cancers in young patients. *Jpn J Cancer Res.* 90, 993-999.
- Salmaggi, A., Maderna, E., Calatozzolo, C., Gaviani, P., Canazza, A., Milanesi, I., *et al.* (2009). CXCL12, CXCR4 and CXCR7 expression in brain metastases. *Cancer Biol Ther*. 8(17), 1608-1614.
- Schafer, Z.T., Grassian, A.R., Song, L., Jiang, Z., Gerhart-Hines, Z., Irie, H.Y., Gao, S., Puigserver, P., Brugge, J.S. (2009). Antioxidant and oncogene rescue of metabolic defects caused by loss of matrix attachment. *Nature.* 461(7260), 109-113. doi: 10.1038/nature08268
- Scherz-Shouval, R., Shvets, E., Fass, E., Shorer, H., Gil, L., Elazar, Z. (2007). Reactive oxygen species are essential for autophagy and specifically regulate the activity of Atg4. *The EMBO Journal*. 26(7), 1749-1760.
- Schioppa, T., Uranchimeg, B., Saccani, A., Biswas, S. K., Doni, A., Rapisarda, A., *et al*. (2003). Regulation of the Chemokine Receptor CXCR4 by Hypoxia. *J Exp Med*. 198(9), 1391-1402.
- Schmidt, M., Fernandez de Mattos, S., van der Horst, A., Klompmaker, R., Kops, G. J. P. L., Lam, E. W-F., *et al*. (2002). Cell cycle inhibition by FoxO forkhead transcription factors involves downregulation of cyclin D. *Mol Cell Biol*. 22(22), 7842-7852.
- Schwartzenberg-Bar-Yoseph, F., Armoni, M., Karnieli, E. (2004). The tumor suppressor p53 down-regulates glucose transporters *GLUT1* and *GLUT4* gene expression. *Cancer Research*. 66, 2627-2633.
- Seagroves, T.N., Ryan, H.E., Lu, H., Wouters, B.G., Knapp, M., Thibault, P., Laderoute, K., Johnson, R.S. (2001). Transcription factor HIF-1 is a necessary mediator of the Pasteur effect in mammalian cells. *Molecular and Cellular Biology*. 21(10), 3436-3444. doi: 10.1128/MCB.21.10.3436–3444.2001.

- Shi, Y., Massagué, J. (2003). Mechanisms of TGF-β signalling from cell membrane to the nucleus. *Cell*. 113, 685-700.
- Shiga, K., Hara, M., Nagasaki, T., Sato, T., Takahashi, H., Takeyama, H. (2015). Cancer-associated fibroblasts: Their characteristics and their roles in tumour growth. *Cancers*. 7, 2443-2458. doi:10.3390/cancers7040902
- Shintani, T., Klionsky, D.J. (2004). Autophagy in health and disease: a double-edged sword. Science. 306(5698), 990–995.
- Silva, T.A., Smuczek, B., Valadäo, I.C., Dzik, L.M., Iglesia, R.P., Cruz, M.C., *et al*. (2016). AHNAK enables mammary carcinoma cells to produce extracellular vesicles that increase neighboring fibroblast cell motility. *Oncotarget*. 7(31), 49998-50016.
- Singer, C.F., Kronsteiner, N., Marton, E., Kubista, M., Cullen, K.J., Hirtenlehner, K., Seifert, M., Kubista, E. (2002). MMP-2 and MMP-9 expression in breast cancer-derived human fibroblasts is differentially regulated by stromal-epithelial interactions. *Breast Cancer Res Treat*. 72, 69–77.
- Singh, M., Lima, A., Molina, R., Hamilton, P., Clermont, A.C., Devasthali, V., *et al*. (2010). Assessing therapeutic responses in *Kras* mutant cancers using genetically engineered mouse models. *Nature Biotechnology*. 28(6), 585-595. doi:10.1038/nbt.1640.
- Singh, S., Srivastava, S.K., Bhardwaj, A., Owen, L.B., Singh, A.P. (2010). CXCL12-CXCR4 signalling axis confers gemcitabine resistance to pancreatic cancer cells: a novel target for therapy. *Brit J Cancer*. 103, 1671-1679.
- Sobral-Leite, M., Wesseling, J., Smit, V.T.H.B.M., Nevanlinna, H., van Miltenburg, M.H., Sanders, J., *et al*. (2015). Annexin A1 expression in a pooled breast cancer series: association with tumor subtypes and prognosis. *BMC Medicine*. 13(156). doi: 10.1186/s12916-015-0392-6.

- Sommermann, T.G., O'Neill, K., Plas, D.R., Cahir-McFarland, E. (2011). IKKb and NF-kB transcription govern lymphoma cell survival through AKT-induced plasma membrane trafficking of GLUT1. *Cancer Res*. 71(23), 7291–7300.
- Song, J. (2007). EMT or apoptosis: a decision for TGF-β. *Cell Research*. 17, 289-290. doi: 10.1038/cr.2007.25.
- Sonveaux, P., Copetti, T., De Saedeleer, C.J., Végran, F., Verrax, J., Kennedy, K.M., *et al*. (2012). Targeting the lactate transporter MCT1 in endothelial cells inhibits lactate-induced HIF-1 activation and tumor angiogenesis. *PLoS ONE.* 7(3), e33418. doi:10.1371/journal.pone.0033418
- Sonveaux, P., Végran, F., Schroeder, T., Wergin, M.C., Verrax, J., Rabbani, Z.N., *et al.* (2008). Targeting lactate-fueled respiration selectively kills hypoxic tumor cells in mice. *The Journal of Clinical Investigation*. 118(12), 3930-3942.
- Sossey-Alaoui, K., Downs-Kelly, E., Das, M., Izem, L., Tubbs, R., Plow, E.F. (2011). WAVE3, an actin remodeling protein, is regulated by the metastasis suppressor microRNA, miR-31, during the invasion-metastasis cascade. *Int. J. Cancer*. 129, 1331-1343. doi: 10.1002/ijc.25793.
- Sotgia, K., Hara, M., Nagasaki, T., Sato, T., Takahashi, H., Takeyama, H. (2012). Cancer-associated fibroblasts: their characteristics and their roles in tumor growth. *Cancers*. 7, 2443–2458. doi:10.3390/cancers7040902
- Spano, D., Heck, C., De Antonellis, P., Christofori, G., Zollo, M. (2012). Molecular networks that regulate cancer metastasis. *Seminars in Cancer Biology*. 22, 234-249. doi: 10.1016/j.semcancer.2012.03.006.
- Stemke-Hale, K., Gonzalez-Angulo, A.M., Lluch, A., Neve, R.M., Kuo, W-L., Davies, M., *et al.* (2008). An integrative genomic and proteomic analysis of PIK3CA, PTEN, and AKT mutations in breast cancer. *Cancer Res*. 68(15), 6084-6091.

- Stemmler, M.P. (2008). Cadherins in development and cancer. *Mol. BioSyst*. 4, 835–850. doi: 10.1039/b719215k.
- Stephanenko, A.A., Dmitrenko, V.V. (2015). Pitfalls of the MTT assay: Direct and off-target effects of inhibitors can result in over/underestimation of cell viability. *Gene*. 574, 193-203. doi: 10.1016/j.gene.2015.08.009.
- Stockinger, A., Eger, A., Wolf, J., Beug, H., Foisner, R. (2001). E-cadherin regulates cell growth by modulating proliferation-dependent β–catenin transcriptional activity. *The Journal of Cell Biology*. 154(6), 1185–1196. doi: 10.1083/jcb.200104036.
- Strnad, H., Lacina, L., Kolář, M., Čada, Z., Čestmír,V., Dvořánková, B., *et al*. (2010). Head and neck squamous cancer stromal fibroblasts produce growth factors influencing phenotype of normal human keratinocytes. *Histochem Cell Biol*. 133, 201–211. doi: 10.1007/s00418-009-0661-6
- Stuelten, C.H., DaCosta Byfield, S., Arany, P.R., Karpova, T.S., Stetler-Stevenson, W.G., Roberts, A.B. (2005). Breast cancer cells induce stromal fibroblasts to express MMP-9 via secretion of TNF-α and TGF-β. *J Cell Sci*. 118, 2143-2153.
- Sugimoto, H., Mundel, T.M., Kieran, M.W., Kalluri, R. (2006). Identification of fibroblast heterogeneity in the tumour microenvironment. *Cancer Biology & Therapy*. 5(12), 1640-1646.
- Sui, X., Kong, N., Ye, L., Han, W., Zhou, J., Zhang, Q., He, C., Pan, H. (2014). p38 and JNK MAPK pathways control the balance of apoptosis and autophagy in response to chemotherapeutic agents. *Cancer Letters*, 344, 174-179. Doi: 10.1016/j.canlet.2013.11.019.
- Sung, S-Y., Hsieh, C-L., Law, A., Zhau, H.E.., Pathak, S., Multani, A., *et al*. (2008). Coevolution of prostate cancer and bone stroma in three-dimensional coculture: implications for cancer growth and metastasis, *Cancer Res*. 68, 9996–10003.

- Takahashi, M., Fukami, S., Iwata, N., Inoue, K., Itohara, S., Itoh, H., Haraoka, J., Saido, T.C. (2002). In vivo glioma growth requires host-derived matrix metalloproteinase 2 for maintenance of angioarchitecture. *Pharmacol Res*. 46,155–163.
- Taki, M., Verschueren, K., Yokoyama, K., Nagayama, M., Kamata, N. (2005). Involvement of Ets-1 transcription factor in inducing matrix metalloproteinase-2 expression by epithelial-mesenchymal transition in human squamous carcinoma cells. *International Journal of Oncology*. 28, 487-496. doi: 10.3892/ijo.28.2.487.
- Tanner, K., Gottesman, (2015). Beyond 3D culture models of cancer. *Sci Transl Med.* 7(283), 283ps9. doi: 10.1126/scitranslmed.3009367.
- Tardito, S., Oudin, A., Ahmed, S.U., Fack, F., Keunen, O., Zheng, L., *et al*. (2015). Glutamine synthase activity fuels nucleotide biosynthesis and supports growth of glutamine-restricted glioblastoma. *Nat Cell Biol*. 17(12), 1556-1568. doi: 10.1038/ncb3272.
- Tezcan, O., Gündüz, U. (2014). Vimentin silencing effect on invasive and migration characteristics of doxorubicin resistant MCF-7 cells. *Biomedicine & Pharmacotherapy*. 68, 357-364. doi: 10.1016/j.biopha.2014.01.006.
- Thiery, J.P., Acloque, H., Huang, R.Y.J., Nieto, M.A. (2009). Epithelial-mesenchymal transitions in development and disease. *Cell*. 139(5). 871-890. doi: 10.1016/j.cell.2009.11.007.
- Thiery, J.P., Sleeman. J.P. (2006). Complex networks orchestrate epithelial–mesenchymal transitions. *Nat Rev*. 7, 131-142.
- Thijssen, V.L.J.L., Brandwijk, R.J.M.G.E., Dings, R.P.M., Griffioen, A.W. (2004). Angiogenesis gene expression profiling in xenograft models to study cellular interactions. *Exp. Cell Res*. 299, 286–293. doi: 10.1016/j.yexcr.2004.06.014
- Thomasset, N., Lochter, A., Sympson, C.J., Lund, L.R., Williams, D.R., Behrendtsen, O., Werb, Z., Bissell, M.J. (1998). Expression of autoactivated stromelysin-1 in mammary

glands of transgenic mice leads to a reactive stroma during early development. *Am J Pathol*. 153, 457–467.

- Tong, R.T., Boucher, Y., Kozin, S.V., Winkler, F., Hicklin, D.J., Jain, R.K. (2004). Vascular Normalization by Vascular Endothelial Growth Factor Receptor 2 Blockade Induces a Pressure Gradient Across the Vasculature and Improves Drug Penetration in Tumors. *Cancer Research*. 64, 3731-3736.
- Toullec, A., Gerald, D., Despouy, G., Bourachot, B., Cardon, M., Lefort, S., *et al*. (2010). Oxidative stress promotes myofibroblast differentiation and tumour spreading. *EMBO Mol Med*. 2(6), 211-230.
- Tracy, K., Dibling, B.C., Spike, B.T., Knabb, J.R., Schumacker, P., Macleod, K.F. (2007). BNIP3 is an RB/E2F target gene required for hypoxia-induced autophagy. *Molecular and Cellular Biology*. 27(17), 6229-6242. doi:10.1128/MCB.02246-06.
- Tse, J.C., Kalluri, R. (2007). Mechanisms of metastasis: Epithelial-to-mesenchymal transition and contribution of tumour microenvironment. *J Cell Biochem*. 101, 816-829. doi: 10.1002/jcb.21215.
- Tsun, Z-Y., Possemato, R. (2015). Amino acid management in cancer. *Cell Dev Biol*. 43, 22-32. doi: 10.1016/j.semcdb.2015.08.002.
- Tuxhorn, J.A., Ayala, G.E., Smith, M.J., Smith, V.C., Dang, T.D., Rowley, D.R. (2002). Reactive stroma in human prostate cancer: induction of myofibroblast phenotype and extracellular matrix remodeling. *Clin Cancer Res*. 8, 2912–2923.
- Tóth, S., Nagy, K., Pálfia, Z., Réz, G. (2002). Cellular autophagic capacity changes during azaaerine-induced tumor progression in the rat pancreas. *Cell Tissue Res.* 309, 409-416. doi: 10.1007/s00441-001-0506-7.
- Ueno, T., Saji, S., Sugimoto, M., Masuda, N., Kuroi, K., Sato, N., *et al.* (2016). Clinical significance of the expression of autophagy-associated marker, beclin 1, in breast

cancer patients who received neoadjuvant endocrine therapy. *BMC Cancer*, 16(230), doi: 10.1186/s12885-016-2270-9.

- Urbich, C., Knau, A., Fichtlscherer, S., Walter, D. H., Brühl, T., Potente, M., *et al*. (2005). FOXO-dependent expression of the apoptotic protein Bim: pivitol role for apoptosis signalling in endothelial progenitor cells. *FASEB J*. 19(8), 974-976.
- Valadi, H., Ekström, K., Bossios, A., Sjöstrand, M., Lee, J. J., Lötvall, J. O. (2007). Exosome-mediated transfer of mRNAs and microRNAs is a novel mechanism of genetic exchange between cells. *Nat Cell Biol*. 9(6), doi: 10.1038/ncb1596.
- Valastyan, S., Weinberg, R.A. (2011). Tumor metastasis: molecular insights and evolving paradigms. *Cell.* 147(2), 275-292. doi:10.1016/j.cell.2011.09.024.
- Valenciano, A., Henríquez-Hernández, L.A., Moreno, M., Lloret, M., Lara, P.C. (2012). Role of igf-1 receptor in radiation response. Transl Oncol. 5, 1-9. doi: 10.1593/tlo.11265.
- van de Loosdrecht, A.A., Beelen, R.H.J., Ossenkoppele, G.J., Broekhoven, M.G., Langenhuijsen, M.M.A.C. (1994). A tetrazolium-based colorimetric MTT assay to quantitate human monocyte mediated cytotoxicity against leukemic cells from cell lines and patients with acute myeloid leukemia. *Journal of Imuunological Methods*. 174, 311-320.
- Van der Heiden, M.G., Cantley, L.C., Thompson, C.B. (2009). Understanding the Warburg effect: The metabolic requirements of cell proliferation. *Science*. 324(5930), 1029-1033.
- Végran, F., Boidot, R., Michiels, C., Sonveaux, P., Feron, O. (2011). Lactate influx through the endothelial cell monocarboxylate transporter mct1 supports an nf-kb/il-8 pathway that drives tumor angiogenesis. *Cancer Res*. 71(7), 2550-2560. doi: 10.1158/0008-5472.CAN-10-2828

- Velaei, K., Samadi, N., Soltani, S., Barazvan, B., Rad, J.S. (2016). NFκBP65 transcription factor modulates resistance to doxorubicin through ABC transporters in breast cancer. *Breast Cancer*. 24, 552-561. doi: 10.1007/s12282-016-0738-8.
- Vincan, E., Barker, N. (2008). The upstream components of the Wnt signalling pathway in the dynamic EMT and MET associated with colorectal cancer progression. *Clin Exp Metastasis*. 25, 657-663. doi: 10.1007/s10585-008-9156-4.
- Von Burstin, J., Eser, S., Paul, M.C., Seidler, B., Brandl, M., Messer, M., *et al*. (2009). E-cadherin regulates metastasis of pancreatic cancer in vivo and is supressed by a SNAIL/HDAC2 repressor complex. *Gastroenterology*. 137, 361-371. doi: 10.1053/j.gastro.2009.04.004.
- Wald, O., Izhar, U., Amir, G., Kirshberg, S., Shlomai, Z., Zamir, G., *et al*. (2011). Interaction between neoplastic cells and cancer-associated fibroblasts through the CXCL12/CXCR4 axis: Role in non-small cell lung cancer tumour proliferation. *J Thorac Cardiovasc Surg*. 141(6), 1503-1512.
- Walter *et al*., 2009). Interleukin 6 secreted from adipose stromal cells promotes migration and invasion of breast cancer cells. *Oncogene*. 28(30), 2745-2755. doi: 10.1038/onc.2009.130.
- Wandel, E., Graßhoff, A., Mittag, M., Haustein, U.F., Saalbach, A. (2000). Fibroblasts surrounding melanoma express elevated levels of matrix metalloproteinase-1 (MMP-1) and intercellular adhesion molecule-1 (ICAM-1). in vitro. *Exp Dermatol*. 2000; 9:34–41.
- Wang, M., Zhang, J., Huang, Y., Ji, S., Shao, G., Feng, S., Chen, D., Zhao, K., Wang, Z., Wu, A. (2017a). Cancer-associated fibroblasts autophagy enhances progression of triple-negative breast cancer cells. *Med Sci Monit*. 23, 3094-3912. doi: 10.12659/MSM.902870.

- Wang, Y., Gan, G., Wang, B., Wu, J., Cao, Y., Zhu, D., *et al*. (2017b). Cancer-associated fibroblasts promote irradiated cancer cell recovery through autophagy. *EBiomedicine*. 17, 45-56. doi: 10.1016/j.ebiom.2017.02.019.
- Wang, Z., Hill, S.J., Luther, J.M., Hachey, D.L., Schey, K.L. (2012). Proteomic Analysis of Urine Exosomes by Multidimensional Protein Identification Technology (MudPIT). Proteomics. 12(2), 329-338. doi: 10.1002/pmic.201100477.
- Warburg, O., Wind, F., Negelein, E. (1926). The metabolism of tumors in the body. *Klin Wochschr*. 5, 829-832.
- Ward, P.S., Thompson, C.B. (2012). Metabolic reprograming: A cancer hallmark even Warburg did not anticipate. *Cancer Cell*. 21, 297-306.
- Watanabe, H., de Caestecker, M.P., Yamada, Y. (2001). Transcriptional cross-talk between Smad, ERK1/2, and p38 mitogen-activated protein kinase pathways regulates transforming growth factor-β-induced aggrecan gene expression in chondrogenic ATDC5 cells. *The Journal of Biological Chemistry.* 276(17), 14466–14473. doi: 10.1074/jbc.M005724200.
- Waterhouse, C., Keilson, J. (1969). Cori Cycle Activity in Man. *The Journal of Clinical Investigation*. 48, 2359-2366.
- Wei, H., Li, F., Fu, P., Liu, X. (2013). Effects of the silencing of hypoxia-inducible actor-1 alpha on metastasis of pancreatic cancer. *Eur Rev Med Pharmacol Sci*. 17, 436-446.
- Wei, J., Xu, G., Wu, M., Zhang, Y., Li, Q., Liu, P., *et al*. (2008). Overexpression of vimentin contributes to prostate cancer invasion and metastasis via Src regulation. *Anticancer Research*. 28, 327-334.
- Whitaker-Menezes, D., Martinez-Outschoorn, U.E., Lin, Z., Ertel, A., Flomenberg, N., Witkiewicz, A.K., *et al*. (2011). Evidence for a stromal-epithelial “lactate shuttle” in human tumors. *Cell Cycle*. 10(11), 1772-1783. doi: 10.4161/cc.10.11.15659.

- Wieman, H.L., Wofford, J.A., Rathmell, J.C. (2007). Cytokine Stimulation promotes glucose uptake via phosphatidylinositol-3 kinase/Akt regulation of Glut1 activity and trafficking. *Mol Biol Cell*. 18, 1437-1446.
- Wietkiewicz, A.K., Dasgupta, A., Sotgia, F., Mercier, I., Pestell, R.G., Sabel, M., *et al.* (2009). An absence of stromal caveolin-1 expression predicts early tumour recurrence and poor clinical outcome in human breast cancers. *AM J Pathol*. 174(6), 2023-2034.
- Wilker, E., Yaffe, M.B. (2004). 14-3-3 proteins - a focus on cancer and human disease. *Journal of Molecular and Cellular Cardiology*. 37, 633-642. doi: 10.1016/j.yjmcc.2004.04.015.
- Williams, C.S., Tsujii, M., Reese, J., Dey, S.K., DuBois, R.N. (2000). Host cyclooxygenase-2 modulates carcinoma growth. *J. Clin. Invest*. 105, 1589-1594.
- Winkler, F., Kozin, S.V., Tong, R.T., Chae, S-S., Booth, M.F., Garkavtsev, I., Xu, L., Hicklin, D.J., Fukumura, D., di Tomaso, E., Munn, L.L., Jain, R.K. (2004). Kinetics of vascular normalization by VEGFR2 blockade governs brain tumor response to radiation: Role of oxygenation, angiopoietin-1, and matrix metalloproteinases. *Cancer Cell*. 6, 553-563.
- Wise, D.R., Ward, P.S., Shay, J.E.S., Cross, J.R., Gruber, J.J., Sachdeva, U.M., Platt, J.M., DeMatteo, R.G., Simon, M.C., Thompson, C.B. (2011). Hypoxia promotes isocitrate dehydrogenase-dependent carboxylation of α-ketoglutarate to citrate to support cell growth and viability. *PNAS*. 108(49), 19611-19616. doi: 10.1073/pnas.1117773108.
- Wong, P-M., Feng, Y., Wang, J., Shi, R., Jiang, X. (2015). Regulation of autophagy by coordinated action of mTORC1 and protein phosphatase 2A. *Nat Commun*. 6, 8048. doi: 10.1038/ncomms9048.
- Wu *et al*., 2009). Stabilization of Snail by NF-κB is required for inflammation-induced cell migration and invasion. *Cancer Cell*. 15(5), 416-428. doi: 10.1016/j.ccr.2009.03.016.

- Wu, J.J., Quijano, C., Chen, E., Liu, H., Cao, L., Fergusson, M. M., *et al*. (2009). Mitochondrial dysfunction and oxidative stress mediate the physiological impairment induced by the disruption of autophagy. *Aging*. 1(4), 425-437.
- Wu, K.N., Queenan, M., Brody, J.R., Potoczek, M., Sotgia, F., Lisanti, M.P., *et al.* (2011). Loss of stromal caveolin-1 expression in malignant melanoma metastasis predicts poor survival. *Cell Cycle*. 10(24), 4250-4255.
- Wu, Y., Zhou, B.P. (2010). Snail. More than EMT. *Cell Adh Migr*. 4(2), 199-203.
- Xiao, X., Yu, S., Li, S., Wu, J., Ma, R., Cao, H., *et al*. (2014). Exosomes: Decreased sensitivity of lung cancer A549 cells to cisplatin. *PLOS One*. 9(2). doi:10.1371/journal.pone.0089534
- Xie, H., Hanai, J-I., Ren, J-G., Kata, L., Burgess, K., Bhargava, P., *et al*. (2014). Targeting lactate dehydrogenase-a inhibits tumorigenesis and tumor progression in mouse models of lung cancer and impacts tumor-initiating cells. *Cell Metabolism*. 19, 795–809.
- Xing, F., Saidou, J., Watabe, K. (2010). Cancer associated fibroblasts (CAFs) in tumour microenvironment. *Front Biosci*. 15, 166-179.
- Yang, L., Pang, Y., Moses, H.L. (2010). TGF-β and immune cells: an important regulatory axis in the tumour microenvironment and progression. *Trends Immunol*. 31(6), 220-227.
- Yang, M-H., Wu, M-Z., Chiou, S-H., Chen, P-M., Chang, S-Y., Liu, C-J., *et al*. (2008). Direct regulation of TWIST by HIF-1α promotes metastasis. *Nat Cell Biol*. 10(3), 295-305.
- Yang, Q-L., Zhang, L-Y., Wang, H-F., Li, Y., Wang, Y-Y., Chen, T-T., *et al*. (2017). The N-terminal polypeptide derived from viral macrophage inflammatory protein II reverses

breast cancer epithelial-to-mesenchymal transition via a PDGFRα-dependent mechanism. *Oncotarget*. 8(23), 37448-37463.

- Yaromina, A., Quennet, V., Zips, D., Meyer, S., Shakiran, G., Walenta, S., Mueller-Klieser, W., Baumann, M. (2009). Co-localisation of hypoxia and perfusion markers with parameters of glucose metabolism in human squamous cell carcinoma (hSCC) xenografts. *Int. J. Radiat. Biol*. 85(11), 972–980. doi: 10.3109/09553000903232868
- Yeh, C-R., Slavin, S., Da, J., Hsu, I., Luo, J., Xiao, G-Q., *et al.* (2016). Estrogen receptor α in cancer associated fibroblasts supresses prostate cancer invasion via reducing CCL5, IL6 and macrophage infiltration in the tumour microenvironment. *Mol Cancer*. 15(7), doi: 10.1186/s12943-015-0488-9.
- Yokoyama, K., Kamata, N., Hayashi, E., Hoteiya, T., Ueda, N., Fujimoto. R., Nagayama, M. (2001). Reverse correlation of E-cadherin and snail expression in oral squamous cell carcinoma cells in vitro. *Oral Oncology.* 37, 65-71.
- Yook, J.I., Li. X-Y., Ota, I., Hu, C., Kim, H.S., Kim, N.H., *et al*. (2006). A Wnt-Axin2-GSK3beta cascade regulates Snail1 activity in breast cancer cells. Nat Cell Biol. 8(12), 1398-406. doi:10.1038/ncb1508.
- Yoshii, Y., Furukawa, T., Waki, A., Okuyama, H., Inoue, M., Itoh, M., *et al*. (2015). High-throughput screening with nanoimprinting 3D culture for efficient drug development by mimicking the tumor environment. *Biomaterials*. 51, 278e289. doi: 10.1016/j.biomaterials.2015.02.008.
- Zavadil, J., Haley, J., Kalluri, R., Muthuswamy, S.K., Thompson, E. (2007). Epithelial-mesenchymal transition. *Cancer Res*. 68(23), 9574-9577. doi:10.1158/0008-5472.CAN-08-2316.
- Zeigerer, A., Lampson, M.A., Karylowski, O., Sabatini, D.D., Adesnik, M., Ren, M., McGraw, T.E. (2002). GLUT4 retention in adipocytes requires two intracellular insulin-

regulated transport steps. *Molecular Biology of the Cell*. 13, 2421-2435. doi: 10.1091/mbc.E02–02–0071.

- Zeisberg, M., Kalluri, R. (2013). Cellular mechanisms of tissue fibrosis. 1. Common and organ-specific mechanisms associated with tissue fibrosis. *Am. J. Physiol. Cell Physiol*. 304(4), C216–C225. doi: 10.1152/ajpcell.00328.2012.
- Zhang, H-G., Liu, C., Su, K., Yu, S., Zhang, L., Zhang, S., Wang, J., Cao, X., Grizzle, W., Kimberly, R.P. (2006). A membrane form of TNF-alpha presented by exosomes delays T cell activation-induced cell death. *J Immunol*. 176(12), 7385-7393. doi: 10.4049/jimmunol.176.12.7385.
- Zhang, L., Zhang, W., Li, Y., Alvarez, A., Li, Z., Wang, Y., Song, L., Lv, D., Nakano, I., Hu, B., Cheng, S-Y., Feng, H. (2016). SHP-2-upregulated ZEB1 is important for PDGFRα-driven glioma epithelial-mesenchymal transition and invasion in mice and humans. *Oncogene*. 35, 5641-5652. doi: 10.1038/onc.2016.100.
- Zhang, Z., Vuori, K., Reed, J.C., Ruoslahti, E. (1995). The α5β1 integrin supports survival of cells on fibronectin and up-regulates Bcl-2 expression. *P Natl Acad Sci USA*. 92, 6161-6165.
- Zheng, X., Carstens, J.L., Kim, J., Scheible, M., Kaye, J., Sugimoto, H., Wu, C-C., LeBleu, V.S., Kalluri, R. (2015). EMT program is dispensable for metastasis but induces chemoresistance in pancreatic cancer. *Nature*. 527(7579). 525-530. doi: 10.1038/nature16064.
- Zhou, F., Yang, Y., Xing, D.(2011). Bcl-2 and Bcl-xL play important roles in the crosstalkbetween autophagy and apoptosis. *FEBS Journal*. 278, 403–413. doi:10.1111/j.1742-4658.2010.07965.x.
- Zimmer, A.D., Walbrecq, G., Kozar, I., Behrmann, I., Haan, C. (2016). Phosphorylation of the pyruvate dehydrogenase complex precedes HIF-1-mediated effects and pyruvate

dehydrogenase kinase 1 upregulation during the first hours of hypoxic treatment in hepatocellular carcinoma cells. *Hypoxia*. 4, 135–145.

Chapter 7: Appendices

7.1. Proteomics – List of Proteins

7.1.1. Proteomics Analysis of E0771 conditioned media

Table 7.1: List of differentially expressed proteins in E0771 control conditioned media (E0771 C).

Group	Accession Number	Description	Confidence score	Anova (p)	Fold Change
E0771_C	I3L145	Sex hormone-binding globulin	5.205962709	5.34E-05	11.57035277
E0771_C	P43652	Afamin	3.781422089	0.0001793	2.196765224
E0771_C	Q96D15	Reticulocalbin-3	13.30528088	0.000212	17.92971387
E0771_C	P04004	Vitronectin	17.98074799	0.0003757	2.706463703
E0771_C	Q06033	Inter-alpha-trypsin inhibitor heavy chain H3	35.41013703	0.000733	2.16369489
E0771_C	Q14118	Dystroglycan	23.47307826	0.0008326	3.080225771
E0771_C	Q8NDW8	Tetratricopeptide repeat protein 21A	2.268184612	0.0015768	3.329415209
E0771_C	P05543	Thyroxine-binding globulin	22.21085603	0.0017916	5.454819359
E0771_C	P02647	Apolipoprotein A-I	15.41758964	0.0024173	4.214960073
E0771_C	A0A087WSY9	Thioredoxin reductase 1, cytoplasmic	10.10739902	0.0034767	4.512266001
E0771_C	Q99497	Protein DJ-1	7.668671354	0.003866	2.204523717
E0771_C	P05452	Tetranectin	11.07079683	0.0050455	3.509300867
E0771_C	P02461	Collagen alpha-1(III) chain	68.80913822	0.0050637	5.070493532
E0771_C	Q92520	Protein FAM3C	4.448114427	0.0052545	4.886536663
E0771_C	Q8NF91	Nesprin-1	24.71886474	0.00594	2.231554617
E0771_C	Q16718	NADH dehydrogenase [ubiquinone] 1 alpha subcomplex subunit 5	1.385617891	0.0060123	6.897579225
E0771_C	P68871	Hemoglobin subunit beta	29.83783544	0.0061377	3.131500028
E0771_C	P02753	Retinol-binding protein 4	11.77082489	0.0065332	4.421631083
E0771_C	D6RF35	Vitamin D-binding protein	94.4880968	0.0094468	6.210660712
E0771_C	P51884	Lumican	24.51921047	0.0122448	2.625482934
E0771_C	Q06323	Proteasome activator complex subunit 1	36.37396179	0.0143785	2.365973585
E0771_C	P08697	Alpha-2-antiplasmin	19.56058745	0.0145895	4.528110877
E0771_C	E7ER44	Lactotransferrin	32.76727595	0.0231877	2.361678455
E0771_C	P69905	Hemoglobin subunit alpha	70.79701702	0.0240917	2.233877481
E0771_C	P09960	Leukotriene A-4 hydrolase	13.90659489	0.024128	2.016656464
E0771_C	P55072	Transitional endoplasmic reticulum ATPase	193.0158475	0.0243696	3.397644393
E0771_C	P02748	Complement component C9	9.250128838	0.0275597	2.598960383
E0771_C	Q6ZU64	Cilia- and flagella-associated protein 65	1.469533219	0.0290416	3.565396709

Table 7.2: List of differentially regulated proteins in glucose deprived E0771 conditioned media (E0771 GD)

Group	Accession Number	Description	Confidence score	Anova (p)	Fold Change
E0771_GD	P05019	Insulin-like growth factor I	27.18266803	4.00E-07	100.9117103
E0771_GD	Q92896	Golgi apparatus protein 1	13.85584627	2.79E-06	124.3286638
E0771_GD	P50454	Serpin H1	22.80631544	5.71E-06	22.26215147
E0771_GD	P78330	Phosphoserine phosphatase	17.47569586	9.16E-06	199.4467577
E0771_GD	P35527	Keratin, type I cytoskeletal 9	2.275532567	9.57E-06	37.68567626
E0771_GD	P48506	Glutamate--cysteine ligase catalytic subunit	4.367829656	2.65E-05	48.36694635
E0771_GD	P14543	Nidogen-1	42.11164221	3.81E-05	8.904518968
E0771_GD	Q99536	Synaptic vesicle membrane protein VAT-1 homolog	35.4234255	4.39E-05	31.52992635
E0771_GD	O43852	Calumenin	12.42646181	5.15E-05	84.9097467
E0771_GD	P25786	Proteasome subunit alpha type-1	35.74063221	9.61E-05	35.92075316
E0771_GD	P30101	Protein disulfide-isomerase A3	18.56128015	0.0001062	5.254872763
E0771_GD	P47755	F-actin-capping protein subunit alpha-2	11.84349912	0.0001155	125.7207973
E0771_GD	A0A075B7D9	TATA-binding protein-associated factor 2N	2.723973745	0.0001225	17.96232547
E0771_GD	P07237	Protein disulfide-isomerase	54.8232496	0.0001311	6.60750763
E0771_GD	P05198	Eukaryotic translation initiation factor 2 subunit 1	16.39010559	0.0001396	57.05598229
E0771_GD	O43707	Alpha-actinin-4	150.87147	0.000145	11.2233816
E0771_GD	Q15404	Ras suppressor protein 1	16.22518375	0.0001466	31.96150798
E0771_GD	P11021	78 kDa glucose-regulated protein	163.6413764	0.0001506	11.3600147
E0771_GD	Q9HC38	Glyoxalase domain-containing protein 4	2.240987264	0.0001539	201.137088
E0771_GD	A0A0A0MTS2	Glucose-6-phosphate isomerase (Fragment)	35.92159293	0.0001728	98.51070454
E0771_GD	P17174	Aspartate aminotransferase, cytoplasmic	21.27582497	0.0001729	51.0418461
E0771_GD	P35268	60S ribosomal protein L22	11.36012289	0.0001806	154.1847734
E0771_GD	P14625	Endoplasmin	58.01996899	0.0001895	45.3519957
E0771_GD	P08243	Asparagine synthetase [glutamine-hydrolyzing]	33.94811192	0.0001934	24.69495924
E0771_GD	P26196	Probable ATP-dependent RNA helicase DDX6	14.80218148	0.0002096	6.730056045
E0771_GD	P23526	Adenosylhomocysteinase	26.47191433	0.0002272	17.77492161
E0771_GD	P06733	Alpha-enolase	144.3654213	0.00023	21.96717627
E0771_GD	P61981	14-3-3 protein gamma	28.52762339	0.0002485	24.56096903
E0771_GD	P31946	14-3-3 protein beta/alpha	29.01540539	0.0002509	9.35160291
E0771_GD	Q96KP4	Cytosolic non-specific dipeptidase	15.23104494	0.0002727	14.87396388

E0771_GD	K7ESG5	Proteasome activator complex subunit 3	15.28695245	0.0002831	19.93834724
E0771_GD	A0A0A0MT01	Gelsolin	61.7798389	0.0002904	4.326626433
E0771_GD	P16989	Y-box-binding protein 3	20.35567549	0.0002918	38.86421734
E0771_GD	Q15393	Splicing factor 3B subunit 3	27.57274331	0.0003076	77.96245178
E0771_GD	P31939	Bifunctional purine biosynthesis protein PURH	14.30122551	0.000311	5.502952087
E0771_GD	P60900	Proteasome subunit alpha type-6	23.75948401	0.0003199	21.83285015
E0771_GD	P34932	Heat shock 70 kDa protein 4	119.9358079	0.0003464	18.43800541
E0771_GD	O15511	Actin-related protein 2/3 complex subunit 5	11.53761872	0.0003529	102.9519305
E0771_GD	Q9Y333	snRNA-associated Sm-like protein LSm2	9.608326012	0.0003582	17.79172191
E0771_GD	P22626	Heterogeneous nuclear ribonucleoproteins A2/B1	58.26867651	0.0003676	38.44655884
E0771_GD	P11142	Heat shock cognate 71 kDa protein	419.5409654	0.0003722	18.94990834
E0771_GD	P14550	Alcohol dehydrogenase [NADP(+)]	25.4247084	0.0003807	32.97295381
E0771_GD	P40925	Malate dehydrogenase, cytoplasmic	19.59996273	0.000409	21.77753032
E0771_GD	J3KTL2	Serine/arginine-rich-splicing factor 1	22.64515346	0.0004264	39.31116722
E0771_GD	Q04917	14-3-3 protein eta	27.68847628	0.0005319	526.4568285
E0771_GD	P13797	Plastin-3	54.92559414	0.0005333	6.615250793
E0771_GD	Q01995	Transgelin	26.09286228	0.0005475	11.14295467
E0771_GD	P20290	Transcription factor BTF3	4.072192706	0.000552	20.07061817
E0771_GD	P26038	Moesin	123.0576281	0.0005636	23.66602474
E0771_GD	H0YL52	Tropomyosin alpha-1 chain (Fragment)	86.19312822	0.0005665	19.95933505
E0771_GD	P36955	Pigment epithelium-derived factor	42.25616633	0.0005666	4.288011783
E0771_GD	P60981	Destrin	19.11083247	0.0006551	51.67840279
E0771_GD	Q9Y266	Nuclear migration protein nudC	21.17417674	0.0006648	31.76922728
E0771_GD	P63104	14-3-3 protein zeta/delta	51.81710983	0.0007014	9.926934748
E0771_GD	P12081	Histidine--tRNA ligase, cytoplasmic	18.0798167	0.0007155	64.41617409
E0771_GD	P62258	14-3-3 protein epsilon	89.45852815	0.0007341	17.55090253
E0771_GD	J3QQX2	Rho GDP-dissociation inhibitor 1	24.35314005	0.0007552	36.16010318
E0771_GD	P25398	40S ribosomal protein S12	2.426077818	0.0008165	50.11784675
E0771_GD	Q00577	Transcriptional activator protein Pur-alpha	4.315667173	0.0008398	20.68473769
E0771_GD	P62495	Eukaryotic peptide chain release factor subunit 1	15.87442813	0.0008428	17.21459969
E0771_GD	P22392	Nucleoside diphosphate kinase B	77.94623192	0.0008681	17.72287615
E0771_GD	P49721	Proteasome subunit beta type-2	29.7717515	0.000869	5.249568663
E0771_GD	P12814	Alpha-actinin-1	135.9385131	0.0008773	8.236881737

E0771_GD	P15121	Aldose reductase	3.156545481	0.0009088	10.02671543
E0771_GD	Q15056	Eukaryotic translation initiation factor 4H	13.01107154	0.0009515	49.09596288
E0771_GD	P61160	Actin-related protein 2	5.068111751	0.0010003	9.732465305
E0771_GD	E9PAV3	Nascent polypeptide-associated complex subunit alpha, muscle-specific form	44.57516428	0.0010148	11.37474143
E0771_GD	P28838	Cytosol aminopeptidase	13.25727622	0.0010156	41.66120379
E0771_GD	P26447	Protein S100-A4	10.80759821	0.0010209	13.03488612
E0771_GD	P00338	L-lactate dehydrogenase A chain	60.81994037	0.0010325	22.39194496
E0771_GD	Q9Y617	Phosphoserine aminotransferase	19.11834003	0.0010523	26.95235973
E0771_GD	P30050	60S ribosomal protein L12	60.48927603	0.0010684	12.10680745
E0771_GD	Q09666	Neuroblast differentiation-associated protein AHNAK	105.5206309	0.001118	7.385812706
E0771_GD	Q5T3N1	Annexin (Fragment)	22.29151562	0.0011323	7.148271985
E0771_GD	O75436	Vacuolar protein sorting-associated protein 26A	3.023696422	0.0011345	48.06475372
E0771_GD	P05388	60S acidic ribosomal protein P0	38.48232022	0.0011409	13.47304982
E0771_GD	P25788	Proteasome subunit alpha type-3	23.07187084	0.0011546	13.07494708
E0771_GD	Q9H444	Charged multivesicular body protein 4b	14.22018781	0.0012056	113.893564
E0771_GD	P24534	Elongation factor 1-beta	17.24048202	0.0012171	54.06454884
E0771_GD	Q8NEV1	Casein kinase II subunit alpha 3	14.00826212	0.001254	57.59737427
E0771_GD	P20618	Proteasome subunit beta type-1	17.66082493	0.001292	28.13805107
E0771_GD	P61088	Ubiquitin-conjugating enzyme E2 N	35.41492654	0.0012957	13.65754205
E0771_GD	P18206	Vinculin	142.6392357	0.001301	6.6939887
E0771_GD	P09417	Dihydropteridine reductase	17.62223854	0.001322	30.8429989
E0771_GD	P61086	Ubiquitin-conjugating enzyme E2 K	17.32208458	0.0013324	32.07035282
E0771_GD	F8WCF6	Actin-related protein 2/3 complex subunit 4	24.29611519	0.0013614	44.49991079
E0771_GD	P07900	Heat shock protein HSP 90-alpha	213.9144792	0.0013713	12.84012893
E0771_GD	P43490	Nicotinamide phosphoribosyltransferase	13.7263839	0.001376	12.8982451
E0771_GD	A0A0C4DFV9	Protein SET	34.04941749	0.0013861	16.89099393
E0771_GD	Q5HYB6	Epididymis luminal protein 189	73.36451715	0.0013926	29.32104725
E0771_GD	P61604	10 kDa heat shock protein, mitochondrial	19.98617907	0.0013965	44.13686282
E0771_GD	P60709	Actin, cytoplasmic 1	249.1469143	0.0014048	5.343437634
E0771_GD	P15090	Fatty acid-binding protein, adipocyte	14.23845041	0.0014528	19.04684404
E0771_GD	P56537	Eukaryotic translation initiation factor 6	18.6117551	0.0014588	90.80153572
E0771_GD	P30086	Phosphatidylethanolamine-	14.02810625	0.0014752	10.05761132

		binding protein 1			
E0771_GD	P18669	Phosphoglycerate mutase 1	131.5371954	0.0015324	13.86821352
E0771_GD	P28070	Proteasome subunit beta type-4	18.07024651	0.0015696	52.30637204
E0771_GD	O14818	Proteasome subunit alpha type-7	28.06374998	0.0015888	43.13663362
E0771_GD	P35241	Radixin	70.44512818	0.0016249	110.6631766
E0771_GD	D6RBL5	Annexin	63.98054264	0.0016527	20.13347112
E0771_GD	P30041	Peroxiredoxin-6	19.54424544	0.001717	16.63084012
E0771_GD	P16949	Stathmin	20.95897788	0.0017462	9.512590349
E0771_GD	P50395	Rab GDP dissociation inhibitor beta	51.21330209	0.0017658	11.88023666
E0771_GD	P49720	Proteasome subunit beta type-3	35.61487044	0.0017795	7.351094514
E0771_GD	Q9UNZ2	NSFL1 cofactor p47	16.14487173	0.0018055	43.06861523
E0771_GD	P35052	Glypican-1	31.3686554	0.0018074	4.648628876
E0771_GD	P31153	S-adenosylmethionine synthase isoform type-2	26.88696816	0.0018299	7.492477447
E0771_GD	A0A087WTT1	Polyadenylate-binding protein	44.50320919	0.001865	6.55602266
E0771_GD	E7EQR4	Ezrin	65.28155066	0.001934	15.65419309
E0771_GD	F5H018	GTP-binding nuclear protein Ran (Fragment)	16.71268999	0.0019795	5.067810675
E0771_GD	A0A0A0MSI0	Peroxiredoxin-1 (Fragment)	40.56018373	0.0020625	20.43352992
E0771_GD	O75368	SH3 domain-binding glutamic acid-rich-like protein	2.414711319	0.0021171	40.9104179
E0771_GD	P11047	Laminin subunit gamma-1	34.91880231	0.0022402	5.448408607
E0771_GD	P62857	40S ribosomal protein S28	15.30735046	0.0022646	16.27778204
E0771_GD	P62942	Peptidyl-prolyl cis-trans isomerase FKBP1A	19.99314866	0.0022744	15.57283435
E0771_GD	P12004	Proliferating cell nuclear antigen	28.42660156	0.0023071	8.193243287
E0771_GD	P07355	Annexin A2	111.8606583	0.0023201	14.67871844
E0771_GD	Q9Y3F4	Serine-threonine kinase receptor-associated protein	8.465085033	0.0023689	9.633715604
E0771_GD	P54136	Arginine--tRNA ligase, cytoplasmic	29.7001631	0.0024244	14.1914355
E0771_GD	A0A1C7CYX9	Dihydropyrimidinase-related protein 2	61.55114303	0.002467	32.04000096
E0771_GD	O00303	Eukaryotic translation initiation factor 3 subunit F	16.56597614	0.0024879	10.79219191
E0771_GD	F8W1I6	Dynactin subunit 2	13.93919298	0.0024891	13.94591096
E0771_GD	P60174	Triosephosphate isomerase	88.16869552	0.0025154	7.241575821
E0771_GD	P26641	Elongation factor 1-gamma	47.86005903	0.00253	15.45695806
E0771_GD	P13667	Protein disulfide-isomerase A4	35.21866854	0.0025649	13.25902836
E0771_GD	P00491	Purine nucleoside phosphorylase	4.985312953	0.002639	36.49561633

E0771_GD	P08572	Collagen alpha-2(IV) chain	4.552047911	0.0026574	18.20379026
E0771_GD	Q6P452	Annexin	31.13235259	0.0027218	6.705898436
E0771_GD	P63244	Receptor of activated protein C kinase 1	11.76338043	0.0027324	10.02347918
E0771_GD	Q9HB71	Calcyclin-binding protein	21.38135904	0.0027361	13.35003289
E0771_GD	O14737	Programmed cell death protein 5	19.20361583	0.0027507	37.26724714
E0771_GD	B4DXW1	Actin-related protein 3	41.0734679	0.0028313	3.989451697
E0771_GD	P50990	T-complex protein 1 subunit theta	32.51208573	0.0028378	11.22403974
E0771_GD	P54577	Tyrosine--tRNA ligase, cytoplasmic	14.98249373	0.0029068	95.00745671
E0771_GD	P27797	Calreticulin	3.630604717	0.0030247	6.171153844
E0771_GD	P23528	Cofilin-1	48.95576562	0.0032264	8.856963346
E0771_GD	X6RJP6	Transgelin-2 (Fragment)	59.22518039	0.0032284	8.199977373
E0771_GD	P60660	Myosin light polypeptide 6	33.57707942	0.0033157	8.614175117
E0771_GD	P13929	Beta-enolase	74.2433916	0.0033193	14.40020733
E0771_GD	P17987	T-complex protein 1 subunit alpha	23.61830161	0.0034827	8.354177175
E0771_GD	Q15084	Protein disulfide-isomerase A6	32.87948727	0.0035249	9.821288795
E0771_GD	P12955	Xaa-Pro dipeptidase	11.38883424	0.0035489	6.63436214
E0771_GD	P08865	40S ribosomal protein SA	51.57748296	0.0035746	4.147811317
E0771_GD	Q99471	Prefoldin subunit 5	14.78491305	0.00369	11.12798189
E0771_GD	P08238	Heat shock protein HSP 90-beta	326.6901234	0.0037918	8.246171054
E0771_GD	P51858	Hepatoma-derived growth factor	32.06325485	0.0038253	4.774944941
E0771_GD	P46108	Adapter molecule crk	9.509125916	0.0039168	25.33114856
E0771_GD	P62937	Peptidyl-prolyl cis-trans isomerase A	81.88757395	0.0039775	7.93440443
E0771_GD	P04075	Fructose-bisphosphate aldolase A	68.55165946	0.0040727	7.362172059
E0771_GD	E9PGT1	Translin	25.61779411	0.0041932	40.5495951
E0771_GD	P07737	Profilin-1	23.04368405	0.0044326	5.710632245
E0771_GD	O15212	Prefoldin subunit 6	18.2558432	0.0046145	30.82969036
E0771_GD	E9PF17	Versican core protein	20.14070083	0.0048299	9.399178079
E0771_GD	P42167	Lamina-associated polypeptide 2	19.29821901	0.0049617	50.73426189
E0771_GD	Q96C86	m7GpppX diphosphatase	2.035682075	0.0050653	3.310530542
E0771_GD	Q5PY61	Polyubiquitin-C	33.00610944	0.0053567	11.05634782
E0771_GD	P30520	Adenylosuccinate synthetase isozyme 2	2.07675278	0.0056083	10.57552564
E0771_GD	Q9Y262	Eukaryotic translation initiation factor 3 subunit L	15.28873387	0.0056966	168.0510296
E0771_GD	O00148	ATP-dependent RNA helicase DDX39A	21.5750899	0.00573	10.3588676
E0771_GD	Q3BDU5	Prelamin-A/C	117.4170305	0.0057681	12.36559143
E0771_GD	P31150	Rab GDP dissociation inhibitor alpha	30.46551202	0.0058626	10.74325911

E0771_GD	P37837	Transaldolase	16.93206375	0.0059913	6.864507858
E0771_GD	P12429	Annexin A3	15.65324113	0.0060379	718.7246173
E0771_GD	R4GMT0	Alpha-centractin	8.747653768	0.0061034	5.349816694
E0771_GD	P40926	Malate dehydrogenase, mitochondrial	23.53498419	0.0062363	12.67831485
E0771_GD	P28066	Proteasome subunit alpha type-5	39.12310879	0.0062656	13.03324322
E0771_GD	Q92626	Peroxidasin homolog	18.32735215	0.0063618	10.44706722
E0771_GD	P84077	ADP-ribosylation factor 1	51.07551082	0.0063821	13.26285689
E0771_GD	P54727	UV excision repair protein RAD23 homolog B	18.62965095	0.0063837	2.790122965
E0771_GD	P12268	Inosine-5'-monophosphate dehydrogenase 2	18.30885909	0.0065278	24.31346318
E0771_GD	P23284	Peptidyl-prolyl cis-trans isomerase B	40.49443876	0.0066615	7.157678277
E0771_GD	Q9Y265	RuvB-like 1	30.02748556	0.006671	13.08236372
E0771_GD	K7ES31	Eukaryotic translation initiation factor 3 subunit K	4.697122713	0.0068126	12.71679842
E0771_GD	P47989	Xanthine dehydrogenase/oxidase	3.342303305	0.0069782	6.608001147
E0771_GD	P68032	Actin, alpha cardiac muscle 1	111.3026141	0.0072859	10.51306663
E0771_GD	P13639	Elongation factor 2	176.6888796	0.007471	8.311274646
E0771_GD	Q02809	Procollagen-lysine,2-oxoglutarate 5-dioxygenase 1	3.005564943	0.0078867	3.731769855
E0771_GD	P06748	Nucleophosmin	79.61927002	0.0080428	8.090073104
E0771_GD	Q6UVK1	Chondroitin sulfate proteoglycan 4	4.674650553	0.0083273	138.1705557
E0771_GD	E7EM57	Glucose-6-phosphate 1-dehydrogenase (Fragment)	24.38034691	0.0085039	6.689857273
E0771_GD	O15144	Actin-related protein 2/3 complex subunit 2	8.988264466	0.0092017	2.682215798
E0771_GD	P04406	Glyceraldehyde-3-phosphate dehydrogenase	13.71045553	0.0092146	6.633323351
E0771_GD	P45877	Peptidyl-prolyl cis-trans isomerase C	14.01299334	0.0095438	2.844549735
E0771_GD	B4DNK4	Pyruvate kinase	143.4995821	0.0095721	4.048009313
E0771_GD	P54578	Ubiquitin carboxyl-terminal hydrolase 14	11.63630836	0.0096358	11.81433337
E0771_GD	Q92743	Serine protease HTRA1	30.18318982	0.0097863	3.601502734
E0771_GD	P49368	T-complex protein 1 subunit gamma	36.63937881	0.0102291	8.51266966
E0771_GD	Q14847	LIM and SH3 domain protein 1	15.01765103	0.0102912	21.77965629
E0771_GD	Q8NFI4	Putative protein FAM10A5	5.004166077	0.0105949	2.905479756
E0771_GD	Q96E39	RNA binding motif protein, X-linked-like-1	16.29530805	0.0113433	11.07678801
E0771_GD	P21810	Biglycan	81.33259475	0.011553	2.291050985
E0771_GD	Q92688	Acidic leucine-rich nuclear phosphoprotein 32 family member B	4.430843064	0.0119703	9.046775964
E0771_GD	Q15046	Lysine--tRNA ligase	13.50486486	0.0123956	15.6381417

E0771_GD	P17931	Galectin-3	17.6179048	0.0125497	6.064707764
E0771_GD	Q9BS26	Endoplasmic reticulum resident protein 44	18.63773741	0.0126871	8.040439191
E0771_GD	Q8NC51	Plasminogen activator inhibitor 1 RNA-binding protein	30.73792272	0.0129015	11.0169867
E0771_GD	G3V213	Adenylate kinase 2, isoform CRA_a	14.87611305	0.0134286	409.3987188
E0771_GD	P63000	Ras-related C3 botulinum toxin substrate 1	4.004296155	0.0138767	7.942737962
E0771_GD	P61221	ATP-binding cassette sub-family E member 1	38.61225812	0.0142311	9.623481034
E0771_GD	P19338	Nucleolin	56.83687246	0.0142443	12.83643062
E0771_GD	P31948	Stress-induced-phosphoprotein 1	33.01403816	0.0142532	15.9651215
E0771_GD	Q15257	Serine/threonine-protein phosphatase 2A activator	9.40876143	0.0143895	923.1228835
E0771_GD	P00390	Glutathione reductase, mitochondrial	13.16686601	0.0143962	304.4120026
E0771_GD	Q00839	Heterogeneous nuclear ribonucleoprotein U	10.96310806	0.0144464	8.776007587
E0771_GD	Q9NUQ9	Protein FAM49B	16.27709457	0.0147385	16.12807098
E0771_GD	E9PK01	Elongation factor 1-delta (Fragment)	10.34346365	0.0148448	15.85849785
E0771_GD	Q5SZU1	D-3-phosphoglycerate dehydrogenase	20.39647605	0.0159053	8.578555236
E0771_GD	A0A0G2JL54	Complement C4-B	23.30479865	0.0161831	3.274646021
E0771_GD	P25787	Proteasome subunit alpha type-2	29.98958476	0.0169424	9.90208828
E0771_GD	P09382	Galectin-1	31.27442255	0.0175186	2.967614746
E0771_GD	P09012	U1 small nuclear ribonucleoprotein A	11.79659915	0.017725	254.160116
E0771_GD	O75822	Eukaryotic translation initiation factor 3 subunit J	1.857363001	0.0183003	124.8261837
E0771_GD	P62805	Histone H4	40.2800152	0.0184892	2.728730422
E0771_GD	Q9BXX0	EMILIN-2	13.97977926	0.0188567	10.88501761
E0771_GD	P68036	Ubiquitin-conjugating enzyme E2 L3	15.39378171	0.0192643	9.800277814
E0771_GD	J3KP15	Serine/arginine-rich-splicing factor 2 (Fragment)	10.96662803	0.0194526	30.77341944
E0771_GD	D6RAH7	Ubiquitin-conjugating enzyme E2 D3	11.07867708	0.0195856	30.83260776
E0771_GD	F8W6I7	Heterogeneous nuclear ribonucleoprotein A1	14.80474899	0.0198982	11.24102904
E0771_GD	P61978	Heterogeneous nuclear ribonucleoprotein K	45.81466189	0.0207411	3.625346631
E0771_GD	P13928	Annexin A8	23.40497842	0.0210746	2.848626695
E0771_GD	P05387	60S acidic ribosomal protein P2	21.39648349	0.0225001	36.84159485
E0771_GD	P55327	Tumor protein D52	12.69666249	0.0231827	30.52443045
E0771_GD	P13645	Keratin, type I cytoskeletal 10	22.11270389	0.0235383	6.327520074
E0771_GD	Q9UKY7	Protein CDV3 homolog	8.645760564	0.0248908	254.8258074

E0771_GD	J3KQ32	Obg-like ATPase 1	2.057474481	0.0254672	26.45053206
E0771_GD	E7ETZ0	Calmodulin	18.41873969	0.0270125	12.78815221
E0771_GD	P22314	Ubiquitin-like modifier-activating enzyme 1	10.08000373	0.0285251	4.357973535
E0771_GD	O00622	Protein CYR61	10.8300273	0.0305074	2.811365881
E0771_GD	Q14974	Importin subunit beta-1	13.91818923	0.0306267	3.66264864
E0771_GD	P14678	Small nuclear ribonucleoprotein-associated proteins B and B'	4.102182284	0.0323491	34.66788912
E0771_GD	Q04760	Lactoylglutathione lyase	19.0899903	0.0330204	6.850529196
E0771_GD	P68104	Elongation factor 1-alpha 1	104.7595316	0.0367757	3.169286028
E0771_GD	Q9P258	Protein RCC2	13.61000298	0.0373669	45.35112037
E0771_GD	B0YIW6	Archain 1, isoform CRA_a	12.03770228	0.0387714	2.614687833
E0771_GD	Q99832	T-complex protein 1 subunit eta	1.733462994	0.0392465	3.783963018
E0771_GD	P08670	Vimentin	187.4989487	0.0420206	2.896464371
E0771_GD	P63241	Eukaryotic translation initiation factor 5A-1	32.73388319	0.0452708	2.813513233
E0771_GD	P00558	Phosphoglycerate kinase 1	90.93888147	0.046696	3.129548188

7.1.2. Proteomics Analysis of MEF conditioned media

Table 7.3: List of differentially regulated proteins in MEF control conditioned media (MEF_C)

Group	Accession Number	Description	Confidence score	Anova (p)	Fold Change
MEF_C	P14174	Macrophage migration inhibitory factor	12.77878926	2.85E-06	7.564200324
MEF_C	P00747	Plasminogen	20.45311285	4.56E-05	21.69418352
MEF_C	P09429	High mobility group protein B1	21.06562199	7.60E-05	10.73004674
MEF_C	P00558	Phosphoglycerate kinase 1	90.93888147	9.77E-05	3.79384269
MEF_C	Q86VP6	Cullin-associated NEDD8-dissociated protein 1	4.759442803	0.0001404	11.60533532
MEF_C	P22314	Ubiquitin-like modifier-activating enzyme 1	10.08000373	0.0004287	4.374880395
MEF_C	B0YIW6	Archain 1, isoform CRA_a	12.03770228	0.000506	3.556512783
MEF_C	P62937	Peptidyl-prolyl cis-trans isomerase A	81.88757395	0.0006568	3.306751805
MEF_C	P09382	Galectin-1	31.27442255	0.0007813	4.150264026
MEF_C	E9PIA8	Palmitoyl-protein thioesterase 1 (Fragment)	17.29199112	0.000959	3.051644669
MEF_C	B4DNK4	Pyruvate kinase	143.4995821	0.0010078	3.959793987
MEF_C	Q06323	Proteasome activator complex subunit 1	36.37396179	0.0012721	3.290128673
MEF_C	Q14974	Importin subunit beta-1	13.91818923	0.0013138	3.670455458
MEF_C	Q01995	Transgelin	26.09286228	0.0018977	3.076369832
MEF_C	P04075	Fructose-bisphosphate aldolase A	68.55165946	0.0032034	3.242566541
MEF_C	P07737	Profilin-1	23.04368405	0.0032754	3.015715679
MEF_C	P12004	Proliferating cell nuclear antigen	28.42660156	0.0036523	3.607955032
MEF_C	Q12841	Follistatin-related protein 1	61.8950355	0.0046812	4.395455115
MEF_C	E9PK01	Elongation factor 1-delta (Fragment)	10.34346365	0.0048529	5.422384798
MEF_C	P60174	Triosephosphate isomerase	88.16869552	0.0057625	3.354651694
MEF_C	Q8NFI4	Putative protein FAM10A5	5.004166077	0.0071957	2.115886625
MEF_C	Q07954	Prolow-density lipoprotein receptor-related protein 1	1.822362664	0.0101923	2.111399629
MEF_C	Q14847	LIM and SH3 domain protein 1	15.01765103	0.0118117	36.49210367
MEF_C	P05387	60S acidic ribosomal protein P2	21.39648349	0.0133154	4.256357453
MEF_C	Q15637	Splicing factor 1	4.921340739	0.0158422	6.400020015
MEF_C	P27797	Calreticulin	3.630604717	0.0212682	2.963129109
MEF_C	P23142	Fibulin-1	24.3109702	0.0385416	2.002286373
MEF_C	P40926	Malate dehydrogenase, mitochondrial	23.53498419	0.0470423	3.132641773
MEF_C	P63000	Ras-related C3 botulinum toxin substrate 1	4.004296155	0.0474118	2.405405586

Table 7.4: List of differentially regulated proteins in MEF untreated conditioned media (MEF UTCM)

Group	Accession Number	Description	Confidence score	Anova (p)	Fold Change
MEF_EUM	P07339	Cathepsin D	24.70351857	3.91E-07	20.20902204
MEF_EUM	E9PBF6	Lamin-B1	3.040874728	7.31E-07	12.05598322
MEF_EUM	Q99497	Protein DJ-1	7.668671354	1.46E-06	4.37208887
MEF_EUM	Q8IUX7	Alpha-2-HS-glycoprotein	52.37726794	5.56E-05	34.33673973
MEF_EUM	P22692	Adipocyte enhancer-binding protein 1	27.75316991	5.65E-05	12.72143831
MEF_EUM	D6RF35	Insulin-like growth factor-binding protein 4	31.20025893	5.86E-05	46.44737396
MEF_EUM	E7ER44	Vitamin D-binding protein	94.4880968	0.0003304	12.78641855
MEF_EUM	Q6ZU64	Lactotransferrin	32.76727595	0.0004445	2.772133956
MEF_EUM	F5GY55	Cilia- and flagella-associated protein 65	1.469533219	0.0006223	5.57361659
MEF_EUM	Q14118	DNA damage-binding protein 1	41.21515873	0.001816	2.557396391
MEF_EUM	Q15149	Dystroglycan	23.47307826	0.0018748	2.682154846
MEF_EUM	P02765	Plectin	46.10077906	0.0026239	3.128565474
MEF_EUM	Q02790	Peptidyl-prolyl cis-trans isomerase FKBP4	4.377302955	0.0036246	3.912809212
MEF_EUM	H0YMZ1	Transthyretin	10.33210583	0.0065524	25.06316252
MEF_EUM	P02766	Proteasome subunit alpha type (Fragment)	20.19146079	0.006681	4.21324574
MEF_EUM	J3KMX3	Alpha-fetoprotein	28.10762696	0.0075399	2.728096788
MEF_EUM	P43652	Afamin	3.781422089	0.0095422	2.307227725
MEF_EUM	Q92520	Protein FAM3C	4.448114427	0.0114107	3.109329026
MEF_EUM	P07602	Prosaposin	23.39733244	0.0129487	5.766958707
MEF_EUM	P05452	Tetranectin	11.07079683	0.018398	2.318315941
MEF_EUM	P01008	Antithrombin-III	36.55639853	0.02029	2.002620074
MEF_EUM	P08697	Alpha-2-antiplasmin	19.56058745	0.0261311	3.366791859
MEF_EUM	P02461	Collagen alpha-1(III) chain	68.80913822	0.0308634	3.597210887
MEF_EUM	P20929	Nebulin	3.546539557	0.0340621	5.927327888

Table 7.5: List of differentially regulated proteins in MEF treated conditioned media (MEF CM)

Group	Accession Number	Description	Confidence score	Anova (p)	Fold Change
MEF_ECM	P09486	SPARC	99.15823693	9.46E-09	3.605443198
MEF_ECM	P06865	Beta-hexosaminidase subunit alpha	4.592586031	2.28E-07	18.47288292
MEF_ECM	O15144	Actin-related protein 2/3 complex subunit 2	8.988264466	2.84E-07	21.84305318
MEF_ECM	P35052	Glypican-1	31.3686554	3.13E-07	181.9229737
MEF_ECM	Q02809	Procollagen-lysine,2-oxoglutarate 5-dioxygenase 1	3.005564943	3.44E-07	6.013931359
MEF_ECM	P05019	Insulin-like growth factor I	27.18266803	9.34E-07	32.94904762
MEF_ECM	P12268	Inosine-5'-monophosphate dehydrogenase 2	18.30885909	1.04E-06	93.76989051
MEF_ECM	P45877	Peptidyl-prolyl cis-trans isomerase C	14.01299334	5.54E-06	16.97948783
MEF_ECM	Q15113	Procollagen C-endopeptidase enhancer 1	32.96217797	6.60E-06	13.16524648
MEF_ECM	Q8NBP7	Proprotein convertase subtilisin/kexin type 9	13.81429275	1.21E-05	39.86114126
MEF_ECM	Q9Y265	RuvB-like 1	30.02748556	1.23E-05	29.28067993
MEF_ECM	P61221	ATP-binding cassette sub-family E member 1	38.61225812	1.50E-05	7.070787786
MEF_ECM	O00154	Cytosolic acyl coenzyme A thioester hydrolase	13.66437377	1.55E-05	71.27723437
MEF_ECM	P50990	T-complex protein 1 subunit theta	32.51208573	2.23E-05	9.779899159
MEF_ECM	P20618	Proteasome subunit beta type-1	17.66082493	2.69E-05	37.11879069
MEF_ECM	O75436	Vacuolar protein sorting-associated protein 26A	3.023696422	3.08E-05	71.36600412
MEF_ECM	P07355	Annexin A2	111.8606583	3.22E-05	39.61265247
MEF_ECM	A0A075B7D9	TATA-binding protein-associated factor 2N	2.723973745	4.10E-05	10.10915742
MEF_ECM	P11047	Laminin subunit gamma-1	34.91880231	4.95E-05	11.3209345
MEF_ECM	P17931	Galectin-3	17.6179048	5.56E-05	6.572031651
MEF_ECM	D6RBL5	Annexin	63.98054264	7.03E-05	44.6026168
MEF_ECM	P54136	Arginine--tRNA ligase, cytoplasmic	29.7001631	8.37E-05	11.50800378
MEF_ECM	F8WCF6	Actin-related protein 2/3 complex subunit 4	24.29611519	9.27E-05	53.39536859
MEF_ECM	A0A0C4DFV9	Protein SET	34.04941749	9.68E-05	8.27237306
MEF_ECM	P49368	T-complex protein 1 subunit gamma	36.63937881	0.0001137	10.23846865
MEF_ECM	P11021	78 kDa glucose-regulated protein	163.6413764	0.0001178	6.521059166
MEF_ECM	E7EM57	Glucose-6-phosphate 1-dehydrogenase (Fragment)	24.38034691	0.000118	19.54911756
MEF_ECM	Q9UNZ2	NSFL1 cofactor p47	16.14487173	0.0001266	13.71943513
MEF_ECM	Q9Y266	Nuclear migration protein nudC	21.17417674	0.0001303	22.07304387
MEF_ECM	Q92743	Serine protease HTRA1	30.18318982	0.0001499	7.896707029
MEF_ECM	Q02818	Nucleobindin-1	83.37053992	0.0001571	7.448348442

MEF_ECM	P07900	Heat shock protein HSP 90-alpha	213.9144792	0.0001649	5.185647396
MEF_ECM	P19338	Nucleolin	56.83687246	0.0001808	26.43263861
MEF_ECM	P23284	Peptidyl-prolyl cis-trans isomerase B	40.49443876	0.0001905	14.43957878
MEF_ECM	P63244	Receptor of activated protein C kinase 1	11.76338043	0.0002138	9.609555685
MEF_ECM	A0A0A0MTS2	Glucose-6-phosphate isomerase (Fragment)	35.92159293	0.0002273	45.39718663
MEF_ECM	Q8NEV1	Casein kinase II subunit alpha 3	14.00826212	0.0002505	44.72304
MEF_ECM	P48506	Glutamate--cysteine ligase catalytic subunit	4.367829656	0.0002528	24.99311748
MEF_ECM	P31948	Stress-induced-phosphoprotein 1	33.01403816	0.000257	43.03005038
MEF_ECM	P61088	Ubiquitin-conjugating enzyme E2 N	35.41492654	0.0002731	6.177626818
MEF_ECM	O00303	Eukaryotic translation initiation factor 3 subunit F	16.56597614	0.0002868	11.22867526
MEF_ECM	P08238	Heat shock protein HSP 90-beta	326.6901234	0.0002957	5.283039516
MEF_ECM	P68032	Actin, alpha cardiac muscle 1	111.3026141	0.0002976	4.975532316
MEF_ECM	P13929	Beta-enolase	74.2433916	0.000302	12.11008746
MEF_ECM	P28070	Proteasome subunit beta type-4	18.07024651	0.0003225	40.8216952
MEF_ECM	P50991	T-complex protein 1 subunit delta	25.39158072	0.0003534	27.68682388
MEF_ECM	P23246	Splicing factor, proline- and glutamine-rich	5.789375976	0.0003942	5.486943163
MEF_ECM	P00390	Glutathione reductase, mitochondrial	13.16686601	0.0003975	60.96463606
MEF_ECM	K7ESG5	Proteasome activator complex subunit 3	15.28695245	0.000414	6.894054314
MEF_ECM	P17987	T-complex protein 1 subunit alpha	23.61830161	0.0004293	6.789096659
MEF_ECM	Q6P452	Annexin	31.13235259	0.0004486	8.805750573
MEF_ECM	Q15046	Lysine--tRNA ligase	13.50486486	0.0004842	22.18081367
MEF_ECM	P28838	Cytosol aminopeptidase	13.25727622	0.0005221	10.01769177
MEF_ECM	P11142	Heat shock cognate 71 kDa protein	419.5409654	0.0005287	5.708618564
MEF_ECM	P15090	Fatty acid-binding protein, adipocyte	14.23845041	0.0005699	23.51281093
MEF_ECM	P62857	40S ribosomal protein S28	15.30735046	0.0005862	5.333414866
MEF_ECM	P22626	Heterogeneous nuclear ribonucleoproteins A2/B1	58.26867651	0.000605	7.116743277
MEF_ECM	Q15393	Splicing factor 3B subunit 3	27.57274331	0.0006479	34.1105804
MEF_ECM	P20290	Transcription factor BTF3	4.072192706	0.0006482	7.895818755
MEF_ECM	P61086	Ubiquitin-conjugating enzyme E2 K	17.32208458	0.0006581	15.24428797
MEF_ECM	P34932	Heat shock 70 kDa protein 4	119.9358079	0.0006744	9.225842753
MEF_ECM	B4DXW1	Actin-related protein 3	41.0734679	0.0006822	2.990269952
MEF_ECM	Q9P258	Protein RCC2	13.61000298	0.0007529	477.0052906
MEF_ECM	P60981	Destrin	19.11083247	0.000763	10.78770483
MEF_ECM	P36955	Pigment epithelium-derived factor	42.25616633	0.0008088	2.684722162

MEF_ECM	P00338	L-lactate dehydrogenase A chain	60.81994037	0.0008264	12.55381661
MEF_ECM	P68036	Ubiquitin-conjugating enzyme E2 L3	15.39378171	0.0009029	6.091791719
MEF_ECM	Q96KP4	Cytosolic non-specific dipeptidase	15.23104494	0.0009628	5.796643656
MEF_ECM	Q9Y333	U6 snRNA-associated Sm-like protein LSm2	9.608326012	0.0009741	6.589097474
MEF_ECM	P30041	Peroxiredoxin-6	19.54424544	0.0010085	8.040433576
MEF_ECM	P12814	Alpha-actinin-1	135.9385131	0.0010117	5.564014072
MEF_ECM	Q00577	Transcriptional activator protein Pur-alpha	4.315667173	0.0010272	25.3897925
MEF_ECM	P60842	Eukaryotic initiation factor 4A-I	36.85229005	0.0010298	5.053309115
MEF_ECM	P25787	Proteasome subunit alpha type-2	29.98958476	0.0010503	18.15917369
MEF_ECM	O14818	Proteasome subunit alpha type-7	28.06374998	0.0010516	21.17066879
MEF_ECM	P17174	Aspartate aminotransferase, cytoplasmic	21.27582497	0.0011038	16.27978407
MEF_ECM	J3QQX2	Rho GDP-dissociation inhibitor 1	24.35314005	0.0011468	9.166165824
MEF_ECM	P40925	Malate dehydrogenase, cytoplasmic	19.59996273	0.0011878	5.805742005
MEF_ECM	P50454	Serpin H1	22.80631544	0.0012022	6.836089806
MEF_ECM	P23526	Adenosylhomocysteinase	26.47191433	0.0012051	9.230900531
MEF_ECM	Q9HB40	Retinoid-inducible serine carboxypeptidase	15.80621185	0.0013997	8.034601757
MEF_ECM	P12429	Annexin A3	15.65324113	0.0014836	14.81975507
MEF_ECM	E7EQR4	Ezrin	65.28155066	0.0015004	6.943780963
MEF_ECM	R4GMT0	Alpha-centractin	8.747653768	0.0015288	7.09259762
MEF_ECM	P13928	Annexin A8	23.40497842	0.0015312	7.155816712
MEF_ECM	F8VQ14	T-complex protein 1 subunit beta	18.31020378	0.0015754	8.290674209
MEF_ECM	P35241	Radixin	70.44512818	0.0016782	17.70868518
MEF_ECM	Q9HB71	Calcyclin-binding protein	21.38135904	0.0020453	14.21027596
MEF_ECM	P60900	Proteasome subunit alpha type-6	23.75948401	0.0020861	11.03239509
MEF_ECM	A0A1C7CYX9	Dihydropyrimidinase-related protein 2	61.55114303	0.0024641	13.996752
MEF_ECM	O14737	Programmed cell death protein 5	19.20361583	0.0024778	17.95434479
MEF_ECM	O43852	Calumenin	12.42646181	0.0024931	26.83904677
MEF_ECM	E9PAV3	Nascent polypeptide-associated complex subunit alpha, muscle-specific form	44.57516428	0.0025044	4.495296949
MEF_ECM	J3KQ32	Obg-like ATPase 1	2.057474481	0.0025091	19.00549393
MEF_ECM	P14625	Endoplasmin	58.01996899	0.0025136	11.61822017
MEF_ECM	P43490	Nicotinamide phosphoribosyltransferase	13.7263839	0.0025198	12.32924574
MEF_ECM	P28066	Proteasome subunit alpha type-5	39.12310879	0.0025762	11.45178936
MEF_ECM	P55327	Tumor protein D52	12.69666249	0.0026762	15.31758237
MEF_ECM	P15121	Aldose reductase	3.156545481	0.002699	5.973819171

MEF_ECM	P78330	Phosphoserine phosphatase	17.47569586	0.0030526	102.1512124
MEF_ECM	P13667	Protein disulfide-isomerase A4	35.21866854	0.0030877	5.531724164
MEF_ECM	P35527	Keratin, type I cytoskeletal 9	2.275532567	0.003188	8.283451964
MEF_ECM	Q15257	Serine/threonine-protein phosphatase 2A activator	9.40876143	0.00337	396.205298
MEF_ECM	P06748	Nucleophosmin	79.61927002	0.0033762	10.86986247
MEF_ECM	Q99536	Synaptic vesicle membrane protein VAT-1 homolog	35.4234255	0.0035306	4.887990838
MEF_ECM	P30520	Adenylosuccinate synthetase isozyme 2	2.07675278	0.0035407	4.334989747
MEF_ECM	A0A0G2JL54	Complement C4-B	23.30479865	0.0036636	6.919384844
MEF_ECM	Q14563	Semaphorin-3A	35.67553254	0.0037111	6.695348738
MEF_ECM	P09417	Dihydropteridine reductase	17.62223854	0.0038692	9.482017172
MEF_ECM	P25786	Proteasome subunit alpha type-1	35.74063221	0.0041639	18.81838379
MEF_ECM	P12110	Collagen alpha-2(VI) chain	23.5741394	0.0044072	6.374719566
MEF_ECM	Q92896	Golgi apparatus protein 1	13.85584627	0.0044345	39.28319961
MEF_ECM	P60709	Actin, cytoplasmic 1	249.1469143	0.004766	2.461971433
MEF_ECM	P62258	14-3-3 protein epsilon	89.45852815	0.0050134	8.159645689
MEF_ECM	E9PGT1	Translin	25.61779411	0.0051955	12.68110738
MEF_ECM	P18669	Phosphoglycerate mutase 1	131.5371954	0.00532	4.761661215
MEF_ECM	P16035	Metalloproteinase inhibitor 2	60.53373099	0.0055238	2.474458381
MEF_ECM	Q9Y262	Eukaryotic translation initiation factor 3 subunit L	15.28873387	0.0057268	277.6428121
MEF_ECM	P26641	Elongation factor 1-gamma	47.86005903	0.0058307	8.535410383
MEF_ECM	P47989	Xanthine dehydrogenase/oxidase	3.342303305	0.005861	2.718817663
MEF_ECM	O43707	>sp|O43707|ACTN4_HUMAN Alpha-actinin-4	150.87147	0.0058805	5.577634365
MEF_ECM	P22392	Nucleoside diphosphate kinase B	77.94623192	0.0059457	6.15089058
MEF_ECM	P13639	Elongation factor 2	176.6888796	0.0061044	3.69656157
MEF_ECM	Q08752	Peptidyl-prolyl cis-trans isomerase D	18.80003183	0.0062396	5.773316813
MEF_ECM	P25398	40S ribosomal protein S12	2.426077818	0.0065573	7.94089657
MEF_ECM	P84077	ADP-ribosylation factor 1	51.07551082	0.0066131	8.417716449
MEF_ECM	P12081	Histidine--tRNA ligase, cytoplasmic	18.0798167	0.006852	20.3827
MEF_ECM	Q92626	Peroxidasin homolog	18.32735215	0.0069114	23.39501459
MEF_ECM	P46108	Adapter molecule crk	9.509125916	0.0074471	12.56253001
MEF_ECM	P06733	Alpha-enolase	144.3654213	0.0076636	6.40860101
MEF_ECM	F8W1I6	Dynactin subunit 2	13.93919298	0.0077509	5.177639163
MEF_ECM	P51858	Hepatoma-derived growth factor	32.06325485	0.0080764	3.035724985
MEF_ECM	Q3BDU5	Prelamin-A/C	117.4170305	0.0081776	11.21609294
MEF_ECM	Q99471	Prefoldin subunit 5	14.78491305	0.0085546	4.412037791
MEF_ECM	P49721	Proteasome subunit beta type-2	29.7717515	0.0086381	4.21711785
MEF_ECM	Q15404	Ras suppressor protein 1	16.22518375	0.0096962	9.438348293
MEF_ECM	P61160	Actin-related protein 2	5.068111751	0.0099821	4.600273498

MEF_ECM	O75822	Eukaryotic translation initiation factor 3 subunit J	1.857363001	0.0101962	24.84973395
MEF_ECM	P16989	Y-box-binding protein 3	20.35567549	0.0103461	4.280511776
MEF_ECM	P47755	F-actin-capping protein subunit alpha-2	11.84349912	0.0105393	22.17359515
MEF_ECM	P31153	S-adenosylmethionine synthase isoform type-2	26.88696816	0.0107121	4.093519293
MEF_ECM	P42167	Lamina-associated polypeptide 2, isoforms beta/gamma	19.29821901	0.0108101	9.411338879
MEF_ECM	P24534	Elongation factor 1-beta	17.24048202	0.0108399	5.20226479
MEF_ECM	P30086	Phosphatidylethanolamine-binding protein 1	14.02810625	0.0114798	3.52084203
MEF_ECM	P31150	Rab GDP dissociation inhibitor alpha	30.46551202	0.0116165	4.548028555
MEF_ECM	O75368	SH3 domain-binding glutamic acid-rich-like protein	2.414711319	0.0116792	11.49590187
MEF_ECM	P12955	Xaa-Pro dipeptidase	11.38883424	0.0118667	15.11063735
MEF_ECM	P16949	Stathmin	20.95897788	0.0125873	2.599283939
MEF_ECM	Q99832	T-complex protein 1 subunit eta	1.733462994	0.0127299	12.90157742
MEF_ECM	Q16181	Septin-7	18.59617012	0.0139076	14.40931327
MEF_ECM	J3KTL2	Serine/arginine-rich-splicing factor 1	22.64515346	0.0139504	17.36692056
MEF_ECM	P35268	60S ribosomal protein L22	11.36012289	0.013986	33.55002354
MEF_ECM	Q92688	Acidic leucine-rich nuclear phosphoprotein 32 family member B	4.430843064	0.0151632	10.38968587
MEF_ECM	P14550	>sp|P14550|AK1A1_HUMAN Alcohol dehydrogenase [NADP(+)]	25.4247084	0.0151806	5.263829452
MEF_ECM	J3KR44	Ubiquitin thioesterase	16.17578218	0.0152034	4.294969352
MEF_ECM	P61978	Heterogeneous nuclear ribonucleoprotein K	45.81466189	0.0164366	7.223612415
MEF_ECM	A0A087WTT1	Polyadenylate-binding protein	44.50320919	0.0167812	6.833016817
MEF_ECM	P31949	Protein S100-A11	19.43224453	0.0171565	4.968403585
MEF_ECM	O15212	Prefoldin subunit 6	18.2558432	0.0171665	10.18382323
MEF_ECM	Q5SZU1	D-3-phosphoglycerate dehydrogenase	20.39647605	0.0171969	16.490005
MEF_ECM	P08670	Vimentin	187.4989487	0.0173837	4.210940104
MEF_ECM	P68104	Elongation factor 1-alpha 1	104.7595316	0.0180475	3.215160776
MEF_ECM	P00491	Purine nucleoside phosphorylase	4.985312953	0.0185877	9.172146463
MEF_ECM	Q9BXX0	EMILIN-2	13.97977926	0.0190658	5.583255667
MEF_ECM	P08243	Asparagine synthetase [glutamine-hydrolyzing]	33.94811192	0.0191626	9.809759358
MEF_ECM	F8W6I7	Heterogeneous nuclear ribonucleoprotein A1	14.80474899	0.0195646	5.951677308
MEF_ECM	Q5HYB6	Epididymis luminal protein 189	73.36451715	0.0205258	4.879795231
MEF_ECM	A0A0U1RRM4	Polypyrimidine tract-binding protein 1	4.17401055	0.0205955	2.948856719
MEF_ECM	Q04917	14-3-3 protein eta	27.68847628	0.0224323	10.7151933
MEF_ECM	Q96E39	RNA binding motif protein, X-	16.29530805	0.0225953	7.410021956

		linked-like-1			
MEF_ECM	Q15056	Eukaryotic translation initiation factor 4H	13.01107154	0.0228567	6.88219021
MEF_ECM	P54578	Ubiquitin carboxyl-terminal hydrolase 14	11.63630836	0.0235592	4.295532361
MEF_ECM	Q9NUQ9	Protein FAM49B	16.27709457	0.0260215	6.518540441
MEF_ECM	P23528	Cofilin-1	48.95576562	0.0269823	2.524999932
MEF_ECM	Q5T3N1	Annexin (Fragment)	22.29151562	0.0276463	4.333201774
MEF_ECM	P07237	Protein disulfide-isomerase	54.8232496	0.0281085	3.300320292
MEF_ECM	P05388	60S acidic ribosomal protein P0	38.48232022	0.0288343	3.517194072
MEF_ECM	P04264	Keratin, type II cytoskeletal 1	41.43977023	0.0296036	3.786299894
MEF_ECM	J3KP15	Serine/arginine-rich-splicing factor 2 (Fragment)	10.96662803	0.0299526	40.04680892
MEF_ECM	Q9UKY7	Protein CDV3 homolog	8.645760564	0.0301626	11.68680738
MEF_ECM	P49720	Proteasome subunit beta type-3	35.61487044	0.0309348	4.473751899
MEF_ECM	H0YL52	Tropomyosin alpha-1 chain (Fragment)	86.19312822	0.0357489	3.074466096
MEF_ECM	P13797	Plastin-3	54.92559414	0.0369476	2.937397332
MEF_ECM	Q15084	Protein disulfide-isomerase A6	32.87948727	0.0380449	3.457893932
MEF_ECM	P08572	Collagen alpha-2(IV) chain	4.552047911	0.0391399	22.48815316
MEF_ECM	P63241	Eukaryotic translation initiation factor 5A-1	32.73388319	0.0400551	4.060502477
MEF_ECM	P62277	40S ribosomal protein S13	11.71976658	0.0406664	449.7241649
MEF_ECM	Q9H444	Charged multivesicular body protein 4b	14.22018781	0.044152	3.814376892
MEF_ECM	P61981	14-3-3 protein gamma	28.52762339	0.0446285	5.296363815
MEF_ECM	P56537	Eukaryotic translation initiation factor 6	18.6117551	0.0448056	6.275252457
MEF_ECM	Q04760	Lactoylglutathione lyase	19.0899903	0.0454793	4.007332552
MEF_ECM	Q9UK55	Protein Z-dependent protease inhibitor	11.22333628	0.0481182	3.44906279

7.2. Flow Cytometry

7.2.1. Assessment of mitochondrial superoxide levels in E0771 murine breast cancer cells following glucose deprivation

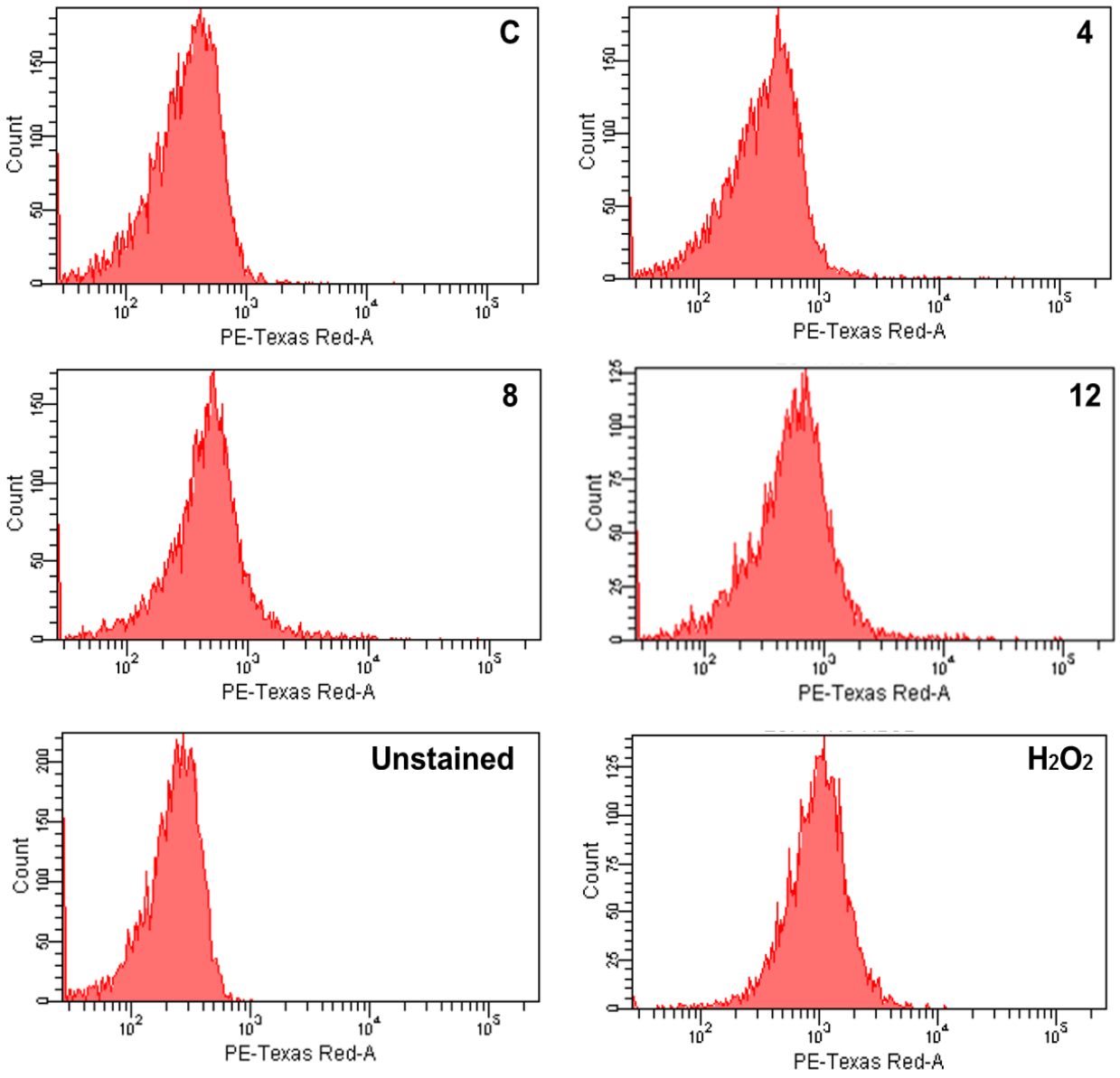

Figure 7.1: Representative flow cytometry histograms of E0771 breast cancer cells assessing mitochondrial $O_2^{\bullet-}$ levels following glucose deprivation. E0771 cells were incubated in 25 mM glucose containing DMEM (Control), or glucose free (0 mM) DMEM for 4, 8 and 12 hours. Mitochondrial oxidative stress was assessed by means of flow cytometry using MitoSox.

7.2.2. Assessment of mitochondrial superoxide levels in MEF cells following treatment with E0771 conditioned media

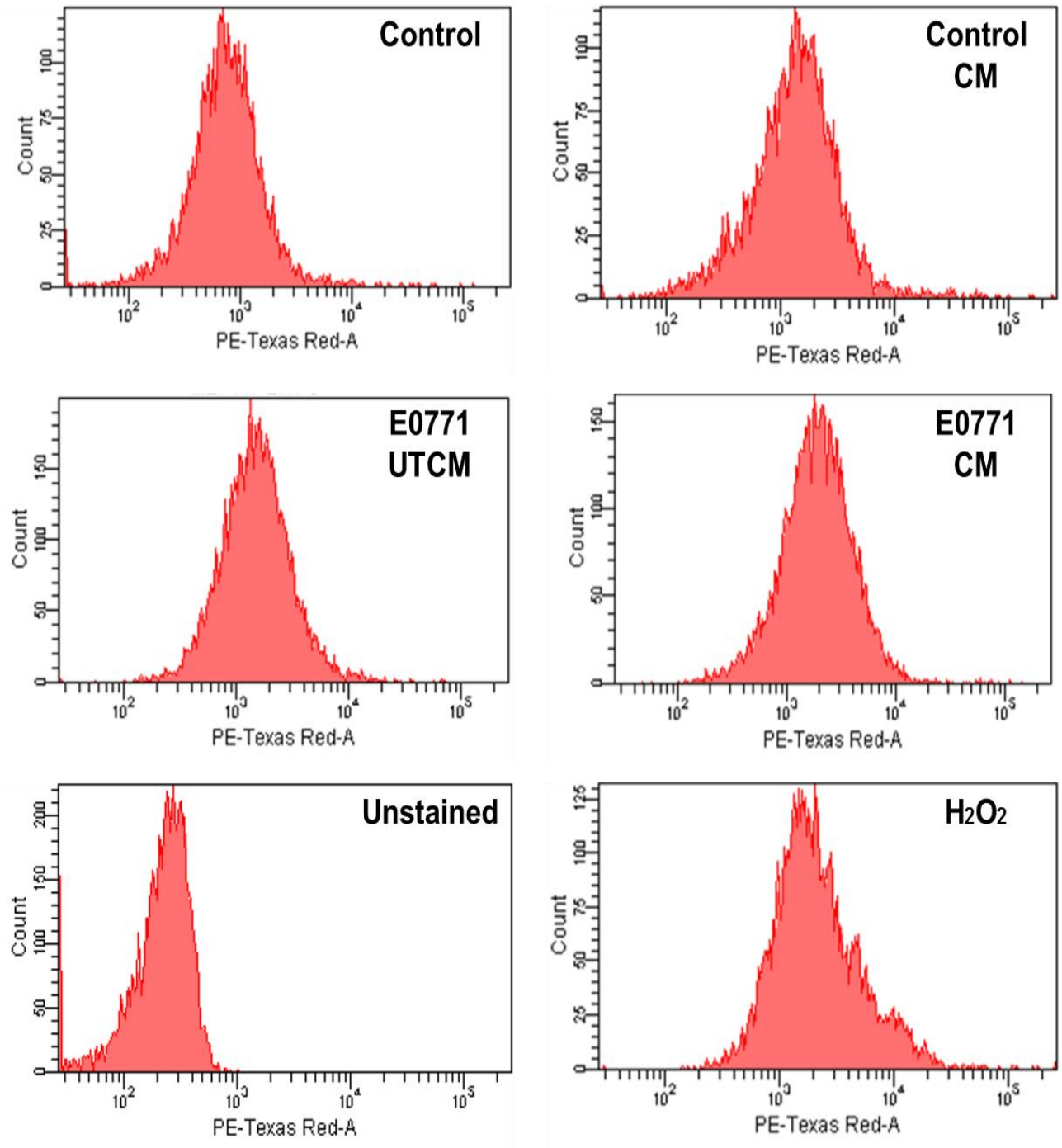

Figure 7.2: Representative flow cytometry histograms of MEF cells assessing mitochondrial $O_2^{\bullet}$- levels following treatment with E0771 conditioned media. MEF cells were subjected to (1) Control, (2) Control conditioned media (Control-CM), (3) E0771 untreated conditioned media (E0771-UTCM) and (4) glucose deprived E0771 conditioned media (E0771-CM) for 24 hours. Oxidative stress was assessed by means of flow cytometry following staining with MitoSox.

7.2.3. Assessment of cytoplasmic hydrogen peroxide levels in E0771 murine breast cancer cells following glucose deprivation

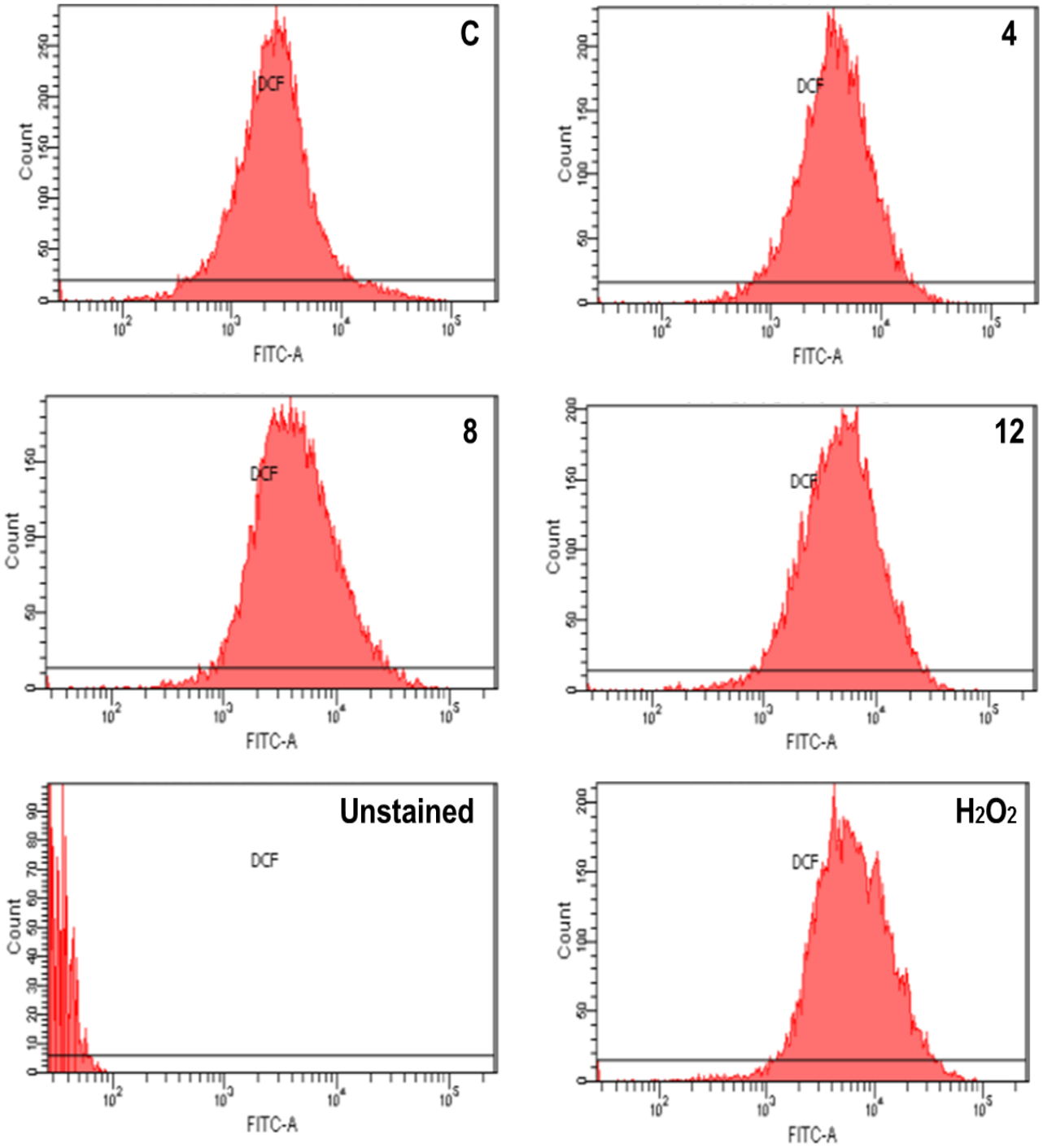

Figure 7.3: Representative flow cytometry histograms of E0771 breast cancer cells assessing cytoplasmic H_2O_2 levels following glucose deprivation. E0771 cells were incubated in 25 mM glucose containing DMEM (Control), or glucose free (0 mM) DMEM for 4, 8 and 12 hours. Mitochondrial oxidative stress was assessed by means of flow cytometry using DCF.

7.2.4. Assessment of cytoplasmic hydrogen peroxide levels in MEF cells following treatment with E0771 conditioned media

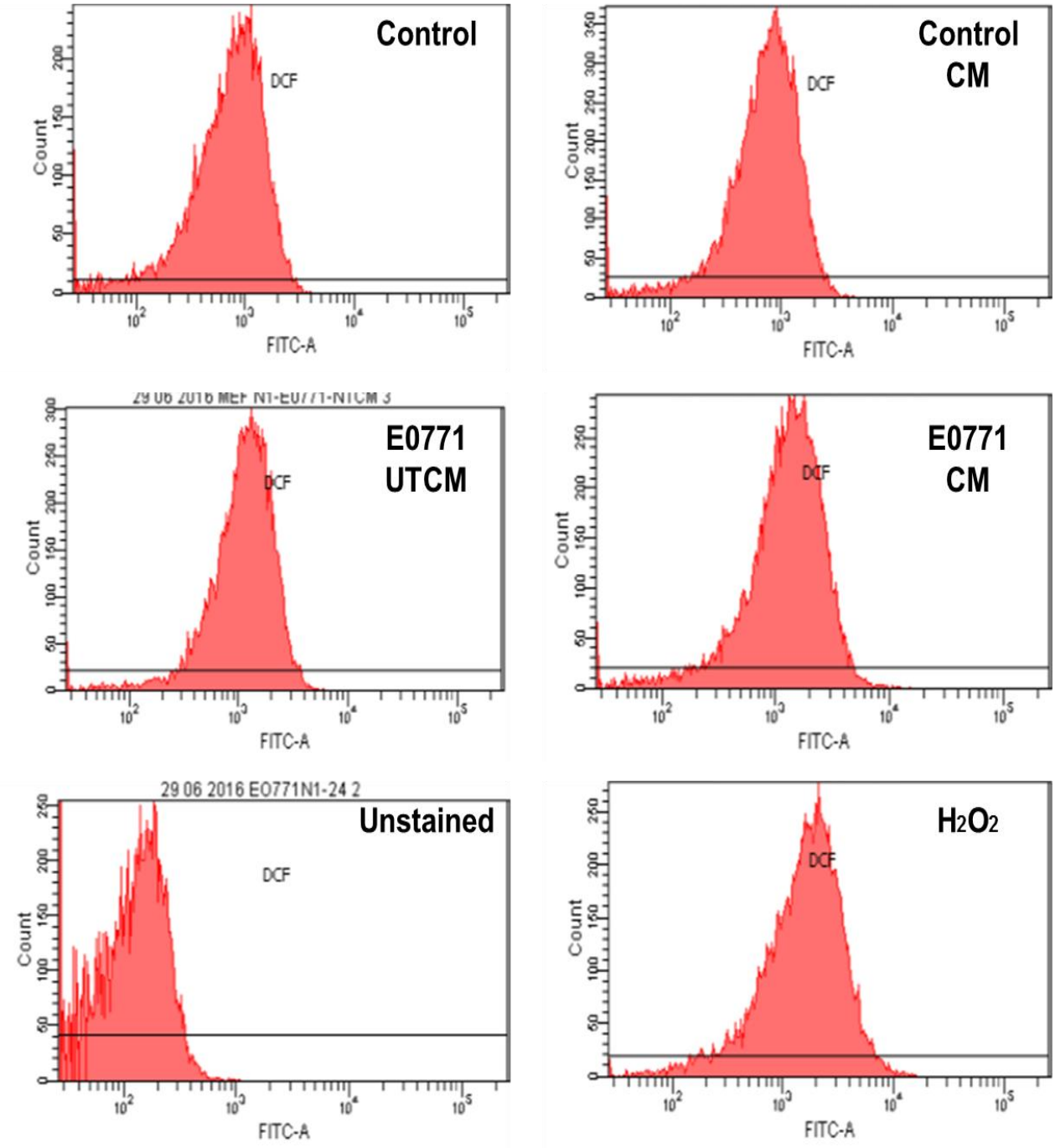

Figure 7.4: Representative flow cytometry histograms of MEF cells assessing cytoplasmic H_2O_2 levels following E0771 conditioned media treatment. MEF cells were subjected to (1) Control, (2) Control conditioned media (Control-CM), (3) E0771 untreated conditioned media (E0771-UTCM) and (4) glucose deprived E0771 conditioned media (E0771-CM) for 24 hours. Oxidative stress was assessed by means of flow cytometry following staining with either DCF.

7.2.5. Assessment of glucose uptake in MEF cells following treatment with E0771 conditioned media

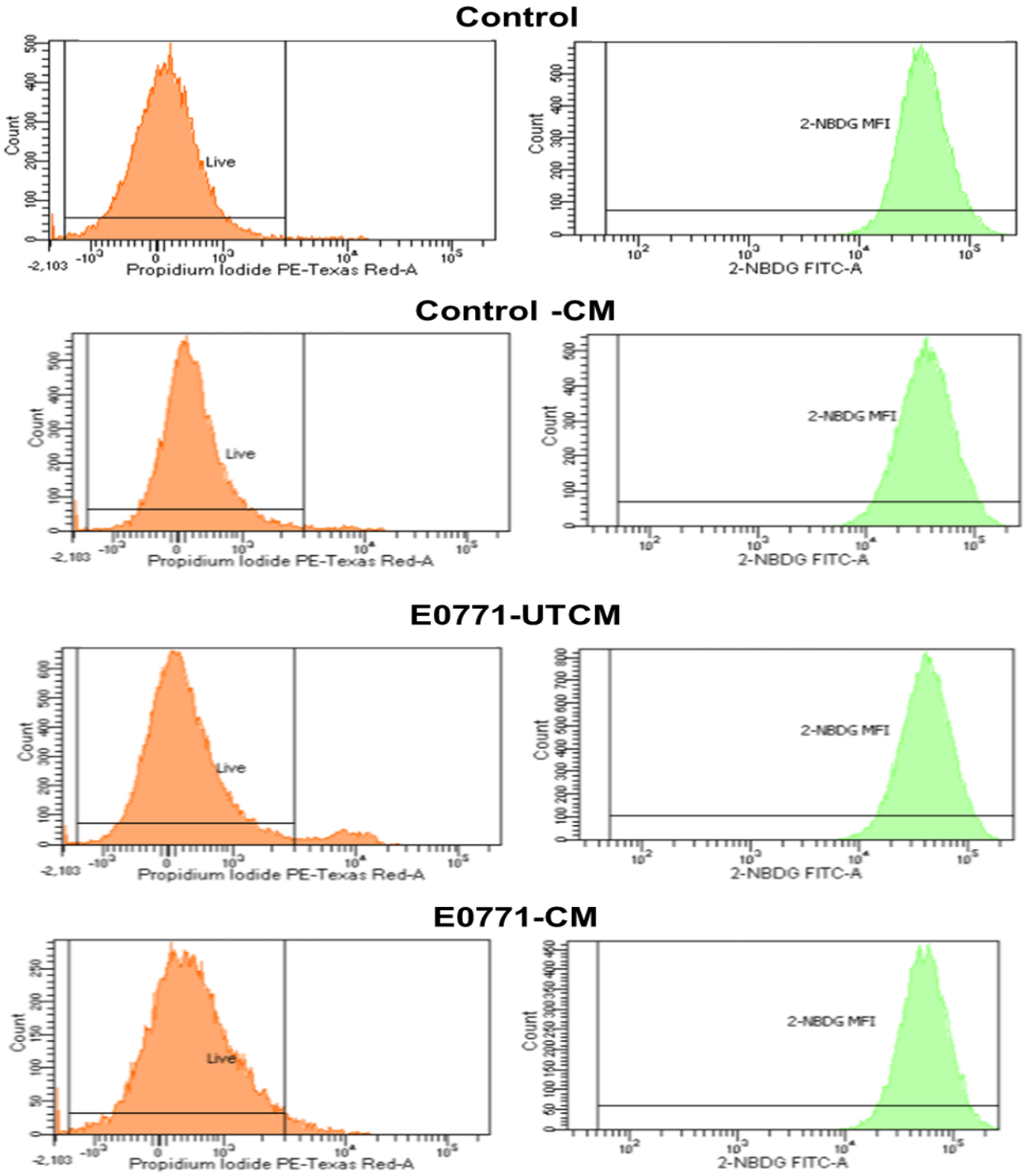

Figure 7.5: Representative flow cytometry histograms of MEF cells assessing cytoplasmic H_2O_2 levels following E0771 conditioned media treatment. MEF cells were subjected to (1) Control, (2) Control conditioned media (Control-CM), (3) E0771 untreated conditioned media (E0771-UTCM) and (4) glucose deprived E0771 conditioned media (E0771-CM) for 24 hours.

7.2.6. Assessment of cell death in E0771 breast cancer cells following treatment with MEF conditioned media

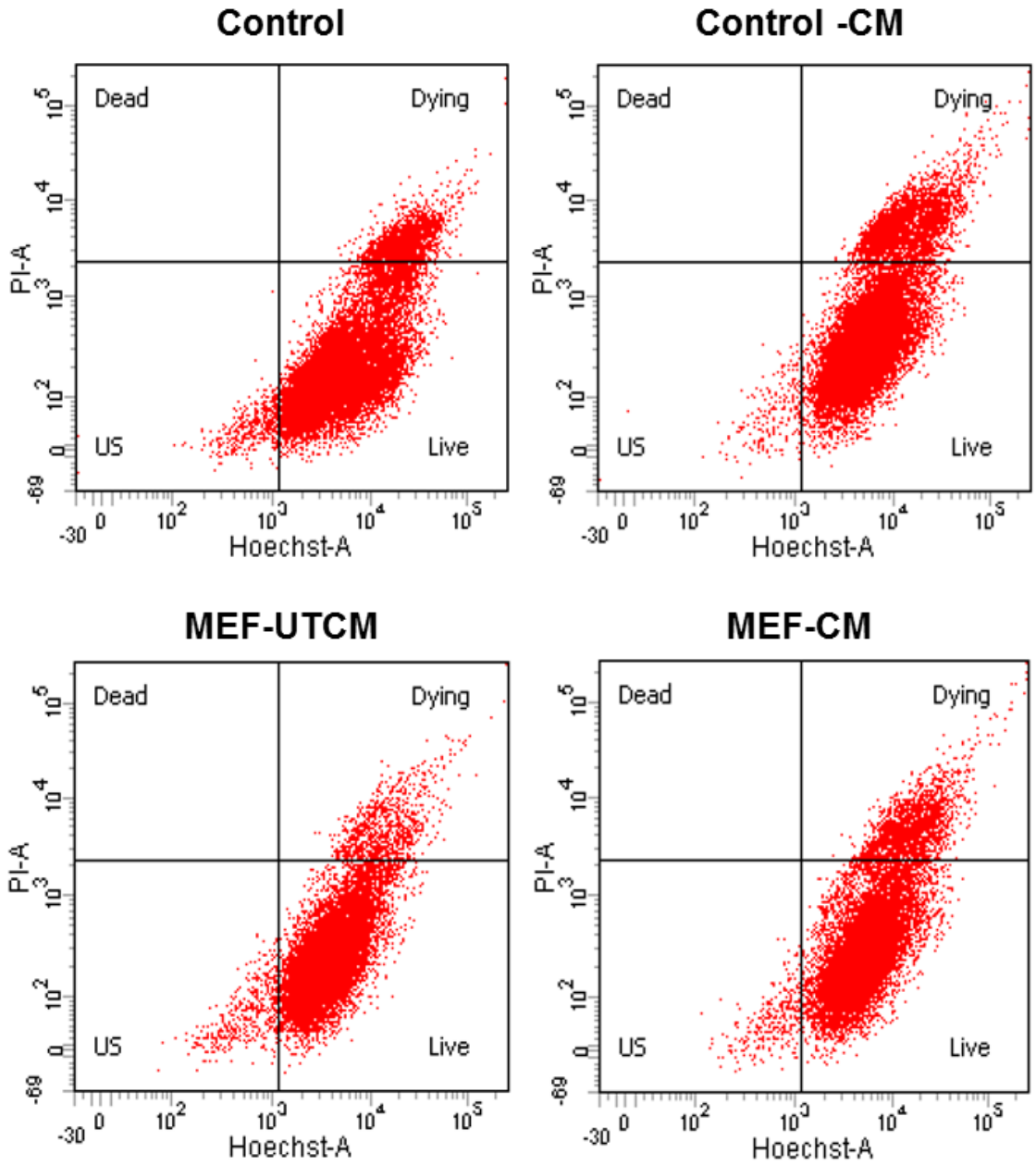

Figure 7.6: Representative flow cytometry plots of E0771 breast cancer cells assessing cell death following MEF conditioned media treatment. Subsequent to 12 hours of glucose deprivation (0 mM glucose DMEM), E0771 cells were subjected to (1) Control, (2) Control conditioned media (Control-CM), (3) Untreated MEF conditioned media (MEF-UTCM) and (4) E0771 treated MEF conditioned media (MEF-CM) for 24 hours.

7.2.7. Assessment of cell death in E0771 breast cancer cells following treatment with Doxorubicin and MEF conditioned media

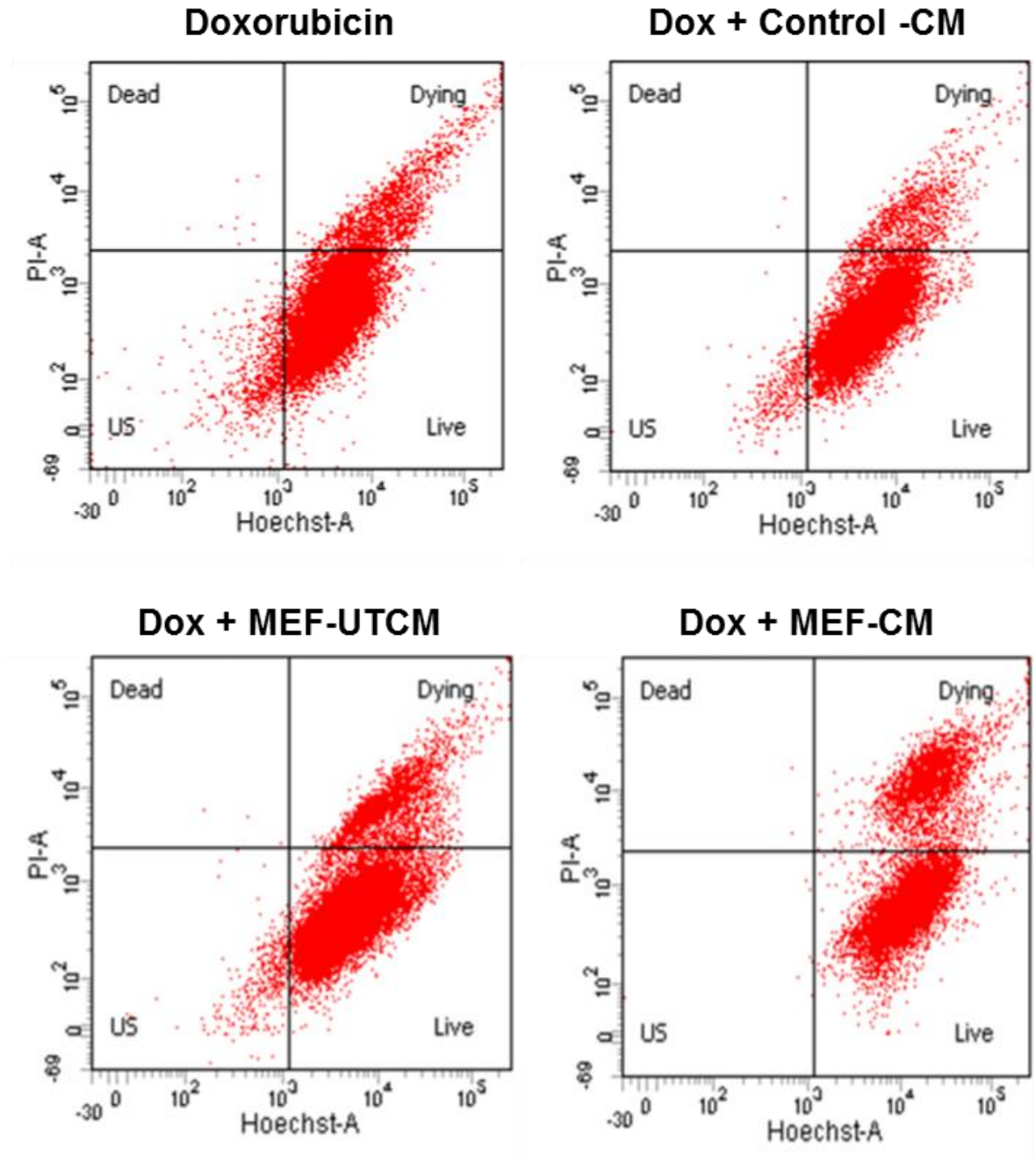

Figure 7.7: Representative flow cytometry plots of E0771 breast cancer cells assessing cell death following Doxorubicin and MEF conditioned media treatment. Subsequent to 12 hours of glucose deprivation (0 mM glucose DMEM), E0771 cells were subjected to (1) Doxorubicin, (2) Doxorubicin + Control conditioned media, (3) Doxorubicin + Untreated MEF conditioned media (Dox + MEF-UTCM) and (3) Doxorubicin + E0771 treated MEF conditioned media (Dox + MEF-CM) for 24 hours.